BODLEIAN LIBRARY OXFORD
DEPOSITED
THESIS
7.1.84

ELECTROCHEMISTRY OF METALLOPROTEINS

B. Nigel Oliver

Thesis submitted in partial fulfilment of the requirements for the degree of Doctor of Philosophy in the Faculty of Physical Sciences

St. John's College, Oxford September 1985

Abstract

Electrochemistry of Metalloproteins

B. Nigel Oliver St. John's College, Oxford

Submitted for the Degree of Doctor of Philosophy

Michaelmas Term, 1985

The direct (unmediated) electrochemistry of a variety of redox proteins has been studied at a range of electrode materials. Electrochemical studies using cytochromes, iron-sulphur proteins and copper proteins show a marked enhancement of the heterogeneous electron-transfer rate at the "edge" plane of pyrolytic graphite. Parallel ESCA studies have shown that mechanical polishing of edge graphite provides an electrode with a high surface coverage of oxidised functional groups. These results indicate the importance of oxidised functional groups in facilitating productive interactions with the proteins.

The importance of multivalent cations has also been established. For proteins with negatively-charged physiological interaction domains, such as plastocyanin or 2[4Fe-4S] ferredoxin, electroactivity at "edge"-oriented graphite is promoted and stabilised in the presence of multivalent cations such as $Cr(NH_3)_6^{3+}$. On the other hand, the electrochemistry of positively-charged cytochrome c is inhibited and destabilised in the presence of such cations. Promotion and inhibition profiles for a range of proteins, together with various cations, indicate the participation of specific electrode-cation-protein interactions.

Studies on plastocyanin, whose electrochemistry is troubled by a time-dependent deterioration of response, have demonstrated the importance of low protein concentration, low pH, low temperatures (3^oC) and, in particular, $Pt(NH_3)_6^{4+}$ at stabilising faradaic responses.

Surface modification of edge pyrolytic graphite has been achieved electrochemically by exploiting the contrasting substitutional reactivity of chromium(III) and chromium(II). The modified-surface, incorporating chromium(III) complexes, promoted reversible direct electrochemistry of plastocyanin.

The direct electrochemistry of plastocyanin, at pH 4, has provided an insight into the possible importance of a kinetically-inactive protonated form of the reduced protein. The $t_{1/2}$ for deprotonation of Cu(I)-plastocyanin is estimated to be < 1 ms. Finally, the direct electrochemistry of azurin was exploited in the design of an electrocatalytic system. The electrochemical oxidation of p-cresol to p-hydroxybenzaldehyde was effected enzymically.

ACKNOWLEDGEMENTS

Firstly, I would like to thank my supervisor, Dr. Allen Hill for renewing my interest in biochemistry several years ago and for providing the opportunity to work in a stimulating research environment.

Thanks are also due to Dr. Fraser Armstrong, whose help throughout the last three years has been invaluable. This thesis has arisen out of his expert guidance.

Many people have helped in the individual chapters. In particular, Adrian and Phil from 10 Parks Road, who gave up much of their own time to run ESCA spectra. Thanks also go to Val and to three Davids (Whitford, Hopper and Page) for providing protein samples, and much-needed assistance with experimental work.

Finally, I am deeply grateful to Malcolm, Margaret and Sharon for being only too willing to help with proof-reading, typing or corrections (or to provide much-needed "Yorkshire Tea"), at any time of day (or night).

CONTENTS

Abbreviations

Asp	aspartic acid
Az	azurin
CV	cyclic voltammetry
Cys	cysteine
DM	decamethonium
Fd	ferredoxin
Fl	flavodoxin
Glu	glutamic acid
HEPES	N-2-[hydroxyethyl]piperazine-N´-2-ethane sulphonate
HM	hexamethonium
MES	2-[N-morpholino]ethane sulphonate
NHE	normal hydrogen electrode
Rd	rubredoxin
SCE	saturated calomel electrode
SWV	square-wave voltammetry
Tris	N-[tris(hydroxymethyl)aminomethane]
Tricine	N-{tris(hydroxymethyl)methyl}glycine

"Biological molecules such as proteins and enzymes hate conventional electrodes and vice versa; as a result biologists and electrochemists do not talk!"

(Albery and Hillman, 1983)

CHAPTER 1

INTRODUCTION

1.1 The Biological Importance Of Redox Proteins.

The efficient acquisition, storage and allocation of energy is central to the continuation of cellular activity. In order to permit a maximal efficiency of energy coupling, biological systems have evolved complex mechanisms of intermolecular redox reactions. These act to conserve efficiently the free energy acquired by cells through the synthesis of adenosine triphosphate (ATP) from adenosine diphosphate (ADP) and inorganic phosphate. ATP is the most useful form of chemical energy for cellular functions such as biosynthesis, mechanical work (e.g. locomotion and contraction) or the osmotic work required to transport materials into the cell.

For the primieval organism, the source of energy was derived from the fermentation of organic matter formed non-biologically in the anoxic environment. However, fermentation is an inefficient source of energy (1 mol of glucose yields 2 mols ATP) leading to rapid depletion of organic materials. The advent of photosynthesis in primitive cells provided a significant biological adaptation, viz., the ability to accomplish fundamental organic syntheses and so self-generate the substrate required for catabolic processes. This earliest mode of

photosynthesis was entirely anaerobic, employing H_2S and releasing sulphur, and remained coupled to the production of energy through inefficient fermentative processes. Thus, the early prokaryotes were, in general, highly prolific but lacked the ability to undergo significant evolutionary elaboration. Another significant feature of these primitive bacteria was the capacity to reduce N_2 to NH_3, an essential process in the anoxic environment where other sources of nitrogen were in short supply.

The Fe-S proteins are among the simplest electron-transfer proteins found in biological systems, and have a good claim to be the first produced during chemical evolution. The 4Fe-4S clusters of bacterial ferredoxins readily assemble themselves from a mixture of iron salts, sulphide, and peptide containing cysteine residues (1) under anaerobic conditions similar to those supposed to have existed in the primieval enviroment. In fact, ferredoxins containing 4Fe-4S clusters are particularly diverse in fermentative bacteria and are used as mediators of reducing equivalents in a variety of metabolic processes. There are at least 18 ferredoxin-dependent enzymes of fermentative bacteria (2), Figure 1.1. Of considerable recent interest are the multiple electron-transfer events leading to the reduction of N_2 to NH_3. The nitrogenase system requires (3) a source of reducing equivalents (ferredoxin) and at least 12 mols of ATP per mol of N_2 reduced to NH_3.

Somewhat later in evolution, bacteria gave rise to the first organisms capable of aerobic photosynthesis, the precursors of the modern cyanobacteria. One of the by-products of aerobic photosynthesis is dioxygen and it is the gradual appearance of an oxygen-enriched atmosphere which effected a second cycle of biological evolution, the development of oxygen-dependent

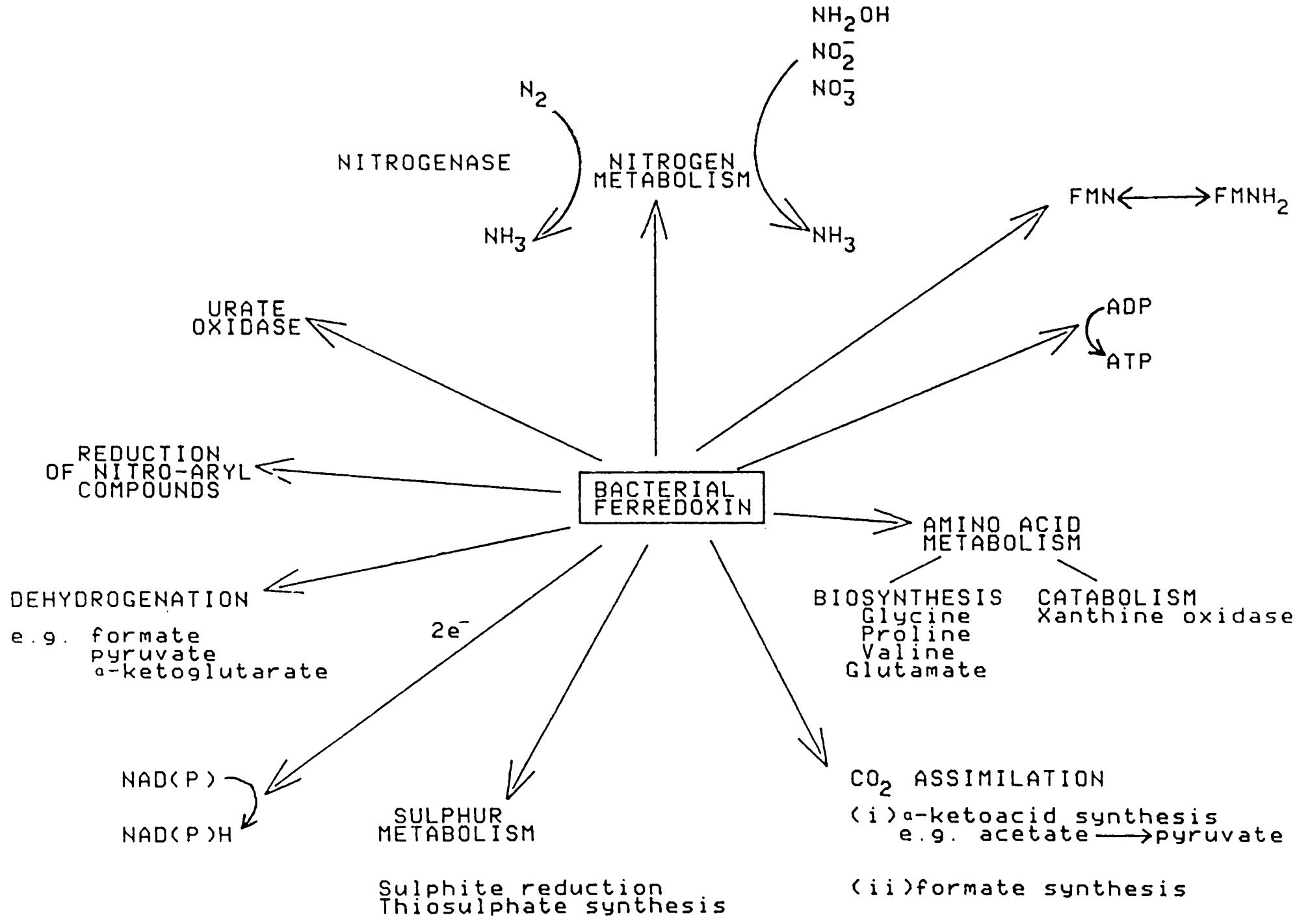

Figure 1.1: The ferredoxin-dependent enzymes and reactions of fermentative bacteria.

(aerobic) biochemistry and, in particular, aerobic respiration. This marked a profound enhancement in the efficiency of energy production and the capacity to create a surplus of energy. In the aerobic organism, the main source of ATP is the flow of reducing equivalents through a series of redox-active carrier molecules (redox proteins). Surplus energy is reserved in long-term energy storage compounds, such as creatine phosphate or polysaccharides, formed through the intermediary of ATP.

1.1.1 Aerobic Respiration.

The catabolic reactions of eukaryotic organisms terminate in an electron-transfer chain located in the inner mitochondrial membrane. This is illustrated schematically in Figure 1.2. The important features of this chain are the directed flow of electrons, the coupling of electron flow to substrate oxidation, and the coupling of electron flow to energy (ATP) production.

The citric acid cycle.

The overall effect of the citric acid cycle is to break down the carbon chain of organic substrates (amino acids, fatty acids and sugars) to carbon dioxide, and to deliver the reducing equivalents made available by this oxidation, to the oxidised carrier nicotinamide adenine dinucleotide ($NAD^+ + 2e^- + H^+ \rightleftharpoons NADH$). NADH is the principal intermediary between the citric acid cycle and the electron-transport chain in the inner mitochondrial membrane.

The respiratory chain.

The driving force of the respiratory chain is the transfer

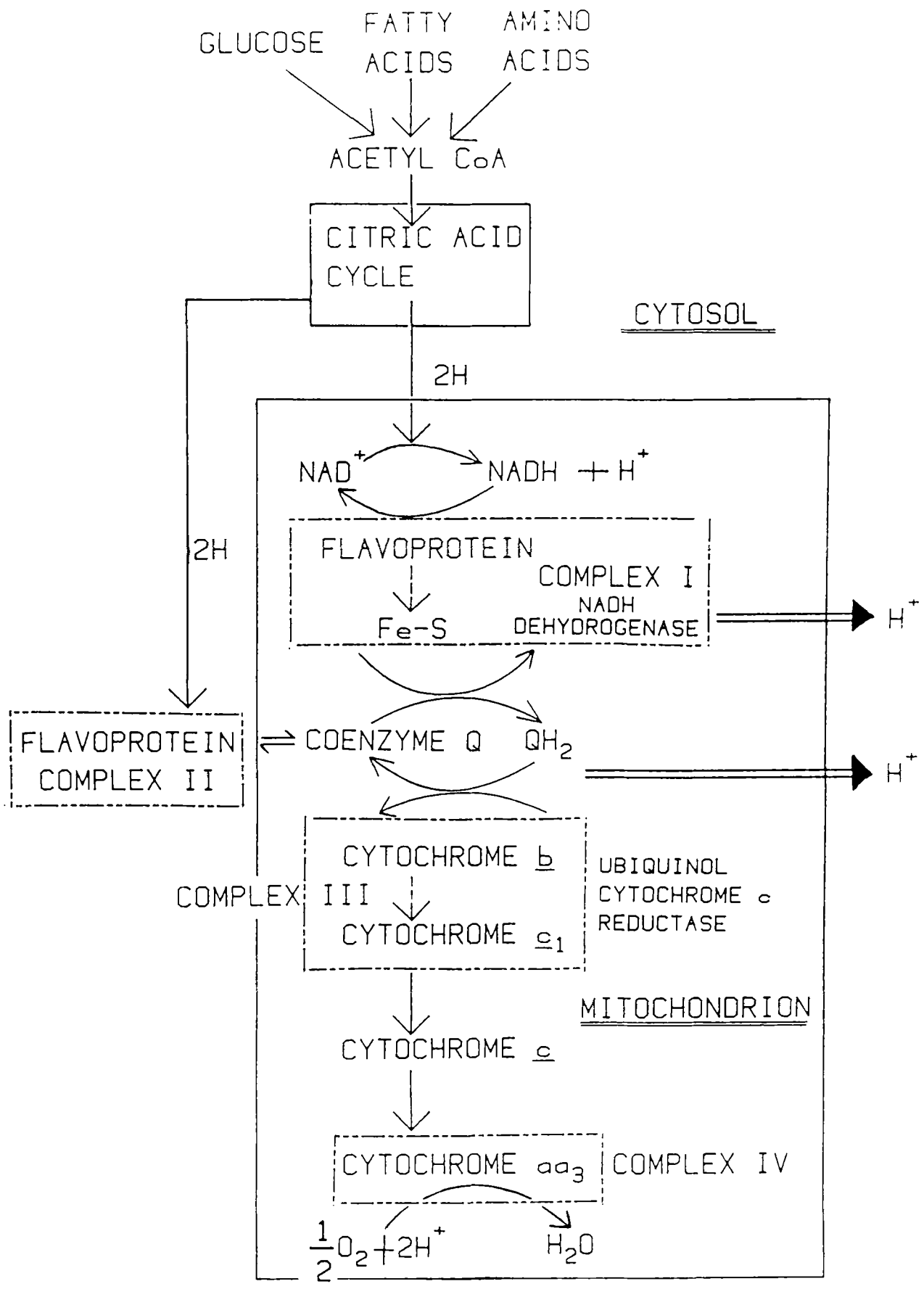

Figure 1.2: Scheme of electron transfer through the complexes of the mitochondrial respiratory chain.

of electrons from NADH (E^o = -0.56 V vs. SCE) to O_2 (E^o = 0.57 V vs. SCE). The free energy of transfer corresponds to -220.1 $kJmol^{-1}$. This energy is released in a series of controlled redox reactions between the components of the electron-transport chain. Three of these steps are sufficiently exergonic to drive the synthesis of ATP (requires 30.5 $kJmol^{-1}$). This is in accordance with the experimental observation that three mols of ATP are formed per mol of mitochondrial NADH (4). Thus, coupled phosphorylation of ADP yields ca. 40% of the free energy decline from NADH to O_2. For each mol of glucose entering the citric acid cycle (via pyruvate), 36 phosphate bonds are formed, a net energy yield to the cell some 18-fold greater than from fermentation or glycolysis alone.

The electron carriers of the respiratory chain are a quinone derivative with an isoprenoid side chain (coenzyme Q), which is soluble in the lipid matrix, and a series of redox proteins containing flavin (FMN), iron-sulphur (Fe-S) and haem centres. With the exception of the haemoprotein cytochrome c, these are all embedded in the rigid matrix of the inner mitochondrial membrane.

Oxidative phosphorylation.

A hypothetical mechanism for the coupling of electron transport to ATP synthesis is the chemiosmotic theory of Mitchell (5). According to this theory, each pair of electrons transferred from NADH to O_2 results in the outward translocation of six protons across the membrane. The redox cycling of coenzyme Q and the FMN centre ($FMN \rightleftharpoons FMNH_2$) of NADH dehydrogenase is postulated to convey protons across the membrane. Thus, the free energy

release occurring in electron transport is conserved in the form of a concentration gradient (H^+) and potential difference across the impermeable inner membrane. The resultant gradients drive the process of ATP synthesis by a proton influx through the membrane-bound ATP-synthase complex (F_1-F_o). Other processes are also powered by this proton gradient. These include the reduction of a phosphorylated derivative of NAD^+, $NADP^+$ to NADPH (the source of reducing equivalents for biosynthesis), the transport of Ca^{2+} and Na^+, and the exchange of ADP for ATP across the mitochondrial membrane.

1.1.2 Aerobic Photosynthesis.

Photosynthetic electron transport, in organisms that evolve O_2, has redox-active carrier molecules similar to those of mitochondrial respiration. Thus, the electron transport chain includes a membrane-soluble quinone (plastoquinone) and redox proteins containg haem (cytochrome b_6-f complex), Fe-S (2Fe-2S ferredoxin) and Cu centres (plastocyanin). Plastocyanin and the 2Fe ferredoxin are the only water-soluble proteins of the photosynthetic chain.

The photosynthetic chain begins with the oxidation of water and produces reducing power in the form of NADPH. Currently, the accepted model (6) for photosynthetic electron transport is that in which two photosystems (photosystems I and II) act co-operatively in series, linked by the chain of electron-carriers which are asymmetrically located across the inner membrane of the chloroplast. This is illustrated schematically in Figure 1.3. The two primary events of photosynthesis are light-activated electron transfers, against

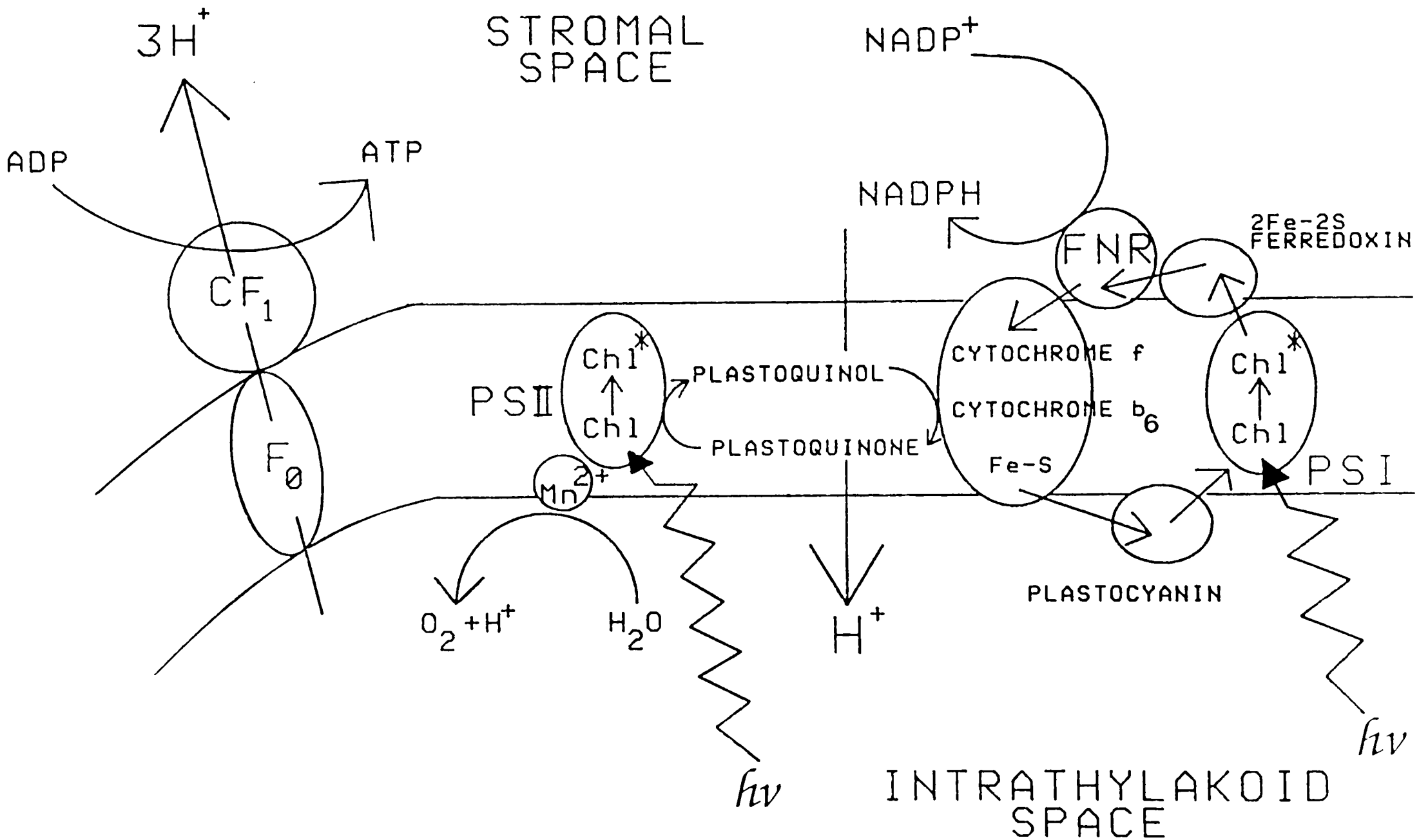

Figure 1.3: Schematic representation of the thylakoid membrane showing the distribution of the components of the photosynthetic electron transport chain.

the free energy gradient, driven by the excitation of chlorophyll molecules located in photosynthetic antenna complexes. The steps following these excitations proceed via electron transport chains in the gradient direction, without the influence of light, and are coupled to the formation of NADPH and ATP. Both of these metabolites participate in the photosynthetic fixation of CO_2 to produce carbohydrate. Superimposed on this lineal, unidirectional redox chain, is a cyclic electron flow around photosystem I linked to the synthesis of ATP, Figure 1.3.

The chemiosmotic theory for the coupling of electron transport to ATP synthesis has also been applied to photosynthetic phosphorylation. However, in chloroplasts, the direction of proton flow is opposite to that of mitochondria. As a result the interior matrix of the chloroplast becomes strongly acidic upon illumination (the pH gradient is about 2-3 units (7)), and phosphorylation may be driven by an **efflux** of protons through a membrane-bound ATP-synthase complex (CF_1-F_o).

1.1.3 Bacterial Respiration.

The respiratory chain of the bacterium Pseudomonas aeruginosa incorporates several components analogous to those found in mitochondrial and photosynthetic membranes, Figure 1.4, and may operate according to similar principles. However, the bacterial respiratory chain is simpler than the eukaryotic analogues, although the precise role of the small haem (cytochrome $\underline{c}_{551}$) and copper (azurin) proteins is not well-defined (8). Both appear to be electron-donors to the terminal cytochrome c-d_1 complex, which is capable of reducing nitrite and dioxygen. The former is thought to be the physiologically-

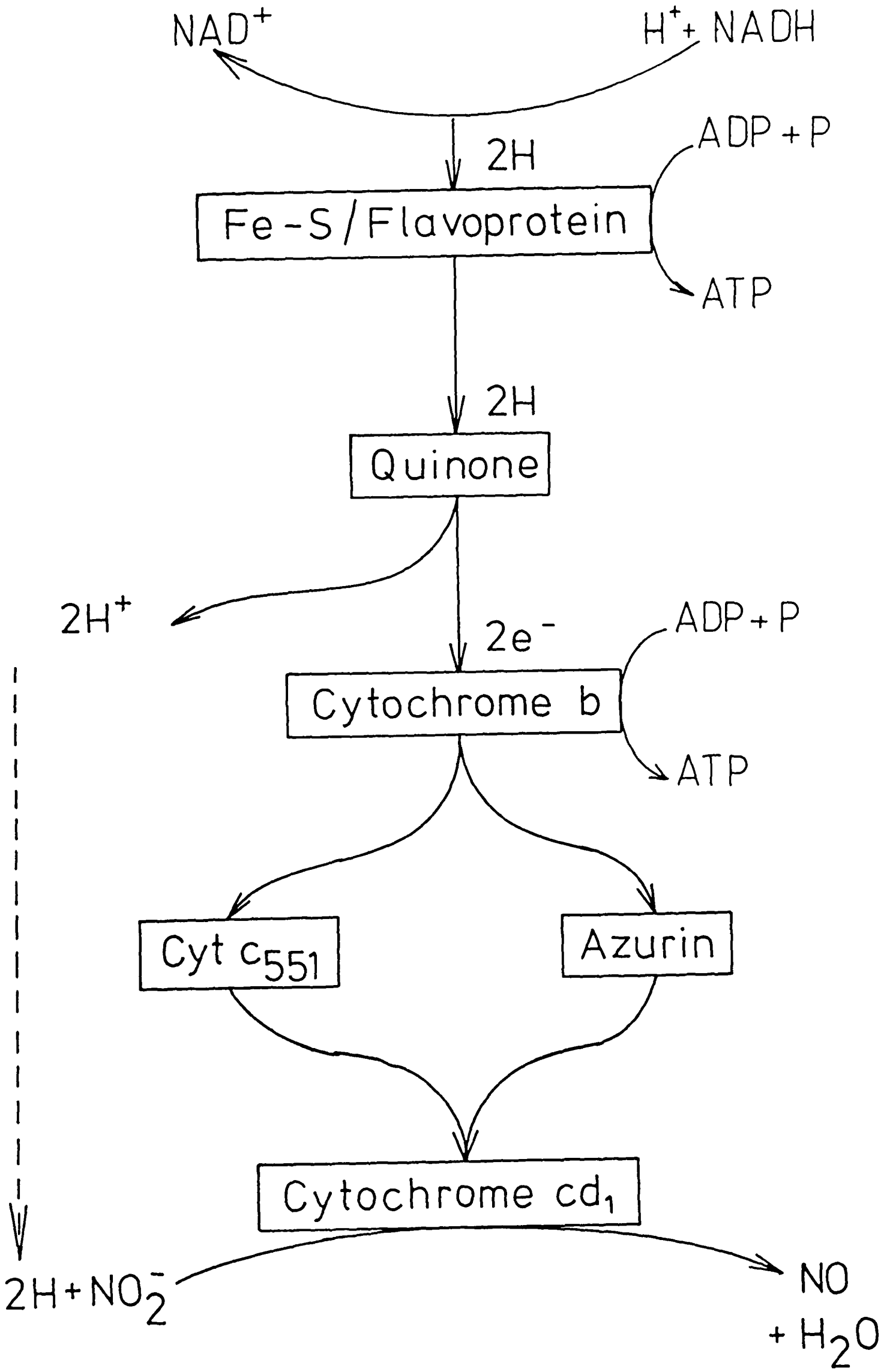

Figure 1.4: The respiratory chain of the bacterium Pseudomonas aeruginosa.

relevant couple. It seems likely (8) that the chain is associated with the cytoplasmic membrane, similar to that of E. coli (9), to facilitate coupling of respiratory activities to oxidative phosphorylation, active transport and related energy-requiring phenomena, although the terminal cytochrome is unusually water-soluble, as isolated.

1.1.4 The Role of Iron-Sulphur Proteins in Biosynthesis.

There are several well-defined electron transport chains to be found in prokaryotic and eukaryotic organisms associated with biosynthetic processes. These utilise reducing equivalents (in the form of NAD(P)H) generated in catabolic reactions, and are exemplified by systems effecting the hydroxylation of hydrocarbons. This is a necessary step in biotransformation reactions (prokaryotes and eukaryotes), particularly of steroids, in the initial functionalisation of hydrocarbons prior to further metabolism (prokaryotes) and in conferring water-solubility on lipophilic molecules prior to excretion (eukaryotes). Typical examples are the cytochrome P-450 (10), benzene dioxygenase (11) and ω-alkane hydroxylase (12) systems, Figure 1.5. These all utilise low molecular-weight Fe-S proteins as mediators of reducing equivalents between NADH dehydrogenases (flavoproteins) and redox-active, dioxygen-dependent hydroxylases.

1.2 The Structures and Properties of Redox Proteins.

There are four main classes of redox proteins associated with biological electron transport chains, namely the iron-sulphur (Fe-S) proteins (13), the flavoproteins (14), the haemoproteins (15), and the copper proteins (16).

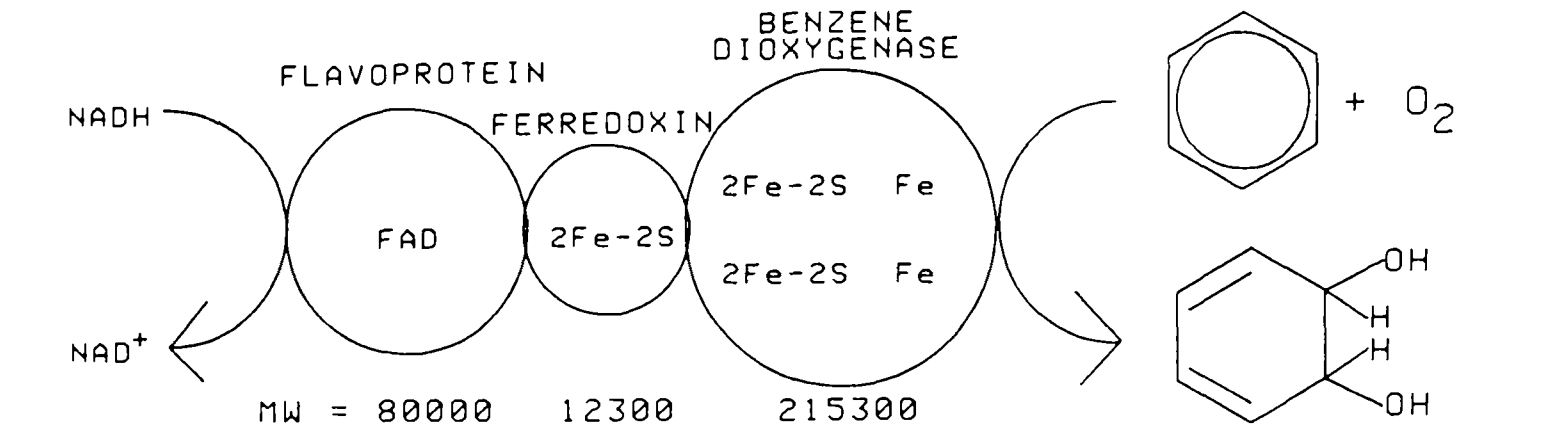

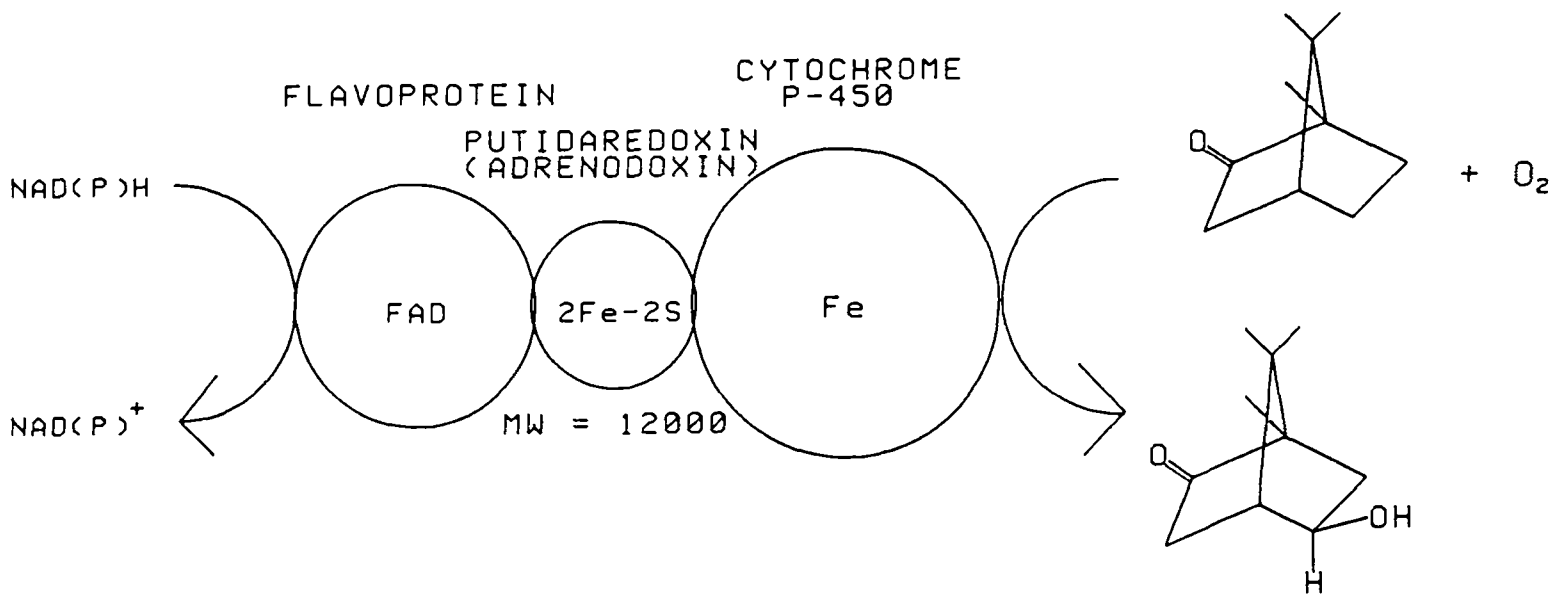

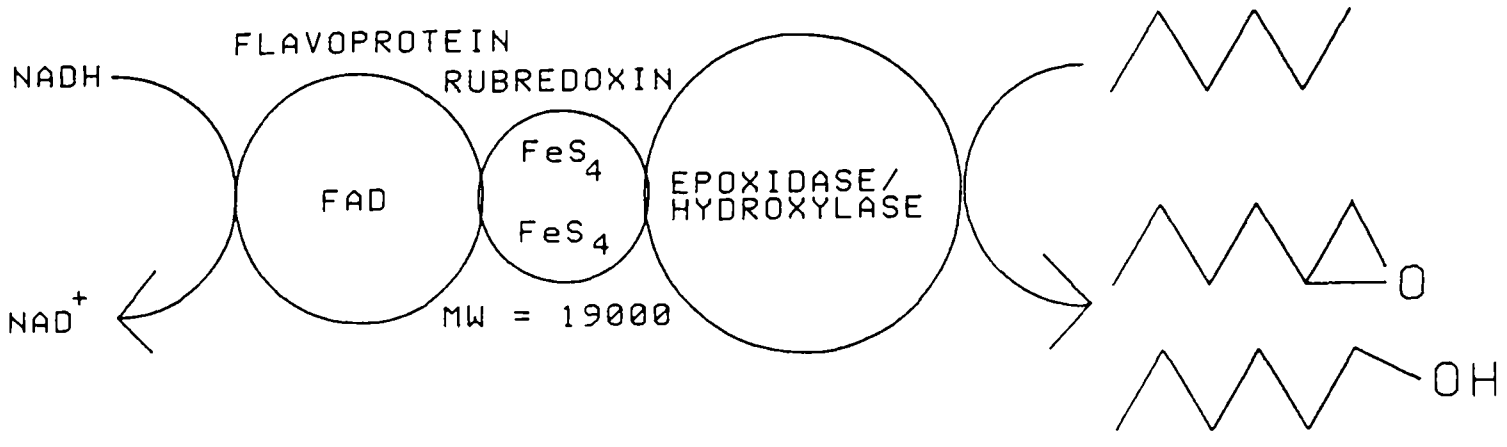

Figure 1.5: The incorporation of iron-sulphur proteins into bacterial electron transfer chains catalysing synthetic processes.

1.2.1 Iron-Sulphur Proteins.

Iron-sulphur proteins contain iron and, usually, non-cysteinyl sulphur ('inorganic sulphur'). The iron centre is bound to the polypeptide chain by four cysteinyl sulphur linkages. Iron-sulphur redox proteins of relatively low molecular weight (ca. 6000 - 20000) are best classified in terms of the amount of iron and sulphide (S^*) per molecule: (1) $1Fe\text{-}0S^*$ (rubredoxins, Rd), bacterial; (2) $2Fe\text{-}2S^*$, plant-type (ferredoxins, Fd), bacterial (e.g. putidaredoxin, Pd) and mammalian (e.g. adrenodoxin); (3) $4Fe\text{-}4S^*$, photosynthetic (high potential iron protein, HIPIP, $E^o \sim +100$ mV vs. SCE), and non-photosynthetic bacterial (ferredoxins, Fd, $E^o \sim -600$ mV); (4) $2[4Fe\text{-}4S^*]$, bacterial (ferredoxins, Fd). The crystal structures of proteins from classes 1-4 have been determined to 1.2 to 2 Å resolution. These are shown in Figure 1.6(a,b,c) for Rd (Clostridium pasteurianum) (17), 2Fe Fd (Spirulina platensis; algal) (18) and 8Fe Fd (Peptococcus aerogenes) (19). A particularly noteworthy feature of the polypeptide conformation of Fe-S proteins is the utilisation of -Cys-X-X-Cys- peptide fragments in binding the Fe-S centre.

1.2.1a Proteins with one Fe per centre: rubredoxins.

Rubredoxin is a small protein (RMM 6127) containing iron in a distorted tetrahedral co-ordination environment, Figure 1.6(a). The co-ordination geometry is essentially the same in both oxidised and reduced proteins. The protein displays pronounced structural asymmetry both in terms of the location of the redox centre and in terms of the amino acid composition and distribution. The amino sequence reveals an absence of both

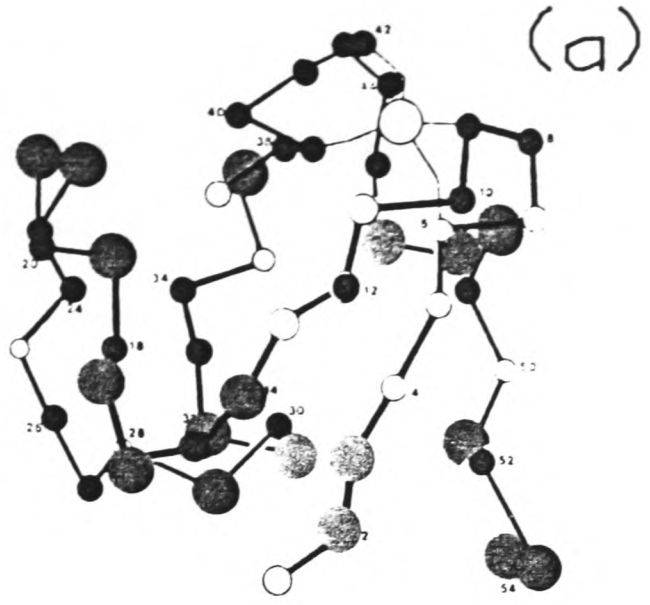

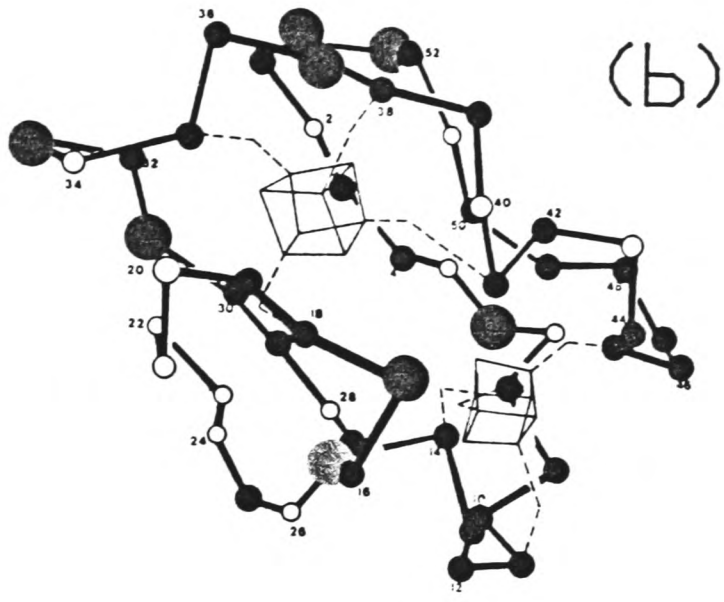

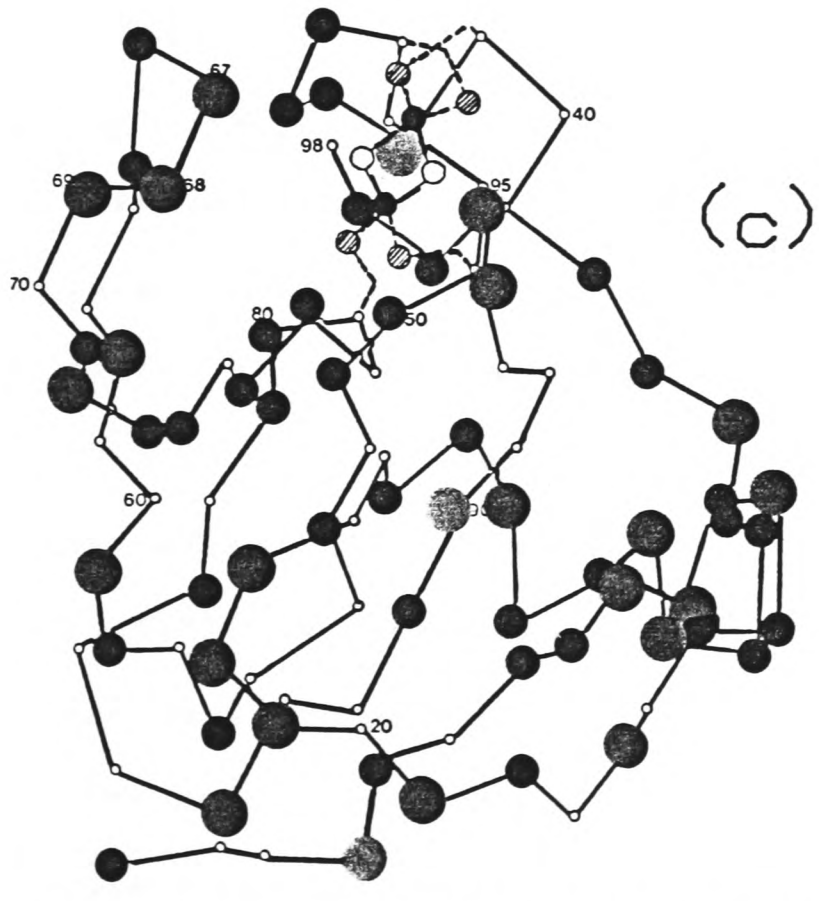

Figure 1.6: Three-dimensional structures of iron-sulphur proteins and Fe-S clusters. (a) Rubredoxin, C. pasteurianum. (b) 2[4Fe-4S] ferredoxin, P. aerogenes. (c) 2Fe-2S ferredoxin, S. platensis. The protein structures show the α-carbon atoms and the position of the Fe-S centres. Acidic [●], basic [●], hydrophobic (non-polar) [●], and polar, non-ionic [○] amino acid residues are marked.

arginine and histidine and an abundance of acidic aspartate and glutamate residues. The surface region in the vicinity of the FeS_4 complex is distinguished by the presence of hydrophobic groups and a total lack of hydrophilic groups.

No physiological function distinct from those which the 8Fe ferredoxin will fulfill has been found for this protein. However, the protein from the aerobe P. oleovorans has a well-defined role in a hydrocarbon hydroxylation system (Figure 1.5), although this rubredoxin is atypical, in that it has a molecular weight of 19,000 and contains two closely similar iron-binding sites.

1.2.1b Proteins containing 4Fe-4S clusters.

The Fe-S centres in the 4Fe and 8Fe proteins are organised into compact clusters of cubane-like geometry, Figure 1.6(b). The cluster geometries in reduced HIPIP, oxidised 8Fe ferredoxin, and a ferredoxin analogue, $[Fe_4S_4(SCH_2C_6H_5)_4]^{2-,3-}$ are essentially identical (20). The basic structure is that of a distorted cube consisting of two interpenetrating and concentric tetrahedra of Fe and S atoms. The vertices bearing the Fe atoms are slightly inside those of the S atoms (Fe-Fe distance ~2.8 Å, S-S distance ~3.5 Å). Each Fe has a tetrahedral environment of four S atoms. The difference in geometry between oxidised and reduced clusters in HIPIP is confined to small changes (<0.1 Å) in the mean Fe-S and Fe...Fe distances. Similarly, the unconstrained, idealised core structural change accompanying electron-transfer in the 4Fe site analogue (21) is:

$$[Fe_4S_4(SPh)_4]^{2-} \text{ (compressed } D_{2d}) \rightleftharpoons [Fe_4S_4(SPh)_4]^{3-} \text{ (elongated } D_{2d})$$

It is unlikely that the Fe-S centre in bacterial ferredoxin undergoes a significant conformational change upon reduction (21).

The physical properties of $HIPIP_{red}$ and Fd_{ox} are remarkably similar. Both these states are diamagnetic and, furthermore, the optical spectra are identical. Given these observations together with the likely similarity of the cluster geometry in all four oxidation states ($HIPIP_{red}$, $HIPIP_{ox}$, Fd_{red}, Fd_{ox}), then the difference in half-wave potential exhibited by the 4Fe-4S cluster in these two proteins is surprisingly large (*ca.* 800 mV). This has led to the proposal of a three-state hypothesis (20), in which three oxidation states are accessible to Fe_4S_4 clusters, and $HIPIP_{red}$ and Fd_{ox} are isoelectronic states:

$Fd_{red} \rightleftharpoons Fd_{ox} + e^-$	$\longleftrightarrow$	$HIPIP_{red} \rightleftharpoons HIPIP_{ox} + e^-$
$Fe_4S_4(SR)_4^{3-}$		$Fe_4S_4(SR)_4^{2-}$		$Fe_4S_4(SR)_4^{1-}$
PARAMAGNETIC		DIAMAGNETIC		PARAMAGNETIC

The question then arises as to what feature restricts HIPIP to the $Fe_4S_4(SR)_4^{2-/1-}$ couple and Fd to the $Fe_4S_4(SR)_4^{3-/2-}$ couple. It seems probable that this results from differences in the polypeptide environment in the vicinity of the cluster. There are clear differences in the exposure of the two clusters to solvent. In HIPIP, the redox cluster is deeply buried in a hydrophobic pocket; in the bacterial ferredoxin, the cluster is close to the surface, also in a non-polar site, but one cysteine of each cluster is solvent exposed. A more specific suggestion has focussed upon the observation of NH....S hydrogen bonds between backbone amide groups and the sulphur atoms of Fe-S clusters, in all Fe-S proteins (22). There is an approximate

correlation between the number of hydrogen-bonds in the environment of a given (Cys-S)-Fe cluster (Fd [P. aerogenes], 15 - 18; Rd [C. pasteurianum], 6; HIPIP [C. vinosum] 3 - 5) and its redox potential. The suggestion was made that a large number of NH....S hydrogen-bonds contributes to the stabilisation of a more negatively-charged cluster.

The direct validity of the three-state concept and the role of the polypeptide moiety in selecting the preferred redox couple has been confirmed experimentally. It has been demonstrated (23) that the cluster in HIPIP can be 'super-reduced', in the presence of the denaturant DMSO, to the lowest state accessible to ferredoxin. This process can be reversed by the addition of an oxidant, $Fe(CN)_6^{3-}$. However, 'super-oxidation' of ferredoxin by $Fe(CN)_6^{3-}$ leads to a facile cluster degradation into a [3Fe-xS] state (24,25). Clearly, the polypeptide in HIPIP is very important in stabilising the $[4Fe-4S]^{3+}$ state. The oxidation of $[Fe_4S_4(SPh)_4]^{2-}$ in a range of non-aqueous media also leads to cluster degradation, although, an inert hydrocarbon medium has recently been described (26) which allows a completely reversible, four-membered electron-transfer chain to be observed ($[Fe_4S_4(SPh)_4]^{n-}$, n = 1 to 4). Thus, the protein portion of tetrameric Fe-S clusters has an important function. It modulates the environment of the cluster to stabilise the preferred redox couple and, thereby, 'tunes' the redox potential.

In regard to the structure of the 8Fe ferredoxin (P. aerogenes), the polypeptide conformation displays a remarkable two-fold symmetry axis. The two clusters are about 12 Å apart and in very similar protein environments. This results from the similarity of the first and second halves of the amino acid

sequence. Interestingly, there are two groups of four cysteine residues in the amino acid sequence (8-11-14-18 and 35-38-41-45). However, these groups are not incorporated one in each cluster as might be expected. Instead, Cys-8,11,14 and 45 are ligands for one cluster and Cys-35,38,41 and 8 for the other. Similar structural features are expected in other bacterial (e.g. C. pasteurianum) 8Fe ferredoxins. The invariant amino acids [acidic amino acids] in the five known sequences of bacterial ferredoxins involve 26 [4] of the 54 [7] in P. aerogenes. It has been concluded on the basis of homogeneous kinetic and chronoamperometric studies (27) that the two clusters act independently and non-cooperatively when undergoing oxidation or reduction.

1.2.1c Proteins with two Fe per centre.

The structure of just one protein (S. platensis) with a 2Fe-2S cluster has been completed, Figure 1.6(c). The 2Fe-2S cluster (Figure 1.6(c)), in its environment of four cysteine ligands, exhibits tetrahedral coordination about each Fe atom, with the [2Fe-2S] core forming a planar four atom ring. The cluster is located near the molecular surface with both Fe atoms within 5 Å of the surface. The amino acid sequence of this protein indicates a large excess of acidic residues. Of the 98 residues [20 acidic residues] in the amino acid sequence of this ferredoxin 65 [14] are common to the sequence of spinach 2Fe-2S ferredoxin.

1.2.2 Flavoproteins.

The prosthetic groups of flavoproteins (Fl) are the tricyclic flavins: riboflavin, flavin mononucleotide (riboflavin

phosphate, FMN) and flavin adenine dinucleotide (FAD), Figure 1.7(b). These prosthetic groups can undergo two-electron ($Fl_{ox} \rightleftharpoons FlH_{2,red}$) or one-electron redox reactions ($Fl_{ox} \rightleftharpoons FlH^{\bullet}$ ($Fl^{\bullet -}$) or $FlH^{\bullet}$ ($Fl^{\bullet -}$) $\rightleftharpoons FlH_{2,red}$). In free flavin, the equilibrium for conproportionation ($Fl_{ox} + FlH_2 \rightleftharpoons FlH^{\bullet}$) lies far to the left (28). Thus, one-electron transfer processes involving flavoproteins require stabilisation of the intermediate semiquinone radical state. This occurs through apoprotein-dependent hydrogen-bond formation (29).

Through the capacity to undergo two distinct one-electron transfer steps, flavoproteins have evolved as transforming redox switches between obligate two-electron donors (e.g. NADH) and one-electron acceptors (e.g. iron-sulphur proteins and haemoproteins). This confers a unique role upon flavoproteins as indispensible mediators in all biological electron-transfer chains. In the respiratory chain, flavoproteins are the collecting point for reducing equivalents from all catabolic processes. A minimum of three cooperating redox-active sites are required for two-electron to one-electron conversion (14), so that many flavoproteins display flavin-flavin-haem or flavin-flavin-(Fe-S) combinations.

Flavodoxins (28) are flavoproteins of relatively low molecular weight (ca. 16000), containing one equivalent of FMN. Flavodoxins do not react directly with pyridine nucleotides and function solely as low-potential, one-electron mediators, shuttling between the semiquinone and hydroquinone states. In these reactions, flavodoxins are often interchangeable with ferredoxins. Indeed, in certain micro-organisms the synthesis of flavodoxin occurs only during growth in iron-poor media,

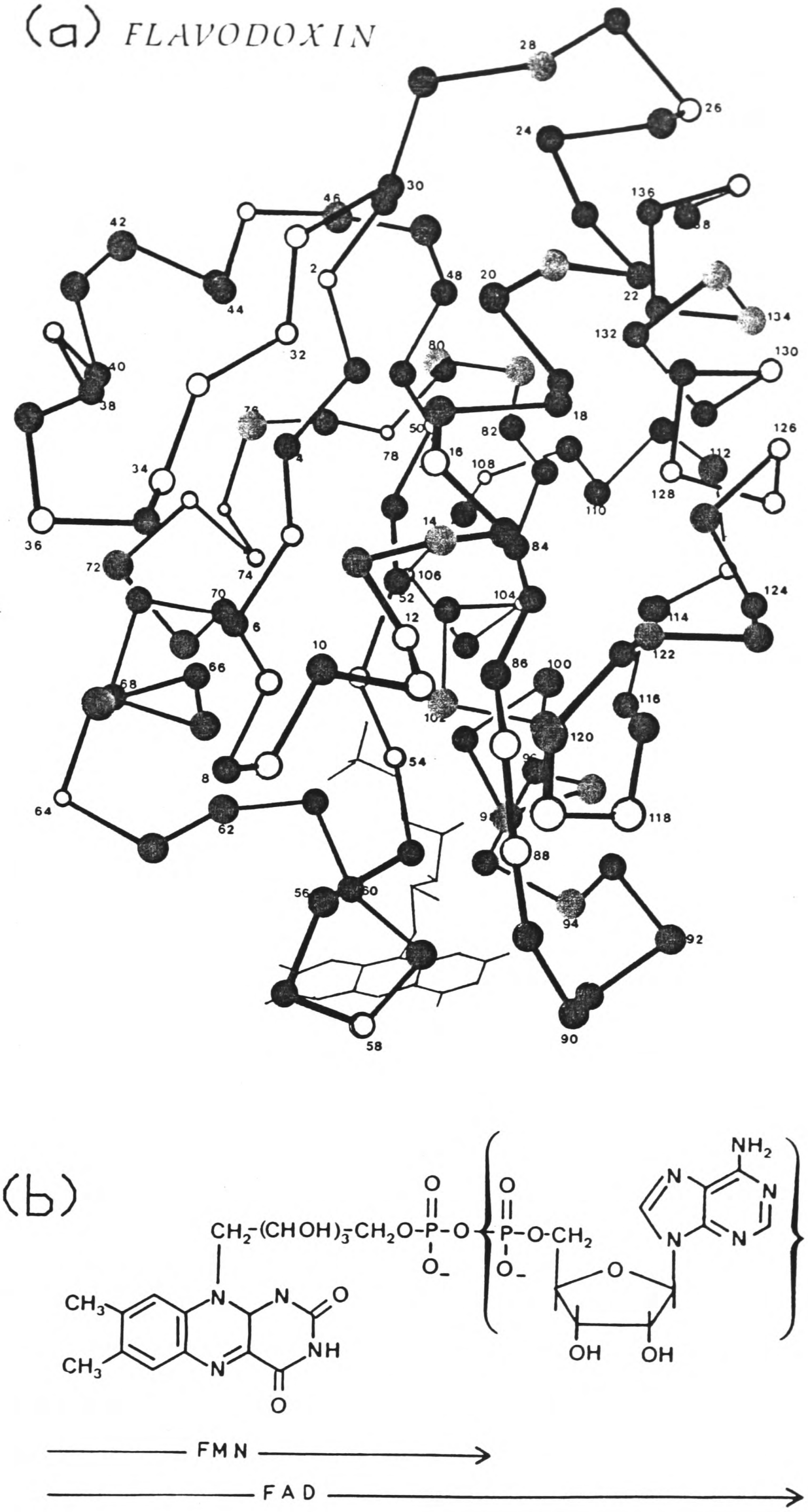

Figure 1.7: (a) Three-dimensional structure of Clostridium MP flavodoxin showing the α-carbon atoms and the position of the FMN site. Acidic [●], basic [●], hydrophobic (non-polar) [●], and polar, non-ionic [○] amino acid residues are marked. (b) Structure of the flavin nucleotides.

suggesting that iron deficiency stimulates the synthesis of flavodoxin as a replacement for ferredoxin.

The three-dimensional structure of the flavodoxin from Clostridium MP has been reported for the oxidised (30) (Figure 1.7(a)), semiquinone and hydroquinone states. The structure reveals flavodoxin to be highly structurally asymmetric. The isoalloxazine ring is located at the periphery of the molecule with the dimethylbenzene end accessible to solvent and the pyrimidine portion 'buried' in the protein. Two clusters of uncompensated negative charge occur on the surface of the molecule. One acidic region, around residues 62-72, is near the exposed dimethylbenzene ring of the flavin group.

Comparison of the sequences of C. pasteurianum, M. elsdenii, Clostridium MP, and D. vulgaris flavodoxins demonstrates that the first three proteins are closely related. In addition, in all four flavodoxins, acidic residues are predominant over basic residues. However, the sequences and crystal structures of the latter two proteins are notably different in the vicinity of the prosthetic group (for a review see ref. (28)). Nevertheless, the overall three-dimensional folding is conserved in these two proteins (132 α-C atoms occupy equivalent positions (30) in the two structures.

There are several differences between the oxidised and semiquinone structures of Clostridium MP flavodoxin (31) indicative of a conformational change close to the flavin group. A similar conclusion is suggested (32) by the slow rate of electron exchange between the oxidised and semiquinone states of M. elsdenii flavodoxin (2 s^{-1}). In contrast, the conformations of the fully-reduced and semiquinone states of flavodoxin are very

similar (28) and electron exchange is favoured (100 s^{-1}). Similarly, dithionite reduction of the oxidised flavodoxin is two orders of magnitude slower than for reduction of the semiquinone (33). These results indicate that the preferred one-electron transfer mode of flavodoxins arises from a kinetic barrier to electron-shuttling between the oxidised and semiquinone states.

1.2.3 Copper Proteins.

The coordination site of the copper ion in plastocyanin and azurin has been shown to involve a cysteine, a methionine and two histidine residues. The disposition of these ligands imposes an irregular distorted tetrahedral geometry upon the copper centre (34), resulting in unique spectroscopic and thermodynamic properties. The intense optical absorption near 600 nm (Cu(II) azurin, $\epsilon_{625} \sim 5700\ M^{-1}cm^{-1}$; Cu(II) plastocyanin, $\epsilon_{597} \sim 4900\ M^{-1}cm^{-1}$) contrasts markedly with that of d-d transitions in normal Cu(II) complexes ($Cu(NH_3)_4^{2+}$, $\epsilon_{600} < 100\ M^{-1}cm^{-1}$) and is attributed to ligand(S)-Cu charge transfer. The redox potentials of these proteins (ca. +0.3 to +0.4 V vs. NHE) are much higher than those of all Cu(II) complexes (ca. -0.5 to +0.2 V vs. NHE), except those with a strong distortion from tetragonal symmetry, indicative of a destabilisation of Cu(II) with respect to Cu(I). In the case of plastocyanin, this effectively 'tunes' the redox potential to the high value necessary for the role of this protein in photosynthesis (10).

The geometry of the protein-Cu(II) sites can be considered as a compromise between the coordination preferences of Cu(II) [typically tetragonal with N,O ligands] and Cu(I) [tetrahedral with S ligands]. There is little change in the geometry of the

Cu(II) site (plastocyanin, pH 8) upon reduction (35).

The crystal structures of P. aeruginosa azurin (36) and poplar plastocyanin (37) are shown in Figure 1.8(a,b). In both proteins, the Cu site is at, but not on, the surface of the protein, and is surrounded by a group of semi-invariant or conservatively-substituted hydrophobic residues. These form large hydrophobic surfaces close to the copper centre. In plastocyanin there is a striking imbalance in the distribution of charged residues. There are only three conserved (based on 67 complete or partial amino acid sequences of plant plastocyanins (35)) lysine (positively-charged) residues. None of the eight conserved acidic residues lies in the top one-third of the molecule. Six of them form an elongated acidic patch close to tyrosine-83. In azurin, the invariant acidic and basic residues occur in pairs, with few exceptions.

1.2.4 c-Type cytochromes.

The cytochromes possess one or more haem centres. The haem c prosthetic group of c-type cytochromes (Figure 1.9(b)) is covalently linked to the amino terminal half of the polypeptide chain through one or more thioether linkages. The fifth and sixth haem ligands are histidine and methionine.

The crystal structures of nine c-type cytochromes have been determined to atomic resolution (15). A ribbon diagram of the structure of tuna cytochrome c is shown in Figure 1.9(a). All c-type cytochromes have similar tertiary structures and side-chain packing arrangements around the haem. The haem group is deeply buried and similarly oriented in all structures with one edge exposed to solvent. There are slight differences in the

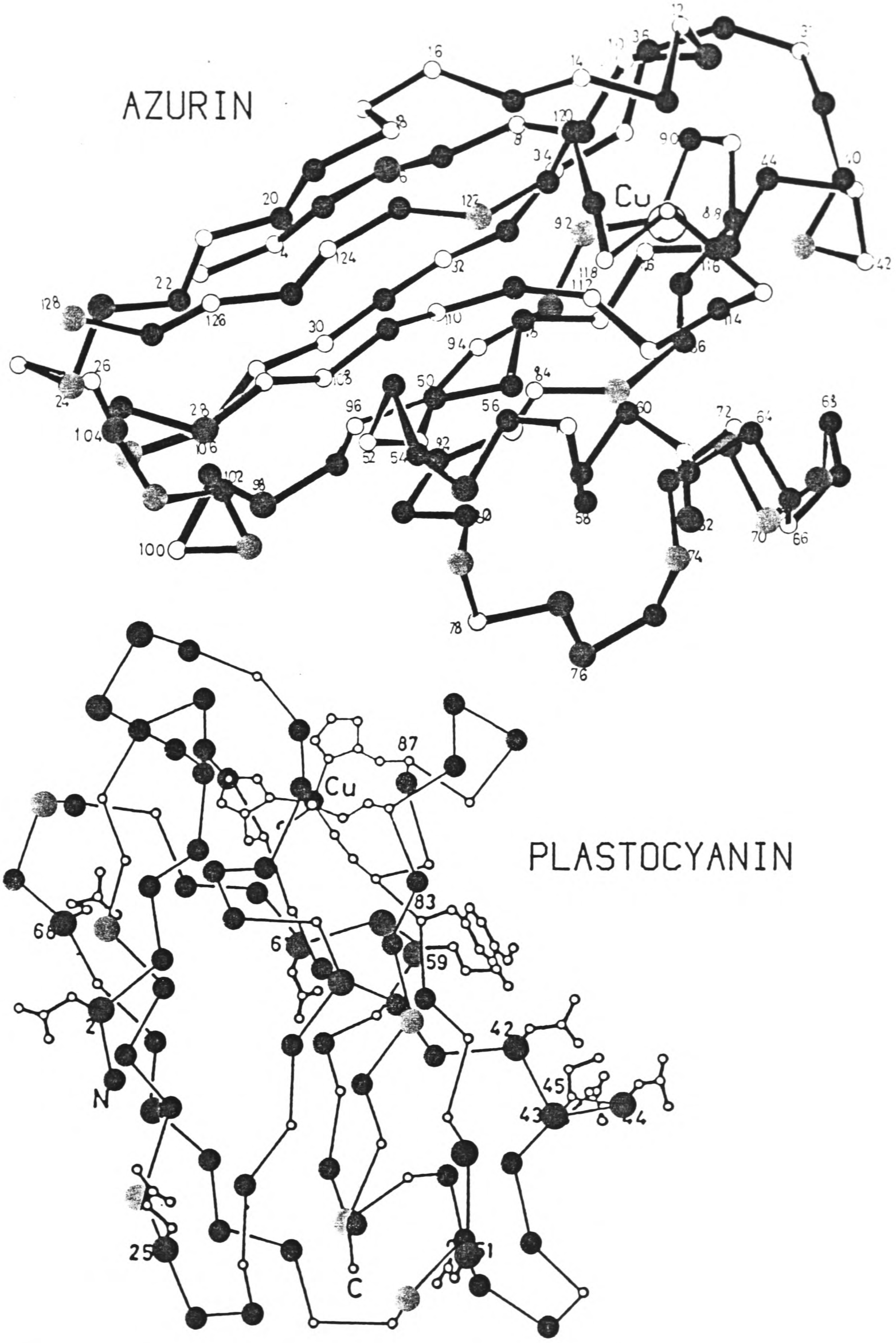

Figure 1.8: Three-dimensional structures of P. aeruginosa azurin and poplar plastocyanin showing the α-carbon atoms and the position of the Cu site. Acidic [●], basic [●], hydrophobic (non-polar) [●], and polar, non-ionic [○] amino acid residues are marked.

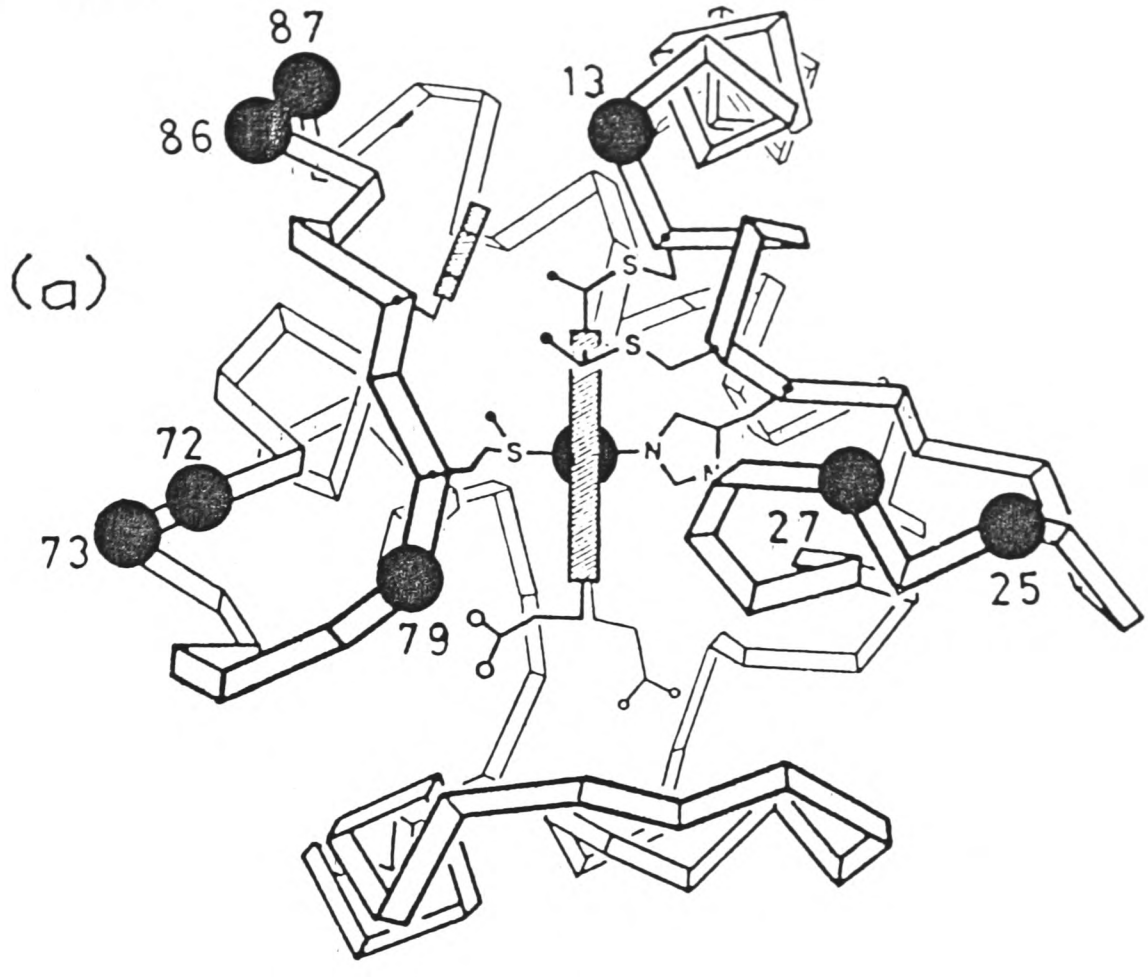

Figure 1.9: (a) Ribbon-diagram of the structure of tuna cytochrome c showing the position of the α-carbon atoms. The molecule is viewed from the side bearing the exposed haem edge and the haem-face lysine residues are marked (●).
(b) The haem c prosthetic group of cytochrome c.

polypeptide conformation in the haem pocket of oxidised and reduced tuna cytochrome c.

The eukaryotic cytochromes c are very basic with a pronounced asymmetry in the distribution of charged residues. Horse heart cytochrome c (pI = 10) has 19 lysine (positively-charged) residues and 12 negatively-charged residues. The excess lysine residues are clustered around the mouth of the haem crevice. In contrast, the centre of negative charge is at the 'back' of the molecule. This gives rise (38) to a dipole moment of 303 debye (oxidised horse cytochrome c) and 286 debye (reduced horse cytochrome c). The positive part of the dipole axis crosses the protein surface at a point close to the exposed haem edge (alanine-83 in tuna cytochrome c).

1.3 The Specificity of Biological Electron-Transfer.

It is evident that there are a number of important structural features common to all four types of redox protein. Thus, each protein possesses a metal ion or organic structure which acts as an electron sink and is usually close to the protein surface. Secondly, these prosthetic groups are chemically atypical and are constructed so that there is a minimum of local structural change concomittant with electron-transfer. Finally, the polypeptide micro-environment in the vicinity of the prosthetic group strongly influences the electron-transfer properties of a particular protein. These features ensure that a redox protein exhibits the appropriate redox potential and undergoes rapid intermolecular electron-transfer.

An additional constraint upon the properties of the individual components of an organised electron-transfer chain is

that they should direct the flow of electrons to a specific acceptor protein. To a certain degree, the close association of complex electron-transferring systems with a rigid membrane matrix, as e.g. in the mitochondrion or chloroplast, allows the requisite spatial organisation of a system for intermolecular electron transfer, such that the constituent proteins are constrained to act in parallel, through tight and specific binding to the membrane. The disposition of proteins across a membrane also allows efficient coupling to vectorial processes such as proton translocation. It is also evident (10) that the difference in redox potential, between components of a membrane-bound electron transport chain, is small (80 mV or less). This may be a direct consequence of a membrane system, in that the rate of electron-transfer between two components does not require a large difference in redox potentials to ensure diffusion-controlled rates of electron-transfer. Alternatively, this may reflect that reduction or re-organisation of substrate is the rate-determining step.

The coupling of electron-transfer in prokaryotic organisms requires special consideration of the role of specific protein-protein interactions. Individual redox proteins are free-floating in the cytoplasm and may, like the Fe-S protein rubredoxin, be of high intrinsic reactivity. It would be surprising if these prokaryotic redox proteins could transfer electrons freely through random collision processes. In these systems the flow of electrons needs to be modulated by specific donor-acceptor recognition. A similar consideration may apply to the small, water-soluble redox proteins, such as plastocyanin or cytochrome c, which are electron-carriers in the photosynthetic and

mitochondrial electron transport chains, respectively. However, the motion of these latter proteins may be restricted to two-dimensional diffusion at the membrane surface (39). From a mechanistic viewpoint, intermolecular electron-transfer rates are expected to be influenced by the asymmetric distribution of polar and non-polar residues across the surface of proteins.

The matching of protein tertiary structure has been postulated as a means of regulating donor-acceptor electron-transfer activity in electronic pathways. In a study (40) of the reaction between azurin and cytochrome $\underline{c}_{551}$ (from *P. aeruginosa*) the apparent second order reaction rate is 3×10^6 $M^{-1}s^{-1}$; however, when mammalian cytochrome *c* is used in place of cytochrome $\underline{c}_{551}$, the apparent second order reaction rate drops to about 10^3 $M^{-1}s^{-1}$. It was proposed (40) that the rationale for this dramatic difference in the rates of electron-transfer is that azurin and cytochrome $\underline{c}_{551}$ are a biological donor-acceptor pair with complementary tertiary structures. Mammalian cytochrome *c* is not a redox partner of azurin and so lacks this specificity.

A specific binding interaction between donor and acceptor molecules has also been postulated to define the functional role of cytochrome *c*. The case of the interaction between cytochrome *c* and its peroxidase is particularly interesting (41). These proteins undergo efficient electron transfer ($k \sim 10^8$ $M^{-1}s^{-1}$) close to the diffusion-controlled limit. A model based on the individual crystal structures of the two proteins suggests that a triangle of lysine residues on cytochrome *c* fits together with a triangle of aspartate residues on cytochrome *c* peroxidase. Furthermore, four additional coulombic and hydrogen-bonded side chain interactions are involved in complex formation. The

combined structure contains no empty spaces or gaps between its component proteins. Moreover, the planes of the haem groups are in almost perfect alignment and linked by a number of parallel aromatic and conjugated residues across the molecular interface. The foregoing discussion suggests that a 'docking' of complementary protein surfaces provides an electron-transfer pathway between the haem groups of cytochrome c and cytochrome c peroxidase. Chemical modification studies (42) provide direct experimental support for similar binding interactions between cytochrome c and its oxidase or reductase in the mitochondrial respiratory chain.

The 2Fe-2S ferredoxin is involved in a variety of metabolic processes in the chloroplast (43). Numerous ferredoxin:enzyme electrostatic complexes have been implicated in the regulation of these processes. An interesting role of binding interactions is suggested by studies of the Fd:Fd-$NADP^+$ oxidoreductase complex of the photosynthetic electron transport chain. Potentiometric titrations (44) performed on this system show that complex formation lowers the ferredoxin reduction potential by 22 mV while raising that of the enzyme by 23 mV, a feature that results in a significant increase in the thermodynamic driving force for electron-transfer.

The observations described above serve to emphasize that an organised pathway for electron transport may be a direct consequence of complementary donor-acceptor interactions.

1.4 Direct Electrochemical Studies of Redox Proteins.

The search for reversible, direct (unmediated) electron transfer between electrodes and redox proteins has received

considerable attention in the last decade or so. The main interest in these studies has been the development of enzyme-based electrochemical devices for specific substrate transformations, and the possibility of gaining insights in to the mechanisms of *in vivo* electron-transfer systems. In contrast, however, to the rapid heterogeneous electron transfer observed for small organic and inorganic redox systems at a wide range of electrode surfaces, redox proteins rarely undergo reversible electron transfer at conventional electrode surfaces. For cytochrome *c*, electron transfer is essentially undetectable at gold (45) and platinum (46) electrodes, while the electrochemistry of ferredoxins is complicated by irreversible adsorption and degradation at mercury electrodes (47). Recent developments in surface modification have led to several reports of direct electron transfer between various small redox proteins and Au (48,49), Pt (50), Hg (51) and carbon (52,53) electrodes. Surface-modifiers have included compounds such as 4,4´-bipyridyl and related reagents (54), poly-lysine (51) or methyl viologen (49). However, the latter might be expected to perform in a mediatory fashion to the low potential redox proteins with which it has been used.

The quasi-reversible, direct electrochemistry of cytochrome *c* at a gold electrode surface-modified by an adsorbed layer of 4,4´-bipyridyl involves binding of the protein at the electrode surface (55). Free energy profiles derived from rotating ring-disc experiments showed that the binding energy is important in reducing the activation barrier for electron transfer. However, it has been noted (55) that for quasi-reversible electrochemistry the binding should be weak such that

on-off rates are sufficiently fast. It appears that for cytochrome c on Hg electrodes (56) the adsorption is too strong leading to less reversible direct electrochemical responses. On the basis of these results it is apparent that any observation of well-behaved diffusion-dominated electrochemistry of redox proteins, without the use of mediators, signals the successful execution, within the experimental time domain, of a sequence of events. Broadly, these may be represented as:

a) Diffusion of reactant protein to the electrode surface.

b) Association of reactant.

c) Electron transfer.

d) Dissociation of product.

e) Diffusion of product protein away from the electrode surface.

The importance of binding in the direct electrochemistry of redox proteins resembles physiological electron-transfer processes where binding interactions and variations in surface structure are necessary to achieve kinetic control and specificity.

The successful observation of reversible direct electrochemistry of cytochrome c, at surface-modified Au electrodes, had immediate application in the construction of an electrocatalytic system, using an artificial electron transport chain to stimulate the reduction of dioxygen to water by a terminal oxidase (57). More recently, the direct electrochemistry of cytochrome c has been applied to the study of intact systems, using rat liver mitochondria and Pseudomonas denitrificans protoplasts (58), and photosystem I particles (59). Similarly,

the direct electrochemistry of the 2[4Fe-4S] ferredoxin at pyrolytic graphite has been applied (60) to the study of facile cluster oxidation processes, most likely proceeding through the 'super-oxidised' $[4Fe\text{-}xS]^{3+}$ oxidation level.

1.5 The Aims of this Thesis.

The aim of this thesis is to achieve and capitalise upon the direct (unmediated) electrochemistry of a range of redox proteins, with a view to defining more closely the general requirements for the design of functional, bio-active electrode surfaces. In order to develop an informative picture, studies have been restricted to small, soluble redox proteins which have well-defined crystal structures.

In Chapter 4, quasi-reversible direct electrochemical responses of Fe-S, haem, flavin and copper-containing redox proteins are observed at pyrolytic graphite electrodes. A marked dependence of the heterogeneous electron-transfer rate on the lattice orientation of pyrolytic graphite is observed, and a general role for mobile, multivalent cations as regulators of the direct electrochemistry of highly-charged redox proteins is established. This observation makes striking analogies with the role of cations in physiologically-relevant interactions. Chapter 5 uses ESCA to define the chemical composition of edge and basal-plane pyrolytic graphite electrodes. This is followed by a return to *in situ* studies of the nature of biologically-active electrode surfaces (Chapter 6). Chapters 7, 8 and 9 explore, in more detail, aspects of the direct electrochemistry of Fe-S proteins, the copper protein plastocyanin, and c-type cytochromes, respectively, with a view to defining more closely the role of

the multivalent cations in direct electrochemical studies. Chapter 10 summarises the results of these three chapters. In Chapters 8, 11 and 12 applications of direct electrochemical studies of redox proteins are described. Chapter 8 probes a problem of biological relevance - the redox inactivity of Cu(I) plastocyanin. Chapter 11 describes the construction of a chemically-modified bio-active electrode surface and Chapter 12 the development of a biosynthetic device.

References - Chapter 1

1) Hagen, K. S., Reynolds, J. G. and Holm, R. H., J. Am. Chem. Soc. 103, 4054 (1981).

2) Yoch, D. C. and Valentine, R.C., Ann. Rev. Microbiol. 26, 139, (1972).

3) Mortenson, L. E. and Thorneley, R. N. F., Ann. Rev. Biochem. 48, 387, (1979).

4) Lehninger, A. L. Biochemistry. New York: Worth (1970).

5) Mitchell, P., Biol. Rev. 41, 445, (1966).

6) Carrillo, N. and Vallejos, R. H., TIBS 2, 52, (1983).

7) Portis, A. R. and McCarty, R. E., J. Biol. Chem. 251, 1610, (1976).

8) Saraste, M. and Kuronen, T., Biochim. Biophys. Acta 513, 117, (1978).

9) Hinkle, P. C. and McCarty, R. E., Sci. Am. 104, 238, (1978).

10) Dryhurst, G., Kadish, K. M., Scheller, F., and Renneberg, R. Biological Electrochemistry. New York: Academic Press, 1, (1982).

11) Crutcher, S. E. and Geary, P. J., Biochem. J. 177, 393, (1979).

12) May, S. W., Lee, L. G., Katopodis, A. G., Kuo, J-Y., Wimalasena, K. and Thowsen, J. R., Biochemistry 23, 2187, (1984).

13) Palmer, G. in: The Enzymes. Boyer, P. D. ed. New York: Academic Press, 12, 1, (1975).

14) Hemmerich, P., Nagel Schneider, G. and Veeger, C., FEBS Lett. 8, 69, (1970).

15) Mathews, F. S., Prog. Biophys. Molec. Biol. 45, 1, (1985).

16) Metal Ions in Biology. Volume 3: Copper Proteins. Spiro, T.G. ed. New York: Wiley (1981).

17) Watenpaugh, K. D., Sieker, L. C. and Jensen, L. H., J. Mol. Biol. 131, 509, (1979).

18) Tsukihara, T., Fukuyama, K., Nakamura, M., Katsube, Y., Tanaka, N., Kakudo, M., Wada, K., Hase, T. and Matsubara, H., J. Biochem. 90, 1763, (1981).

19) Adman, E. T., Sieker, L. C. and Jensen, L.H., J. Biol. Chem. 248, 3987, (1973).

20) Carter, C. W., Kraut, J., Freer, S. T., Alden, R. A., Sieker, L. C., Adman, E. T. and Jensen, L. H., Proc. Nat. Acad. Sci. U.S.A. 69, 3526, (1972).

21) Laskowski, E. J., Reynolds, J. G., Frankel, R. B., Foner, S., Papaefthymiou G. C., and Holm, R.H., J. Am. Chem. Soc. 101, 6562, (1979).

22) Adman, E. T., Watenpaugh, K. D. and Jensen, L. H., Proc. Nat. Acad. Sci. U.S.A. 72, 4854, (1975).

23) Cammack, R., Biochem. Biophys. Res. Commun. 54, 548, (1973).

24) Johnson, M. K., Spiro, T. G., and Mortensen, L. E., J. Biol. Chem. 257, 2447, (1982).

25) Thomson, A. J., Robinson, A-E., Johnson, M. K., Cammack, R. Rao, K. K. and Hall, D. O., Biochim, Biophys, Acta. 637, 423, (1981).

26) Pickett, C. J., J. Chem. Soc. Chem. Commun. 323, (1985).

27) see, for example: Feinberg, B. A., Tuschel, D. D. and Ryan, M. D., Bioelectrochem. Bioenerg. 12, 575, (1984).

28) Mayhew, S. G. and Ludwig, M. L. in: The Enzymes. Boyer, P. D. ed. New York: Academic Press, 12, 57, (1975).

29) Dreyer, J. L., Experientia 40, 653, (1984).

30) Burnett, R. M., Darling, G. D., Kendall, D. S., LeQuesne, M.E., Mayhew, S. G., Smith, W. W. and Ludwig, M. L., J. Biol. Chem. 249, 4383, (1974).

31) Smith, W. W., Burnett, R. M., Darling, G. D. and Ludwig, M.L., J. Mol. Biol. 117, 195, (1977).

32) Moonen, C. T. W. and Muller, F., Biochemistry. 21, 408, (1982).

33) Mayhew, S. G. and Massey, V., Biochim. Biophys. Acta. 315, 181, (1973).

34) Garrett, T. P. J., Clingeleffer, D. J., Guss, J. M., Rogers, S. J. and Freeman, H. C., J. Biol. Chem. 259, 2822, (1984).

35) Freeman, H. C., in: Coordination Chemistry-21. Laurent, J. P. ed. Oxford: Pergamon (1981).

36) Adman, E. T. and Jensen, L. H., Isr. J. Chem. 21, 8, (1981).

37) Colman, P. M., Freeman, H. C., Guss, J. M., Murata, M., Norris, V. A., Ramshaw, J. A. M., and Venkatappa, M. P., Nature 272, 319, (1978).

38) Koppenol, W. H., Vroonland, C. A. J. and Braams, R., Biochim. Biophys. Acta. 503, 499, (1978).

39) Crofts, A. R. and Wraight, C. A., Biochim. Biophys. Acta. 726, 149, (1983).

40) Antonini, E., Finnazi-Argo, A., Avigliano, L., Guerrieri, P., Rotilio, G. and Mondovi, B., J. Biol. Chem. 245, 4847, (1970).

41) Kraut, J., Biochem. Soc. Trans. 9, 197, (1981).

42) Koppenol, W. H. and Margoliash E., J. Biol. Chem. 257, 4426, (1982), and references therein.

43) Orme-Johnson, W. H., Ann. Rev. Biochem. 42, 159, (1973).

44) Smith, J. M., Smith, W. H. and Knaff, D. B., Biochim. Biophys. Acta. 635, 405, 1981.

45) Heineman, W. R., Norris, B. J. and Goelz, J. F., Anal. Chem. 47, 79, (1975).

46) Kono, T. and Nakamura, S., Bull. Agric. Chem. Soc. Japan 22, 399, (1958).

47) Ikeda, T., Toriyama, K. and Senda, M., Bull. Chem. Soc. Jpn. 52, 1937, (1979).

48) Eddowes, M. J. and Hill, H. A. O., J. Am. Chem. Soc. 101, 4461, (1979).

49) Landrum, H. L., Salmon, R. T. and Hawkridge, F. M., J. Am. Chem. Soc. 99, 3154, (1977).

50) Taniguchi, I., Murakami, T., Toyosawa, K., Yamaguchi, H. and Yasukouchi, K., J. Electroanal. Chem. 131, 397, (1982).

51) van Dijk, C., van Leeuwen J. W., Veeger C., Schreurs, J. P. G. M. and Barendrecht, E., Bioelectrochem. Bioenerg. 9, 743, (1982).

52) van Dijk, C., van Eijs, T., van Leeuwen, J. W. and Veeger, C., FEBS Lett., 166, 76, (1984).

53) Dhesi, R., Cotton, T. M. and Timkovich, R., J. Electroanal. Chem. 154, 129, (1983).

54) Allen, P. M., Hill, H. A. O. and Walton, N. J., J. Electroanal. Chem. 178, 69, (1984).

55) Albery, W. J., Eddowes, M. J., Hill, H. A. O. and Hillman, A.R., J. Am. Chem. Soc. 103, 3904, (1981).

56) Betso, S. R., Klapper, M. H. and Anderson, L. B., J. Am. Chem. Soc. 94, 8197, (1972).

57) Hill, H. A. O. and Walton, N. J., J. Am. Chem. Soc. 104, 6515, (1982).

58) Coleman, J. O. D., Hill, H. A. O., Walton, N. J. and Whatley, F. R., FEBS Lett. 154, 319, (1983).

59) Hill, H. A. O., Walton, N. J. and Whitford, D., J. Electroanal. Chem. 187, 109, (1985).

60) Armstrong, F. A., Hill, H. A. O. and Walton, N. J., FEBS Lett. 150, 214, (1982).

CHAPTER 2

ELECTROCHEMICAL THEORY AND METHODS

2.1 Introduction

This chapter is concerned with the theory of controlled potential techniques in which the response of a system to a potential perturbation is followed by current measurements. The principles of potential sweep and potential pulse techniques will be described, with particular reference to aspects of cyclic voltammetry and square wave voltammetry.

2.2 Basic Principles of Charge Transfer Reactions

The mathematical formulation of charge transfer processes at planar, stationary electrodes, follows directly from the potential dependence of heterogeneous electron transfer rates and the laws of diffusion. Thus, for the simplest electrochemical reaction (equation 2.1) in which there is only heterogeneous electron transfer:

$$A + ne^- \underset{k_b}{\overset{k_f}{\rightleftharpoons}} B \qquad (2.1)$$

the reaction steps to be considered are the transport of electroactive species between bulk solution and the interface, and electron transfer at the electrode surface.

The rate of heterogeneous electron transfer is determined by the sum of forward and back reactions, equation (2.2).

$$\text{Rate} = \frac{i}{nFA} = k_f C_A(o,t) - k_b C_B(o,t) \qquad (2.2)$$

$C_x(o,t)$ is the surface concentration of species x.

k_y are potential-dependent rate constants.

i is the faradaic current at an electrode area A.

The potential dependence of the rate constants for electron transfer, e.g. k_f in equation (2.2), is given by a rate expression of the form:

$$k_f = k_s \exp\left[\frac{-\alpha nF(E-E^o)}{RT}\right] \qquad (2.3)$$

where E is the electrode potential, α is the transfer coefficient describing the symmetry of the overlapping potential energy curves (reactant and product), n is the number of the electrons transferred in the rate-limiting step, and E^o is the formal potential, which fixes the value of the pre-exponential factor (i.e $k_f = k_s$, the standard heterogeneous rate constant, when $E = E^o$). Combining equations (2.2) and (2.3) yields the relation between current and applied potential:

$$i = nFAk_s\left\{C_A(o,t)\exp\left[\frac{-\alpha nF(E-E^o)}{RT}\right] - C_B(o,t)\exp\left[\frac{(1-\alpha)nF(E-E^o)}{RT}\right]\right\} \qquad (2.4)$$

The potential-dependent conversion of A into B reduces the concentration of A immediately adjacent to the electrode surface. The difference between the surface concentration $C_A(o,t)$ and the

bulk concentration of A (C_A^{BULK}) establishes a concentration gradient, as a result of which there is diffusional mass transport towards the electrode, according to equation (2.5). The reduced species, B, is generated at the electrode giving rise to a mass flux away from the electrode:

$$-D_B \frac{\delta C_B(o,t)}{\delta x} = D_A \frac{\delta C_A(o,t)}{\delta x} = J_A(o,t) = \frac{i}{nFA} \qquad (2.5)$$

D_x is the diffusion coefficient of species x

J_A is the flux of species A

Thus, the measurable current has two components; the rate of heterogeneous flux (equation 2.4), determined by the surface concentrations, $C_x(o,t)$, the applied potential E and the constants k_s, α and E^o; and the diffusional flux controlled by the slope of the interfacial concentration profiles (equation (2.5)). If the electrode processes are sufficiently rapid, then $C_A(o,t) \longrightarrow 0$ and the current is influenced solely by mass transport (diffusional control). Under these conditions the diffusion layer expands in a non-linear manner, and the slope of the concentration profile decreases according to Fick's second law (equation (2.6)), giving a decrease in current.

$$\frac{\delta C_A}{\delta t} = D_A \frac{\delta^2 C_A}{\delta x^2} \qquad (2.6)$$

The magnitude of the faradaic current, at a given time, arising from the application of a potential transient, is

determined by the potential dependence of reaction rate (equation (2.4)) and the solution of the partial differential equations describing the fluxes of reactants and products (equations (2.5) and (2.6)). The general approach to the solution of these boundary problems is through the application of Laplace transform techniques (1). If the potential applied to a planar electrode (at t = 0) is sufficient to maintain the electrode surface concentration of A at zero, the solution of the linear diffusion equations under semi-infinite boundary conditions ($C_A(x,t) = C_0^{BULK}$ as $x \longrightarrow \infty$) gives a basic electrochemical relation, the Cottrell equation:

$$i(t) = \frac{nFAD_A^{1/2}C_A^{BULK}}{\pi^{1/2}t^{1/2}} \qquad (2.7)$$

This states that the decrease in the concentration gradient due to the depletion of an electroactive species near the surface of an electrode, is characterised by an inverse $t^{1/2}$ function.

2.3 Cyclic Voltammetry

In D.C. cyclic voltammetry (2) the potential applied to a stationary working electrode is a triangular wave form. The electrode potential E is a function of time (t) and scan rate (υ):

$$E = E_i - \upsilon t \qquad 0<t<\lambda$$

$$E = E_i - 2\upsilon\lambda + \upsilon t \qquad \lambda<t$$

where E_i is the starting potential and

$t = \lambda$ at the reversal potential E_λ.

The integral equations derived from the relevant boundary problems for cyclic voltammetry, have been solved numerically by Nicholson and Shain (3) (for a system in which $C_A(o,t) = C_A^{BULK}$ and $C_B(o,t) = C_B^{BULK} = 0$, at $t = 0$) to establish diagnostic criteria for charge transfer processes termed reversible, irreversible and quasi-reversible (4).

Reversible Case

In an electrochemically reversible process, the faradaic current is influenced solely by the rate of diffusional mass transport. Under these conditions a thermodynamic equilibrium is established at the phase boundary and surface concentrations are given by the Nernst equation (a limiting form of equation (2.4)). The solution of the boundary problem generates a current-potential relation:

$$i = nFAC_A^{BULK}(\pi D_A a)^{1/2}\chi(at) \qquad (2.8)$$

$$\text{where } at = \frac{nF\upsilon t}{RT} = \frac{nF}{RT}(E(t) - E_i)$$

The cathodic current function, $\pi^{1/2}\chi(at)$, reaches a maximum value of 0.4463 at $n(E - E_{1/2}) = -28.5$ mV at 298K. Thus, the cathodic peak current (i_{pc}) is given by:

$$i_{pc} = 2.69 \times 10^5 D_A^{1/2} C_A^{BULK} A \upsilon^{1/2} \qquad (2.9)$$

The form of the cyclic voltammetric response (Figure 2.1(a)) is determined by the coupling of the heterogeneous electron transfer and diffusional rate processes. The current decay in the

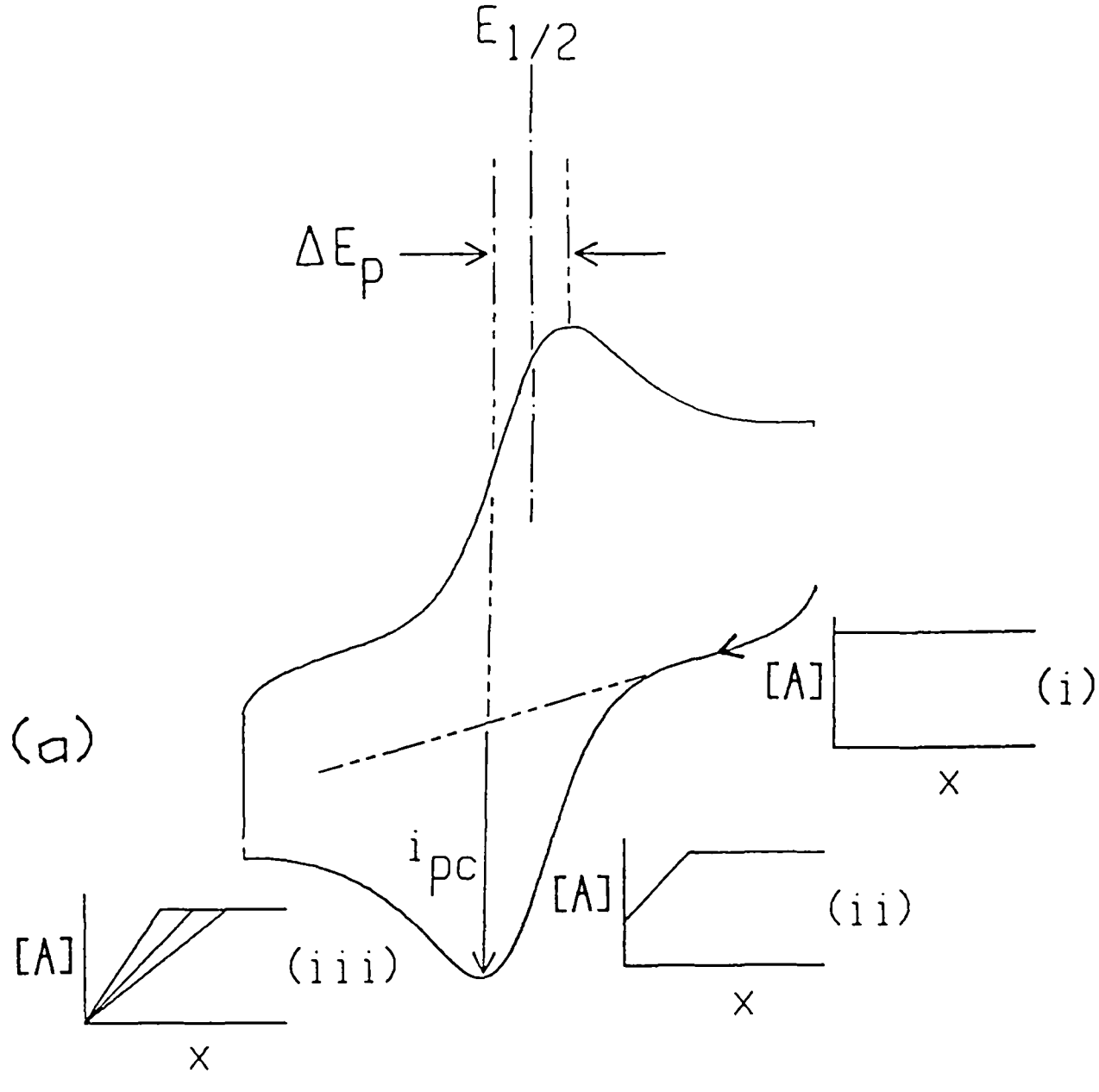

Figure 2.1: (a) Cyclic voltammogram for the reversible case. Concentration([A]) - distance(x) profiles during the potential scan are shown below the voltammogram. (b) Variation of the reversible cyclic voltammetric response with scan rate. The increase of peak current with increasing scan rate (5, 10, 20, 50 and 100 mVs^{-1}) is shown.

portion of the wave beyond the peak exhibits a simple Cottrell ($i \propto t^{-1/2}$) relationship (5), independent of potential, as expected when the concentration of the reacting species at the electrode surface approaches zero (Figure 2.1(a), concentration-distance profile iii). The decrease in current is due to a decreasing flux of the electroactive species towards the electrode. The rising portion of the voltammogram is determined by a potential-dependent decrease in the surface concentration of the oxidised species according to the Nernst equation (profiles i,ii).

In a single-scan voltammetric experiment the cathodic peak current can be measured by extrapolating the baseline current preceding the peak (Figure 2.1(a)). However, the height of the anodic peak is a function of reversal potential (3). Various empirical methods of evaluating the anodic peak current have been proposed and are discussed in detail by Adams (6). According to equation (2.9), the cathodic peak current for a diffusion-limited charge transfer process is proportional to (scan rate)$^{1/2}$. This is illustrated by the set of cyclic voltammograms in Figure 2.1(b) . The reason for the increase in peak current with increasing scan rate, is that less time is available, at high scan rates, for depletion of the solution adjacent to the electrode, resulting in steeper concentration profiles and, consequently, an increase in diffusional flux to the electrode.

The experimental criteria required to establish reversible one-electron transfer are a peak separation (ΔE_p) of 57 mV, independent of scan rate; a ratio of cathodic to anodic peak currents, i_{pc}/i_{pa}, of unity (for $\alpha = 0.5$); and $i_{pc}/v^{1/2}$ = constant (Figure 2.2, case a).

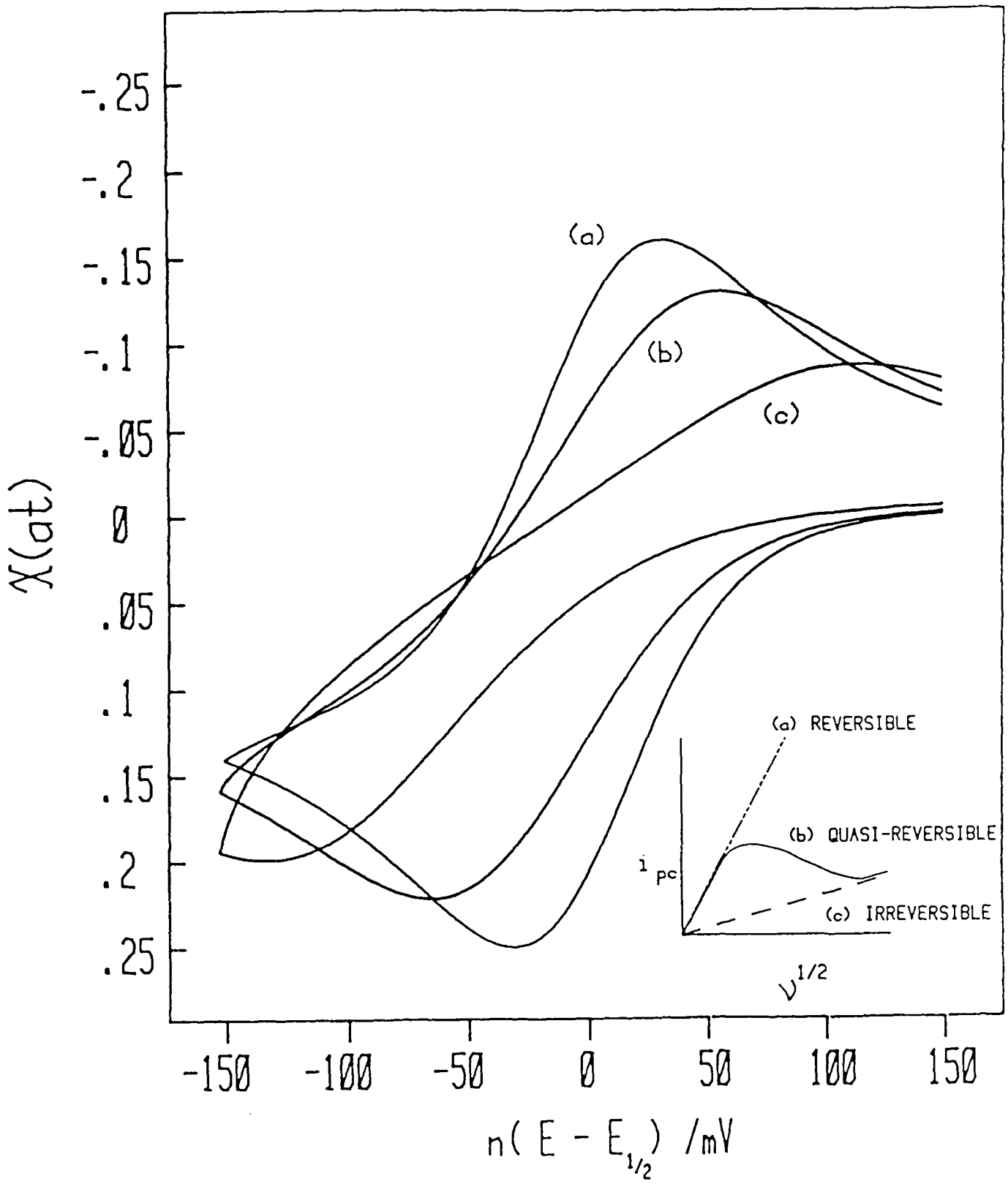

Figure 2.2: Dimensionless cyclic voltammograms calculated for the case of (a) reversible, (b) quasi-reversible, and (c) irreversible electron transfer. The variation of peak current (i_{pc}) with scan rate is also shown for each case.

Irreversible case

Under conditions where the rate of diffusional mass transport is much faster than the rate of electron transfer, the electrochemical process is designated as electrochemically-irreversible. The current-potential functions, computed according to the method of Allen et. al. (7), for reversible (k_s = 1.1×10^{-3} $m.s^{-1}$) and irreversible ($k_s = 1.1 \times 10^{-6}$ $m.s^{-1}$) processes are shown in Figure 2.2(a,c). In the irreversible case, the current in the initial portion of the voltammetric response may be analysed solely on the basis of the heterogeneous rate process without reference to diffusion (4). The boundary condition for a totally-irreversible cathodic process can be written as:

$$D_A \frac{\delta C_A(o,t)}{\delta x} = k_f(E).C_A(o,t) \qquad (2.10)$$

$$\text{where } k_f(E) = k_s \exp\left[-\frac{\alpha n_a F(E_i - \upsilon t - E^o)}{RT}\right]$$

The solution to equation (2.10) gives that:

$$i_{pc} = (2.99 \times 10^5).n.(\alpha n_a)^{1/2} A D_A^{1/2} C_A^{BULK} \upsilon^{1/2} \qquad (2.11)$$

where n_a is the number of electrons transferred in the rate-determining step of the electrode process. The cathodic peak current of an irreversible process is also proportional to (scan rate)$^{1/2}$. However, the magnitudes of the current function (χ_{MAX}(at)) and peak separation (ΔE_p) for an irreversible process

0.2, 244 mV; Figure 2.2(c)) are markedly different from those of a reversible process (0.25, 59 mV; Figure 2.2(a)).

Quasi-reversible case

In the quasi-reversible case (e.g Figure 2.2(b); ΔE_p= 93 mV, $\chi_{MAX}(at)$ = 0.233, k_s = 1.1 x 10^{-5} $m.s^{-1}$) both the charge transfer and the diffusion rate processes determine the faradaic current. The rising portion of the voltammetric response is a complex function of potential (8).

The transition from essentially reversible to irreversible electrochemistry can be achieved by increasing the rate of diffusional processes in the interfacial region, through an increase in scan rate (see inset, Figure 2.2). A quasi-reversible couple approaches the reversible limit ($i_{pc} \propto v^{1/2}$ and ΔE_p = 57 mV) at low scan rates.

Solution of the boundary problem for the quasi-reversible case (i.e those reactions described by equation (2.4)) led (9) to a simple procedure for determining the standard heterogeneous rate constant (k_s). The peak separation ΔE_p, can be correlated with the value of k_s for a particular electrode reaction using a kinetic parameter Ψ (equation (2.12)) and a working curve, Figure 2.3, (constructed from data in ref. (2) or (9) for α = 0.5) relating ΔE_p to Ψ.

$$\Psi = \frac{D_A^{\alpha/2} . D_B^{-\alpha/2} . k_s}{\left(D_A \pi n F v / RT\right)^{1/2}} \simeq \frac{k_s}{\left(D_A \pi n F v / RT\right)^{1/2}} \qquad (2.12)$$

$$\Delta E_p = f(\Psi)$$

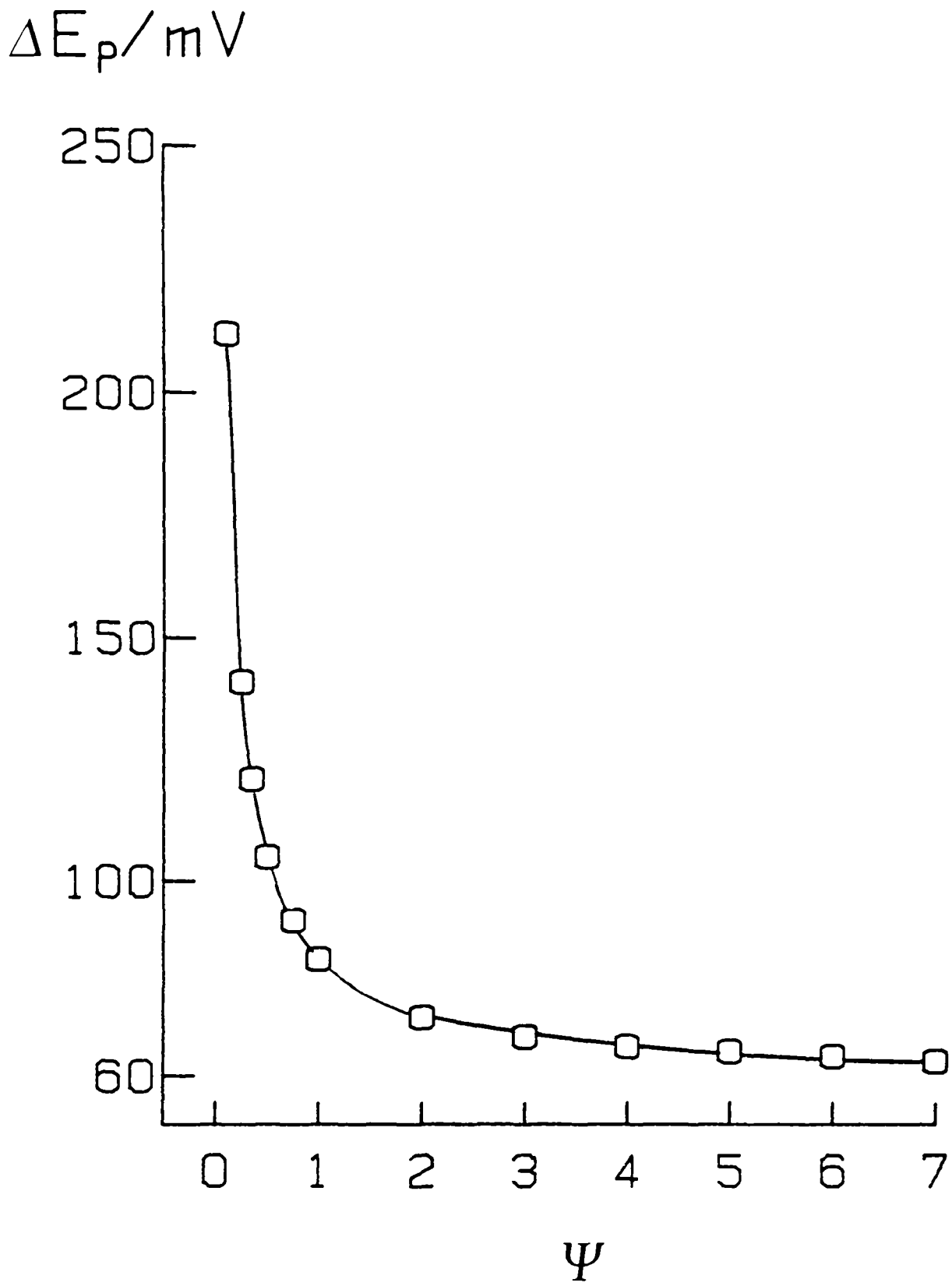

Figure 2.3: Working curve relating peak separation to the kinetic parameter Ψ.

It should be noted that equation (2.12) only applies to single scan cyclic voltammetric studies and for $\alpha = 0.5$. However, values of ΔE_p are nearly independent of α in the range $0.3 < \alpha < 0.7$ providing that $\Psi > 0.5$ ($\Delta E_p < 105/n$ mV) (9).

2.3.1 Cyclic Voltammetry with Coupled Chemical Reactions

The theory of cyclic voltammetry has also been extended to describe chemical reactions which either precede or follow charge transfer. The following scheme illustrates a series of kinetic systems, incorporating reversible heterogeneous electron transfer, for which theoretical treatments have been provided by Shain et. al. (3, 10). These include the adsorption of electroactive species (equ. (2.13)), charge transfer followed by reversible (equ. (2.15)) and irreversible (equ. (2.16)) reactions, a coupled catalytic reaction (equ. (2.17)), and a preceeding reversible chemical reaction (equ. (2.14)):

$$A + ne^- \rightleftharpoons B \quad ; \quad X_{SOLUTION} \rightleftharpoons X_{ADSORBED} \qquad (2.13)$$

where X can be either A or B or both.

$$Z \underset{k_b}{\overset{k_f}{\rightleftharpoons}} A \quad ; \qquad A + ne^- \rightleftharpoons B \qquad (2.14)$$

$$A + ne^- \rightleftharpoons B \quad ; \qquad B \underset{k_b}{\overset{k_f}{\rightleftharpoons}} Z \qquad (2.15)$$

$$A + ne^- \rightleftharpoons B \quad ; \qquad B \xrightarrow[k_f]{} Z \qquad (2.16)$$

$$A + ne^- \rightleftharpoons B \quad ; \qquad A + Z \xrightarrow[k_f]{} B \qquad (2.17)$$

Qualitatively, the effect of a coupled chemical reaction

on a cyclic voltammetric response depends on the time scale of the electrochemical experiment (i.e the scan rate) relative to the rate of the coupled process. A change in scan rate can shift the response from kinetic control by the diffusion-controlled, heterogeneous charge-transfer process to a mixed kinetic control region, and from there to kinetic control by the coupled reaction. By plotting $i_p/v^{1/2}$ versus scan rate, the effect of the scan rate on the diffusional process can be separated from its effect on the kinetics (3). This is illustrated in Figure 2.4 for the systems as given in equations (2.14) to (2.17). The behaviour for each kinetic case approaches that of a simple diffusion-controlled charge transfer ($i_p/v^{1/2}$ = constant) when the rate of voltage scan is such that the chemical reaction cannot proceed significantly before the experiment is over.

The direct evaluation of homogeneous kinetic parameters from cyclic voltammetric respones can be conveniently achieved through the use of theoretical working curves relating experimentally-measured current ratios to dimentionless kinetic parameters (3). The working curves used to interpret electrochemical reaction mechanisms discussed in Chapter 8 (equ. (2.15)) and Chapter 12 (equ. (2.17)) are presented in Figures 2.5 and 2.6.

The accuracy of homogeneous kinetic data derived from cyclic voltammetric studies has been discussed by Cass et. al. (11), for the case of a catalytically-coupled reaction (equ. (2.17)) between a ferrocene and flavocytochrome b_2. The second-order rate constants obtained from cyclic voltammetric and chronoamperometric studies were identical and in good agreement with a value determined by a conventional spectrophotometric

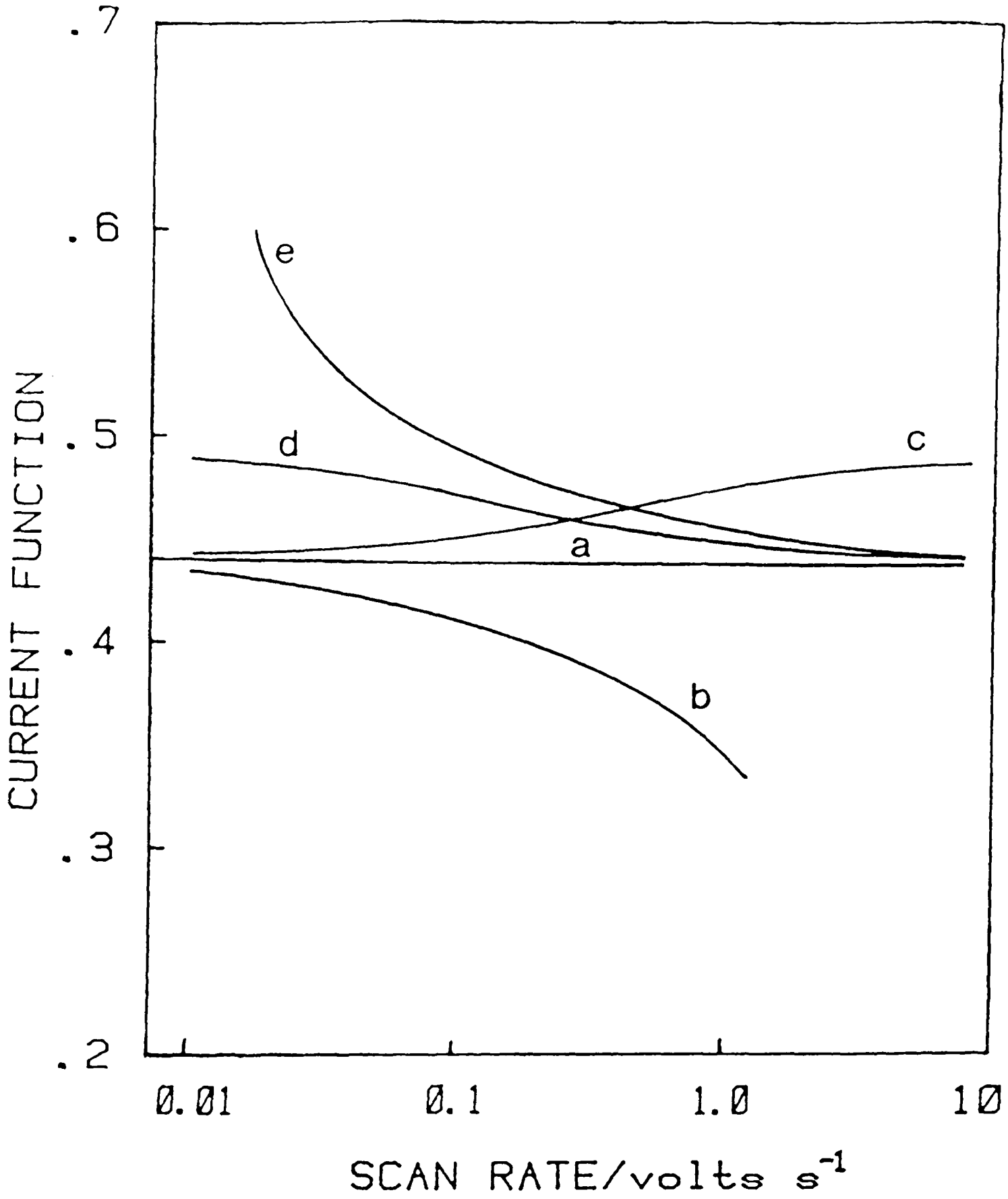

Figure 2.4: Variation of the peak current functions with the rate of voltage scan. Curves (a)-(e) correspond to the coupled reactions shown respectively in eqn. 2.1 and eqns. 2.14 to 2.17.

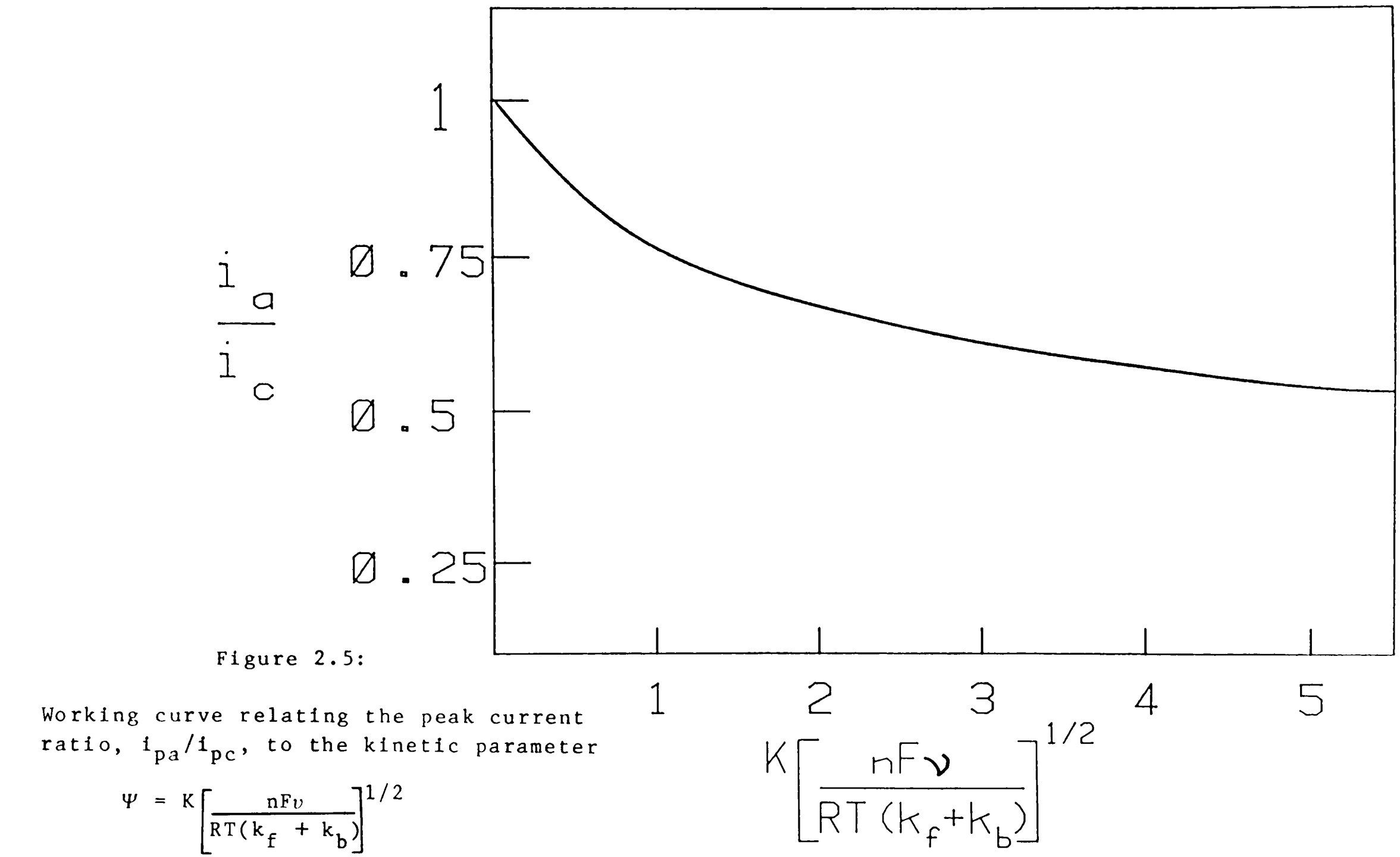

Figure 2.5:

Working curve relating the peak current ratio, i_{pa}/i_{pc}, to the kinetic parameter

$$\Psi = K\left[\frac{nF\upsilon}{RT(k_f + k_b)}\right]^{1/2}$$

for a reversible chemical reaction following charge transfer (eqn. (2.15)).

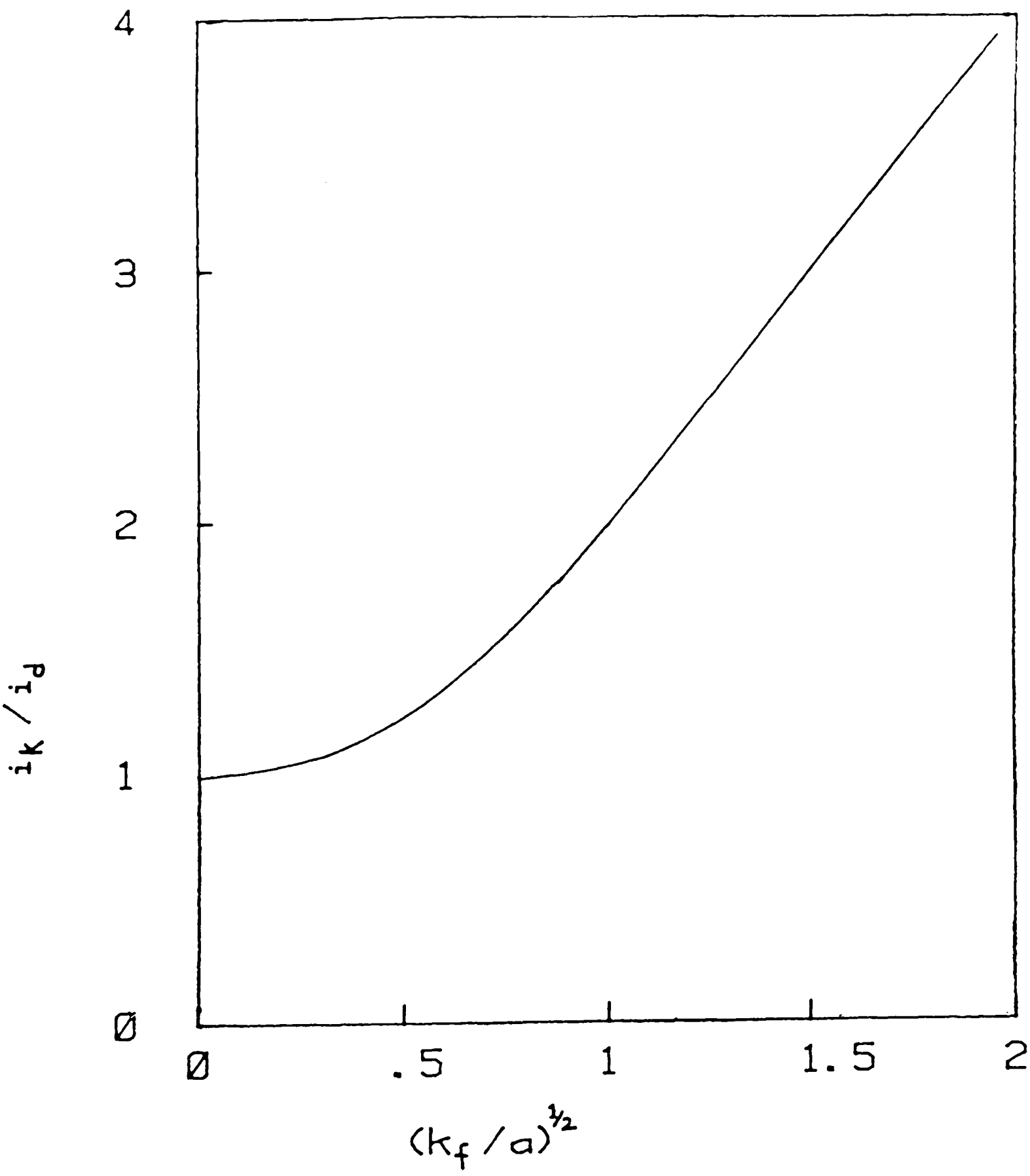

Figure 2.6: Working curve relating the ratio of the kinetic (i_k) to the diffusion-controlled (i_D) current, to the kinetic parameter k_f/a, for a catalytically-coupled reaction (eqn. (2.17)).

method.

The diagnostic criteria for identifying the presence of adsorption in cyclic voltammetric responses (equ. (2.13)) have also been described (10). Strong adsorption of reactant or product is indicated by the observation of symmetrical peaks and a linear dependence of peak current on scan rate ($i_{pc} \propto v$). Weak adsorption of reactant or product, characterised by the enhancement of anodic or cathodic peak currents, is usually more pronounced at higher scan rates or low reactant concentrations.

2.4 General Principles of Pulse Voltammetry.

In pulse voltammetry (12), the potential is held at some initial value E_1 and then stepped instantaneously to a second value E_2. Some time after the pulse is applied (at t_m), the current is measured. This sequence is shown in Figure 2.7(a). Following the application of a potential step of magnitude $(E_2 - E_1)$, the faradaic current, due to an electrochemically-reversible couple, decays according to a modified Cottrell equation:

$$i(t) = nFAC_A^{BULK} \left[\frac{D_A}{\pi t}\right]^{1/2} \left[1 + \left[\frac{C_A}{C_B}\right]_{x=0}\right]^{-1} \qquad (2.18)$$

where $\left[\frac{C_A}{C_B}\right]_{x=0}$ is given by the Nernst equation.

The decay of the charging current, following the application of a potential step, can be derived from a representation of an electrochemical cell as an RC circuit (13). The resulting expression is given in equation (2.19).

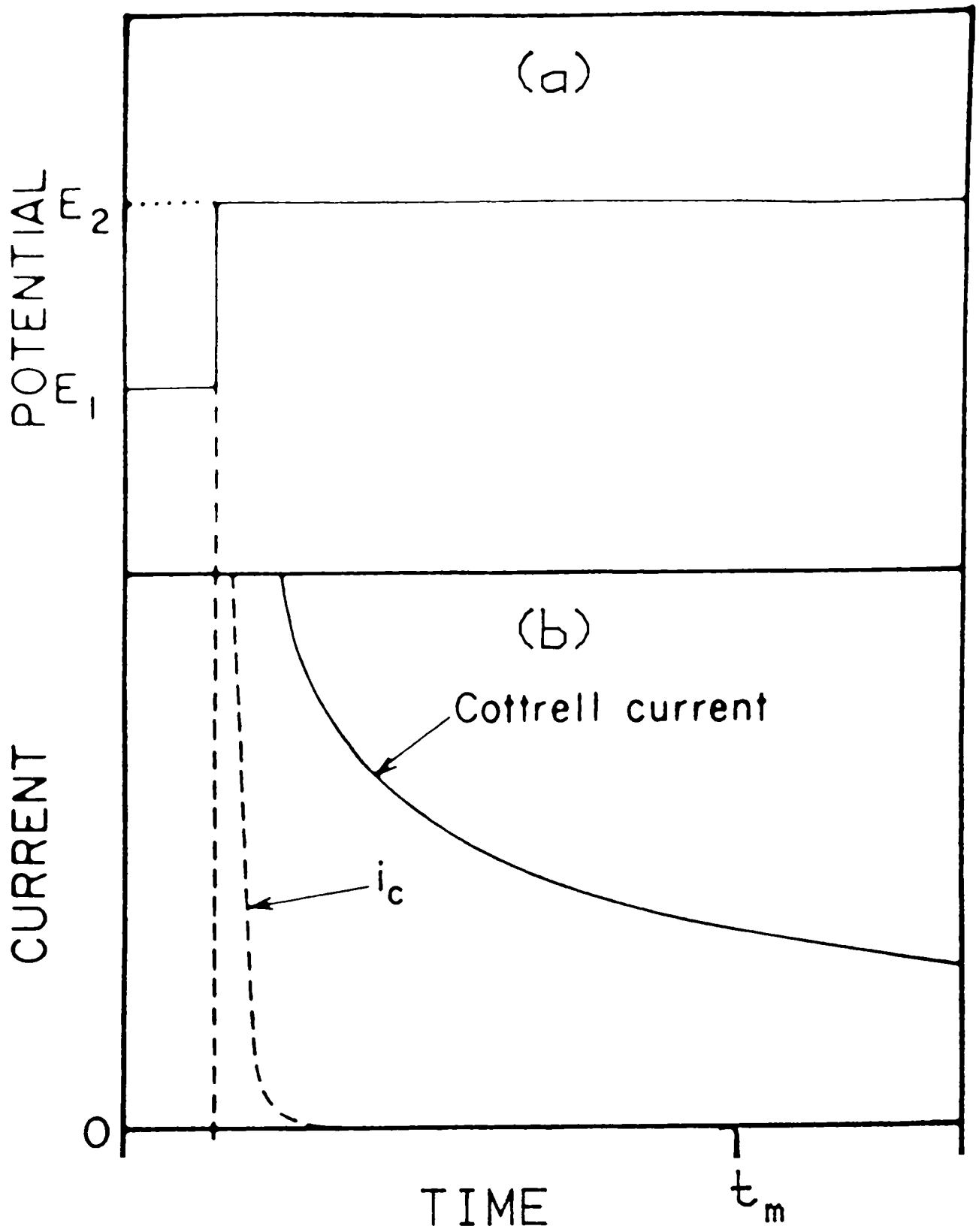

Figure 2.7: Potential-time sequence (a) and resulting current-time response (b) in pulse voltammetry.

$$i_c(t) = \frac{E_2 - E_1}{R_s} \exp(-t/R_s C_d) \qquad (2.19)$$

where C_d is the double layer capacitance and R_s is the solution resistance.

Comparison of equations (2.18) and (2.19) shows that a time-based current-sampling technique provides a means of effective discrimination against charging current contributions, as illustrated in Figure 2.7(b). This forms the underlying principle of all potential step techniques. The charging contribution in potential sweep techniques has a steady-state component given by υC_d (13) and limits sensitivity, particularly at high scan rates.

The general idea of pulse voltammetry has been elaborated by employing a variety of pulse sequences and current sampling schemes (12) and the theory of several techniques has been reappraised recently by Osteryoung and associates (14-16). Of these techniques, the most important may be square-wave voltammetry (SWV). SWV retains the usual advantages of pulse techniques: high current sensitivity (due primarily to short pulse widths) and discrimination against charging currents. However, the particular advantages of SWV, over more established techniques such as differential (DPV) and normal pulse voltammetry, are (14) increased speed and sensitivity coupled with the possibility of recognising systems with kinetic complexities.

2.5 Square-Wave Voltammetry.

Square-wave voltammetry employs a potential-time waveform

(Figure 2.8(a)) consisting of a square wave of half peak-to-peak amplitude, E_{SW}, superimposed on a staircase waveform (step height, ΔE). The basic square wave period, τ, is coincident with the step advance of the base staircase. The current is sampled twice during each staircase period: at time t_1 ($\rho_1\tau$), during a forward pulse of duration $\sigma\tau$, and at time t_2 ($\rho_2\tau$), during a reverse pulse, where the basic time unit t = 0 corresponds to the advance of the staircase. The coefficients σ, ρ_1, and ρ_2 are fractions less than unity and are used (15) to signify asymmetry in the wave-form and in the measurement times. The values of the square-wave parameters used in routine experiments, as described in Chapter 4, were ΔE = 1 - 10 mV, E_{SW} = 50 mV, frequency (= $1/\tau$) = 31 Hz, and $\rho = \sigma$ = 0.5 (symmetric SWV). These values emphasise the advantages of SWV, each potential sweep (ca. 400 mV) taking 1 - 10 secs., with current-sampling every 15 msecs.

For a reversible or quasi-reversible electrode reaction, a reverse current is generated in addition to a forward current, in response to the application of a double potential step in the vicinity of E^o (Figure 2.8(b)). The individual foward and reverse currents in the square-wave procedure (Figure 2.8(c)) ressemble those observed in cyclic voltammetry. At potentials beyond the current maxima, depletion of the analyte in the vicinity of the electrode is apparent. When the forward (i_f) and reverse (i_b) currents of the same period are differenced (Figure 2.8(c)), the forward difference current ($i_f - i_r$) is essentially a symmetric peak (similar to that observed in DPV), larger than either the forward or the reverse current alone. This sampling scheme enhances the sensitivity of SWV measurements (by a factor of ca. 4 at 100 Hz (14)) when compared to the differential measurements

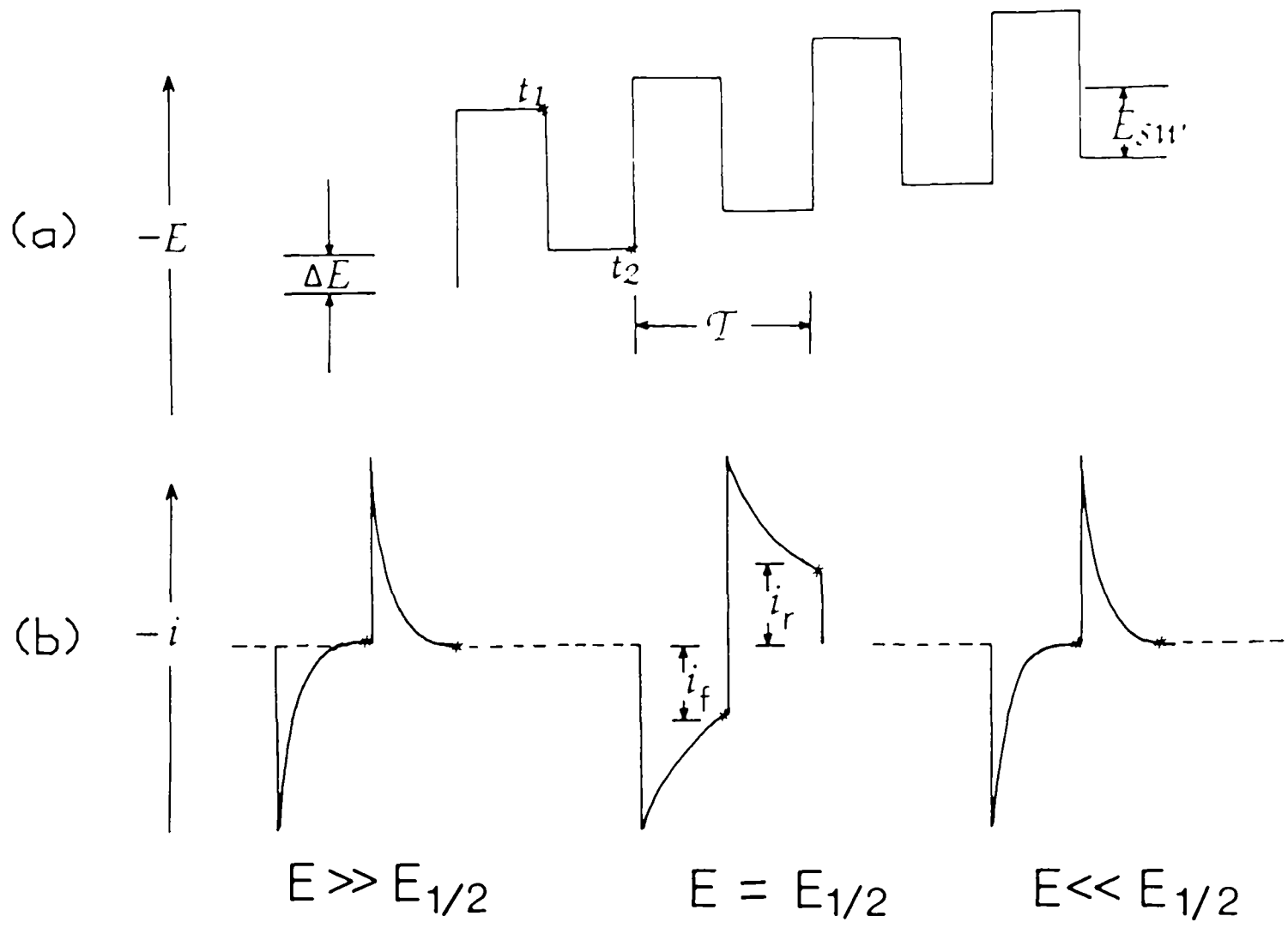

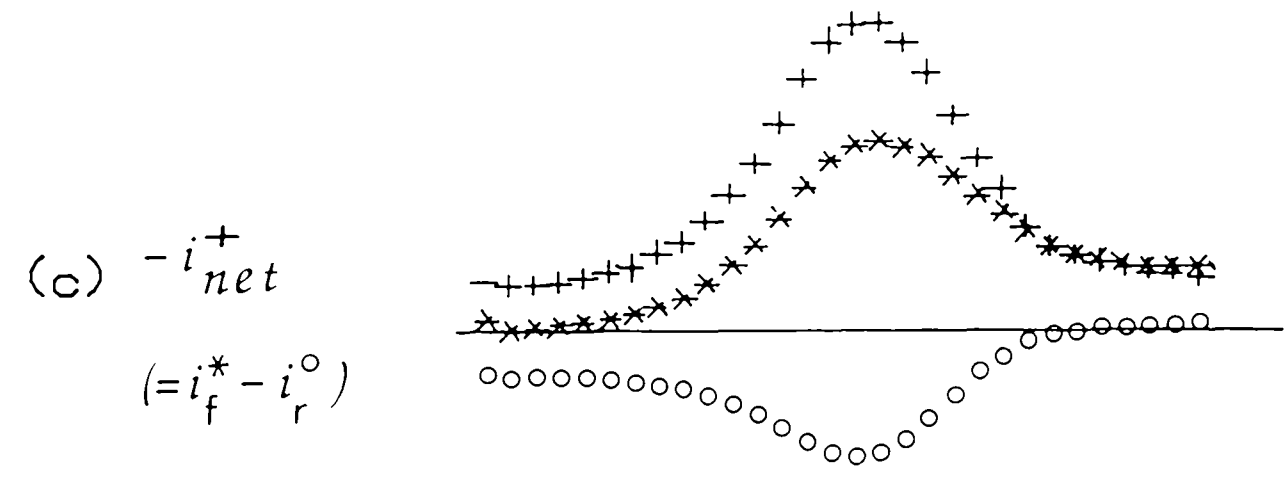

Figure 2.8: Introduction to square-wave voltammetry. (a) the applied potential-time waveform and current-sampling (t_1, t_2) scheme, and (b) the resulting current-time responses as a function of overpotential; (c) a square-wave voltammogram calculated for the case of reversible electron transfer.

employed in DPV studies. In the latter case, the delay between pulses is typically 0.5 to 1 second. Even more marked is the increase in sensitivity over cyclic voltammetric (CV) measurements. An experimental comparison (17) of CV and SWV reported a 16-fold increase in sensitivity in the SWV measurements.

The theoretical aspects of square-wave voltammetry were originally described (15) for a reversible electrode reaction, with only the oxidised form initially present in solution, and later extended (16) to systems complicated by slow heterogeneous electron-transfer or preceeding, following, or catalytic chemical reactions. Theoretical square-wave voltammograms, for a reversible system, can be generated by calculating individual and difference current functions, through the application of the arbitrary waveform equation of Rifkin and Evans (18):

$$i = \frac{nFAD_A^{1/2}C_A^{BULK}}{\pi} \sum_{j=1}^{m} \frac{\Delta\psi_j}{\sqrt{t-\tau_j}} \qquad (2.20)$$

where:

$$\Delta\psi_j = \frac{\theta_{j-1}(\theta_o+\gamma)}{\theta_o(\theta_{j-1}+\gamma)} - \frac{\theta_j(\theta_o+\gamma)}{\theta_o(\theta_j+\gamma)} \qquad (2.22)$$

m is the number of potential changes preceeding time t, $\theta = (C_A/C_B)_{x=0}$ and, $\gamma = (D_R/D_o)^{1/2}$. This expression is an entirely general equation and gives the current after any given potential pulse in an arbitrary series of step-functional potential changes. The equation reduces to the form appropriate to square-wave voltammetry when the appropriate potential-time

relationship is inserted (15).

The square-wave forward difference current function during the kth period (ΔI_k) is given by:

$$\Delta I_k = I_{k,\text{forward}} - I_{k,\text{reverse}}$$

$$= \frac{nFAD_A^{1/2}C_A^{BULK}}{\pi\tau^{1/2}} \cdot \Delta\psi_k(E_{SW}) \qquad (2.22)$$

The dependence of the difference peak current on the experimental parameters is hidden in the $\Delta\psi_k$ terms, but computation of theoretical voltammograms (15) indicated a non-linear increase in the peak current with increasing E_{SW}. The step height, ΔE, has little effect on the height of the difference peak current. Increasing the sweep rate, by increasing the frequency (f) causes the current to increase as $f^{1/2}$. Furthermore, for a reversible system, the position of the peak in the difference current is coincident with the half-wave potential, and the peak position, peak width and peak height are independent of the square-wave frequency.

The changes in the current responses observed (16) in theoretical square-wave voltammograms, for quasi-reversible and irreversible electron-transfer, are similar to those described for cyclic voltammetry. In the quasi-reversible region [$1 > \log(k_s\tau^{1/2}/D_A) > -1$] the peak position, peak width and peak height all vary with $\tau^{1/2}$. As expected, as the square-wave period becomes longer, the voltammetric response approaches that of a reversible system. A totally irreversible process exhibits a peak height and width independent of $\tau^{1/2}$.

2.6 Controlled Potential Techniques in Flowing Solutions.

The current-time responses of cyclic voltammetry and square-wave voltammetry, for near reversible electrochemical behaviour, are determined, in part, by a $t^{1/2}$ expansion of the diffusion layer in quiescent solution. However, if the solution is stirred by rotating the electrode, as in rotating-disc voltammetry, the bulk concentration of electroactive species is maintained at distances close to the electrode, at all times. Thus, a **limiting** current is observed at overpotentials ($|E - E^{o}|$) sufficiently large to ensure diffusion-controlled behaviour [$C_x(o,t) = 0$].

The laminar flow pattern (13) of a rotating-disc electrode is shown in Figure 2.9(a,b). The rate of laminar flow decreases near the electrode due to frictional forces, until a thin layer of stagnant solution is present immediately adjacent to the electrode. The slope of the surface concentration profile and, hence, the faradaic current is determined by the thickness of the stagnant diffusion layer. An increase in the angular velocity (ω) of a disc electrode decreases the diffusion layer thickness, so increasing the diffusional flux. The relation between the limiting current (i_L) and the angular velocity (equation (2.23)) has been derived (13) from a rigorous hydrodynamic treatment of the rotating-disc system:

$$i_L = 0.62nFAC_A^{BULK}D_A^{2/3}\,\bar{\upsilon}^{-1/6}\omega^{1/2} \qquad (2.23)$$

where $\bar{\upsilon}$ is the kinematic viscosity of the fluid

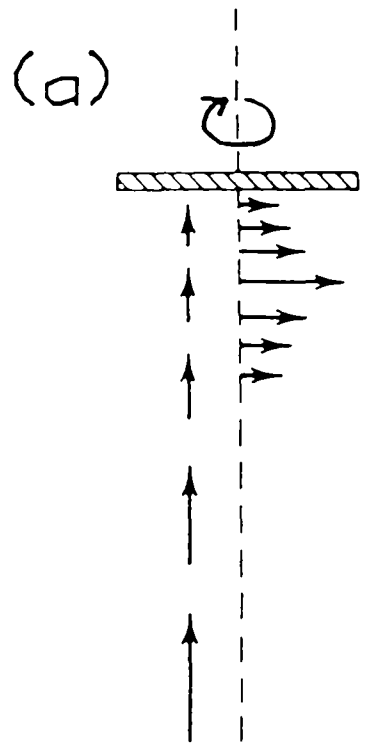

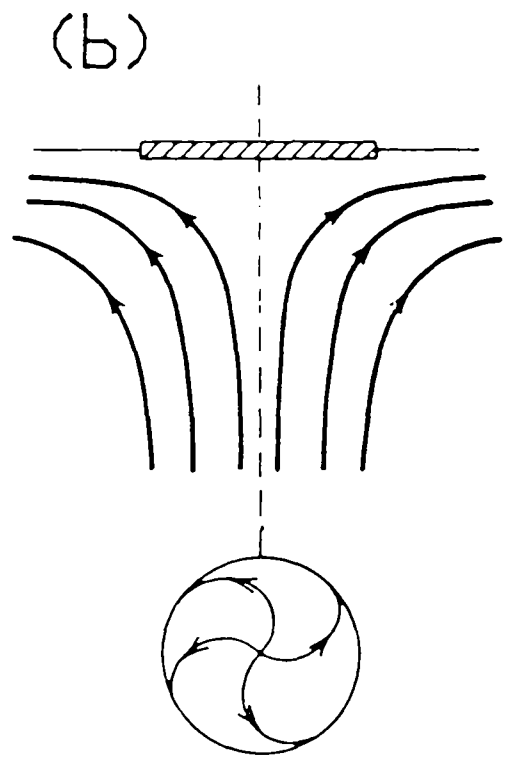

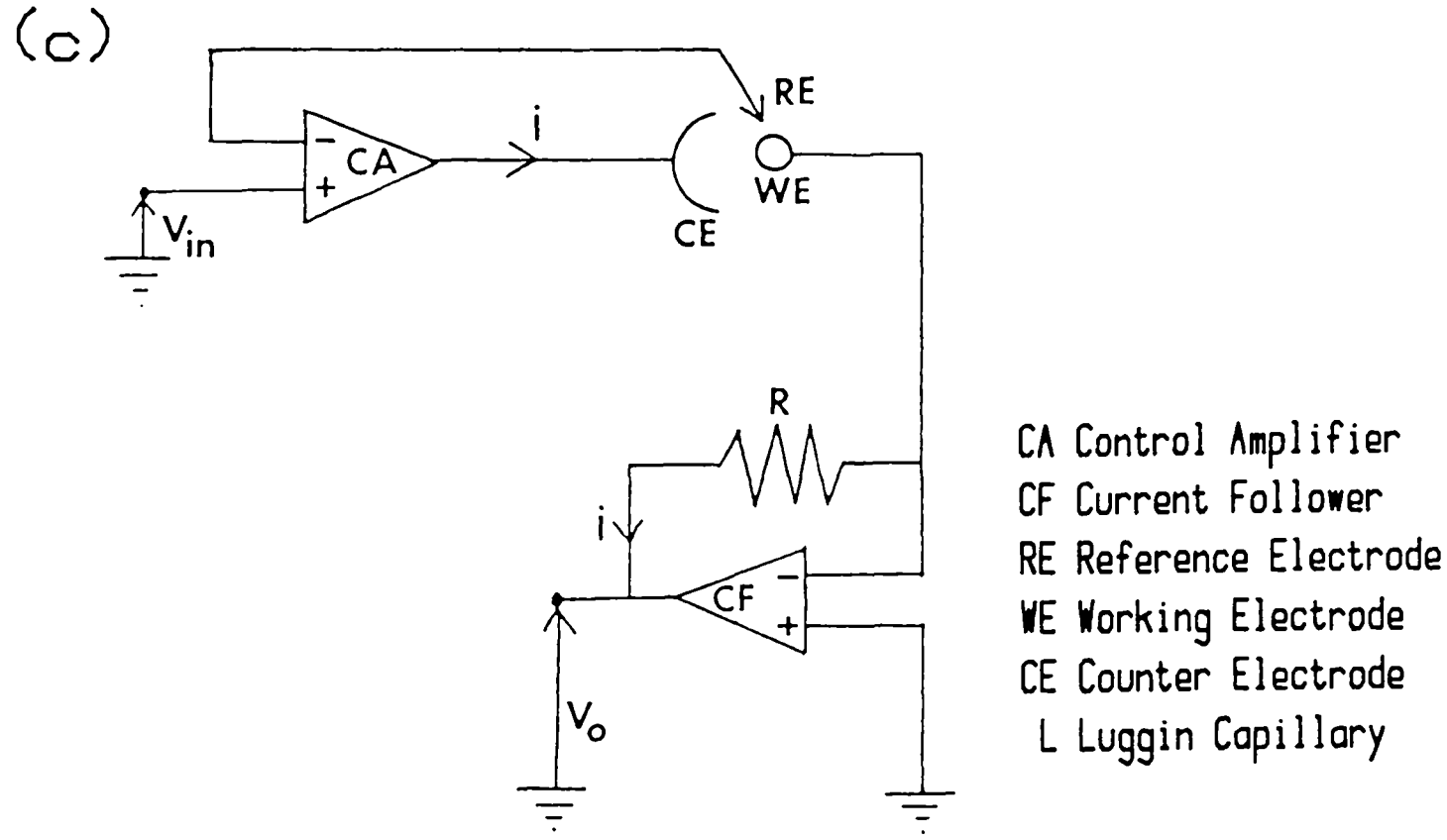

Figure 2.9: TOP- the rotating-disc technique, (a) vector representation of fluid velocities near a rotating disc, and (b) schematic resultant velocity streamlines. BOTTOM- (c) schematic diagram of an operational amplifier potentiostat.

2.7 Analogue Instrumentation and iR Errors.

The basis of all controlled potential techniques is that the potential between a working electrode (WE) and a reference electrode (RE) is controlled by varying the current flow between the working electrode and a counter electrode (CE). Figure 2.9(c) shows a schematic diagram of an operational amplifier potentiostat in which negative feedback around a control amplifier (CA) loop reduces the differential input, $V_- - V_+$, to zero, i.e. $E_{RE} = V_{IN}$, where V_{IN} is the applied potential waveform. The faradaic current is given by V_o/R.

The potential difference between the working and reference electrodes (E_{WR}) is given by:

$$E_{WR} = E_{WE} - iR_u - E_{RE} \qquad (2.24)$$

where R_u is the solution resistance between the working electrode and the Luggin capillary tip, and i is the faradaic current.

but, since the working electrode is maintained at virtual ground potential by the current follower (CF), then:

$$E_{WR} = -iR_u - E_{RE} = -iR_u - V_{IN} \qquad (2.25)$$

According to equation (2.25), the electrode potential is the inverse of the applied potential and contains a term arising from the potential drop due to the finite resistance of the solution between the working electrode and the Luggin tip.

The term iR_u has consequences in both potential sweep and

potential step experiments. In a potential step experiment "iR" or uncompensated resistance effects impose a finite rise time upon the system (13), such that the potential step applied to the control amplifier does not cause the desired instantanous potential pulse at the working electrode. In a potential sweep experiment (19), the current-potential profile becomes distorted so that there is an apparent increase in peak separation and also a deviation from the expected dependence of current on (scan rate)$^{1/2}$. The size of the term in iR_u can be minimised by positioning the working electrode as close to the Luggin tip as possible, by increasing the conductivity of the test solution, and by decreasing the area of the working electrode.

References - Chapter 2

1) Reinmuth, W. H., Anal. Chem. 34, 1446, (1962).

2) Heinze, J., Angew. Chem., Int. Ed. Engl. 23, 831, (1984).

3) Nicholson, R. S. and Shain, I., Anal. Chem. 36, 706, (1964).

4) Klingler, R. J. and Kochl, J. K., J. Phys. Chem. 85, 1731, (1981).

5) Polcyn, D. S. and Shain, I., Anal. Chem. 38, 370, (1966).

6) Adams, R. N. Electrochemistry at Solid Electrodes. New York: Marcel Dekker (1969).

7) Allen, P. M., Hill, H. A. O. and Walton, N. J., J. Electroanal. Chem. 178, 69, (1984).

8) Reinmuth, W. H., Anal. Chem. 33, 1793, (1961).

9) Nicholson, R. S., Anal. Chem. 37, 1351, (1965).

10) Wopschall, R. H. and Shain, I., Anal. Chem. 39, 1515, (1967).

11) Cass, A. E. G., Davis, G., Hill, H. A. O. and Nancarrow, D. J., Biochim. Biophys. Acta 828, 51, (1985).

12) Osteryoung, J., J. Chem. Educ. 60, 296, (1983).

13) Bard, A. J. and Faulkner, L. R. Electrochemical Methods. New York: Wiley (1980).

14) Borman, S. A., Anal. Chem. 54, 698A, (1982).

15) Christie, J. H., Turner, J. A. and Osteryoung, R. A., Anal. Chem. 49, 1899, (1977).

16) O'Dea, J. J., Osteryoung, J. and Osteryoung, R. A., Anal. Chem. 53, 695, (1981).

17) Takeuchi, E. S. and Osteryoung, J., Anal. Chem. 57, 1768, (1985).

18) Rifkin, S. C. and Evans, D. H., Anal. Chem. 48, 1616, (1976).

19) Nicholson R. S., Anal. Chem. 37, 667, (1965).

CHAPTER 3

PROTEIN PURIFICATION

3.1 Introduction.

The majority of the redox proteins studied in this thesis are not commercially available, the only exception being horse heart cytochrome *c* (Sigma Chemical Co.). Thus, the 8Fe ferredoxin and rubredoxin, from *C. pasteurianum*, and azurin and cytochrome c_{551}, from *P. aeruginosa*, were extracted from bacterial cell pastes as described below. The other proteins used in this thesis were prepared by other workers. Plastocyanin and the 2Fe ferredoxin from spinach (Dr. F.A. Armstrong), and 'modified' horse heart cytochrome *c* (Dr. D. Whitford) were prepared in this laboratory according to literature procedures (1,2). *M. elsdenii* and *D. vulgaris* flavodoxins were kind gifts of Prof. Cees Veeger (University of Wageningen) and Dr. G. Moore (University of Oxford), respectively. Azurin (*P. putida*) and *p*-cresol methylhydroxylase (*P. putida* and *P. alcaligenes*) were prepared by Dr. D.J. Hopper (University of Aberystwyth).

Direct electrochemical studies of cytochrome *c* using the protein "as received", without further purification, have shown (3) significantly less-reversible responses, often with the presence of additional voltammetric peaks, than is observed with protein subject to an additional chromatographic purification. This removes a variety of deamidated and polymeric forms which are present in even the best commercially-available cytochrome *c*. The cytochrome used for direct electrochemical studies in this thesis was purchased from Sigma (Type VI) and purified by Dr. F.A. Armstrong according to the method of Brautigan *et. al.*. (4). The

purity of the other redox proteins studied was established by measurement of the optical absorbances of the oxidised protein.

All solutions were prepared in water purified by a combination of reverse osmosis, ion exchange and carbon filtration (Millipore, Milli-Q system).

3.2 Ferredoxin and Rubredoxin from Clostridium Pasteurianum.

Ferredoxin (8Fe) and rubredoxin from Clostridium pasteurianum were isolated using a modification of the method of Thompson et. al. (5). All buffer solutions were purged with argon prior to use. Frozen cells (500 g), obtained from the PHLS Centre for Applied Microbiology and Research at Porton, were suspended in ca. 1200 mL of 25/20 mM Tris-HCl at $0^{o}C$. The suspension was homogenised for ca. 5 minutes in a Waring blender. The homogenate was then sonicated at $-10^{o}C$ in 100 mL portions for ca. 5 minutes, using an MSE sonicator probe. The combined sonicated mixture was centrifuged at 22,000g for 2 hours ($2^{o}C$) after which the grey pellet was discarded. The supernatant was then stirred for ca. 5 minutes with dry DEAE-23 anion exchange cellulose (15 g) The cellulose was filtered-off using a sinter funnel (porosity 1 or 2) and the sludge transferred to a 30 x 5 cm column. The column was washed with ca. 200 mL of 25/20 mM Tris-HCl and 0.1 M NaCl. Ferredoxin and rubredoxin were then eluted by stepping the ionic strength to 0.8 M NaCl.

The proteins were precipitated by the addition of solid $(NH_4)_2SO_4$ (0.6 g per mL) to the stirred solution, and the pH lowered to 5.8 by the dropwise addition of 1 M acetic acid. The suspension was then centrifuged at 30,000g for 30 minutes and the colourless supernatant was discarded. All further purification

was carried out with NaCl solutions buffered with 25/20 mM Tris-HCl. The brown pellet was dissolved in the minimum volume of 0.15 M NaCl and dialysed overnight (Sigma benzoylated dialysis tubing) against the same buffer. The dialysed solution was loaded on to a column of DEAE-23 (50 x 2.6 cm) equilibrated with 0.15 M NaCl, and the column washed with 0.25 M NaCl (ca. 100 mL) to elute rubredoxin as a pinkish solution. This was frozen and stored to await further purification. The ferredoxin was then eluted using NaCl solutions of increasing concentration 0.25 - 0.50 M (ca. 500 mL) and fractions with absorbance ratios $A_{390}/A_{280} > 0.73$ were pooled.

Final purification was achieved by diluting the ferredoxin to a total NaCl concentration of 0.15 M and loading on to a second column of DEAE-23 (50 x 2.6 cm) equilibrated as before with 0.15 M NaCl. After washing with ca. 100 mL of 0.15 M NaCl, the ferredoxin was eluted using NaCl solutions of increasing concentration 0.20 - 0.50 M, retaining fractions with $A_{390}/A_{280} > 0.80$. The protein solution was diluted x 3 and loaded on to a small (2 x 1.6 cm) column of DEAE-23 equilibrated with 0.15 M NaCl. It was eluted as a concentrated solution with 0.5 M NaCl. This was then further concentrated and desalted (against doubly-deionised H_2O) using an Amicon 8MC ultrafiltration unit and YM2 membrane. The final black solution was drop-frozen in liquid N_2 to give pellets of ca. 25 μL volume. The final concentration ranged between 1 - 3 mM (ϵ_{390} = 30.6 $mM^{-1}cm^{-1}$) and the absorbance ratio A_{390}/A_{280} was typically 0.82.

The rubredoxin fractions were thawed and diluted x 2.5 using 25/20 mM Tris-HCl then applied to a column of DEAE-23 (2.5 x 1.5 cm). The red band was eluted in ~20 mL volume using

buffered 0.4 M NaCl. This solution was concentrated to ca. 1 mL using an Amicon 8MC ultrafiltration unit, and then dialysed against 25/20 mM Tris-HCl and 0.1 M NaCl. The final purification used a Pharmacia FPLC system. The solution was applied to a polyanion SI-17 preparative column and eluted by a 0.1 - 1.0 M NaCl gradient (25/20 mM Tris-HCl). The red fractions with an absorbance ratio of A_{490}/A_{280} = 0.43 were combined. The final solution was concentrated and desalted (against doubly-deionised water) using an Amicon 8MC ultrafiltration unit, with a YM2 membrane, then frozen as pellets in liquid N_2.

The spectra of ferredoxin and rubredoxin are shown in Figures 3.1(a) and 3.1(b).

3.3 Azurin from Pseudomonas aeruginosa.

P. aeruginosa azurin, was purified by a slight modification of the method of Parr et al. (6). The Pseudomonas aeruginosa cell paste was provided by Prof. I.J. Higgins of the Cranfield Institute of Technology and was stored at -20°C prior to use. The preparation procedure used is described below.

Approximately 200 g of cell paste was thawed and homogeneously suspended in approximately 1000 mL of 20 mM potassium phosphate buffer (pH 7.0), at 4°C. These cells were then ruptured by mechanical stirring and ultrasonication at 0°C.

The resulting suspension was made 5% in $(NH_4)_2SO_4$ and then centrifuged to remove cell debris. The supernatant was decanted off, and the precipitate re-suspensed in buffer and centrifuged again. The two supernatants were combined and taken to 45% saturation in $(NH_4)_2SO_4$ and then centrifuged to remove unwanted proteins. The golden-yellow supernatant was then taken to 95%

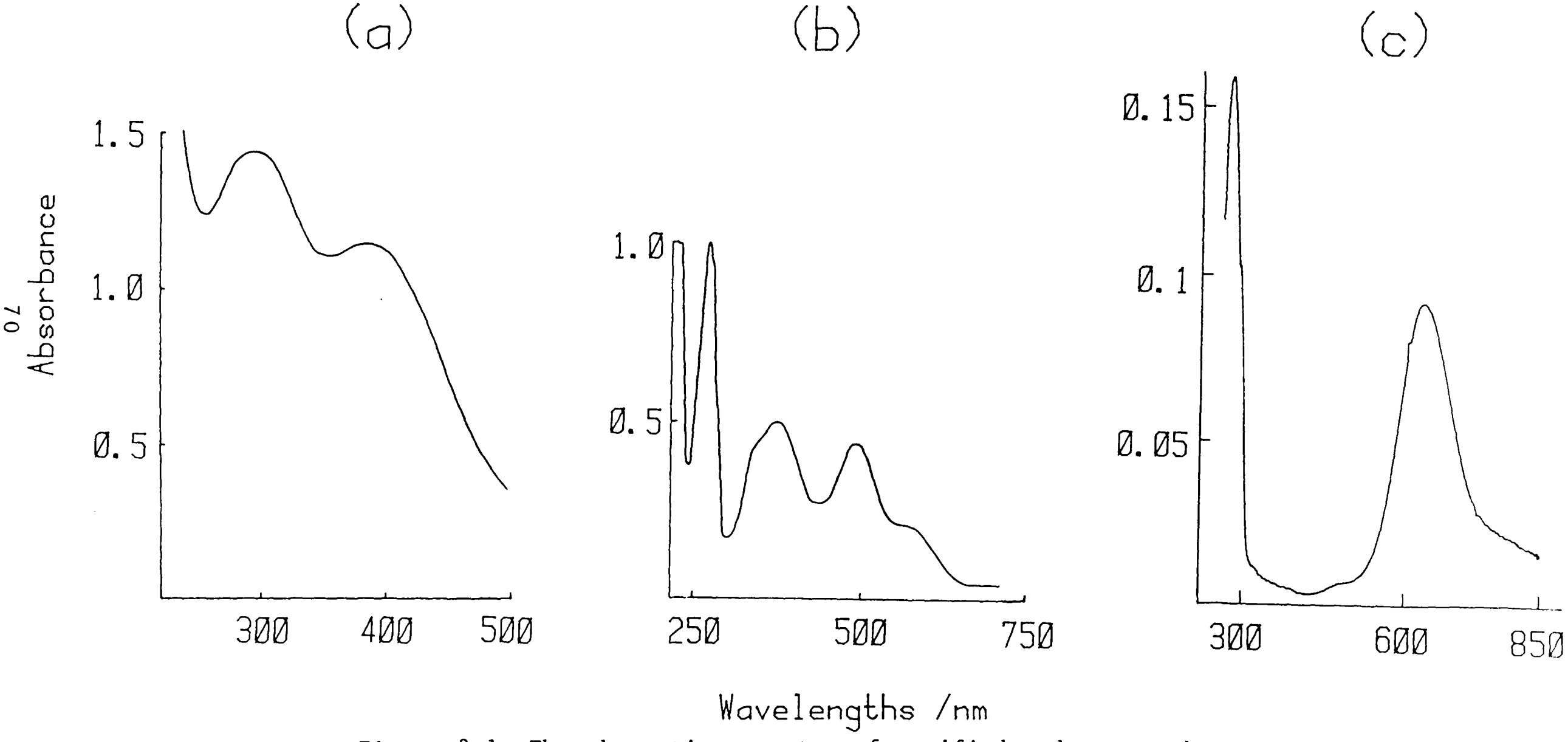

Figure 3.1: The absorption spectra of purified redox proteins.
(a) 2[4Fe-4S] ferredoxin (30 μM) and
(b) rubredoxin (25 μM), from Clostridium pasteurianum
(c) azurin (16 μM) from Pseudomonas aeruginosa.
1 cm pathlength.

saturation in $(NH_4)_2SO_4$ and centrifuged whereupon the azurin, cytochrome $\underline{c}_{551}$ and cytochrome oxidase precipitate out. The precipitate was re-suspended in buffer and then dialysed against a large volume of phosphate buffer overnight.

Approximately 250 g of a slurry of DEAE-52 cellulose, equilibrated in 20 mM potassium phosphate buffer, pH 7.0, was added to the dialysate and stirred for 15 minutes. Unwanted flavoprotein is absorbed on the cellulose which may be removed by centrifugation. The supernatant was then taken to 100% saturation in $(NH_4)_2SO_4$ and centrifuged. The blue/green supernatant was washed through precycled but unequilibrated CM-23 cellulose in a sintered glass funnel, whereupon any remaining azurin precipitates at the surface of the cellulose and can be eluted by washing the gel with distilled H_2O. This eluant was then dialysed, overnight, against a large excess of doubly-deionised H_2O.

The precipitate from the 100% $(NH_4)_2SO_4$ cut was redissolved in a minimum volume of 20 mM Tris-HCl buffer, pH 7.6, and dialysed overnight against a large excess of the same buffer. The solution was concentrated using an Amicon ultrafiltration cell with a Diaflo YM-10 membrane, and then applied to an S-200 gel filtration column, equilibrated in 20 mM Tris-HCl buffer, pH 7.6. This column separates the azurin and cytochrome $\underline{c}_{551}$ fractions from the cytochrome oxidase.

The two azurin/cytochrome $\underline{c}_{551}$ fractions were then combined and the pH adjusted to pH 3.9 with CH_3COOH. The mixture was then applied to a 2.5 x 30 cm CM-23 ion-exchange column, equilibrated in $CH_3CO_2NH_4$ buffer, pH 3.9, and washed at pH 3.9. The cytochrome $\underline{c}_{551}$ was eluted as a broad band by stepping the pH to 4.45. The azurin was then eluted by stepping the pH to 4.65.

To concentrate and further purify the proteins they were applied separately to 1.5 x 20 cm CM-23 ion-exchange columns, equilibrated in $CH_3CO_2NH_4$ buffer, pH 3.9, after adjusting their pH to 3.9, and then eluted by stepping the pH to 6.0.

The eluants were concentrated and desalted (against doubly-deionised H_2O) using an Amicon 8MC ultrafiltration unit with a YM10 membrane. The proteins were stored as pellets in liquid N_2. The final purity ratio of azurin (A_{625}/A_{280}) was 0.57. The concentration was assessed using $\epsilon_{625} = 5700\ M^{-1}cm^{-1}$ (7). The spectrum of azurin is shown in Figure 3.1(c).

3.4 Small Scale Purifications.

Electrochemical samples were re-purified by ion-exchange chromatography on a Pharmacia FPLC system, using a linear salt gradient. The column used for the purification of azurin was a strong cation-exchanger, Mono-S (Pharmacia), equilibrated in acetate, pH 4.0. Ferredoxins, flavodoxin and rubredoxin were purified on a strong anion-exchanger, polyanion SI-17 (Pharmacia), equilibrated in Tris-HCl, pH 7.6.

References - Chapter 3

1) Borchert, M. T. and Wessels, J. S. C., Biochim. Biophys. Acta 197, 78, (1970).

2) Brautigan, D. L., Ferguson-Miller, S. and Margoliash, E., J. Biol. Chem. 253, 130, (1978).

3) see, for example, Bowden, E. F., Hawkridge, F. M., Chlebowski, J. F., Bancroft, E. E., Thorpe, C. and Blount, H. N., J. Am. Chem. Soc. 104, 7641, (1982), and references therein.

4) Brautigan, D. L., Ferguson-Miller, S. and Margoliash, E., Methods Enzymol. 33D, 128, (1978).

5) Thompson, C. L., Johnson, C. E., Dickson, D. P. E., Cammack, R., Hall, D. O., Wesser, U. and Rao, K. K., Biochem. J. 139, 97, (1974).

6) Parr, S. R., Barber, D., Greenwood, C., Phillips, B. W. and Melling, J., Biochem. J. 157, 423, (1976).

7) Kitchen, N. A., D. Phil. Thesis. Oxford (1984).

CHAPTER 4

DIRECT ELECTROCHEMISTRY OF REDOX PROTEINS AT PYROLYTIC GRAPHITE ELECTRODES

4.1 Introduction.

In general, redox proteins do not show reversible electrochemical responses at normal voltammetric electrodes. At the time of beginning this project there were few exceptions to this statement. The most successful studies had focussed upon the readily available, and quite robust, protein, cytochrome c. The use of indium oxide and tin oxide semi-conductor electrodes provided one of the first reports (1) of quasi-reversible direct electrochemistry of this protein. In the same year quasi-reversible direct electron transfer between cytochrome c and a gold electrode, upon which 4,4´-bipyridyl, or a related compound, is adsorbed, was observed (2). Although bacterial and plant ferredoxins can be rapidly reduced at mercury electrodes, there are associated problems of irreversibility and degeneration. Rapid and reversible direct electrochemistry of these proteins had only been observed at a gold electrode modified with methyl viologen [2Fe ferredoxin] (3) or pyrolytic graphite in the presence of Mg^{2+} [8Fe ferredoxin] (4). There were no reports of the reversible electrochemistry of copper proteins or flavoproteins. This chapter describes the observation of direct quasi-reversible electrochemistry of a variety of redox proteins at polished pyrolytic graphite electrodes, and establishes the importance of electrostatic interactions in promoting electrochemical responses at this surface.

Electrostatic effects dominate many aspects of protein and enzyme behaviour, including the folding of polypeptide chains (5), the thermo-stability of enzymes in thermophilic bacteria (6), enzyme-substrate interactions (7), protein-protein interactions (8) and the assembly of virus sub-units (9). In some studies these effects may simply be attributed to the influence of salt-bridge formation upon molecular structure (e.g. the thermo-stability of some proteins). However, in many cases specific electrostatic interactions may control intermolecular phenomena. For example, a 1:1 protein:enzyme complex between the 2Fe-2S ferredoxin and ferredoxin-NADP-oxidoreductase, involving a strong electrostatic interaction ($K_{ass} = 10^7$ at I=0), is thought to be the catalytically-active species in photosynthetic $NADP^+$ reduction (10). In accord with this proposal, the complex is dissociated at high ionic strength. It is interesting that bacterial 8Fe ferredoxin, flavodoxin and rubredoxin, proteins carrying net negative charges similar to the plant ferredoxin, are also capable of stimulating $NADP^+$ reduction. In each case, catalytic activity is reduced at high ionic strength. This suggests that the interactions between the enzyme and these low potential redox proteins are similar and primarily electrostatic.

Inorganic cations such as Ca^{2+}, Mn^{2+}, Mg^{2+} and Na^+ play a central role in many biological processes. The involvement of divalent cations in the ATP cycle (e.g. MgATP) and in contractile and motile responses (e.g. Ca-troponin) clearly involves specific binding and regulation (11). However, there are many examples of salt effects in which the requirement for divalent cations appears to be associated with simple 'screening' of otherwise repulsive intermolecular electrostatic interactions. These

effects are particularly marked in processes involving interactions at, or between, biological membranes, as exemplified by the phase separation and fusion of negatively-charged lipid vesicles (12), membrane stacking (13), chlorophyll fluorescence yields (14), activation of membrane bound enzymes (15,16), the stimulation of chloroplast ferredoxin and plastocyanin linked electron-transport (17,18) and the assembly and activation of membrane-bound chloroplast and mitochondrial ATPases (19,20). All biological membranes contain charged groups on their surfaces derived from both lipids and intrinsic proteins. At neutral pH, these groups commonly give rise to a net negative surface charge density, the isoelectric points being 4.1 - 4.7 for thylakoid membranes (21), 4.8 - 5.4 for rat liver mitochondrial membranes (22) and 4.0 for microsomal membranes (23). The effects of divalent cations are consistent with 'screening' or neutralisation of these membrane charges so facilitating interactions with adjacent membranes or with negatively-charged 'mobile' proteins such as the 2Fe ferredoxin. The observed (15,19) effects of pH, ionised surfactants and the relative efficiency of divalent versus monovalent cations are in agreement with this interpretation.

At near neutral pH most proteins are charged, since few have isoelectric points in this region (24). The approximate net charge of a protein at a pH of ca. 7 may be calculated from the amino acid composition (Table 4.1) assuming that strongly basic amino acid residues (arginine and lysine) are fully ionised and contribute 1+ and that strongly acidic residues (aspartate and glutamate) are similarly ionised and contribute 1-. Additionally, charges associated with individual redox centres may be taken into account in the summation. It is clear that proteins

TABLE 4.1

Amino Acid Compositions of Representative Redox Proteins

	AMINO ACID (Mol %)																			CHARGE	
	ACIDIC				BASIC			HYDROPHOBIC (NON-POLAR)									NON-IONIC, POLAR					COUNT [a]
	STRONG		WEAK		STRONG		WEAK														
	GLU	ASP	CYS	TYR	LYS	ARG	HIS	GLY	ALA	MET	VAL	ILE	LEU	PHE	PRO	TRP	GLN	SER	THR	ASN	pI	pH 7.0
pK	**4.25**	**3.7**	**8.3**	**10.1**	**10.5**	**12.5**	**6.0**															
Cp Fd (8Fe)	3.6	9.1	14.5	1.8	1.8	0	0	7.3	14.5	0	11	9.1	0	1.8	5.5	0	3.6	9.1	1.8	5.5	n.a.	6-
Sp Fd (2Fe)	9.3	11.3	5.2	4.1	4.1	1	1	6.2	9.3	0	7.2	4.1	8.2	2.1	4.1	1	4.1	7.2	8.2	2.1	4.0	16-
Cp Rd	11.1	18.5	7.4	5.6	7.4	0	0	11.1	0	1.9	9.3	3.7	1.9	3.7	9.3	1.9	0	0	5.6	1.9	n.a.	12-
Sp Pc	9.1	6	0	3	6	0	2	14	7.1	2	10.1	4	7.1	6.1	5.1	0	1	7.1	5.1	5.1	4.0	9-
Me Fl	11.7	7.3	1.5	1.5	6.6	1.5	0	10.2	13.1	3.7	9.5	3.7	5.1	2.9	3.7	2.9	0.7	5.1	5.8	3.7	n.a.	15-
Pa Az	3.1	8.6	2.3	1.5	9.4	0.8	3.1	8.6	5.5	4.7	7.8	3.1	7	4.7	3.1	0.8	4.7	7.8	7.8	5.5	5.4	3-
HH Cyt c	8.7	2.9	1.9	3.9	18.2	1.9	2.9	11.5	5.8	1.9	2.9	5.8	5.8	3.9	3.9	1	2.9	0	9.6	4.8	9.0	7+

Key to Table. Cp Fd (Rd): C. pasteurianum 2[4Fe-4S] ferredoxin (rubredoxin); Sp Fd (Pc): Spinach 2Fe-2S ferredoxin (plastocyanin); Me Fl: M. elsdenii flavodoxin; Pa Az: P. aeruginosa azurin; HH Cyt c: Horse Heart Cytochrome c. n.a.: not available

a: based on a count of the number of strongly acidic and strongly basic residues.

representative of most classes of redox proteins carry a large excess of charged residues (Table 4.1), in accord with known pI values. However, specific estimates of total protein charge are expected to be modified by internal compensatory effects such as H-bonding or salt-bridges, and should be treated as maximal values. Experimental evidence for the substantial negative charges carried by low-potential redox proteins at pH ca. 7 is the observation of strong binding to DEAE anion exchangers (ferredoxin, rubredoxin and flavodoxin require >0.3 M Cl^- for elution).

It has been proposed that in order to effect electron-transfer between redox proteins and electrodes, binding of the protein to the electrode surface is required (25). Thus, 4,4´-bipyridyl adsorbed perpendicularly (26) on gold, allows rapid heterogeneous electron transfer to cytochrome c. It is most likely that the protein hydrogen bonds, through its positively-charged lysine residues, to the negative charge density of pyridyl groups. The ability of the divalent cations Mg^{2+} and Mn^{2+} to promote the direct electrochemistry of C. pasteurianum 2[4Fe-4S] ferredoxin at a polished basal plane pyrolytic graphite electrode has been recently reported (4). Oxidised graphite surfaces have been shown to carry a range of surface functional groups including acidic carboxylate residues (27). Divalent cations were proposed to act as a ´transient´ electrostatic bridge between these carboxylate groups and the highly negatively-charged 8Fe ferredoxin. This observation provides an interesting parallel with the role of divalent cations as regulators of heterogeneous processes in vivo.

The hypothesis guiding the work in this chapter is that productive interactions between graphite surfaces and other highly-charged redox proteins may also depend upon association through electrostatic interactions. Thus, for negatively-charged redox proteins such as flavodoxin, rubredoxin and plant-type 2Fe-ferredoxins the addition of multivalent cations may stabilise otherwise repulsive electrostatic interactions between the protein and a graphite electrode surface.

4.2 Experimental Details.

Ferredoxin-NADP reductase (EC 1.18.1.2) was used as supplied (BDH U.K.). Hexamminechromium(III) chloride ($Cr(NH_3)_6Cl_3$) was prepared by V.J. Lowe as described in the literature (28). All other reagents were of AnalaR or AristaR grade. Electrochemical experiments were carried out at 25°C. The glass electrochemical cell (ca. 500 µL volume) incorporated a conventional three electrode configuration. The counter electrode consisted of a semi-cylindrical piece of platinum gauze and the reference electrode (Radiometer K401) was saturated calomel (SCE), E = +244 mV (25°C) vs. the normal hydrogen electrode (NHE).

Table 4.2 lists the size, source and grade of materials used in the preparation of the working electrodes in this thesis. Carbon and gold discs were housed in a teflon electrode sheath or a sheath of epoxy resin. Prior to each experiment, the electrodes were polished using an alumina (particle size 0.3µ)-water slurry, thoroughly rinsed, and then sonicated in distilled water. For experiments in which a freshly cleaved pyrolytic graphite basal surface was required, a graphite disc was glued on to the polished end of a piece of glass capillary tubing (5 mm outer diameter). Electrical contact with a piece of platinum wire glued into the capillary was achieved via a mercury junction. Two methods of sealing the perimeter of the graphite disc and adjoining capillary tubing were tested. Initial trials using heat-shrink polyolefin tubing proved unsatisfactory with leakage of solution between the graphite and the seal, and unstable, tailing voltammetric responses in buffer alone. However, stable voltammetric responses were achieved when the perimeter of the disc was sealed with a girdle of silicone rubber (Dow Corning,

TABLE 4.2

Materials Used in Electrode Preparation

MATERIAL	SOURCE	GRADE	DESCRIPTION
Pyrolytic graphite	Le Carbone (Portslade, Sussex).	Standard	5 mm dia.
Glassy Carbon	Tokai Carbon, Tokyo.	GC-10S	5 mm dia.
Gold	Oxford Electrodes, U.K.	99.9% pure	4 mm dia.
Vacuum-evaporated Gold films	Dept. of Nuclear Physics Oxford Univ.	" "	1000 Å thick 193 $\mu g cm^{-2}$ on glass slides.
Thin film RuO_2	Gift of Dr. M.A. Harmer I.C.L., Oxford.	----	Ti support
Polishing alumina	Banner Scientific Ltd. or BDH, U.K.	'Highly-pure'	0.3μ, 0.05μ
Diamond paste	Engis Ltd., U.K.	Metallographic	0.25μ
Polishing detergent (Micro')	International Products Corp., New Jersey.	----	----
Sonicator	Semat Technical (U.K.)	----	----

U.S.A.), with no suggestion of solution contact at any face other than the exposed basal surface. Exposure of fresh surfaces was carried out by careful slicing with a sharp razor blade.

Anaerobicity of samples was achieved by passing a slow stream of humidifed oxygen-free ('Gas-Clean' oxygen filter, Chrompack) argon across the surface. This proved an efficient means of de-aeration as assessed by measurements of the spectral purity ratio of the oxygen-sensitive 8Fe ferredoxin over a period of 2 - 3 hours in the electrochemical cell. No significant changes in optical absorption were evident throughout this period. Solutions contained 20 mM acetate or Tricine (N-{tris(hydroxymethyl) methyl}glycine) as the support medium. Aliquots of 3.0 M $MgCl_2$ or 0.3 M $Cr(NH_3)_6Cl_3$ stock solutions were added as required via a 25 μL Hamilton syringe.

Symmetric SWV was carried out using microprocessor-based instrumentation. A Research Machines 380-Z microcomputer was interfaced to a rack system containing digital-to-analog and analog-to-digital converters. The potentiostat used was constructed in this laboratory. Parameter input and data manipulation were carried out in BASIC while experimental control software was CALLed from BASIC. D.C. cyclic voltammetry was carried out using an Oxford Electrodes potentiostat.

Experimental Results

4.3 Direct Electrochemical Studies of Redox Proteins at Polished Basal Plane Pyrolytic Graphite Electrodes.

4.3.1 Divalent Cation Promotion Effects: C. pasteurianum Ferredoxin and Rubredoxin.

For pyrolytic graphite electrodes at near neutral pH, the working range or 'potential window' covers a range of ~2 V and encompasses the formal potential of all redox proteins.

In the absence of $MgCl_2$, i.e. with 0.1 M NaCl, 20 mM Tricine as sole supporting electrolyte, no faradaic electrochemistry of ferredoxin or rubredoxin is detectable at a polished basal plane pyrolytic graphite electrode (Figure 4.1(a,c)). The addition of *ca.* 40 mM $MgCl_2$ to the solution is sufficient to promote a single faradaic response with well-defined forward and reverse current contibutions to the SWV net current for each protein (Figure 4.1(b,d)).

Promotion profiles recorded by measuring the peak net current (SWV) at a range of Mg^{2+} concentrations (Figure 4.2) show the optimal concentration of Mg^{2+} to be 50 - 80 mM for ferredoxin and rubredoxin. The large scatter in experimental points is due to the poor reproducibility in polishing the electrode surface between Mg^{2+} additions. This procedure was adopted following the observation of a deterioration in faradaic response, particularly at sub-optimal cation levels, on prolonged immersion and cycling of the electrode in the protein test solution (see Chapter 7).

The rate of the electron-transfer process under optimal cation conditions is manifested in the influence of square wave frequency on the peak width and position, as illustrated in

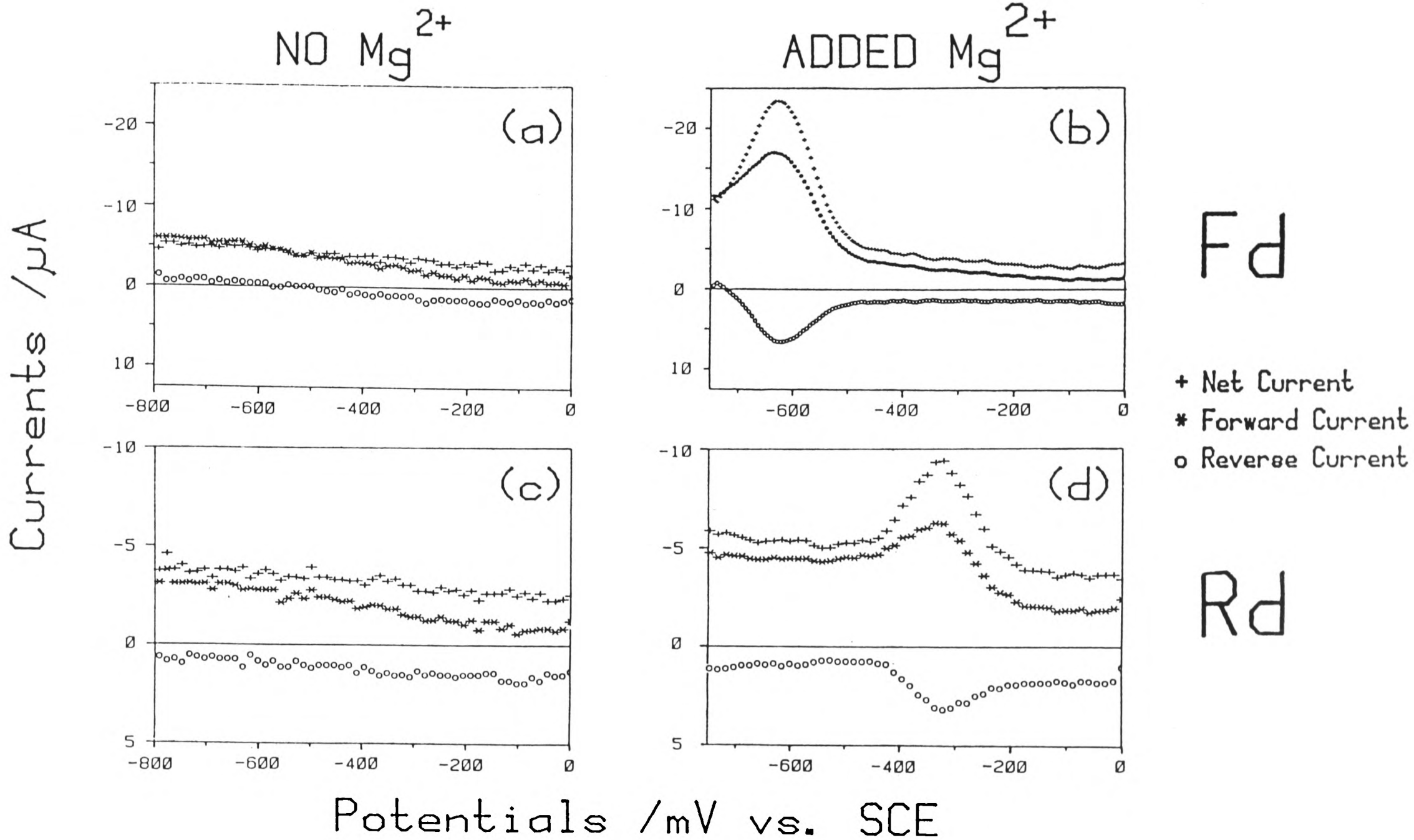

Figure 4.1: Square-wave voltammograms (frequency 31 Hz and amplitude (half peak-to-peak) 50 mV) for: (a) 2[4Fe-4S] ferredoxin, 0.23 mM in 20 mM Tricine, 100 mM NaCl, pH 8.0; (b) as (a), with the addition of 40 mM $MgCl_2$. (c) Rubredoxin, 0.17 mM in 20 mM Tricine, 100 mM NaCl, pH 8.0; (d) as (c), with the addition of 40 mM $MgCl_2$. Polished basal plane graphite electrode.

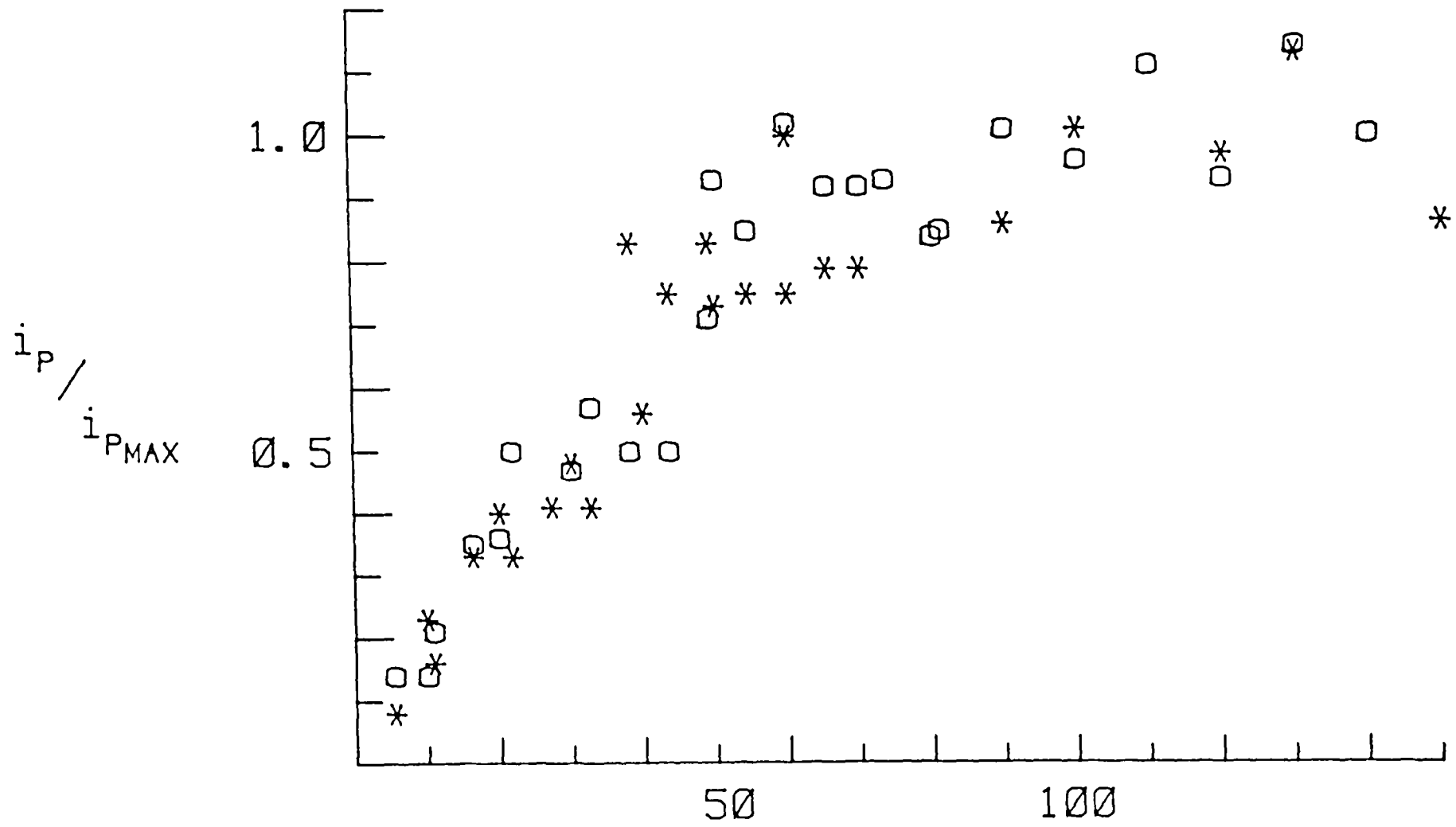

Figure 4.2: Variation of normalised peak net current (square-wave voltammetry) with Mg^{2+} concentration for 0.2 mM *C. pasteurianum* rubredoxin (*) and 2[4Fe-4S] ferredoxin (o). Conditions as given in Figure 4.1.

Figure 4.3. The observed frequency dependence of the peak net-current potential is consistent with quasi-reversible behaviour.

However, there is no simple **empirical** method for estimating values of the heterogeneous rate constant, k_s, from fast scan square-wave voltammograms. It was intended that curves of peak net-current potential versus square-wave frequency, derived from these studies, should be fitted to similar curves generated by computer simulations of square-wave voltammograms, to yield values of k_s. However, this requires a complex multi-parameter optimisation procedure and, to date, no satisfactory fit of theory to experiment has been obtained. Cyclic voltammetric studies gave typical peak-current potential separations ΔE_p (mV) at scan rates 10 [and 50] mVs^{-1} of 70 [80] - [rubredoxin (100 mM Mg^{2+})] and 85 [107] - [ferredoxin (40 mM Mg^{2+})]. Plots of peak current vs. square root of scan rate (v) were linear for rubredoxin up to at least 100 mVs^{-1}, but for ferredoxin small deviations from linearity became apparent above 20 mVs^{-1}. This behaviour again indicates quasi-reversible electrochemistry with values of the standard heterogeneous rate constant (k_s) estimated from electrochemical diffusion coefficients and ΔE_p (50 mVs^{-1}) of 3.4×10^{-3} $cm.s^{-1}$ (Rd) and 8.2×10^{-4} $cm.s^{-1}$ (Fd).

For a reversible electrochemical reaction, the potential of peak net-current corresponds to the redox potential of the system. At sufficiently low frequencies, quasi-reversible systems also give SW voltammograms approaching this reversible limit. The potentials of peak net-current (31 Hz) for rubredoxin and ferredoxin shift to more positive values on increasing the cation concentration in accord with increasing electrochemical reversibility. The limiting values (Table 4.3) are in

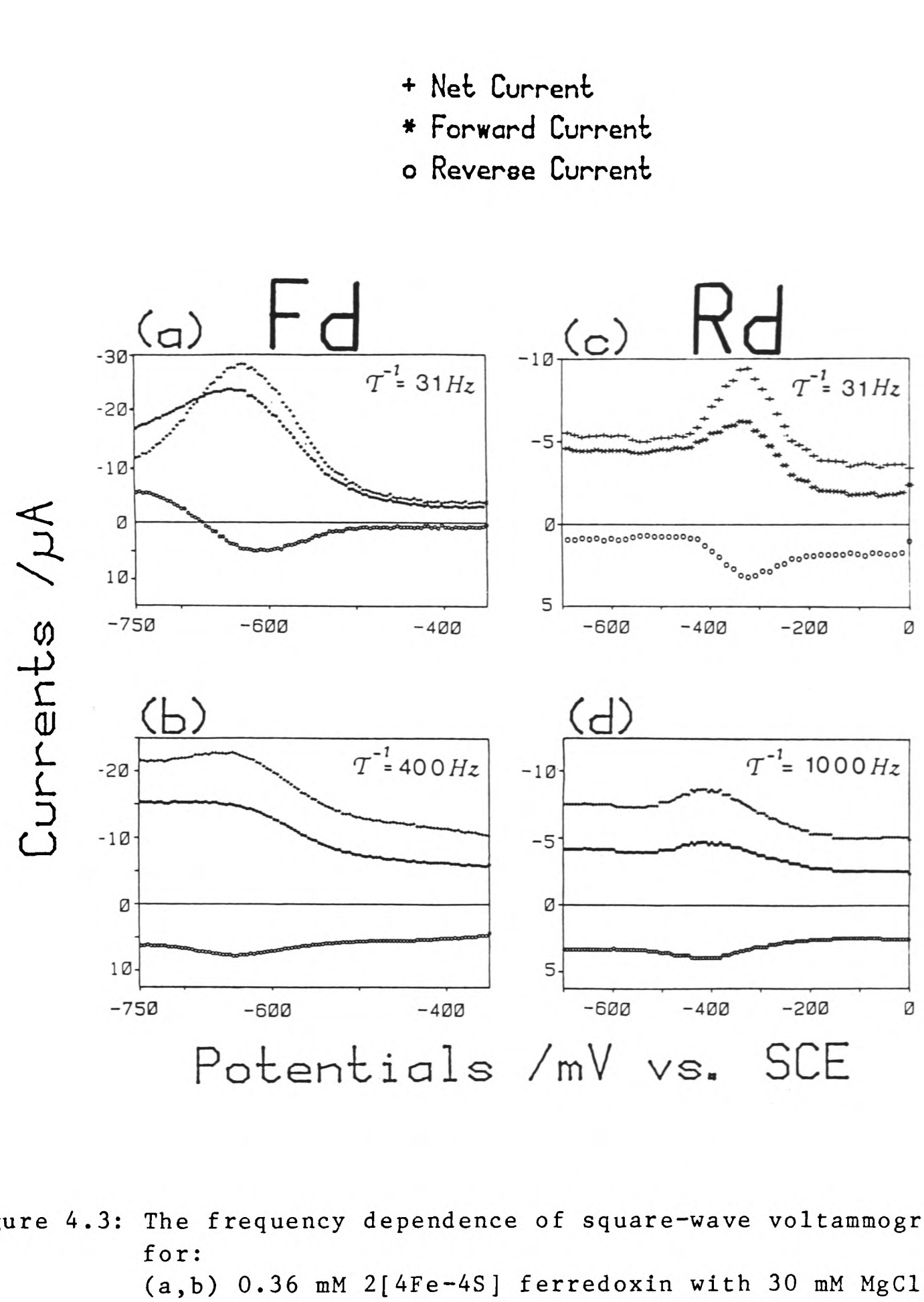

Figure 4.3: The frequency dependence of square-wave voltammograms for:
(a,b) 0.36 mM 2[4Fe-4S] ferredoxin with 30 mM $MgCl_2$.
(c,d) 0.17 mM rubredoxin with 40 mM $MgCl_2$.
Conditions as in Figure 4.1.

TABLE 4.3

Comparison of Electrochemically and Potentiometrically-Determined Redox Potentials for Small Redox Proteins

Protein	Electrochemical Redox Potential (mV vs. NHE)	Potentiometric Redox Potential (mV vs. NHE)
azurin	+323(pH 5.2)[a,j]	+360[b], +330[c]
rubredoxin	-74(pH 8.0)[d,j]	-57[e]
flavodoxin (semiquinone-hydroquinone	-318(pH 5.0)[d,j]	-328[f]
2[4Fe-4S] ferredoxin	-369(pH 8.0)[d,j]	-403[g], -371[h]
cytochrome c	+270(pH 8.0)[k,l]	+257[m]

a) 0.2 mM in 20 mM acetate, 100 mM NaCl; b) pH 5.0, calculated from kinetic data in ref. 29; c) pH 7.0, ref. 30; d) 0.2 mM protein in 20 mM buffer, 100 mM NaCl. $MgCl_2$ concentrations [mM] were rubredoxin [65], ferredoxin [60], and flavodoxin [32]; e) pH 7.0, ref. 31; f) calculated for pH 5.0 from data given in ref. 32; g) pH 7.0, ref. 33; h) calculated redox potential from pH dependence data, pK_{ox} = 7.4, pK_{red} = 8.9, ref. 34; j) SWV net current peak potential; k) from cyclic voltammogram; l) 0.2mM protein in 20 mM Tricine, 100 mM NaCl; m) pH 7.0, ref. 35.

satisfactory agreement with published potentiometric values.

Flavodoxin.

Flavodoxins contain one equivalent of tightly, but not covalently, bound FMN. The two one-electron reduction steps of the oxidised bound FMN (equation 4.1) have distinct potentials which also differ significantly from those of the free prosthetic group, Table 4.4. The consequence of the observed redox potential shifts is that whereas the conproportionation equilibrium of free FMN lies far to the left, addition of one reducing equivalent to flavodoxin produces predominantly the semiquinone.

$$FH + H^{+} \underset{E_2}{\overset{+e^{-}}{\rightleftharpoons}} FH_2^{\bullet} \underset{E_1}{\overset{+e^{-}}{\rightleftharpoons}} FH_2^{-} \underset{pK\,5.8}{\rightleftharpoons} FH_3 \qquad (4.1)$$

QUINONE NEUTRAL HYDROQUINONE

YELLOW SEMIQUINONE COLOURLESS

BLUE

TABLE 4.4.

	E_2	E_1	pH
	(mV vs. NHE)		
FMN	-0.238	-0.172	7
M. e. flavodoxin	-0.241	-0.328	5
	-0.175	-0.365	8

Square wave voltammetry carried out with fully oxidised M. elsdenii flavodoxin at pH 8.0 and pH 5.0 showed a strong response

due to free FMN with the expected pH shift (E vs. SCE -525 mV (pH 8.0), -377 mV (pH 5.0)), as illustrated in Figure 4.4(a). This faradaic response was variable. Additions of Mg^{2+} produced no significant change in the response although there was a marked increase in current as a function of electrode-solution contact time. This is likely to be due to progressive adsorption of FMN on the graphite electrode (36). It is not possible to prepare a flavodoxin solution free of FMN due to the equilibrium between free flavin and the non-covalently bound prosthetic group of the protein.

No electroactivity was discernible at redox potentials corresponding to one-electron reduction of the quinone form of the protein. The flavodoxin semiquinone radical form is conveniently generated in situ in the electrochemical cell by titration with one equivalent of NADPH in the presence of a catalytic amount of ferredoxin-NADP-reductase. The resulting solution shows no electroactivity at pH 8.0 corresponding to flavodoxin. At pH 5.0, the physiologically relevant semiquinone-hydroquinone redox potential is well-separated from that due to free FMN and re-oxidation of the semiquinone is minimised. Addition of Mg^{2+} to the solution under these conditions promotes well-defined direct electrochemistry (Figure 4.4(d,e)) with a peak potential close to the potentiometric redox potential (Table 4.3). The current responses evident at less negative potentials are due to 'free' FMN. Promotion profiles show a similar optimal Mg^{2+} level to that seen for ferredoxin and rubredoxin with a similar impersistence at sub-optimal cation levels. Trace cation-promoted electrochemistry corresponding to this couple is also discernible using solutions of the oxidised protein at pH 5.0.

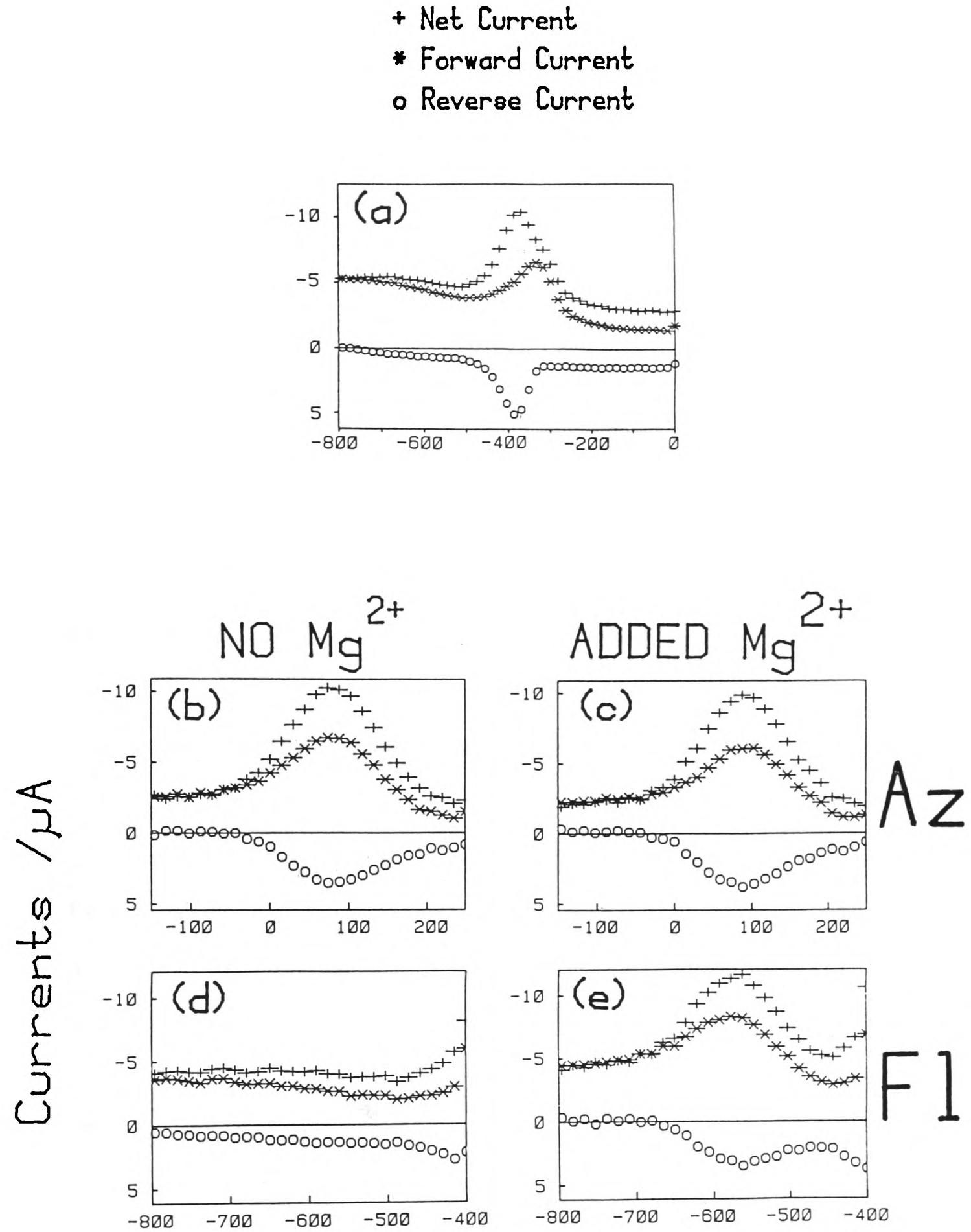

Figure 4.4: Square-wave voltammograms (frequency 31 Hz and amplitude (half peak-to-peak) 50 mV). (a) Flavodoxin (M. elsdenii, fully oxidised), 0.2 mM in 20 mM acetate, 100 mM NaCl, pH 5.0; (d) flavodoxin (semiquinone-hydroquinone), conditions as (a); (e) as (d), with the addition of 32 mM $MgCl_2$. (b) Azurin, 0.2 mM in 20 mM acetate, 100 mM NaCl, pH 5.2; (c) as (b), with the addition of 100 mM $MgCl_2$. Polished basal plane graphite electrode.

One explanation for the absence of a faradaic response corresponding to the quinone-semiquinone redox couple may be in terms of slower electron-transfer rates for this physiologically less relevant redox process (See Chapter 1).

Azurin.

In the case of azurin, direct electrochemistry (pH 5.5) is easily observable without the requirement for divalent cation promoters (Figure 4.4(b)) and addition of 100 mM $MgCl_2$ produces no meaningful change in current, although there is a ca. 10mV positive shift in redox potential (Figure 4.4(c)). Cyclic voltammetric peak separations (mV) at 10(50) mVs^{-1} were 87(122).

4.3.2 Divalent Cation Inhibition Effects: Cytochrome c.

In the absence of multivalent cations, i.e. in 0.1 M NaCl alone, cytochrome c readily undergoes direct electron-transfer at a polished basal plane pyrolytic graphite (Figure 4.5) (ΔE_p 90 mV, 20 mVs^{-1} (Scan 4)). However, the addition of $MgCl_2$ causes a profound inhibition of the electrochemistry.

4.3.3 Trivalent Cation Promotion Effects.

In view of the possible importance of electrostatic interactions in the interfacial region, it was of interest to investigate the effect of a trivalent cation ($Cr(NH_3)_6^{3+}$) on the direct electrochemistry of redox proteins. The particular advantages in the use of this trivalent cation are that it is not subject to base hydrolysis at neutral pH in aqueous solutions and is redox inactive over the potential region of interest. In addition, the substitution inertness of Cr(III) eliminates the

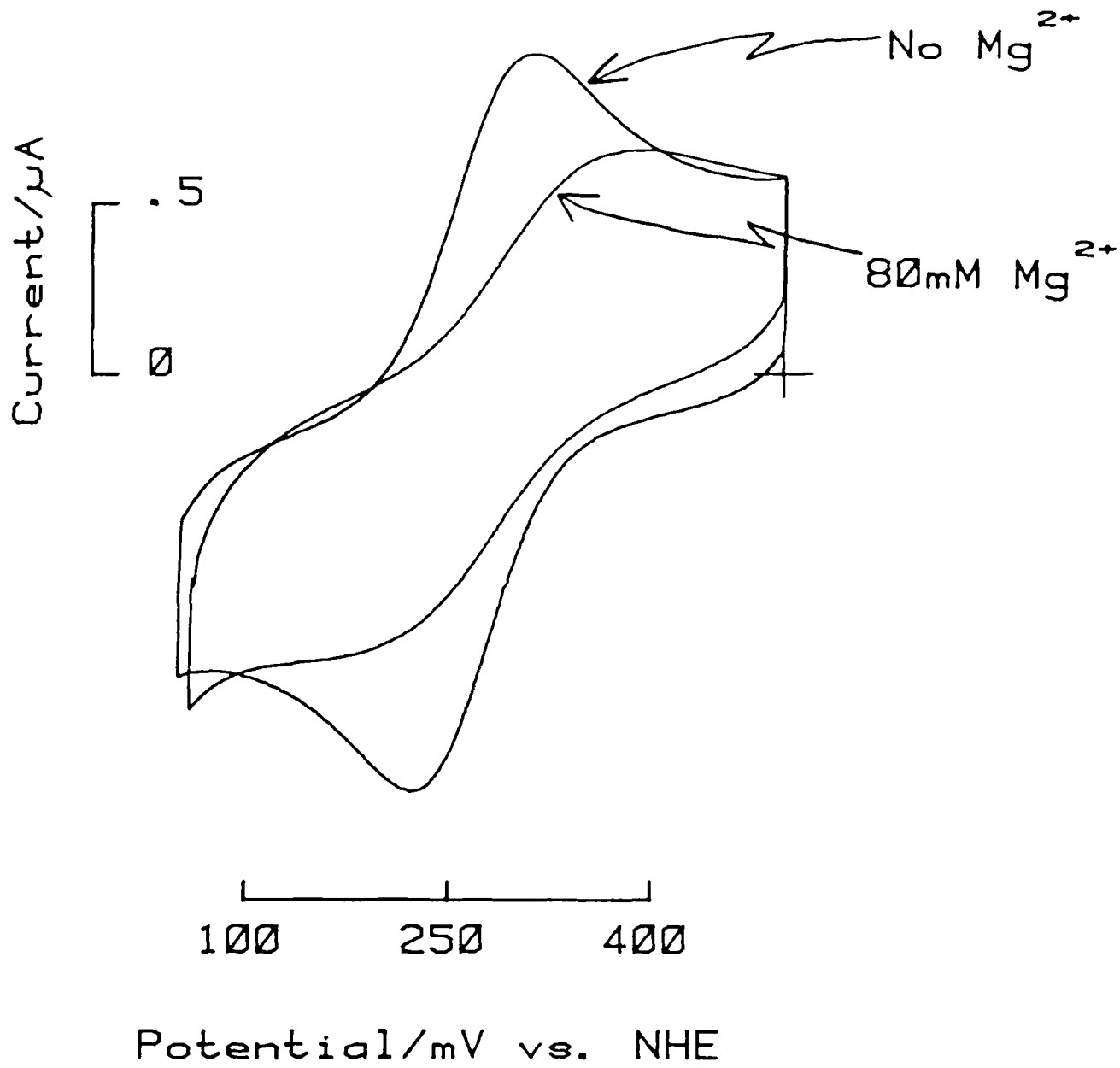

Figure 4.5: The effect of the addition of $MgCl_2$ on the cyclic voltammetry of cytochrome c (0.2 mM in 20 mM phosphate, 100 mM $NaClO_4$, pH 7.0). Polished basal plane pyrolytic graphite electrode. Scan rate 20 mVs^{-1}. Only the 4th voltammetric cycle is shown.

possibility of ligand exchange.

8Fe Ferredoxin, Rubredoxin and Flavodoxin.

Studies with $Cr(NH_3)_6^{3+}$ show this cation also to be an effective promoter of direct electron transfer for C. pasteurianum ferredoxin and rubredoxin, and D. vulgaris flavodoxin, Figure 4.6. A promotion profile for the 8Fe ferredoxin measured from SWV peak net currents showed that the concentration of $Cr(NH_3)_6^{3+}$ required to achieve optimal currents is 4 - 8 mM i.e. an order of magnitude lower than observed for Mg^{2+}.

Plastocyanin and Spinach [2Fe-2S] ferredoxin.

Both these proteins gave weak and poorly-defined faradaic responses in the presence of Mg^{2+}. The addition of $Cr(NH_3)_6^{3+}$ promoted well-defined faradaic responses at a polished basal plane pyrolytic graphite electrode. These proteins will be considered in detail in chapters 7 and 8.

4.4 Comparative Electrochemical Studies at the Edge and Cleaved Basal planes of Graphite.

The previous sections have established that the polished basal plane of pyrolytic graphite allows rapid direct electron transfer to a range of proteins, which encompass representatives of each of the major classes of redox proteins [Fe-S proteins (1Fe, 2Fe and 8Fe proteins), flavoproteins, cytochromes and copper proteins]. In the case of highly negatively-charged redox proteins, such as the Fe-S proteins, there is an additional requirement for multivalent cationic promoters. This was the first electrode surface to have such widespread success. It was

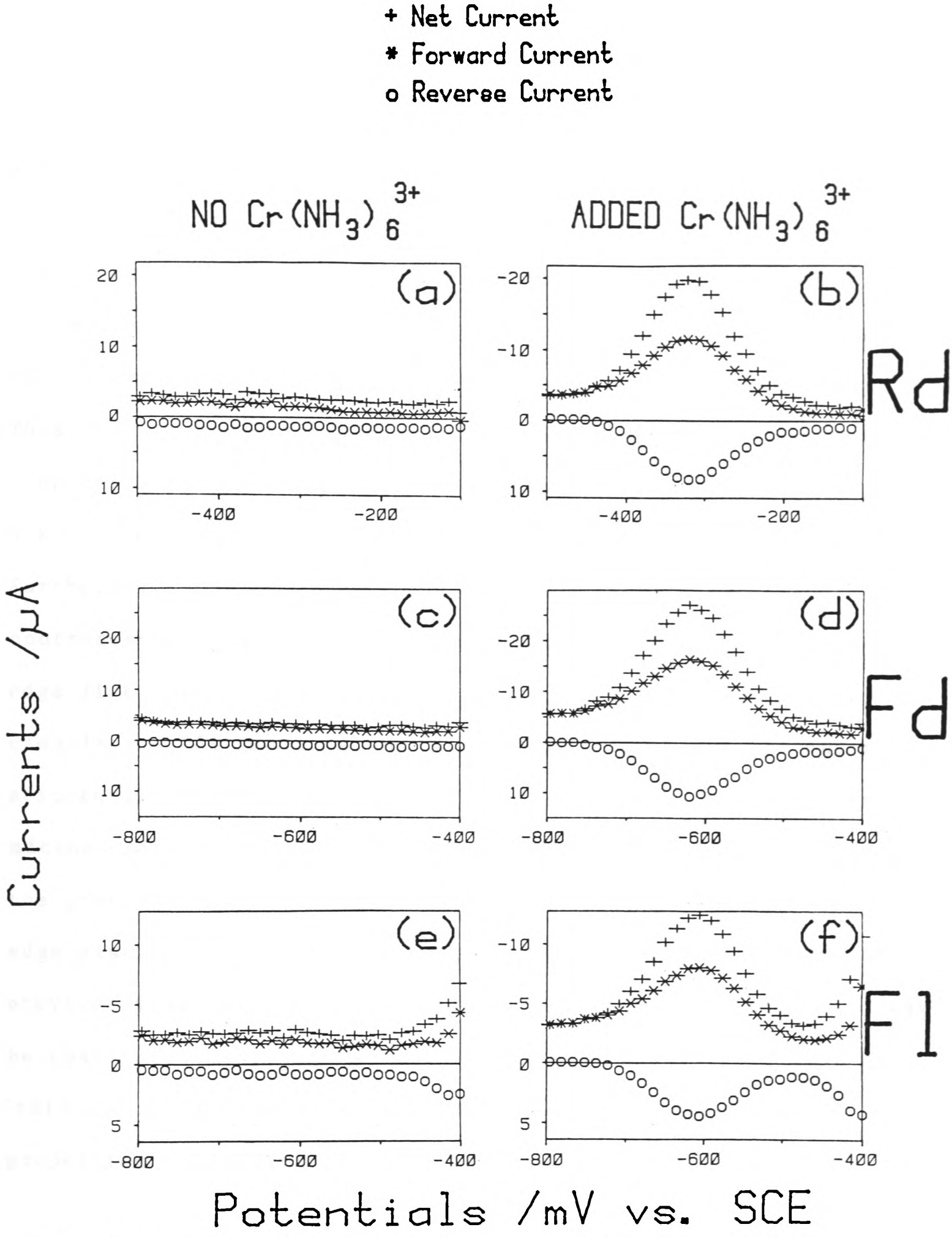

Figure 4.6: Square-wave voltammograms of C. pasteurianum rubredoxin (a,b) and ferredoxin (c,d), and D. vulgaris flavodoxin (semiquinone-hydroquinone) (e,f), showing the effect of adding 9 mM $Cr(NH_3)_6^{3+}$. Voltammograms were obtained with 0.2 mM protein in 20 mM buffer (ferredoxin, rubredoxin: Tricine, pH 8.0; flavodoxin: acetate, pH 5.0), 100 mM NaCl. Square-wave frequency 31 Hz and amplitude (half peak-to-peak) 50 mV. Polished basal plane pyrolytic graphite electrode.

important then, at this point, to pursue the characteristics of this electrode which confer this biological electron-transfer activity.

Pyrolytic graphite has a lattice structure which imparts high anisotropy to this material. The plane parallel to the layers is called the basal (a-b) plane, while the plane perpendicular to the layers is known as the edge (b-c) orientation, see Figure 4.10. These planes have highly-distinctive physical and electrochemical properties (37,38). For example, the electrical resistivity is 4×10^{-5} Ωcm in the (a-b) plane and 0.15 Ωcm in the (b-c) plane. Furthermore, the appearance of a freshly-cleaved basal surface contrasts markedly with that of an alumina-polished and sonicated edge disc. The basal surface has a grey mottled appearance with clearly visible 'nodules' on the surface. These are the chief structural characteristics of pyrolytic graphite resulting from microscopic growth cones formed at imperfections or particles on the graphite surface during deposition (39,40). The surface of an edge disc has a uniform black reflective finish, a feature not previously described in the extensive graphite literature. It may be that in polishing this surface the edge planes fold over or 'roll up' to produce an amorphous or glassy surface with properties resembling those of the polycrystalline material glassy carbon. However, it is interesting to note that pressure annealing of pyrolytic graphite at high temperatures (2800^{o}C) yields a graphite basal surface characterised by a similar mirror-like finish (41). Polishing the basal surface produces a more uniform surface with a grey reflective appearance.

The surface chemistry of pyrolytic graphite differs according to the direction under consideration. The basal surface

has valencies which are satisfied across the layer planes. However, the regular array of atoms within each plane is terminated abruptly at the edge surface, and the degree of coordination of those atoms at the edge must be different from those at the cleavage surface. The differing surface chemistry of these two planes is reflected in their electrocatalytic properties. Thus, there are marked differences in the hydrogen evolution reaction (42), the oxidation of peroxide (43) and the product distribution in electrosyntheses (44,45) at edge and cleaved basal plane electrodes. It has been proposed (25) that for direct electrochemistry of redox proteins to be achieved there must be a transient binding interaction between the redox protein and the electrode surface. In view of this hypothesis, it was important to exploit the anisotropy of pyrolytic graphite to probe the importance of specific protein-electrode interactions in direct electrochemical studies at this surface.

4.4.1 Cytochrome c.

The cyclic voltammograms of cytochrome c at edge and basal electrodes are quite different (Figure 4.7). At the edge electrode the response is reproducible with polishing, stable and well-defined; in contrast, the peak current recorded for the basal surface is at least 2-fold lower than at the edge and largely irreversible. At a scan rate of 20 mVs^{-1} peak separations were typically 60±5 and >150 mV respectively. A plot of cathodic peak current vs. square root of scan rate for the edge surface (see inset, Figure 4.7) was linear up to 100 mVs^{-1} and gave a diffusion coefficient of 5.0×10^{-7} cm^2s^{-1} based on the geometric area of the electrode surface. This value is in good agreement

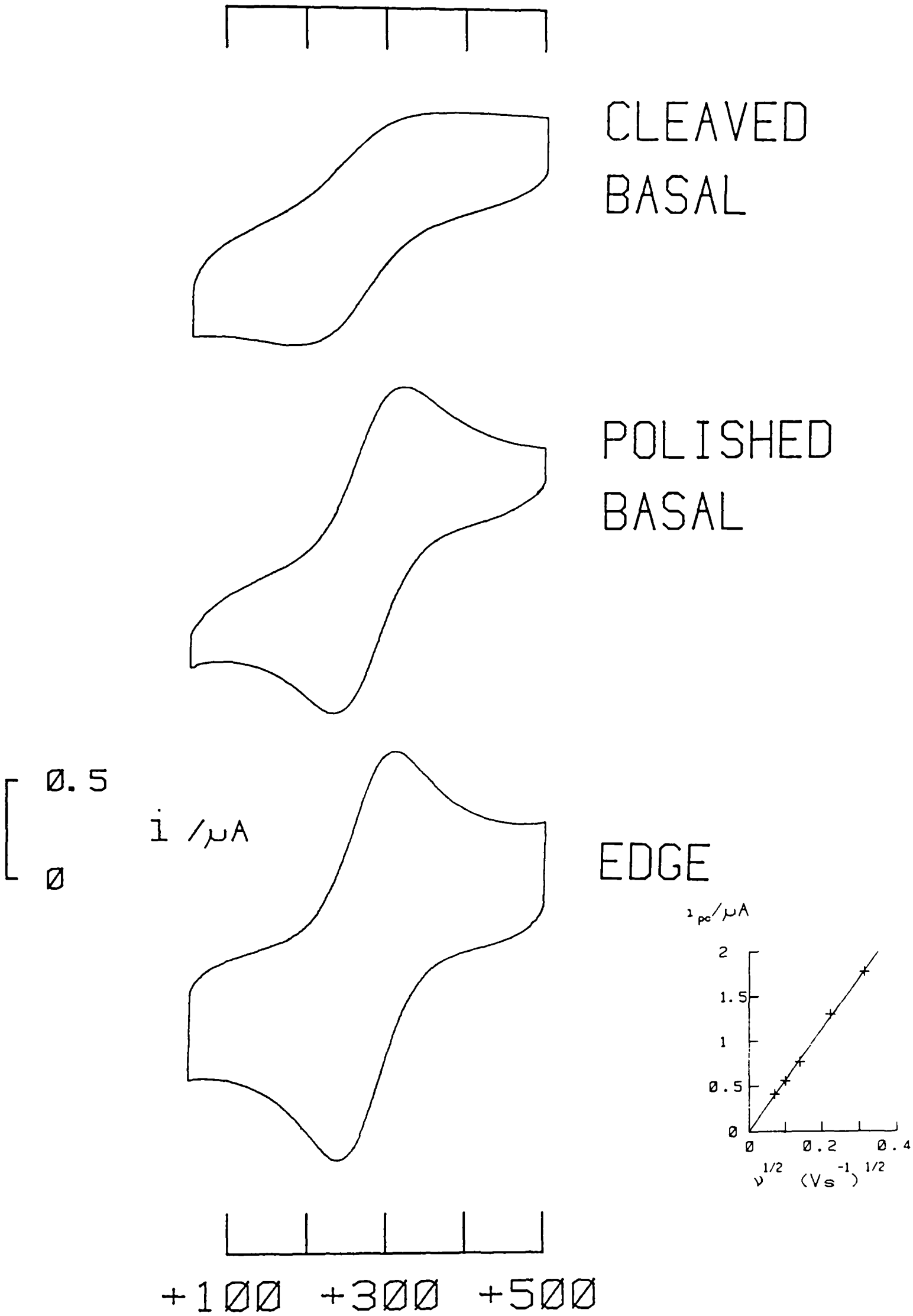

Figure 4.7: Cyclic voltammograms (scan 4: 20 mVs^{-1}) of cytochrome c at pyrolytic graphite electrodes. 0.15 mM protein in 5 mM Tricine, 100 mM NaCl, pH 8.0. A plot of cathodic peak current vs. $(\text{scan rate})^{1/2}$, for the edge surface, is also shown.

with the value (11×10^{-7} cm^2s^{-1}) determined by other methods (46,47). Cyclic voltammograms recorded at graphite electrodes in buffer alone show some residual surface activity (see Chapter 6) and it is possible that this, together with edge planes exposed on cleaving pyrolytic graphite, or at defects in the basal plane, may contribute to the residual electrochemistry at the basal plane. Indeed, polishing a basal surface generates a response intermediate between those recorded at edge and basal electrodes, although the response is less reproducible than at the edge (ΔE_p 70 - 90 mV at 20 mVs^{-1}) (Figure 4.7). Cyclic voltammograms recorded at a glassy carbon surface were indistinguishable from those recorded at the edge.

The observed peak separations may be used to estimate values for the standard heterogeneous rate constant for electron-transfer (k_s) at the two types of graphite surface. A typical value of k_s obtained for the edge surface is 4.5×10^{-3} $cm.s^{-1}$ whilst at the basal surface, k_s is estimated to be lower than 2.5×10^{-4} $cm.s^{-1}$.

4.4.2 2[4Fe-4S] Ferredoxin and Rubredoxin.

Electron-transfer rates are similarly enhanced for *C. pasteurianum* ferredoxin and rubredoxin at an edge-oriented electrode, Figure 4.8, although there is an additional requirement for the presence of multivalent cation promoters. A freshly cleaved basal surface in the **presence or absence of cations** shows only a weak, poorly-defined faradaic response often superimposed on a large tailing background. Typical peak separations (20 mVs^{-1}) observed at the edge in the presence of 4 mM $Cr(NH_3)_6^{3+}$ (100 mM NaCl) were 62.5 mV (67 μM 2[4Fe-4S] ferredoxin) and 67.5 mV (67 μM

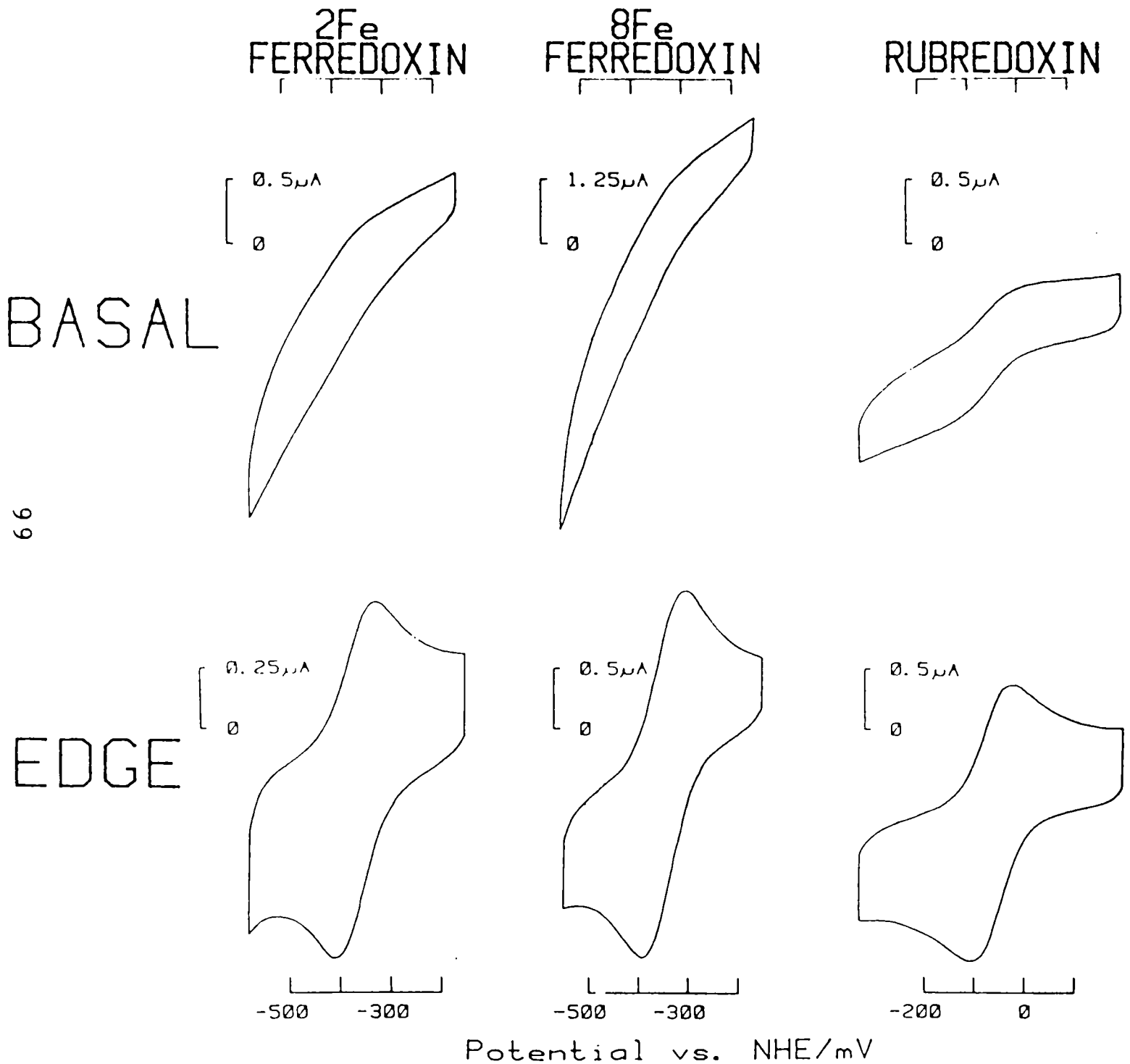

Figure 4.8:
Cyclic voltammograms (20 mVs^{-1}) of iron-sulphur proteins at cleaved basal and polished edge pyrolytic graphite electrodes.
5mM Tricine, pH 8.0.
Spinach [2Fe-2S] ferredoxin: 70 μM in 1 mM NaCl + 3 mM $Cr(NH_3)_6^{3+}$.
C. pasteurianum 2[4Fe-4S] ferredoxin: 100 μM in 100 mM NaCl + 6 mM $Cr(NH_3)_6^{3+}$.
C. pasteurianum rubredoxin: 67 μM in 100 mM NaCl + 8 mM $Cr(NH_3)_6^{3+}$.
Only the 4th voltammetric cycle is shown.

rubredoxin) with plots of cathodic peak current (i_{pc}) vs. square root of scan rate ($v^{1/2}$) linear up to at least 100 mVs^{-1}.

In a further study of the 2[4Fe-4S] ferredoxin under identical conditions (4 mM $Cr(NH_3)_6^{3+}$) the response at a glassy carbon surface was found to be less well-defined than at the edge, with ΔE_p now 87.5 mV at 20 mVs^{-1} and a plot of i_{pc} vs. $v^{1/2}$ showing marked deviations from linearity above 20 mVs^{-1}. This merely reflects a higher cation requirement for optimal electron-transfer rates at glassy carbon (and also polished basal) surfaces when compared to the edge. This is best illustrated by the responses observed in 100 mM NaCl background alone. Whilst no faradaic responses are discernible at glassy carbon and polished basal surfaces, the edge surface shows significant electrochemical activity with an impersistent, largely irreversible response (see Chapter 7).

4.4.3 Spinach 2Fe-2S ferredoxin and plastocyanin.

Under optimal cation conditions at the edge, the faradaic responses of these redox proteins are poorly defined at a cleaved basal plane electrode. This is illustrated in Figure 4.8 for the 2Fe ferredoxin alone, the response of plastocyanin at the basal plane being complicated by surface redox processes.

4.4.4 Azurin.

Electrochemical studies on azurin (pH 5.5 and 8.0) show that this protein is the least surface-selective of all redox proteins studied. Direct electrochemistry is observed at Au electrodes surface-modified with organic promoters [e.g. bis(4-pyridine)bisulphide (Au: Figure 4.9(a)) or 2-(pyridinylmethylene)

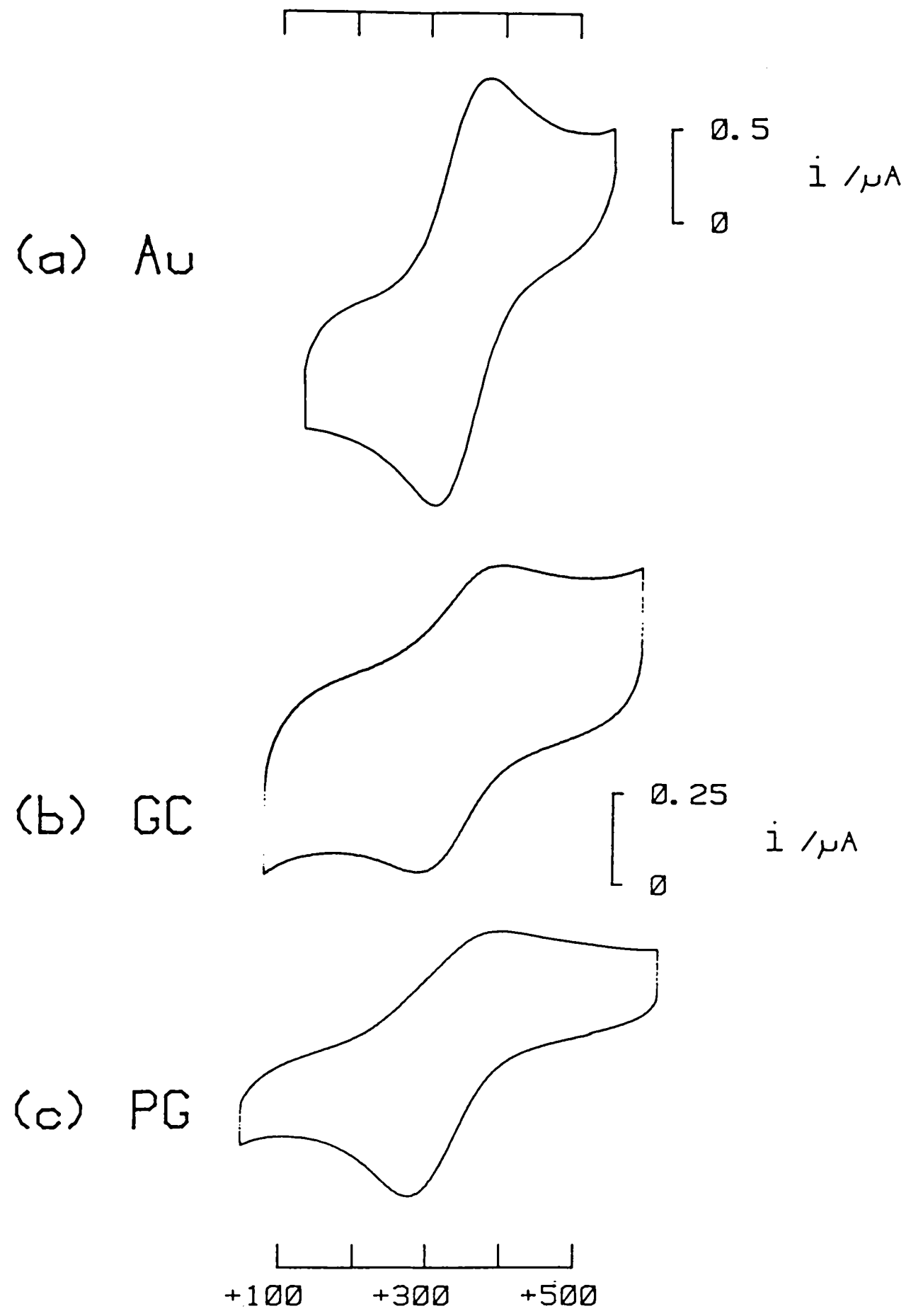

Figure 4.9 : Cyclic voltammograms (20 mVs^{-1}; cycle 4) of azurin at a range of electrode surfaces:
(a) a gold electrode surface-modified with bis(4-pyridyl)bisulphide. 0.2 mM azurin in 20 mM acetate, 100 mM NaCl, pH 5.4.
(b) alumina-polished glassy carbon. 50 μM azurin in 5 mM acetate, 100 mM NaCl, pH 5.5.
(c) alumina-polished pyrolytic graphite (basal plane). Conditions as in (b)

hydrazinecarbothioamide (Chapter 12)], glassy carbon (GC: Figure 4.9(b)), edge graphite, polished basal graphite (PG: Figure 4.9(c)) and cleaved basal plane graphite electrodes, with no effect of added multivalent cations. The observed faradaic responses are more reversible at non-graphitic electrodes (ΔE_p at 20 mVs^{-1}, pH 5.5: 87.5 mV (GC), 72.5 mV (Au), ca. 100 mV (PG)) where the responses tend to be dominated by diffusion-controlled processes. Electrochemistry at graphite typically gives asymmetric cyclic voltammograms particularly at low (<100 μM) protein concentrations, behaviour characteristic of weak adsorption, and is complicated by overlapping 'surface' redox processes especially at high scan rates. However, the responses at polished edge surfaces appear to be more reversible than those observed at cleaved basal plane surfaces.

4.4.5 $Fe(CN)_6^{3-}$ and $Ru(NH_3)_6^{3+}$.

The response of two small inorganic reagents as marker 'probes' for positively-charged cytochrome c ($Ru(NH_3)_6^{3+}$) and negatively-charged proteins e.g. ferredoxin ($Fe(CN)_6^{3-}$) was assessed. For ($Ru(NH_3)_6^{3+}$), electron-transfer rates were essentially identical at both edge and cleaved basal plane surfaces in the presence or absence of multivalent cations (ΔE_p = 60 mV for 0.05 - 0.5 mM $Ru(NH_3)_6^{3+}$, 0 - 120 mM $MgCl_2$, in 5 mM Tricine, 100 mM NaCl pH 8.0). The response of $Fe(CN)_6^{3-}$ at the edge parallels that of ferredoxin in that multivalent cations are required to promote the faradaic response. However, the overall cation requirements (1 mM $MgCl_2$) to optimise the electron-transfer rate (i_{pc} = 0.67 μA, ΔE_p<70 mV, 20 mVs^{-1}) for 50 μM $Fe(CN)_6^{3-}$ (in 5 mM Tricine, 100 mM NaCl, pH 8.0) are significantly lower than

those required for a comparable concentration of ferredoxin (see Chapter 7). Interestingly, the response at a cleaved basal plane electrode is also promoted by the addition of multivalent cations, although the optimal peak separation (ΔE_p = 100 mV at 20 mVs^{-1}, 5 mM $MgCl_2$) and peak current (0.53 μA) indicate a similar, although less marked, contrast in electrochemical reactivity at edge and basal surfaces to that seen for redox proteins.

4.5 Discussion.

An investigation of the electrochemical response of representative redox proteins shows that, with appropriate 'tuning' of solution conditions, quasi-reversible (unmediated) faradaic responses of Fe-S proteins (bacterial 8Fe ferredoxin, plant-type 2Fe ferredoxin and rubredoxin), a flavoprotein (flavodoxin), copper proteins (azurin and plastocyanin) and a cytochrome (cytochrome c) may be readily observed at alumina-polished pyrolytic graphite electrodes. For those proteins carrying a high net negative charge at pH 8.0 (ferredoxin, rubredoxin and flavodoxin) direct electrochemistry may be readily observed following the addition of multivalent cations (Mg^{2+}, $Cr(NH_3)_6^{3+}$) to a solution with a high background level of NaCl (100 mM). By contrast, a redox protein with a high net positive charge at pH 8.0 (cytochrome c) undergoes ready direct electrochemistry in the absence of multivalent cations (100 mM NaCl alone) but this faradaic response is inhibited upon addition of Mg^{2+}. The copper protein azurin carries only a small (ca. 3-) negative charge at pH 8.0 and, as such, the observed faradaic response is insensitive to the presence or absence of multivalent

cations. This is also consistent with the crystal structure which shows (48) extensive charge pairing among side chains. In general, therefore, it appears that due consideration of the net charge of a redox protein provides a basis for controlling electronic communication between the redox protein and a polished graphite electrode, based upon the presence or absence of multivalent cations.

The results in this chapter also clearly show that the electrochemical reactivity of a wide range of redox proteins is critically dependent upon the nature of the carbon surface. Without exception, all proteins examined show weak, largely irreversible electrochemical responses at the cleaved basal plane of pyrolytic graphite. To improve electrochemical reversibility, it appears that an important step is to increase the availability of edge orientation. Previous investigations have focussed mainly upon the basal plane of pyrolytic graphite, or glassy carbon, and attempted to enhance the density of edge sites through chemical (49), electrochemical (50), thermal (51) and plasma treatments (52). However, the results presented here have shown that routine polishing of an edge-oriented pyrolytic graphite electrode in air is sufficient to generate a reproducible surface at which electron-transfer rates for a wide range of redox proteins may be easily optimised. Polishing of the basal plane can result in a surface that yields electrochemistry comparable to that at the edge orientation, but the response is less reproducible and for negatively-charged proteins, overall cation requirements are higher. Similarly, cation requirements are found to be higher at a glassy carbon surface.

The observed dependence of cation requirement upon protein

charge is consistent with a protein-electrode interaction in which an electrostatic contribution is a dominant factor. In accord with this proposal the level of multivalent cations required to regulate faradaic responses is a function of cation charge $M^{3+} > M^{2+} > M^{+}$. On these grounds it would appear that a polished graphite electrode carries a net negative charge in the potential domain ca. +273 mV vs NHE (cytochrome c) to ca. -373 mV vs. NHE (8Fe ferredoxin). This is in satisfactory agreement with estimates of potentials of zero charge for oxidised graphite dust (+160 to +200 mV vs. NHE) (38).

The basal plane of standard pyrolytic graphite used in this study approximates to a regular extended aromatic array. This surface clearly has a hydrophobic character. A cleaved basal plane electrode is very difficult to wet and can be drawn out of aqueous solution to give a surface with an apparent absence of liquid film or droplets. The hydrophobic character of this surface is also evident from the contact angle (83.9^{o}) of a stress-annealed pyrolytic graphite basal plane (53).

The effect of polishing an edge or cleaved basal plane surface with an alumina slurry will be to re-surface the electrode through grinding. The grinding mechanism clearly removes carbon, as evidenced by the substantial grey discoloration of alumina slurries after polishing, and so must rupture strong in-plane C-C bonds. As a consequence of the increase in surface energy and the heat released in breaking bonds, disrupted aromatic arrays may react spontaneously with water or atmospheric oxygen at the plane edges to produce a variety of surface C-O groups, as illustrated in Figure 4.10. These may include quinones, carboxylic acids, phenols and ethers.

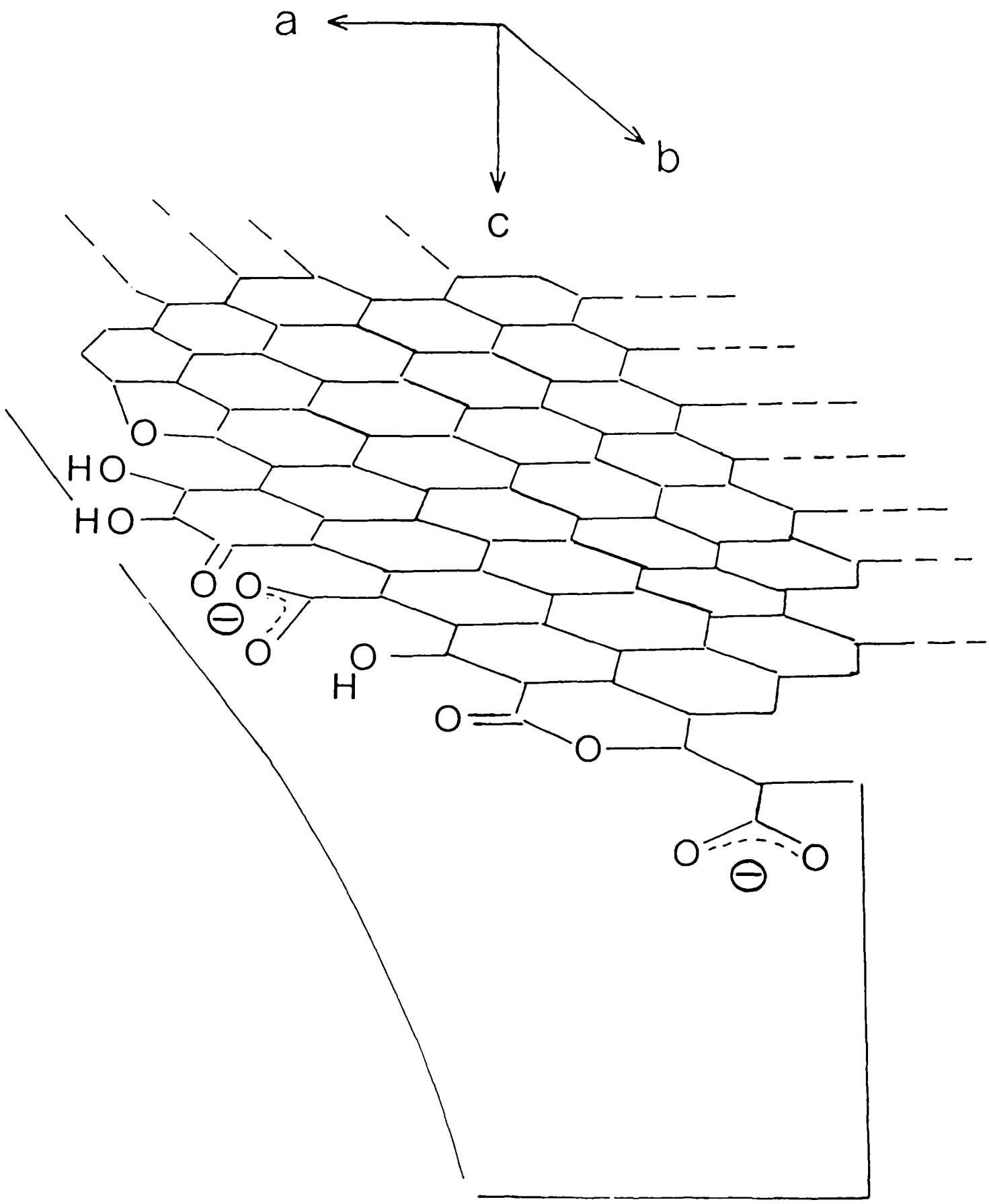

Figure 4.10: Schematic representation of the structure of pyrolytic graphite showing surface C-O groups formed at edge planes.

This is in accord with previous work on microcrystalline carbon blacks and graphite dust (54,55). Oxidation of these surfaces by chemical or thermal pretreatments produces acidic surfaces which may be neutralised by titration with various bases. It is clear that this acidity arises from surface oxygen-containing functional groups, in that CO and CO_2 are evolved on evacuating these oxidised powders. The presence of these surface oxides confers considerable hydrophilicity on the surface. Oxidised carbon blacks disperse spontaneously in water giving very stable suspensions, hence, part of the surface must include strongly hydrophilic groups. That this region of the surface is located at edge planes is clearly demonstrated by the observation that an edge graphite electrode surface is readily wetted by aqueous solutions, and by the decrease in the amount of oxygen fixed by oxidised carbon blacks as the degree of graphitisation increases. Clearly there is definite evidence that oxidised graphite forms chemically detectable, hydrophilic C-O functions at edge planes. The direct electrochemistry of redox proteins is catalysed at the edge surface indicating the importance of these surface functional groups in direct electrochemical studies.

A polished graphite surface may be substantially disordered and may include regions of predominantly basal plane character (non-polar, hydrophobic), regions of acidic 'edge' character bearing C-O functional groups (polar, hydrophilic) and regions with embedded alumina particles. The density of edge sites generated simply by grinding a basal plane will be random and will depend particularly on the pressure applied during polishing. This is consistent with the poor reproducibility and considerable scatter of experimental points seen in the initial

Mg^{2+} titrations at polished basal plane graphite (Figure 4.2).

The acidity of surface oxides produced by polishing may account for the observation of electrostatic contributions to the direct electrochemistry of charged redox proteins. Surface oxides bearing discrete negative charges ($-CO_2^-$) or dipolar character (C=O) may provide a negatively-charged binding domain for a positively-charged redox protein such as cytochrome c. More specifically, surface oxides may bind to the lysine residues around the haem crevice on cytochrome c through salt bridges or hydrogen bonds. This hypothesis is supported by a similar conclusion reached on the basis of a survey (56) of the ability of fifty-four bifunctional organic compounds to act as surface modifiers for the direct electrochemistry of cytochrome c at Au electrodes. Similarly, a potentiometric proton titration (57) of a cytochrome c analogue, bovine pancreas ribonuclease (RNase: pI = 9.2), which has 10 lysine residues, adsorbed on negatively-charged (sulphonato) polystyrene particles suggests the formation of 3 protein($-NH_3^+$)...(^-O_3SO)latex ion-pairs. These results provide a striking analogy with the interaction between cytochrome c and its natural redox partners. This interaction is suggested to be electrostatic in nature (see Chapter 1) involving complementary charge-pair interactions between the lysine groups on cytochrome c and carboxylate residues on cytochrome oxidase, cytochrome b_5 or cytochrome c peroxidase. X-ray crystallographic studies have identified a ring of negatively-charged carboxylates surrounding the haem crevice of both cytochrome b_5 and cytochrome c peroxidase that is complementary to a ring of positively-charged lysines on cytochrome c. Similarly, using a water-soluble carbodiimide, Millet et. al. (58) have identified a ring of four carboxylate

groups on cytochrome oxidase important in binding cytochrome c.

The electron-transfer reactions of photosynthesis take place at and across the complex inner membrane (thylakoid) of the chloroplast. The average net negative charge on the surface of this membrane may be largely due to carboxyl groups of exposed segments of integral membrane protein complexes (59). The efficiency of electron donation between negatively-charged extrinsic redox proteins and membrane proteins, in isolated chloroplast thylakoid membrane fragments, depends (60) on the presence or absence of divalent cations. Addition of 20mM $MgCl_2$ greatly enhances the efficiency of electron-donation from plastocyanin (negatively-charged) to the $P700^+$ reaction centre but severely inhibits electron-transfer to $P700^+$ from the non-physiological partner cytochrome c (positively-charged). This general regulation of in vitro photosynthetic phenomena by Mg^{2+} makes striking analogies with the ability of Mg^{2+} to promote or inhibit electrochemical responses at polished graphite electrodes. However, it must be noted that Mg^{2+} may be irrelevant (61,62) to heterogeneous processes at intact membranes in vivo where protonation and phosphorylation of internal membrane surfaces may regulate charge interactions.

Barber (63) has proposed that general diffuse layer effects and specific binding interactions may be of significance in relation to the cation control of photosynthetic phenomena. Similarly, the role of cations in direct electrochemical studies at polished graphite may involve general diffuse layer 'screening' of a negative surface potential arising from acidic surface oxides, or more specific interactions involving cation-protein association (ion-pairing) or charge neutralisation

through adsorption or binding of cations at the electrode surface. Additionally, intermolecular electrostatic interactions between adjacent protein molecules at the electrode surface may be influenced by the presence of multivalent cations. In accord with these proposals radio-tracer experiments (64) have shown that the adsorption of a negatively-charged protein, human plasma albumin (HPA), at a negatively-charged polystyrene latex is accompanied by the co-adsorption of cations such as Ba^{2+} or Mn^{2+}. The various possible interactions are illustrated schematically in Figure 4.11.

An intriguing proposal is that there may be polydentate Mg^{2+}-carboxylate chelation resulting in close apposition of protein and electrode surfaces through a trans protein($-CO_2^-$)...Mg^{2+}...($^-O_2C-$)electrode complex. This proposal is in keeping with the preferred coordination of Mg^{2+} to oxygen ligands in aqueous solution. However, the increased efficiency of substitution inert trivalent cationic complexes over divalent cations suggests that electrostatic influences may predominate over specific chemical effects in a protein-electrode 'bridge'. Electrostatic bridges of a similar nature have been proposed in studies of HPA at the negatively-charged (sulphonato) polystyrene latex particles (64) and in the polycation-induced fusion of acidic phospholipid vesicles (12).

The importance of 'screening' and binding interactions with respect to cation regulation of direct electrochemical responses at pyrolytic graphite will be examined at length in Chapter 7.

Attention has been previously drawn to the possible

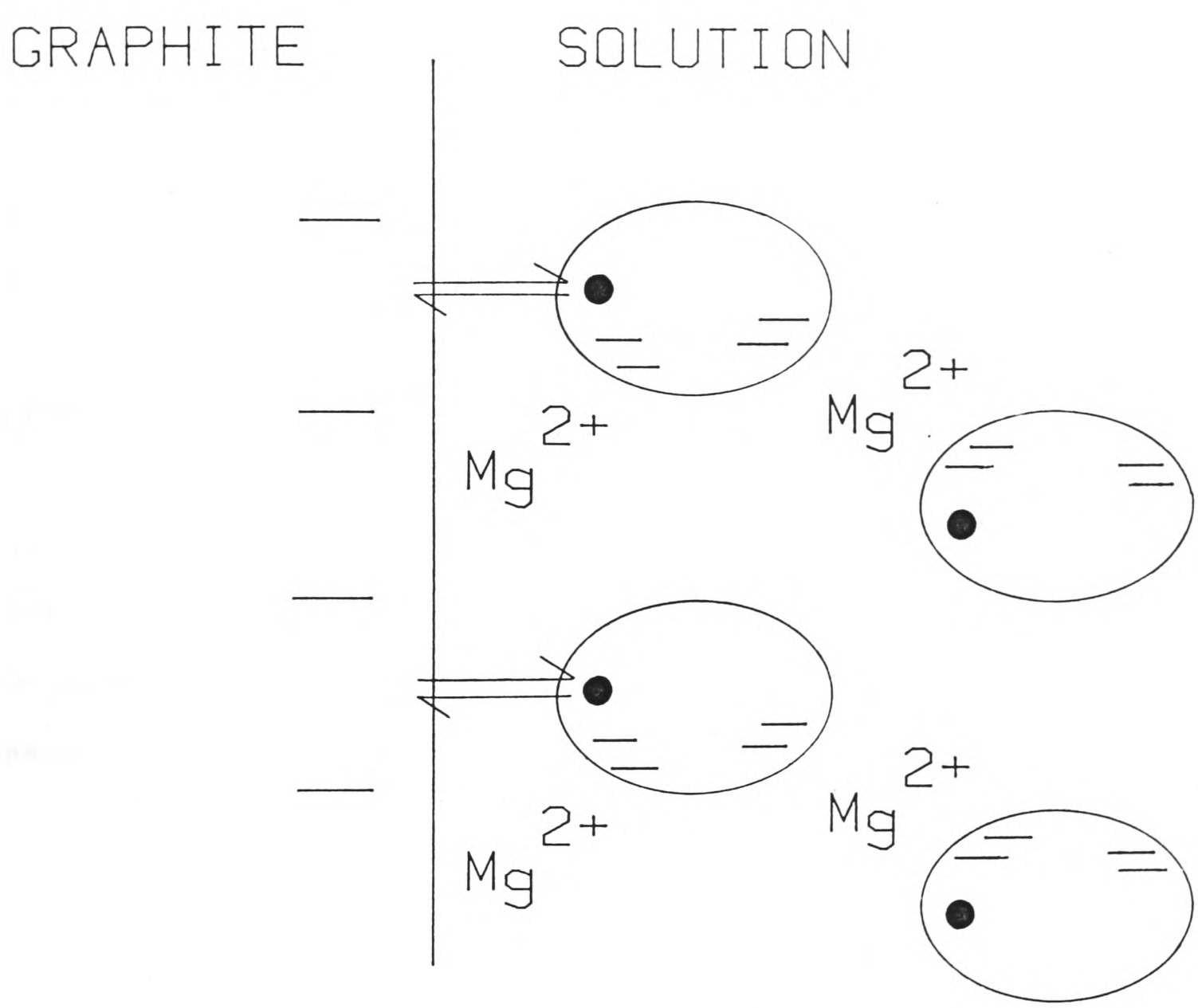

Figure 4.11 : A schematic model for the role of divalent cations in promoting the direct electrochemistry of negatively-charged redox proteins.

importance of hydrophobic interactions for azurin by Adman et. al. (48) and Norris et. al. (65) on the basis of a conserved area of hydrophobic residues around the copper ligand, His-117, and due to the packing of individual molecules within the unit cells of azurin from both Pseudomonas aeruginosa and Alcaligenes denitrificans, such that interactions between this region on different molecules are maximised. The absence of cation sensitivity in direct electrochemical studies of azurin may be consistent with hydrophobic binding interactions at regions of predominantly hydrophobic, non-polar character on the polished graphite surface. However, azurin shows a clear preference for hydrophilic (edge) over hydrophobic (basal) electrode surfaces. This may reflect a favourable interaction between the solvation 'sheath' of the protein (at sites distant from the hydrophobic patch) and the solvent structure at the hydrophilic edge surface.

References - Chapter 4

1) Yeh, P. and Kuwana, T., Chem. Lett. 1145, (1977).

2) Eddowes, M. J. and Hill, H. A. O., J. Chem. Soc. Chem. Commun. 771, (1977).

3) Landrum, H. L., Salmon, R. T. and Hawkridge, F. M., J. Am. Chem. Soc. 99, 3154, (1977).

4) Armstrong, F. A., Hill, H. A. O. and Walton, N. J., FEBS Lett. 145, 241, (1982).

5) Hol, W. G. J., Halie, L. M. and Sander C., Nature 294, 532, (1981).

6) Perutz, M. F. and Raidt, H., Nature 255, 256, (1975).

7) Getzoff, E. D., Tainer, J. A., Weiner, P. K., Kollman, P. A., Richardson, J. S. and Richardson, D. C., Nature 306, 287, (1983).

8) Matthew, J. B., Weber, P. C., Salemme, F. R. and Richards, F. M., Nature 301, 169, (1983), and references therein.

9) Butler, P. J. G. and Klug, A., Sci. Am. 239, 52, (1978).

10) Foust, G. P., Mayhew, S. G. and Massey, V., J. Biol. Chem. 244, 964, (1969).

11) Lehninger, A. L. Biochemistry. New York: Worth (1970).

12) Gad, A. E., Silver, B. L. and Eytan, G. D., Biochim. Biophys. Acta 690, 124, (1982).

13) Barber, J. and Chow, W. S., FEBS Lett. 105, 5, (1979)

14) Barber, J. and Searle, G. F. W., FEBS Lett. 92, 5, (1978).

15) Wojtczak, L. and Nalecz, M. J., Eur. J. Biochem. 94, 99, (1979).

16) Laing, W. A., Stitt, M. A. and Heldt, H. W., Biochim. Biophys. Acta 637, 348, (1981).

17) Harnischfeger, G. and Shavit, N., FEBS Lett. 45, 286, (1974).

18) Takabe, T., Ishikawa, H., Niwa, S. and Itoh, S., J. Biochem. 94, 1901, (1983).

19) Sandri, G., Suranyi, E., Eriksson, L. E. G., Westman, J. and Ernster, L., Biochim. Biophys. Acta 723, 1, (1983).

20) Shahak, Y., FEBS Lett. 145, 223, (1982).

21) Akerlund, H. A., Andersson, B., Persson, A. and Albertsson, P. A., Biochim. Biophys. Acta 552, 238, (1979).
22) Ericson, I., Biochim. Biophys. Acta 356, 100, (1974).

23) Gibrat, R. and Grignon, C., Biochim. Biophys. Acta 692, 462, (1982).

24) Fisher, R. A., Putt, W. and Harris, H., Ann. Hum. Genet. (London) 40, 371, (1977).

25) Eddowes, M. J. and Hill, H. A. O., Biosci. Reports 1, 521, (1981).

26) Elliott, D., Part II Thesis. Oxford (1985).

27) Boehm, H. P., Adv. in Catalysis 16, 198, (1966).

28) Oppegard, A. L. and Bailar, J. C. in: Inorg. Syntheses, Audrieth, L. F. ed. New York: McGraw-Hill, 3, 153, (1950).

29) Lappin, A. G., Segal, M. G., Weatherburn, D. C., Henderson, R. A. and Sykes, A. G., J. Am. Chem. Soc., 101, 2302, (1979).

30) Sailasuta, N., Anson, F. C. and Gray, H. B., J. Am. Chem. Soc. 101, 455, (1979).

31) Lovenberg, W. and Sobel, B. E., Proc. Natl. Acad. Sci. U.S.A. 54, 193, (1965).

32) Mayhew, S. G., Foust, G. P. and Massey, V., J. Biol. Chem. 244, 803, (1969).

33) Stombaugh, N. A., Sundquist, J. E., Burris, R. H. and Orme-Johnson, W. H., Biochemistry, 15, 2633, (1976).

34) Magliozzo, R. S., McIntosh, B. A., Sweeney, W. V., J. Biol. Chem. 257, 3506, (1982).

35) Hawkridge, F. M. and Kuwana, T., Anal. Chem. 45, 1021, (1973).

36) Gorton, L. and Johansson, G., J. Electroanal. Chem. 113, 151, (1980).

37) Spain, I. L., Ubbelohde, A. R. and Young, D. A., Philos. Trans. R. Soc. (London) 262A, 345, (1967).

38) Randin, J. P. in: Encyclopedia of Electrochemistry of the Elements. Bard, A. J., ed. New York: Marcel Dekker, 7, 1, (1976).

39) Panzer, R. E. and Elving, P. J., Electrochim. Acta 20, 635, (1975).

40) Wieck, H. J., Antrim, R. F., Yacynch, A. M. and Greenhut, V. A., Analyst 8, 951, (1982).

41) Ubbelohde, A. R., Young, D. A. and Moore, A. W., Nature 198, 1192, (1963).

42) Brennan, M. P. J. and Brown, O. R., J. App. Electrochem. 2, 43, (1972).

43) Morcos, I. and Yeager, E., Electrochim. Acta 15, 953, (1970).

44) Brennan, M. P. J. and Brettle, R., J. Chem. Soc., Perkin Trans. I, 257, (1973).

45) Firth, B. E., Miller, L. L., Mitani, M., Rogers, T., Lennox, J. and Murray, R. W., J. Am Chem. Soc. 98, 8271, (1976).

46) Theorell, H., Biochem. Z. 285, 207, (1936).

47) Ehrenberg, A., Acta Chem. Scand. 11, 126, (1957).

48) Adman, E. T. and Jensen, L. H., Isr. J. Chem. 21, 8, (1981).

49) Taylor, R. J. and Humffray, A. A., J. Electroanal. Chem. 42, 347, (1973).

50) Wightman, R. M., Palk, E. C., Borman, S. and Dayton, M. A., Anal. Chem. 50, 1411, (1978).

51) Stutts, K. J., Kovach, P. M., Kuhr, W. G. and Wightman, R. M., Anal. Chem. 55, 1632, (1983).

52) Evans, J. F. and Kuwana T., Anal. Chem. 49, 1632, (1977).

53) Morcos, I., J. Chem. Phys. 57, 1801, (1972).

54) Boehm, H. P., Diehl, E., Heck, W. and Sappok, R., Angew. Chem., Internat. Edit. Engl. 3, 669, (1964).

55) Donnet, J. B., Carbon 6, 161, (1968).

56) Allen, P. M., Hill, H. A. O. and Walton, N. J., J. Electroanal. Chem. 178, 69, (1984).

57) Norde, W. and Lyklema, J., J. Coll. Interf. Sci. 66, 266, (1978).

58) Millett, F., de Jong, C., Paulson, L. and Capaldi, R. A., Biochemistry, 22, 546, (1983).

59) Nakatani, H. Y., Barber, J. and Forrester, J. A., Biochim. Biophys. Acta 504, 215, (1978).

60) Davis,D. J., Krogmann, D. W. and San Pietro, A., Plant Physiol. 65, 697, (1980).

61) Williams, R. J. P., Biochim. Biophys. Acta 505, 1, (1978).

62) Hodges, M., Packham, N. K. and Barber, J., FEBS Lett. 181, 83, (1985).

63) Barber, J., Biochim. Biophys. Acta 594, 253, (1980).

64) van Dulm, P., Norde, W. and Lyklema. J., J. Coll. Interf. Sci. 82, 77, (1981).

65) Norris G. E., Anderson, B. F. and Baker, E. N., J. Mol. Biol. 165, 501, (1983).

CHAPTER 5

X-RAY PHOTOELECTRON SPECTROSCOPIC STUDIES OF PYROLYTIC GRAPHITE SURFACES

5.1 Introduction.

In chapter 4, well-behaved direct electrochemistry of a range of redox proteins was observed by the use of pyrolytic graphite electrodes, with appropriate 'tuning' of solution conditions. Through exploiting the anisotropy of this material, distinct differences in electrochemical reactivity can be observed, which show that the most effective surface, in terms of the reproducibility and reversibility of electrochemical responses, is that provided by edge-oriented electrodes. This has led to the proposal that interactions between proteins and carbon electrodes are critically dependent upon the generation of an, as yet, ill-defined surface containing C-O functional groups. This chapter utilizes high-energy photoelectron spectroscopy to observe the differences that exist in the chemistry of the edge-oriented and basal plane electrodes used in direct electrochemical studies, with a view to developing a better understanding of the protein-electrode interaction.

Evidence for the existence and chemical nature of surface functional groups at carbonaceous surfaces is usually obtained by indirect methods of investigation. Thus, techniques such as acid-base titrations (1), specific chemical identification through normal procedures of organic synthesis (2), differential capacitance (3), electrochemistry (4), and specular reflectance (5) have been applied to carbon and graphite surfaces. The most informative studies have been those examining the chemical

reactivity of activated carbons, carbon blacks and graphite dust. The results of these studies are summarised in several excellent reviews (1,2,6). However, there are only a few detailed investigations of pyrolytic graphite because of the small available surface area and the ensuing difficulties in analysing small quantities of C-O groups.

A small number of direct spectroscopic investigations of carbon surfaces have been carried out (7) utilising the techniques of infra-red and X-ray photo-electron spectroscopy. Infra-red studies have largely concentrated on microcrystalline carbons, although it is anticipated that Fourier transform IR spectroscopic (and laser raman) studies should contribute significantly, in the next few years, to the study of graphite electrodes. In the last decade, or so, core-level photoelectron spectroscopy (ESCA) has been applied to a range of carbon surfaces including carbon fibres (8,9), glassy carbon (10,11) and highly-ordered pyrolytic graphite (12,13). The particular advantage of using ESCA (14) is the ability to detect all adsorbed or constitutional surface atoms to a high degree of sensitivity (<1% monolayer coverage) and so yield directly the chemical composition of a surface.

The different methods used to determine the chemistry of carbon surfaces have not yielded comparable results. In particular, the variety and relative amounts of individual C-O functional groups is critically dependent upon the source and type of material and the nature of the pretreatment procedure (chemical, thermal or electrochemical) employed prior to examination. Furthermore, comparative ESCA studies (12) at edge and cleaved basal planes of pyrolytic graphite have been

restricted to single crystals of stress-annealed pyrolytic graphite with no polishing prior to examination. In view of these statements, an ESCA examination of standard pyrolytic graphite electrodes (as used in Chapter 4), subject only to a routine polishing pretreatment in air, was undertaken. The aim of this study was to provide a surface analysis of direct relevance to the observations of surface-selectivity in the direct electrochemistry of redox proteins.

5.2 Experimental Details.

Spectrometer

All the electron spectra presented in this thesis were obtained using an ESCALAB 5 spectrometer (VG Scientific, East Grinstead, U.K.) equipped with facilities for X-ray photoelectron spectroscopy and EELS. The base pressure in the spectrometer main chamber was typically 10^{-8} mbar. A multichannel analyser interfaced to a microcomputer (Research Machines 380-Z) was used for accumulating spectral scans (typically >10). All subsequent data handling and analysis was performed by computer programme.

Radiation Source

X-ray gun: this is a twin anode source giving unmonochromated $MgK\alpha_{1,2}$ ($h\upsilon$ = 1253.6 eV) radiation (soft X-rays).

Samples

For all spectroscopic studies graphite discs cut from standard pyrolytic graphite were used. Basal plane surfaces (15 mm diameter) were generated by cleaving with a sharp razor blade immediately prior to exposure to ultra-high vacuum (UHV). Edge discs (9 mm diameter) were supported by a PVC girdle. All samples were mounted in Pt holders cleaned by sonication in iso-propanol.

Both edge and basal surfaces were polished with an alumina slurry on a cotton wool 'bud', followed by extensive sonication in doubly-deionised water. There was no evidence for 'carry-over' of the edge disc housing during polishing, either from observed spectral features or from parallel studies with polished but unmounted electrodes.

Raman

Raman spectra of pyrolytic graphite discs were recorded by Dr. H. Edwards at the Molecular Spectroscopy Unit, University of Bradford.

5.3 ESCA Studies of Edge and Basal Planes of Pyrolytic Graphite.

Typical examples of broad scan, $MgK\alpha_{1,2}$ excited, X-ray photoelectron spectra for a range of pyrolytic graphite surfaces are shown in Figure 5.1. Comparison of the experimentally observed binding energies with tabulated values (Table 5.1) reveals the presence of only $Al_{2s,2p}$, C_{1s} and O_{1s} peaks on a routinely-polished edge-oriented disc. In contrast, a freshly cleaved basal plane disc and the same surface following alumina polishing show only minor O_{1s} peaks and no detectable $Al_{2s,2p}$ peaks. Following subtraction of background and satellite structure and correction for the linear increase in analyser transmission with kinetic energy (Appendix 5.1) it was possible to derive values for the intensity ratios of observed peaks by integration of the experimental data. A compilation of intensity data for cleaved, polished and cut (no polish) graphite surfaces is given in Table 5.2.

The observed O_{1s} intensities relative to C_{1s} show a marked increase in the oxygen coverage from the cleaved basal - polished

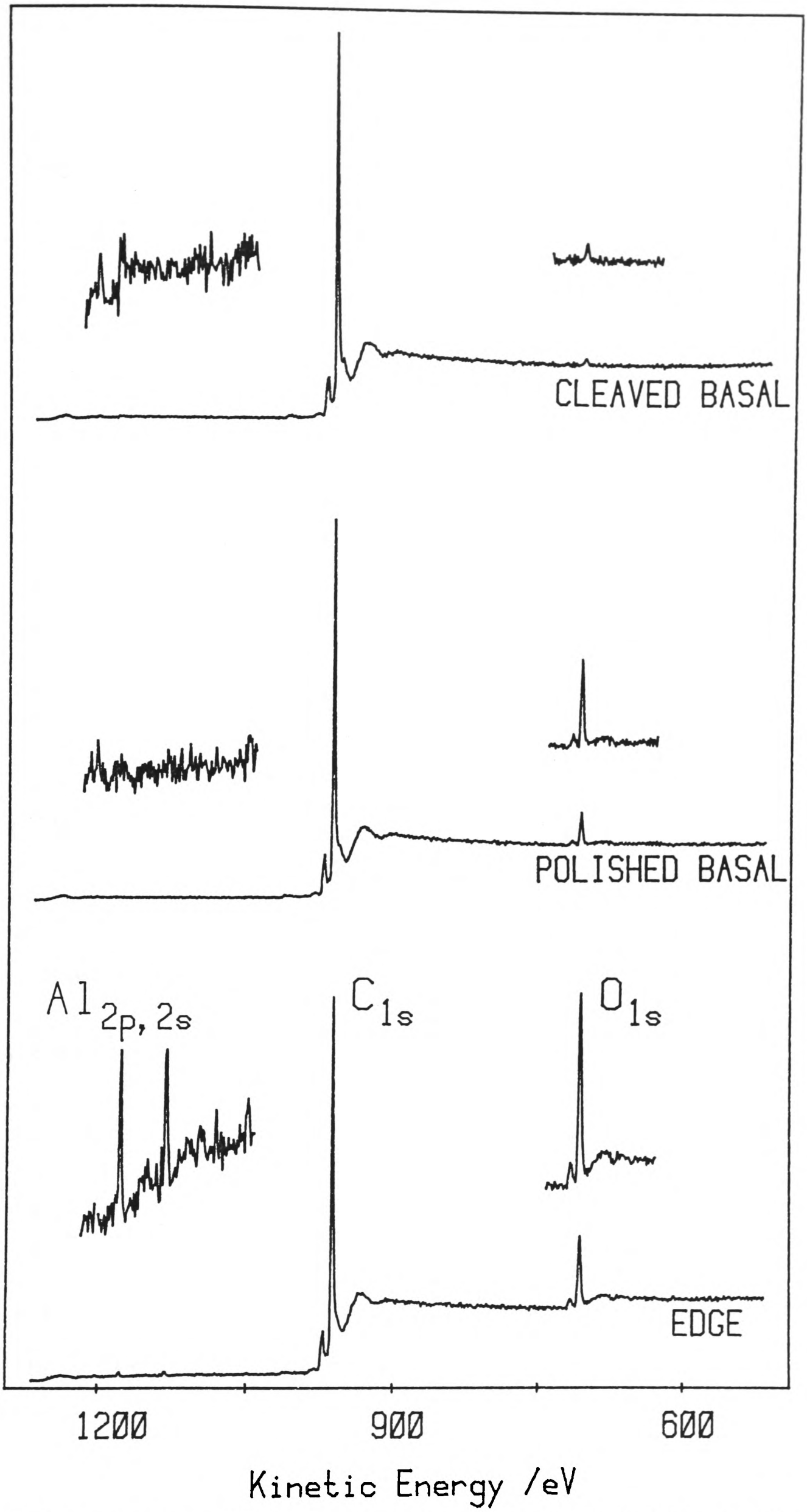

Figure 5.1: Wide-scan ESCA spectra of pyrolytic graphite surfaces, showing scale expansions of the $Al_{2p,2s}$ (x 40) and O_{1s} (x 2.7) regions.

TABLE 5.1

Experimental and Literature ESCA Kinetic Energies

LEVEL	SURFACE	EXPERIMENTAL[a] K.E./eV	LITERATURE[b] K.E./eV
C 1s	Cleaved basal	969	
	Polished basal	969	970
	Edge	968.5	
O 1s	Cleaved basal	720±1	
	Polished basal	719	722
	Edge	719.5	
Al 2s	Edge	1132.5±0.5	1136
Al $2p_{1/2}$	Edge	1177.5±0.5	1180
$2p_{3/2}$		(Not resolved)	1181
Ar 2s	Edge (Etched)	Not observed	934
Ar $2p_{1/2}$	Edge (Etched)	1011	1007
$2p_{3/2}$		(Not resolved)	1009

a. MgKα radiation: hν = 1253.6 eV

Binding energy = 1253.6 - Kinetic Energy

Spectra were not corrected for charging effects and consequently the binding energies as reported are not absolute values. However, the intrinsic conductivity of graphite may prevent significant charging effects.

b. Reference 15.

TABLE 5.2

Summary of Experimentally-Measured ESCA Intensity Ratios[a] for Pyrolytic Graphite Electrodes

SURFACE	C_{1s}/O_{1s}	C_{1s}/Al_{2p}
Edge 0.3μ alumina	3.33±0.73 (8 RUNS)	86±27 (3 RUNS)
Cut Edge- no polish	3.11 (1 RUN)	-
Polished basal	8.95 (1 RUN)	-
Cleaved basal	49.1 (1 RUN)	-

a. All total counts were standardised for the number of sweeps and the width of the scan.

basal - edge surfaces in parallel with the improvement in protein electrochemical reactivity generally observed. In the only previous ESCA study of edge pyrolytic graphite (12), no intensity data were reported for the single crystal surfaces under study. However, a C_{1s}/O_{1s} ratio of 12, estimated from the spectrum presented, is considerably smaller than that found here. A more extensively studied surface is that of alumina-polished glassy carbon where C/O ratios range from 3.2 to 5.9 (11) depending on the initial pretreatment.

5.4 Ion-Etching Studies.

For the soft X-ray photons used in ESCA there is little or no surface damage induced by the probe beam. Ion beams, on the other hand, cause sputtering of all materials. By combining ESCA with sputtering techniques it is possible to get some information about depth distributions and reactivity at the surface of a solid.

A routinely-polished and sonicated edge disc was sputter-etched with argon ions over the whole disc face (5 keV, 30 μA, 10^{-8} T) until no further decrease was observed in the O_{1s} signal (2 mins. etching). The disc was then 'smoothed' with a lower energy ion beam (1 keV, 3 μA, 10^{-8} T for 5 mins.). It was estimated that etching was to a minimum depth of 50 Å. This is in accord with a recent report of electron spectroscopic studies at ion-etched glassy carbon (11). Here sputtering depth was calibrated with an interference microscope and was typically 25 Å/min. at 5 keV, 10^{-8} T.

The resulting broad scan ESCA spectrum (Figure 5.2) shows that the largest residual signals (aside from C_{1s}) are $Al_{2s,2p}$,

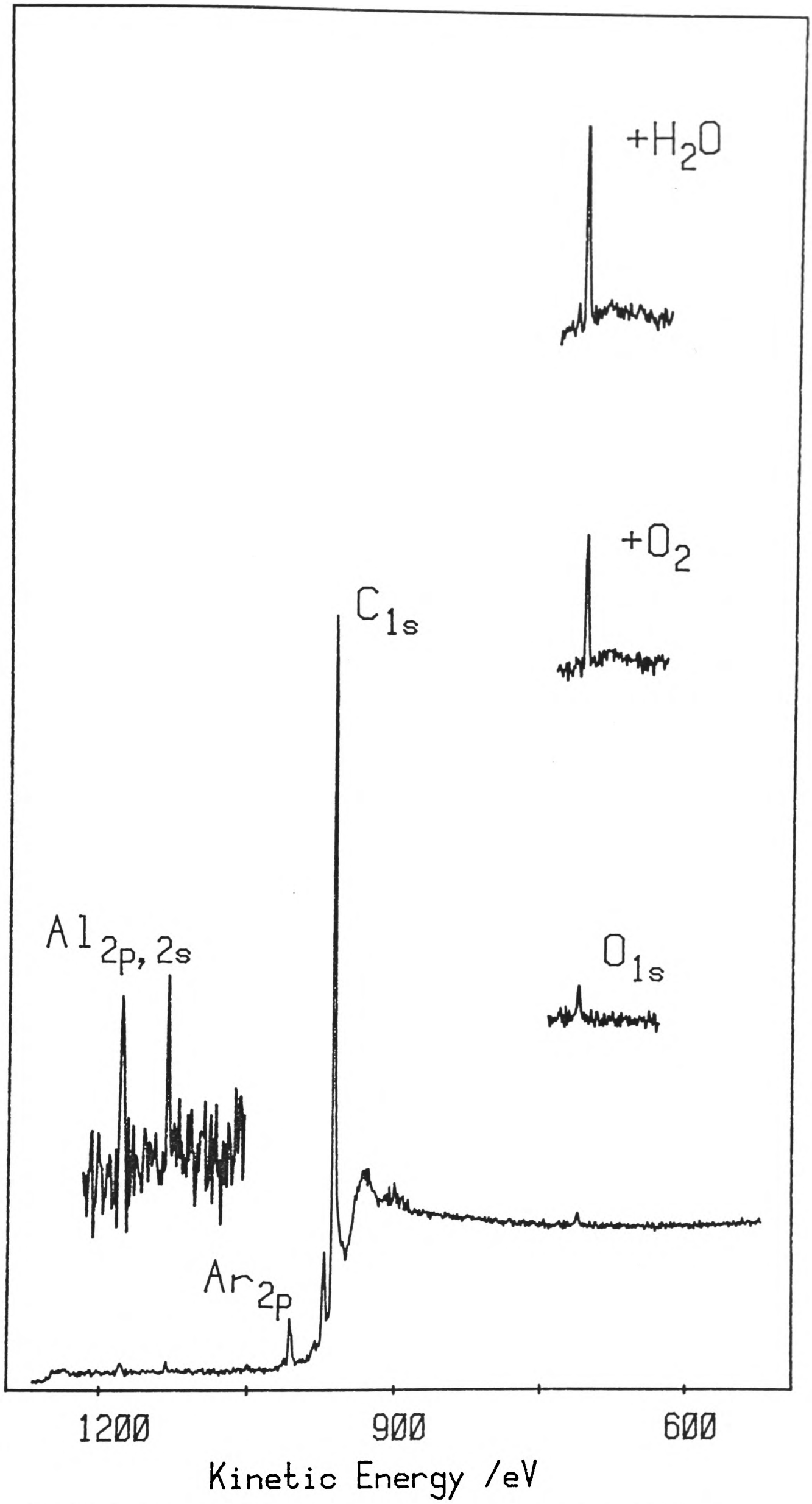

Figure 5.2: Wide scan ESCA spectrum of an ion-etched edge pyrolytic graphite surface. Expansions of $Al_{2p,2s}$ (x 20) and O_{1s} (x 2.7) regions. Also shown are the O_{1s} signals (x 2.7) recorded after exposure of the etched surface to O_2 and then H_2O.

O_{1s} (<0.1 monolayer), and Ar_{2p} (see Table 5.1). The latter presumably are implanted deep within the graphite lattice. The intensity of $Al_{2s,2p}$ signals did not change as a result of ion-etching. In the absence of residual C-O functions, the small O_{1s} signal may arise from the residual alumina still detectable at the sputtered surface.

Following etching, a gas handling line was used to allow controlled exposure of the surface to dry dioxygen and then water vapour. Following each exposure ESCA spectra were recorded (O_{1s} signals are shown in Figure 5.2) and integrated, corrected ESCA intensity ratios (C_{1s}/O_{1s}) were found to be 10.9 (O_2) and 7.0 (H_2O). The increase in O_{1s} relative to C_{1s} presumably results from reaction at vacancies induced by Ar^+ ion bombardment (or adsorption of dioxygen). It can be seen that whilst these results implicate both O_2 and H_2O in surface oxide formation at the edge surface, a significant fraction of the original O_{1s} signal is not recovered through exposure to molecular oxidants. It appears that polishing in the presence of dioxygen or H_2O is not the same as simply introducing dioxygen or H_2O to an 'oxide-free' surface. However, it is possible that reactive 'dangling' vacancies generated by sputtering may recombine in the absence of O_2 or H_2O. It may also be that lateral 'scrambling' of the surface layer by the ion beam or by imbedded Ar produces a partially disordered or 'glassy' surface layer less reactive towards oxidants. In a complementary study (16) at ion-etched basal planes of stress-annealed pyrolytic graphite, Evans and Thomas also reported a sluggish reactivity towards molecular oxygen, but up to two monolayer equivalents of exited molecular oxygen (which will contain some atomic oxygen) were taken up over a prolonged

period. Similarly Ar^+ ion-sputtered glassy carbon (11) shows relatively little uptake of dioxygen at 1 atmosphere pressure.

5.5 Quantitative Estimates of Alumina and Oxide Coverage.

From the preceeding sections it is apparent that the main value of ESCA studies lies in qualitative chemical analysis of surfaces. Nevertheless, the measurement of relative ESCA intensities has practical significance in facilitating quantitative estimates of surface coverage to be made based on calculated, or experimentally-based, relative differential subshell cross-sections, geometric estimates of the lattice dimensions and likely surface structure, and the attenuation of photoelectron flux with depth below the surface as given (17) by equation (5.1):

$$I(x) = I_o(x).\exp(-x/\lambda) \qquad (5.1)$$

$I(x)$ = emerging flux of photoelectrons.

$I_o(x)$ = flux of electrons of energy E originating at a depth x below the surface.

λ = electron escape depth or mean free path length, itself dependent on the kinetic energy (E) of the electron.

5.5.1 Surface Coverage of Alumina.

ESCA studies reveal that, even following sonication, a detectable level of alumina remains at all edge surfaces. In contrast to this, no detectable alumina was observed at polished, sonicated basal surfaces. This difference may simply reflect the

greater ease with which captive environments can be provided for foreign particles by the edge surface, where adjacent planes can easily expand to form microcavities. It is likely that the basal surface will show a greater tendency to exfoliate rather than form surface pits on polishing, so providing fewer sites for the inclusion of alumina.

A possible contribution to the overall O_{1s} intensity at edge surfaces by dispersed alumina cannot be overlooked. Using two experimentally-measured Al_{2p}/C_{1s} intensity ratios (0.013, 0.0089) an estimate of the O_{1s} intensity due to alumina can be calculated taking into account the stoichiometry (2Al:3O) and the experimentally-based sub-shell cross-sections (Al_{2p}/O_{1s} = 1/4). This predicts $O_{1s}(alumina)/C_{1s}$ intensity ratios to be 0.078 and 0.053 compared to the experimentally measured $O_{1s(total)}/C_{1s}$ ratios of 0.246 and 0.27 (net contributions to the O_{1s} signal of 31% and 20%, respectively, from imbedded alumina). These values undoubtedly represent an overestimate of the alumina coverage as no account has been taken of the difference in electron escape depth between Al_{2p} and O_{1s}, levels of widely different kinetic energy (λ in a wide range of materials is dependent on electron energy (E) as $AE^{3/4}$, where A is sample dependent (18)). The attenuation of the O_{1s} signal with respect to that of Al_{2p} may be an important contribution for large imbedded particles (~30% maximum).

A similar calculation for the etched surface yields an $O_{1s}(alumina)/C_{1s}$ ratio of > 0.1 compared to the experimentally measured value of 0.055, so illustrating the **overestimate** of the O_{1s} intensity contribution from alumina, based on cross-sections alone.

A simple calculation of the alumina distribution throughout the ESCA sampling depth (assuming this to be uniform) may be made based on the Al_{2p}/C_{1s} peak area ratio and the ratio of the cross-sections (Al_{2p}/C_{1s} = 0.773). Using the same values as before (Al_{2p}/C_{1s} = 0.013 and 0.0089), the calculated atom ratios are about 1:60 and 1:87 giving a surface concentration of 1 - 2%. Again the difference in electron escape depth for the two levels may put the error as high as 14%.

5.5.2 Surface Coverage of C-O Functionalities.

Any calculation of the density of C-O groups at graphitic surfaces will depend upon the contribution made by alumina to the overall O_{1s} intensity. As estimated in the previous section, this may be as high as 30%. However, in parallel with ESCA studies of alumina-polished edge surfaces, spectra were also run on pyrolytic graphite cut to expose the edge surface but not subsequently polished in any way. Analysis of a typical spectrum gave a C_{1s}/O_{1s} peak intensity ratio (Table 5.2) in close correspondence to those measured for alumina-polished surfaces. This result suggests that the contribution made by alumina to the total O_{1s} intensity, at polished edge surfaces, may be negligible. This would be the case if alumina particles were deeply imbedded in the graphite surface.

A calculation of the atomic number density of O, relative to C, at the various surfaces, can be made based on the attenuation of photoelectron flux with depth (equation 5.1) and a simple model for the surface structure (Appendix 5.2). Such an analysis yields the coverages presented in Table 5.3.

Direct analysis of ESCA intensities to yield surface

TABLE 5.3

Estimated Oxide Coverage[a] of Graphite Surfaces

C-O bond distance[b]/ Å	1.34 (C-OH)	1.2 (C=O)
Edge 0.3μ alumina	1.1±0.15 (4 runs)	1.1±0.15 (4 runs)
Cut Edge - no polish	1.22 (1 run)	-
Polished basal	0.46 (1 run)	-
Cleaved basal	0.087 (1 run)	0.087 (1 run)

a. Oxygen coverage is expressed as the fraction of a monolayer, relative to carbon in the topmost graphitic layer.

b. Coverages calculated, by the method of Appendix 5.2, for overlayers of C-O or C=O functionalities.

coverages is not straightforward and a number of errors are inherent in such an approach. Aside from the somewhat naive assumption of surface homogeneity and smoothness, the major error arising from the reliance on intensity measurements, is the use of ionisation cross-sections to represent the initial emergent intensity of the photoelectron flux. However, a ratio of cross-sections was taken which may lead to a cancelling of errors. The values used were taken from the tabulation of Evans et. al. (19) which are experimentally-based photoionisation cross-sections, and are only expected (19) to prove accurate to 12% or less, on average, in analytical applications. Similar considerations apply to the adoption of experimentally-based mean free paths. In addition, the total emergent intensity of a particular core level is partitioned between the main peak and secondary 'shakeup' and 'shakeoff' features, representing the distribution of kinetic energy between the primary electron flux and secondary electrons. Interaction between one photon and one core level to produce the principal peak is assumed to be the dominant process, although 'shakeoff' effects are virtually impossible to quantify.

Evans et. al. (19) claim that quantitative analysis using an error of better than ESCA may now be possible to λ 10%, and this may indeed be the case for bulk homogeneous solids with well-defined atom positions. However, it seems likely that the errors in estimating the elemental composition of graphite surfaces may be as high as 50%.

Qualitatively the measured intensities suggest that a high (ca. monolayer relative to C) surface coverage of various oxygen functionalities is reproducibly generated at an edge surface upon polishing in air. As expected, the O coverage at a freshly-cleaved

basal surface is low (< 15% monolayer). Prolonged exposure (> 12 hours) of polished edge and cleaved basal surfaces to ultra high vacuum gave no significant variation in the degree of oxide coverage.

5.5.3 Surface Coverage of Alumina as a Function of Particle Size.

ESCA studies of edge surfaces show that the alumina used in the polishing pretreatment is retained in the surface region, even following sonification. The retention of alumina at the surface was examined, by ESCA, as a function of the particle size of the powder used. Figure 5.3 shows spectra recorded for edge discs polished with 0.05μ or 0.3μ alumina, but otherwise treated identically. Estimates of peak intensities made by measuring peak heights are given in Table 5.4. The Al_{2p} intensities indicate that there are significant increases in the alumina levels at a 0.05μ surface (surface concentration ~7 atom percent) compared to a 0.3μ surface (~1%). The increase in the O/C intensity ratio with increasing particle size may also reflect the increased level of alumina at a 0.05μ polished surface. To minimise the retention of alumina at edge graphite electrodes, only 0.3μ particle size powders were used for routine polishing in subsequent electrochemical experiments.

5.6 Characterisation of surface functional groups by ESCA.

The effectiveness of ESCA as a simple qualitative tool to establish the elemental composition of graphite surfaces has already been shown. However, it has also been reported (20) that binding energy shifts may allow the assignment of molecular structure from ESCA. Table 5.5 lists the C_{1s} binding energy

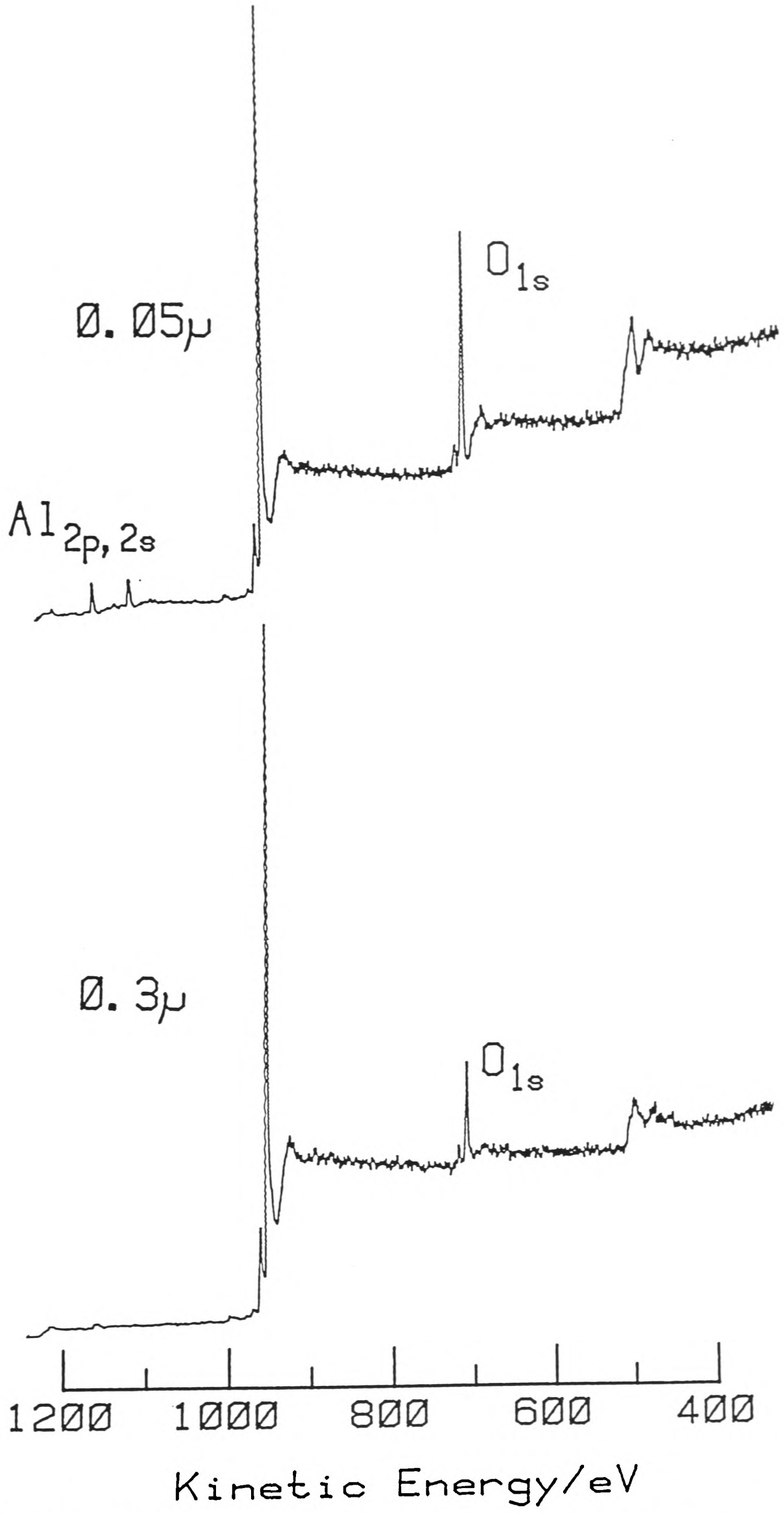

Figure 5.3: Wide scan ESCA spectra of edge pyrolytic graphite surfaces polished with different particle size polishing aluminas (as indicated).

TABLE 5.4

ESCA Analysis of Edge Surfaces Polished with Different Particle Size Polishing Aluminas

LEVEL	PEAK HEIGHT RELATIVE TO C_{1s}	
	0.05μ alumina	0.3μ alumina
O_{1s}	0.42	0.15
Al_{2s}	0.05	--
Al_{2p}	0.053	0.007

TABLE 5.5

C_{1s} Binding Energy Shifts[a] for Various C...O Environments[b]

COMPOUND	$^{*}C_{1s}$ BINDING ENERGY SHIFT / eV
$CH_3{}^{*}CH_2OH$	1.5
$^{*}CH_2O$	2.9
$^{*}(CH_3)_2CO$	3.1
$CH_3{}^{*}CO_2H$	4.5
$CH_3{}^{*}CO_2Et$	4.4
$H{}^{*}C(OCH_3)_3$	4.9
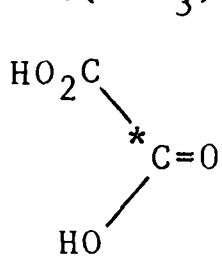	5.1
$(CH_3O)_2C{=}O$	6.4
$O{=}{}^{*}C{=}O$	7.1

a. Binding energy shifts relative to 285.0 eV.

b. Taken from reference 20.

shifts (relative to 285.0 eV) measured for a series of solid samples (20), with reproducibility reported as better than 0.2 eV.

Narrow scan ESCA spectra of the O_{1s} and C_{1s} regions from a routinely-polished edge graphite disc are shown in Figure 5.4. In both cases the fine structure to high kinetic energy of the principal peak is due to satellite lines arising from the inhomogeneity of the X-ray irradiation.

The main C_{1s} peak at 968 - 969 eV, assigned to C in extended aromatic arrays, is followed by a broad feature to low kinetic energy, shifted by 25 - 30 eV, which falls outside the range for a C_{1s} chemical shift (the largest reported shift is 9.9 eV for HCF_3). In view of this and the lack of the discrete structure on this feature it can be assigned to inelastic scattering of photoelectrons generated deep within the graphite lattice. In the intermediate energy loss region there is a noticeable asymmetric tail to the principal peak with a shift of ca. 6 eV. Comparison of spectra from cleaved and polished basal surfaces revealed a similar but more pronounced feature in the same region. The lack of correlation with oxide coverage suggests that this feature may arise from a collective π-electron (plasmon) excitation, or from excitations from the top of the valence band to the bottom of the conduction band, resulting in small energy losses, as suggested for a similar peak in well-ordered graphitic samples (12). The decrease in intensity with increasing functionalisation of the surface may simply arise from exfoliation of the lattice by C-O groupings, or a decrease in the short range order at polished surfaces.

The O_{1s} region shows no low kinetic energy loss features and no obvious asymmetry in the principal peak, although the

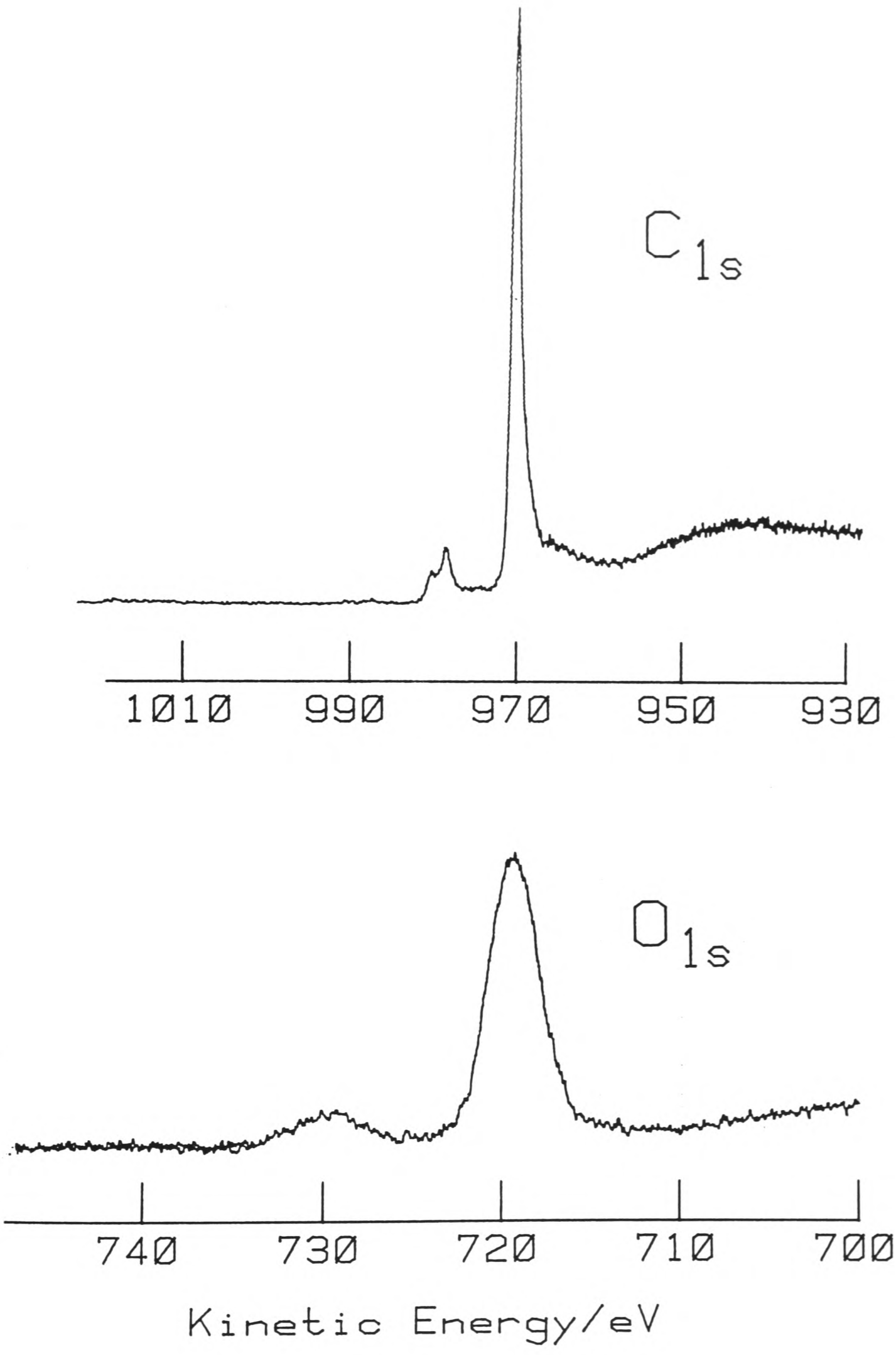

Figure 5.4: Narrow-scan ESCA spectra of the C_{1s} and O_{1s} spectral regions of an edge pyrolytic graphite surface.

width (full width at half maximum: FWHM) of this peak is 3.3 eV compared to that of the C_{1s} peak of only 1.3 eV. The FWHM of O_{1s} in a material with only one type of chemically-bound species is typically 1.4 (Cu-O) (21) to 1.8 eV (anthraquinone) (22) suggesting more than one type of oxygen species on the edge plane.

5.7 EELS and Raman Studies

In an attempt to characterise the specific C-O functional groups present at an edge surface, EELS (electron energy loss spectroscopy) and laser raman studies were undertaken. Vibrational EELS spectra of various graphite surfaces revealed spectral activity close to 2900 cm^{-1} and 1400 cm^{-1}. The intensities of these bands were not linearly related to O_{1s} ESCA intensities. The poor resolution and large band width of EELS spectra made an unambiguous assignment of these bands impossible. The expected frequencies for lattice vibrations, C-O functionalities and hydrocarbon contamination (C-C and C-H stretch, and C-H deformation) all fall within the envelope of observed bands. Electronic EELS spectra were similarly ambiguous and did not aid assignment. In raman spectra, all bands with intensities enhanced at the edge plane were assigned to skeletal vibrations of bulk aromatic structures. Comparison of the observed bands with those previously reported in raman spectroscopic studies of graphite (23), revealed the presence of structural disorder in the surface region of the polished edge graphite electrodes used in this study. In the spectrum of a cleaved basal surface, seven bands can be assigned to surface-adsorbed alkanes and ethers. It is

perhaps significant that these bands are considerably less intense or absent at the edge surface.

5.8 Discussion of ESCA Studies.

Electron spectroscopy conclusively shows that polished edge graphite electrodes carry a high 'surface' oxygen content. Calculations based on the attenuation of photoelectron flux with depth are consistent with *ca.* monolayer coverage of C-O functionalities. The absence of chemical and structural information concerning the state of the surface, together with the assumptions of a smooth surface with no stacking irregularities, means that the result must be treated with caution. In fact, the act of polishing is expected to produce substantial surface disorder. A 'surface', in the context of the measurements described here, is defined by the ESCA sampling depth and is typically 10 - 20 Å. Surface oxide may then be distributed throughout a disordered region at the surface, over a depth of 10 - 20 Å. A simple calculation based on the C_{1s}/O_{1s} intensity ratio (3.33) and the corresponding cross-section ratio (0.36) gives the oxide distribution in terms of atom percent, with respect to carbon, as 10%, throughout the sampled region. Both these calculations show that the edge surface is substantially oxidised following the mild oxidative pretreatment employed - polishing or even cutting the edge is all that is required to functionalise the surface. It appears that the only contaminant at the surface is that introduced by polishing, although at levels of ~1%, no significant role is expected for 'surface' imbedded alumina (0.3μ). Scanning electron microscope studies (24) of glassy carbon have also shown that alumina is retained in the

surface region following polishing.

The range of C-O functional groups proposed at microcrystalline carbons is very wide. For instance, Boehm (1) presented evidence for a strongly acidic carboxyl (pK < 6.4), a phenolic hydroxyl (pK < 15.7) and a hydroxylactone comprising a weakly acidic carboxyl (pK < 10.3) and a carbonyl (pK < 20.6) group, whilst at graphite dust Kiselev et. al. (25) proposed - CO_2H (0.48 mequivs.), -OH (0.16), $-CO_3H$ (0.04) and C=O (0.07). The nature of the oxygen functionalities at graphite relies largely on extrapolations from these reactivity studies. Specific chemical evidence for pyrolytic graphite itself rests mainly on the success of chemical pretreatment and coupling procedures designed to selectively enhance the population of a specific group e.g. heating in air or plasma treatment. Preliminary studies (26,27) of the edge graphite surfaces used in this study have shown that extensive reduction of the surface with $LiAlH_4$ has no deleterious effects on the reversibility of the direct electrochemistry of 2[4Fe-4S] ferredoxin, whilst silylation (ca. 10% coverage of Si with respect to C, as estimated by ESCA studies) leads to a marked decrease in the reversibility of the response observed for cytochrome c. In the latter case control experiments rule out a purely steric role for the covalently-bound alkyl silanes, showing that the removal of acid groups as silyl esters, or hydroxy groups as silyl ethers, is important in 'wiping out' the faradaic response. The involvement of hydroxyl groups in interfacial interactions is suggested by these observations and clearly formation of these groups would require less surface energy than formation of carboxylate, ether or quinone functions where additional surface energy is required in

order to disrupt the aromatic ring structures.

In several recent reports ESCA has been used to characterise the chemical nature of C-O functional groups of carbonaceous materials. Thomas et. al. (16) and Sherwood et. al. (8) used ESCA to assign small (< 10 eV) energy loss features to low kinetic energy of the main C_{1s} peak in graphitic samples to specific surface oxygen functionalities. Curve fitted C_{1s} spectra of electrochemically-oxidised carbon fibres (8) suggest three main chemically-shifted species at 2.1 (C=O), 4.0 (-COO-) and >6.0 eV ($-CO_3$) from the main C_{1s} peak, with corresponding FTIR bands at 1730 - 1740 cm^{-1}, 1690 - 1700 cm^{-1} and 1600 cm^{-1}, respectively. In contrast, Thomas et. al. proposed that C-O-C and C=O surface groups were present in equal proportions on ion-bombarded basal plane surfaces following exposure to excited molecular oxygen. Similarly, asymmetric O_{1s} peaks from oxidised carbon fibres have been resolved (9) into three main component signals with shifts ca. 2 eV (O_2), ca. 5 eV (C=O) and ca. 6.5 ev (C-O) from the main O_{1s} peak.

In the studies described above, low kinetic energy loss features are well-defined. No such features are evident in the ESCA spectra described in this chapter. Similarly, raman studies provide no convincing evidence for the specific nature of surface C-O groups. This suggests that individual groups are present at a low surface concentration at the edge-oriented graphite surface. In view of this, and the high (ca. monolayer) oxide coverage suggested by ESCA studies, it seems that there may be a wide range of C-O functional groups at a routinely-polished edge electrode.

APPENDIX 5.1

The measurement of ESCA intensities.

(A) A non-monochromatised X-ray source gives satellite lines to the high kinetic energy side of principal peaks and can create difficulties in measuring intensities. ESCA spectra were stripped of satellite peaks with intensity > 1% of the main $MgK\alpha_{1,2}$ excitation by computer programme (28).

(B) There is no method for extracting peak areas from raw ESCA data which has any adequate theoretical basis. The major problem lies in background 'stripping' to provide a true spectrum. Nevertheless, the background may be subtracted empirically using a step model for the spectra recorded on the ESCALAB5 spectrometer (28). All peak intensities derived by integration of the resulting spectra were standardised to correct for the number of sweeps and the scan width.

(C) Intensity comparisons between peaks of widely different kinetic energy are affected by the linear increase in electron analyser transmission with kinetic energy. A measure of the transmission characteristic may be obtained by following the intensity of the Au $4d_{5/2}$ and $4f_{7/2}$ levels as a potential bias is applied to a gold sample to perturb the kinetic energy of ejected electrons. A calibration curve generated by this method gives a good measure of the transmission characteristic in the kinetic energy range 400 to 1000 eV and was used to correct raw ESCA peak intensities.

APPENDIX 5.2.

Calculation of the surface oxygen coverage from the ESCA peak intensity ratio O_{1s}/C_{1s}.

If the topmost m monolayers of thickness x contain oxygen functionalities only, then the arrangement of 'surface' layers consists of two superimposed arrays of photoemitters as shown in Figure 5.5(a). Taking the lattice dimensions as those of the AB crystalline form of graphite (29), Figure 5.5(b), and assuming a smooth surface with no stacking irregularities, then the total emergent intensity from oxygen in oxide layers and carbon in the topmost graphitic layers can be calculated.

C_{1s}: From layer n (Figure 5.5), emergent intensity (I_n) is given by:

$$I_n = I_o^c \exp[-(x+nd)/\lambda_c] \qquad (5.2)$$

λ_c is the mean free path length for the C_{1s} region (~12 Å).

I_o^c is the tabulated ionisation cross-section for C_{1s}.

x is the thickness of the oxygen overlayer.

Summing to infinity gives the total emergent intensity arising from periodic carbon sub-layers (I^c). This is given in equation (5.3).

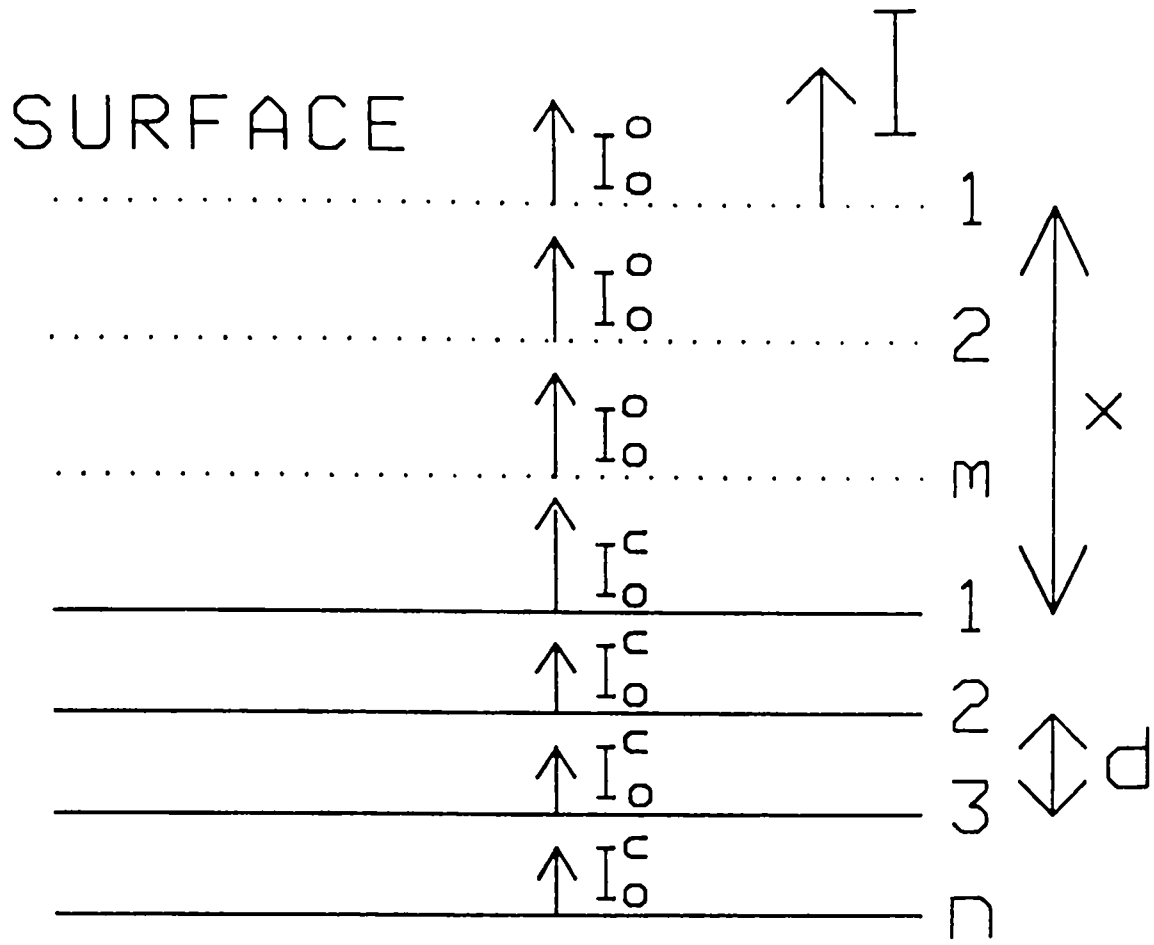

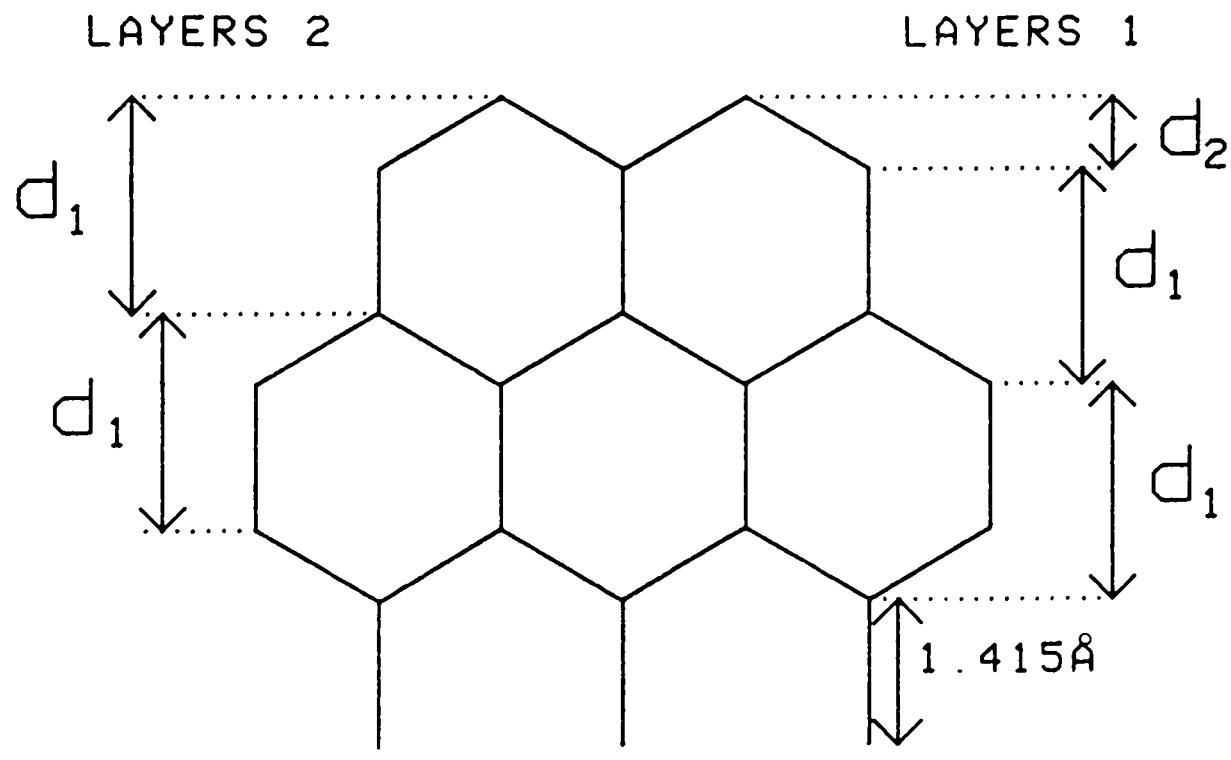

$$d_1 = 1.415 + 1.415\cos 60$$

$$d_1 = 2.1225\text{Å}$$

$$d_2 = 0.7075\text{Å}$$

Figure 5.5: Schematic representations of the lattice structure of pyrolytic graphite with an overlayer of oxygen functionalities. The lattice dimensions and photoelectron fluxes, as discussed in Appendix 5.2, are also indicated.

$$I^C = \Sigma I_n = I_o{}^C \exp[-x/\lambda_c] + \exp[-(x+d)/\lambda_c] + \exp[-(x+2d)/\lambda_c] + \ldots$$

$$= I_o{}^C \frac{\exp[-x/\lambda_c]}{1 - \exp[-d/\lambda_c]} \qquad (5.3)$$

The total C_{1s} intensity from graphitic edge sublayers can be broken down into two parts, each part representing the intensity contributed by one of the two periodic arrays characterised by an interatomic spacing of d_1 (Figure 5.5(b)). Therefore, for an overlayer of thickness x the total C_{1s} intensity will be:

$$I^C = I_o{}^C \frac{\exp[-x/\lambda_c] + \exp[-(x+d_2)/\lambda_c]}{1 - \exp[-d_1/\lambda_c]} \qquad (5.4)$$

O_{1s} overlayer: For an nth of a monolayer of oxygen, the total emergent intensity (I^O) is simply given by:

$$I^O = nI_o{}^O \qquad (5.5)$$

where $I_o{}^O$ is the tabulated ionisation cross-section for O_{1s}.

The resulting C_{1s}/O_{1s} intensity ratio is given by equations (5.4) and (5.5) as:

$$\frac{I^C}{I^O} = \frac{I_o{}^C}{nI_o{}^O} \frac{\exp[-x/\lambda_c] + \exp[-(x+d_2)/\lambda_c]}{1 - \exp[-d_1/\lambda_c]} \qquad (5.6)$$

For a monolayer of sp^2 C-OH functionalities, x = 1.34 Å and:

$$I^c/I^o = \frac{0.225}{0.624} \frac{\exp[-1.34/12] + \exp[-2.0475/12]}{1 - \exp[-2.1225/12]} \quad (5.7)$$

$$= 3.86$$

Correspondingly, for a monolayer of $>C=O$ functionalities, x = 1.2 Å and $I^c/I^o = 3.91$.

The experimentally observed C_{1s}/O_{1s} intensity ratios show similar attenuation factors for the photoelectron flux emitted from the carbon sublayers, relative to the oxygen signal, and so equation (5.6) may be used to predict the atomic number density of oxygen at the surface relative to that of carbon.

References - Chapter 5

1) Boehm, H. P., Diehl, E., Heck, W., Sappok, R., Angew. Chem., Internat. Edit. Engl., 3, 669, (1964).

2) Donnet, J. B., Carbon, 6, 161, (1968).

3) Randin, J. P. and Yeager, E., J. Electroanal. Chem. 58, 313, (1975).

4) Epstein, B. D., Dalle-Molle, E. and Mattson, J. S., Carbon, 9, 609, (1971).

5) Laser, D. and Ariel, M., J. Electroanal. Chem. 52, 291, (1974).

6) Boehm, H. P., Adv. in Catalysis 16, 198, (1966).

7) Britton, W. E., El-Hashash, M., El-Cady, M. and Assubaie, F., J. Electroanal. Chem. 172, 189, (1984), and references therein.

8) Kozlowski, C. and Sherwood, P. M. A., J. Chem. Soc., Faraday Trans. I 80, 2099, (1984).

9) Proctor, A and Sherwood, P. M. A., Carbon 21, 53, (1983).

10) Cabaniss, G. E., Diamantis, A. A., Murphy, W. R., Linton, R.W. and Meyer, T. J., J. Am. Chem. Soc. 107, 1845, (1985).

11) Kamau, G. N., Willis, W. S. and Rusling, J. F., Anal. Chem. 57, 545, (1985).

12) Thomas, J. M., Evans, E. L., Barber, M. and Swift, P., Trans. Faraday Soc. 67, 1875, (1971).

13) Schogl, R. and Boehm, H. P., Carbon 21, 345, (1983).

14) Hercules, D. M. and Hercules, S. H., J. Chem. Educ. 61, 483, (1984).

15) Siegbahn, K., Nordling, C., Fahlman, A., Nordberg, R., Hamrin, K., Hedman, J., Johansson, G., Bergmark, T., Karlsson, S. E., Lindgren, I. and Lingberg, B. ESCA. Uppsala: Almquist and Wiksells (1967).

16) Evans, S. and Thomas, J. M., Proc. R. Soc. (London) 353A, 103, (1977).

17) Orchard, A. F. in: Handbook of X-ray and ultraviolet photoelectron spectroscopy. Briggs, D., ed. London: Heyden (1977).

18) Szajman, J., Liesegang, J., Jenkin, J. G. and Leckey, R. C. G., J. Electron Spectrosc. Relat. Phenom. 23, 97, (1981).

19) Evans, S., Pritchard, R. G. and Thomas, J. M., J. Electron Spectrosc. Relat. Phenom. 14, 341, (1978).

20) Gelius, U., Heden, P. F., Hedman, J., Lindberg, B. J., Manne, R., Nordberg, R., Nordling, C. and Siegbahn, K., Physica Scripta 2, 70, (1970).

21) Evans, S., Evans, E. L., Parry, D. E., Tricker, M. J., Walters, M. J., and Thomas, J. M., Faraday Disc. Chem. Soc. 58, 97, (1974).

22) Marsh, H., Foord, A. D., Mattson, J. S., Thomas, J. M. and Evans, E. L., J. Coll. Interf. Sci. 49, 368, (1974).

23) Vidano, R. and Fischbach, D. B., J. Am. Cer. Soc. 61, 13, (1978).

24) Engstrom, R. C. and Strasser, V. A., Anal. Chem. 56, 136, (1984).

25) Zarif'yants, Y. A., Kiselev, V. F., Lezhnev, N. N., Novikova, I. S. and Fedorov, G. G., Dokl. Akad. Nauk. SSSR 143, 1358, (1962).

26) Armstrong, F. A., unpublished results.

27) Brown, K. J., Part II Thesis. Oxford (1985).

28) Williams, A. A., D. Phil. Thesis. Oxford (1985).

29) Cotton, F. A. and Wilkinson, G. Advanced Inorganic Chemistry. New York: Wiley (1980).

CHAPTER 6

SURFACE EFFECTS IN DIRECT ELECTROCHEMISTRY

6.1 Introduction.

The main goal of this chapter is to establish in what way, and to what extent, does the chemical nature of an electrode surface influence the energetics of biological electron-transfer reactions. The ability to achieve well-behaved direct electrochemistry of a range of structurally-characterised redox proteins, at pyrolytic graphite surfaces (Chapter 4), has provided a convenient approach to address this problem. In Chapter 4 the structure of pyrolytic graphite was successfully exploited to show that direct electrochemistry of redox proteins is selective, and is catalysed at the edge, but not the cleaved basal, plane. Electron spectroscopy was then used in Chapter 5 to define the contrasting chemistry of these two surfaces. Further spectroscopic techniques (EELS and Raman) were also applied to the ex situ characterisation of graphite electrodes. However, the preferred approach to the characterisation of electrode surfaces is an in situ study of electrodes in the relevant electrochemical environment, in this case, aqueous solution. This chapter adopts an electrochemical approach to provide more detailed insights into the fundamental requirements made of pyrolytic graphite, and other, electrode surfaces such that these electrodes confer biological electron-transfer activity.

6.2 Experimental Details

Electrodes and polishing materials.

Table 4.2 lists the size, source and grade of the materials used in electrode preparation.

The perimeter of gold film electrodes was sealed by a silicone rubber girdle. Edge graphite and gold discs were mounted in Teflon electrode sheaths.

Synthetic diamond polishing compounds are supplied suspended in an organic dispersive agent. Electrodes polished with this paste show extensive electroactivity even after sonication in organic solvents. To overcome this, a synthetic diamond polishing powder was prepared by soxhlet extraction of the paste in acetone for 12 hours, followed by washing in doubly-deionised water and drying at 100°C.

pH Titrations.

Controlled potential pH titrations at a rotating-disc electrode were carried out using a microprocessor (Research Machines 380-Z)-controlled electrochemical rack system, constructed in this laboratory, which incorporated an Oxford Electrodes motor and motor controller. Potential and rotation speed control and data acquisition were achieved through assembler language routines which were CALLed from BASIC. The electrochemical cell (ca. 2 mL volume) (Figure 6.1) was held in place on the motor housing with a perspex holder and had a Luggin capillary aligned along the central axis of the working compartment. A combination pH micro-electrode (MI-410, Microelectrodes Inc.) was introduced into the cell via a side arm and retained firmly in place by a thermometer holder. The tip of the probe was positioned to one side of the rotating disc

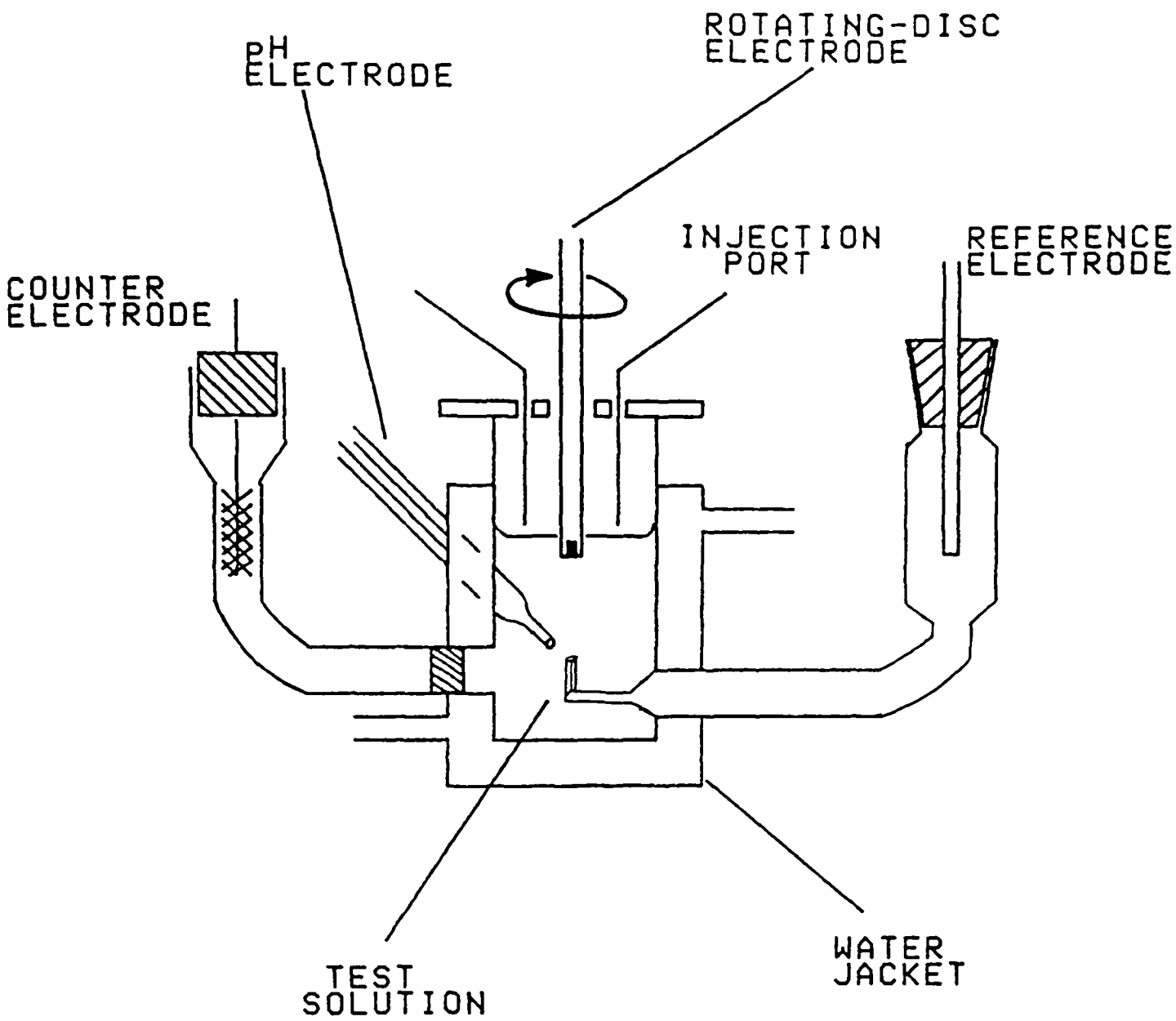

Figure 6.1: Design of electrochemical cell used for pH titrations at a rotating edge graphite electrode

electrode. The platinum counter electrode was in a side arm with electrical contact to the working compartment through a sintered glass frit. The edge graphite working electrode was a 4 mm diameter disc sealed in a machined perpsex tube with a threaded internal iron rod. This provided electrical contact between the disc and a brass electrode holder which attached to the motor through a convenient screw thread fitting. The electrode was polished by mounting in a teflon holder and reproducibly positioned ca. 1.5 cm from the Luggin tip. Cyclic voltammetric studies of ferrocene monocarboxylic acid confirmed that this did not give rise to a significant iR error at low concentrations of supporting electrolyte (1 mM NaCl). Anaerobicity of samples was maintained throughout the experiments as described in Chapter 4.

The solution pH was adjusted over the pH range 3.5 to 8.5 by addition of acid (2 M acetic acid) or base (2 M Tris) components to a mixed buffer system (1.5 mM each of acetate (BDH AnalaR acetic acid), MES (Sigma Chemical Co.) and Trisma base (BDH AristaR)) with a 1mM NaCl background. Injection of de-oxygenated titrant solutions was achieved using Hamilton syringes with the needle inserted between the cell wall and the rotating electrode. Between additions the syringe needle was held above the level of the test solution. The flow of the test solution itself provided an efficient means of mixing added titrant into the solution with a mixing time of <5 secs. The response time of the pH probe, used in conjunction with a Radiometer PH4 pH meter was measured to be <5 secs. for an induced pH change of 0.5 pH units. Following addition of titrant, the faradaic response was continually monitored until a steady value was reached, when the pH and faradaic current were recorded. The electrode potential

was then stepped to an oxidising rest potential whilst further titrant was introduced. This prevented depletion of oxidised electroactive species through bulk electrolysis.

Experimental Results.

6.3 The role of the polishing material in electrochemical studies.

In a recent publication (1) it has been shown that metal oxides, such as alumina, dispersed on glassy carbon surfaces can enhance the rate of electron-transfer to certain inorganic and organic redox couples. Sonication of these electrodes proved an efficient means of removing dispersed particles left by the polishing procedure. ESCA studies (Chapter 5) have shown that alumina is retained at edge graphite surfaces, even following thorough sonication. However, the surface coverage of alumina (0.3μ particle size: ca. 1%) lies well below that (30%) observed to 'activate' glassy carbon surfaces (2).

To assess the role of alumina as a heterogeneous catalyst in the direct electrochemistry of redox proteins, the faradaic response of representative proteins was compared under varying cation conditions at sonicated and non-sonicated electrodes. The faradaic responses at electrodes previously polished with 0.3μ alumina were found to be independent of whether or not the electrode had been sonicated prior to use and the length of the sonication pre-treatment. Polishing with 0.25μ synthetic diamond powder, which does not exert catalytic effects (1), gives identical faradaic responses to those observed at alumina polished electrodes.

Marked differences were evident, however, on comparing alumina powders of differing particle size. Table 6.1 summmarizes

the electrochemical response for 67 μM C. pasteurianum 2[4Fe-4S] ferredoxin at an edge electrode polished with alumina powders of particle size 0.3μ or 0.05μ, followed by sonication. A decrease in faradaic peak current and an increase in peak separation are apparent as the alumina particle size decreases. The decrease in the magnitude of the faradaic response with particle size parallels the decrease in the capacitative current suggesting that a decrease in the effective surface area available for electron-transfer determines the diminished response at the 0.05μ polished electrode.

The ESCA study of alumina-polished edge graphite surfaces (Chapter 5) reveals a greater retention of 0.05μ alumina (ca. 7% coverage) as compared to 0.3μ alumina (ca. 1% coverage) at polished and sonicated surfaces. Thus, a decrease in the reversibility of electron transfer may be correlated with an increase in the surface coverage of alumina. Apparently, alumina can exert inhibitory effects upon the electrochemical responses of redox proteins as the surface coverage of alumina increases.

6.4 Electrochemical Investigations Of Surface Faradaic Processes.

Cyclic voltammograms at edge and polished basal plane electrodes in the region +250 to -700 mV vs. NHE were routinely used as 'diagnostic' runs at the start of experiments to establish cell and electrode performance and deoxygenation efficiency. A reproducible feature of these runs was a rather broad, irreversible peak in the initial scan at ca. -650 mV vs. NHE (pH 8.0), seen to decay essentially to zero by scan 4, Figure 6.2(b). A cleaved basal plane electrode showed no such electroactivity at these negative potentials (Figure 6.2(a)).

TABLE 6.1

Effect of Alumina Particle Size on Faradaic Response at an Edge Electrode for 67 μM C. pasteurianum 2[4Fe-4S] Ferredoxin in 30 mM $MgCl_2$, 5 mM Tricine, 100 mM NaCl, pH 8.0

	ALUMINA PARTICLE SIZE 0.3μ	0.05μ
ΔE_p / mV[a]	75	90
$i_{p(CATHODIC)}$ / μA[a]	0.77 (0.2)[b]	0.51 (<0.1)[b]
$i_{p(ANODIC)}$ / μA[a]	0.71	0.45
$E_{1/2}$ / mV (SCE)	-598	-593
$i_{CHARGING}$ / μA	0.8	0.5

a. 20 mVs^{-1}

b. Figures in brackets refer to the response in the absence of $MgCl_2$ i.e. in 100 mM NaCl alone.

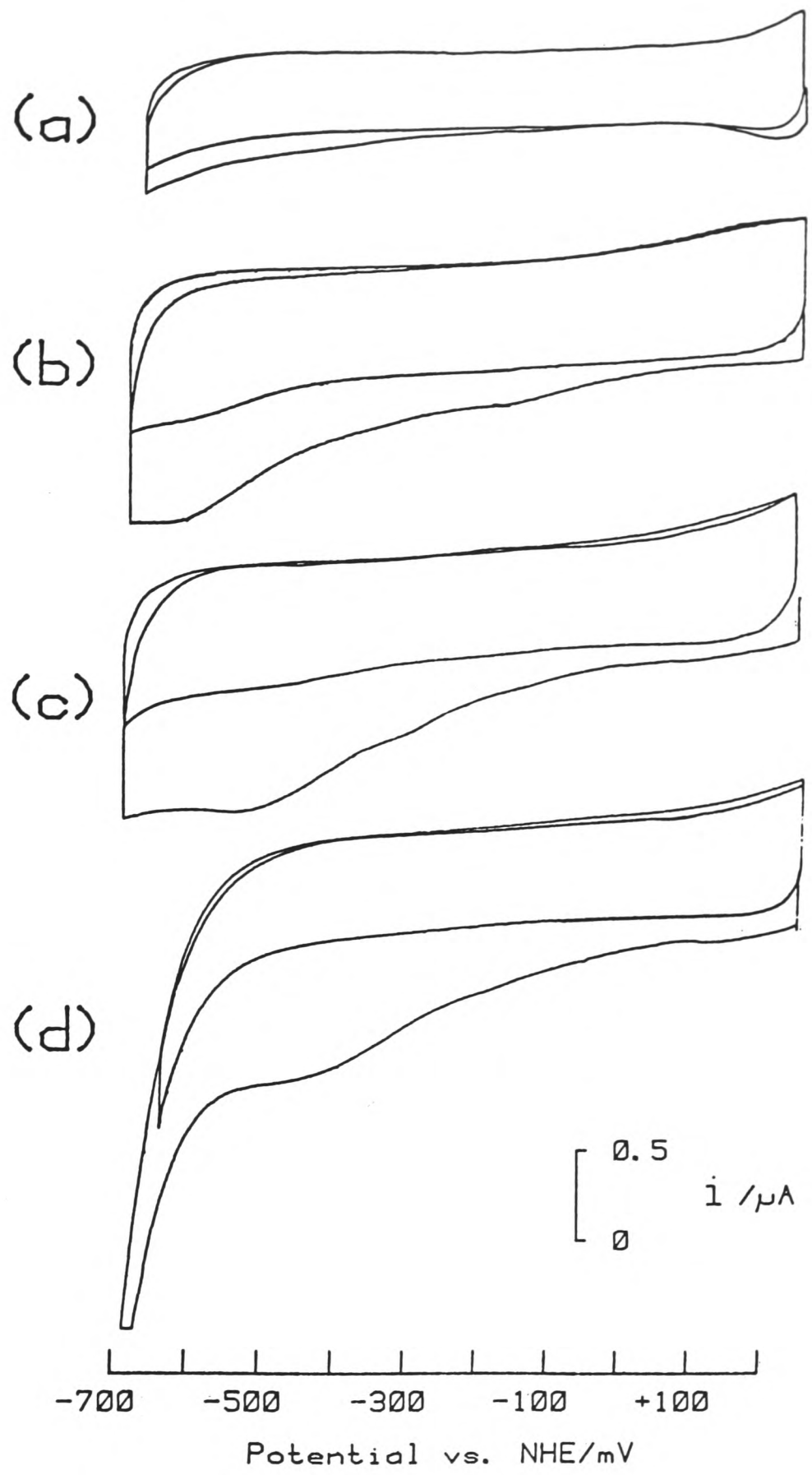

Figure 6.2: Cyclic voltammograms (20 mVs^{-1}) recorded at (a) cleaved basal and (b,c,d) edge plane graphite electrodes, in 5 mM buffer, 100 mM NaCl alone. (a,b) pH 8.0 [Tricine]; (c) pH 6.0 [MES], and (d) pH 4.5 [acetate]. Voltammetric cycles 1 and 4 are shown at each pH.

The peak showed a strong dependence on solution pH as studied by cyclic voltammetry (Figure 6.2(b-d)) and square wave voltammetry. The pH dependence of the peak potential, as estimated from square wave voltammograms, is 50 - 75 mV/pH, close to the theoretical value of 59 mV/pH at 25°C for a $2H^+/2e^-$ redox couple. Extending the potential sweep to +650 mV vs NHE after an initial cathodic sweep revealed a broad anodic peak around +250 mV at pH 8.0, shifted to +500 mV at pH 4.0. By adjusting the cycle limits it is possible to show that these two peaks are related and are probably due to the irreversible reduction and oxidation of the same group. On the evidence of previous studies (3) it seems likely that the observed electrochemistry may involve quinone and hydroquinone groups.

In separate experiments in which the scan range was restricted to the potential region +550 to -50 mV vs. NHE, additional couples to those described above were observed, (Figure 6.3). At pH 8.0 there is a single redox couple which, curiously, is most prominent at a freshly cleaved basal surface, but only weakly evident at the edge and not apparent at a glassy carbon surface. Polishing the cleaved basal surface leads to a diminished response, similar to that at the edge. At the cleaved basal surface the observed behaviour is characteristic of a quasi-reversible surface redox reaction:

$$i_{p(\text{cathodic})} \sim i_{p(\text{anodic})} \propto \text{scan rate}$$

ΔE_p 30 - 40 mV (20 - 200 mVs^{-1})

Symmmetrical peaks

In addition, the couple shows a pH dependence at the cleaved basal surface of ~50 mV/pH. At the edge surface, more complex behaviour is observed at or below pH 5.5, with two

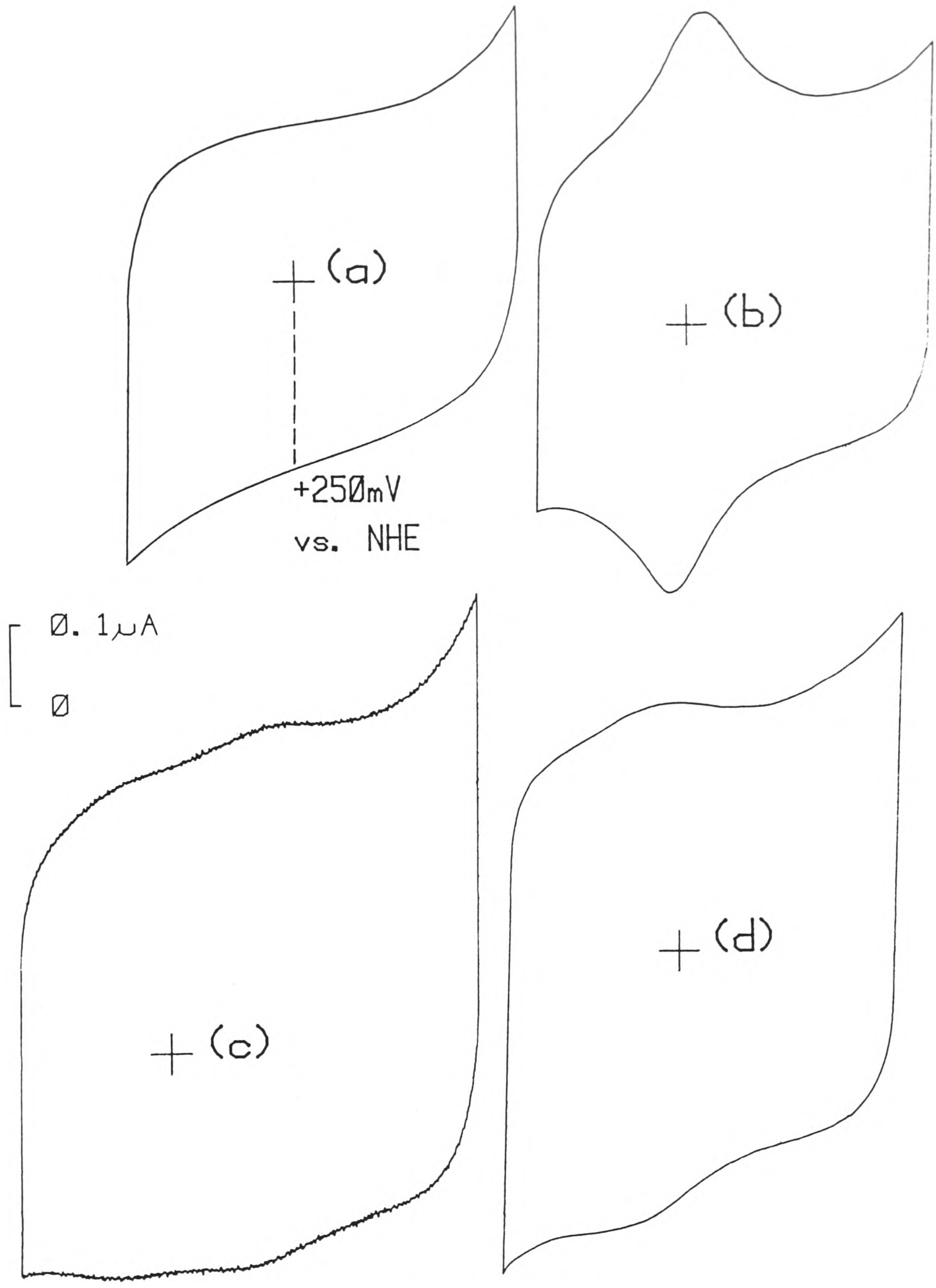

Figure 6.3: Cyclic voltammograms (20 mVs^{-1}) recorded at (a) glassy carbon, (b) cleaved basal plane graphite and (c,d) edge plane graphite, in 5 mM buffer, 100 mM NaCl alone. (a,b,d) pH 8.0 [Tricine]; (c) pH 5.5 [acetate].

couples of ΔE_p <50 mV now discernible.

A non-faradaic adsorption-desorption process or an adsorbed electroactive contaminant seem the only feasible rationalisation of the observed response. Intrinsic contamination of the pyrolytic graphite used to construct these electrodes is unlikely as the electrochemical activity was retained following prolonged (>12 hours) soxhlet extraction of discs in AnalaR acetone. The enhanced activity at the basal surface is best viewed in terms of a solvent replacement reaction and corresponds to the least hydrophilic surface where inner layer water molecules are weakly bound and easily replaced. The exact nature of the process cannot be determined unequivocally, but the ensuing 'redox' behaviour leads to complications when pursuing weak electrochemical responses in the potential region around 0 mV vs. SCE at cleaved basal plane electrodes.

6.5 Faradaic Response pH Titrations.

Initial results indicate that surface functional groups play an important role in promoting direct electrochemistry at graphite surfaces. In addition, the necessity for appropriate 'tuning' of solution conditions through the control of multivalent cation levels suggests the involvement of charge interactions in the electrical double layer. Control of surface protonation equilibria at an edge graphite surface may then prove an efficient means of regulating surface charge at the reaction plane.

6.5.1 Cyclic Voltammetric Studies.

Exploratory studies of protonation effects were made using the 2[4Fe-4S] ferredoxin in the absence of cations (5 mM buffer,

1 mM NaCl at pH 4.0 (acetate) and pH 8.0 (tricine)). The faradaic response was promoted at low pH although the poor response at pH 4.0 (ΔE_p >125 mV, 20 mVs^{-1}) probably reflects oxidative denaturation of ferredoxin at this low pH. Complementary studies using plastocyanin confirmed the importance of protonation effects, in that rapid charge transfer can be promoted by Mg^{2+} ions (pH 6 - 8) or by mild acidification (pH 4 - 6) (Figure 8.4). However, in the case of plastocyanin, discussion is complicated by evidence (see Chapter 8) for the formation of a kinetically-inactive protonated form of the reduced protein with pK5 - 6. In contrast, the direct electrochemistry of azurin is similar at pH 8 and pH 5 with no significant change in response.

6.5.2 Constant Overpotential Studies.

In order to probe the electrochemical effects of edge surface protonation equilibria more closely, titrations of the faradaic current observed as a function of pH were carried out at constant overpotential using a rotating-disc electrode. The responses of cytochrome c (Figure 6.4(a)) and the 'marker' probe $Fe(CN)_6^{3-}$ (Figure 6.5(a)) were examined over the pH range 4 - 9 in a 1 mM NaCl background.

The electrochemistry of $Fe(CN)_6^{3-}$ undergoes a smooth transition from irreversible to essentially diffusion-controlled behaviour (see insets) as the pH drops below 6. A similar trend has also been observed at glassy carbon and carbon paste electrodes but is not apparent at Au or Pt electrodes where the rate of electron-transfer is pH independent (4). The same pH profile was observed on going from high-low or low-high pH, indicating that the effect is not simply one of a titrant-induced increase in

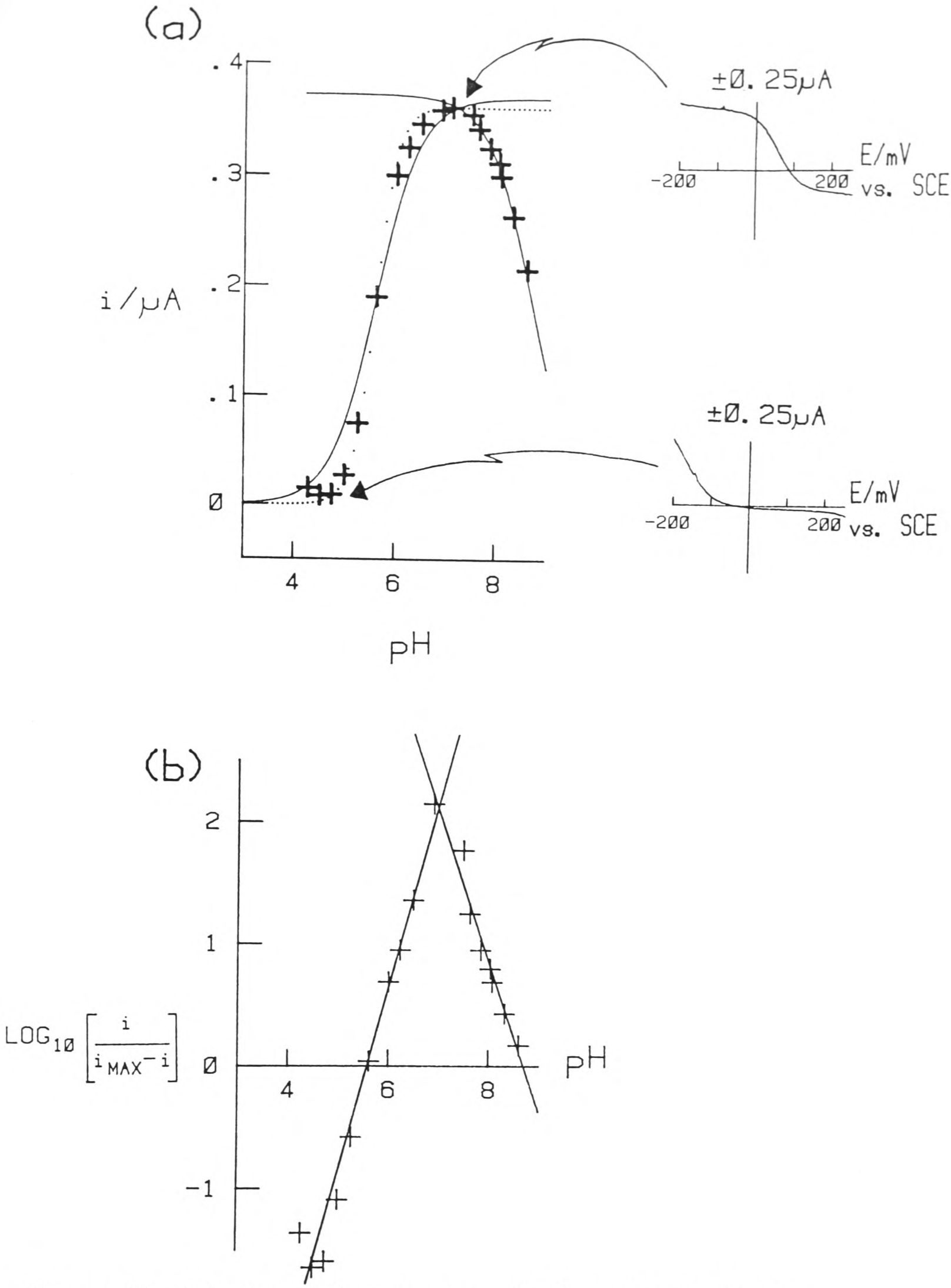

Figure 6.4: **(a)** Faradaic response pH titration of 50 μM cytochrome c in a mixed buffer system (1.5 mM each of Tris, MES, acetate) containing 1 mM NaCl. The insets show the i-E behaviour recorded at the high and low pH limits. All measurements taken at a rotating edge graphite electrode (ω = 20 Hz). The experimental points [+] (E = -75 mV vs. SCE) are compared with the i-pH behaviour predicted, for one (——) and two (·····) proton reactions, from a Henderson-Hasselbach analysis (shown in **(b)**).

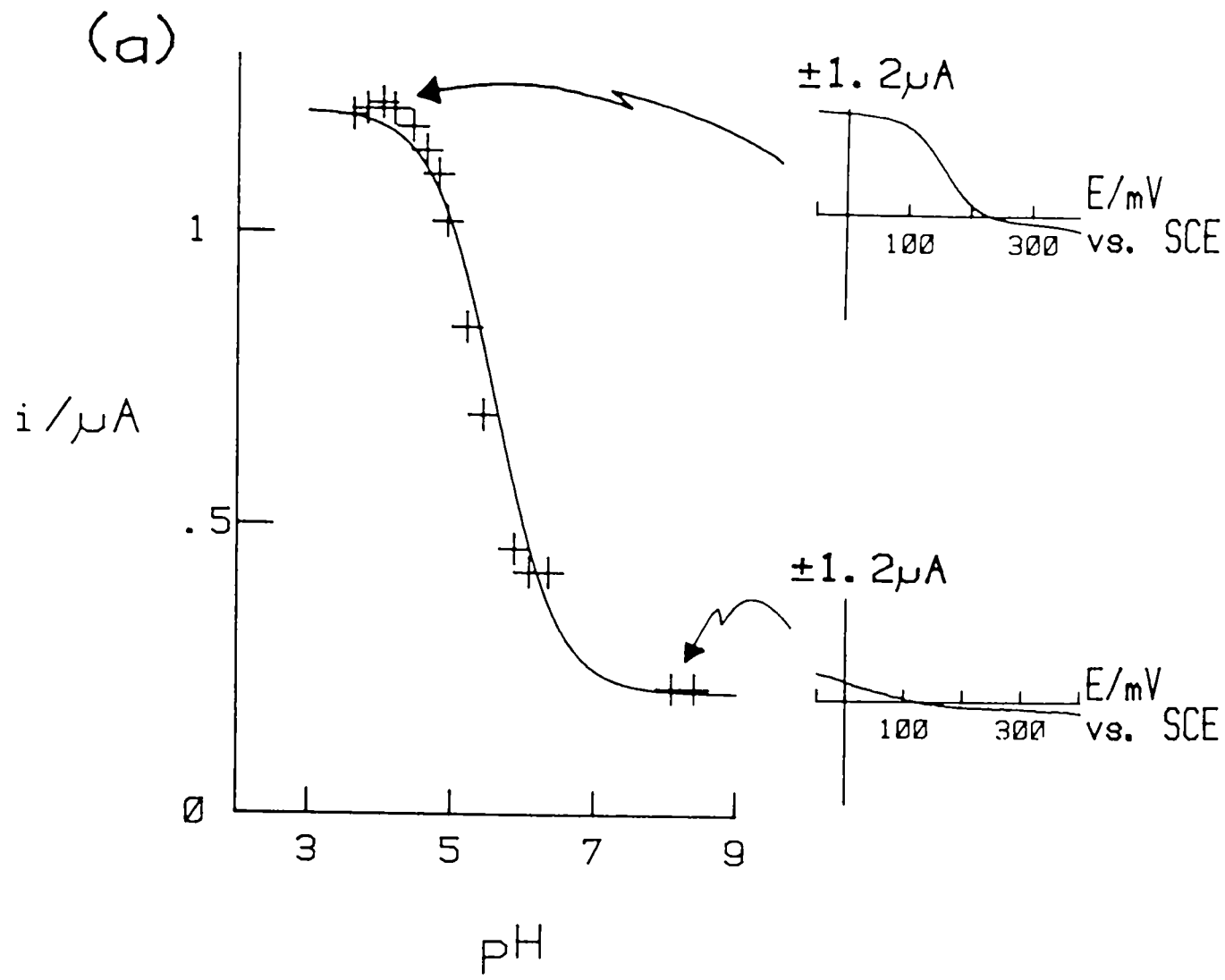

Figure 6.5: **(a)** Faradaic response pH titration of 50 μM $K_3Fe(CN)_6$ in a mixed buffer system (1.5 mM each of Tris, MES, acetate) containing 1 mM NaCl. The insets show the *i*-E behaviour recorded at the high and low pH limits. All measurements taken at a rotating edge graphite electrode (ω = 20 Hz). The experimental points [+] (E = 0 mV vs. SCE) are compared with the i-pH behaviour predicted from a Henderson-Hasselbach analysis (solid line). **(b)** Henderson-Hasselbach analysis of the data in **(a)**.

ionic strength. In parallel with the 'switch-on' of electrochemistry upon lowering the pH, the requirement for multivalent cation promoters decreases. At pH 4 the addition of cations has no detectable effect on the electrochemistry. A similar change in cation requirement is also seen for plastocyanin (Chapter 8). Cyclic voltammetric studies on $Fe(CN)_6^{3-}$, at pH 4, indicated a small additional couple adjacent to the main peaks, with $i_p \propto$ scan rate, indicative of adsorption at this low pH. With respect to the effects of pH it is relevant to note that ferricyanide itself shows no evidence of protonation effects at pH >1 (5). Thus, the observed pH dependence is a property of edge graphite rather than ferricyanide and it seems likely that the chemical origin is protonation of surface functional groups.

Assuming the observed faradaic current to be proportional to the concentration of protonated groups, a Henderson-Hasselbach plot, Figure 6.5(b), may be used to derive a pK value of 5.6 for the surface protonation. The slope of the plot is 1.1 consistent with the involvement of one proton in the reaction. The solid line in Figure 6.5(a) shows the current-pH dependence predicted from this analysis.

For the case of cytochrome c, the observed change of current with pH goes through a maximum at near neutral pH. A Henderson-Hasselbach plot, Figure 6.4(b), gives pK values of 5.6 and 8.7 with associated slopes of 1.45 and 1.2, respectively. The current-pH dependences predicted from these pK values are shown in Figure 6.4(a) for one (——) and two (.....) proton reactions. Cytochrome c itself is structurally sound down to pH 4.0 and has no known pK of 5.6. This pK may, therefore, be ascribed to an electrode surface protonation and may be related to that described

for ferricyanide. The pK of ~8.7 correlates with a known (6,7) reaction of cytochrome c arising from dissociation of the haem-linked S-methionine[80] residue at alkaline pH.

6.6 Direct Electrochemical Studies at 'Clean' Au and Graphite Electrode Surfaces - Electrochemical and Detergent Pretreatments.

The electrochemical responses of redox proteins are critically dependent upon the precise nature of a carbon surface. This may imply significant interactions with the surface. Alternatively, the functional groups at oxidised carbon surfaces may lead to a decrease in the level of surface contamination by providing sites of extensive hydrophilicity (defects) in contaminant overlayers. The hydrophobic basal plane, at which electron transfer rates are retarded, may carry a more extensive 'greasy' contaminant overlayer.

A study of the effect of electrode materials and preparation was undertaken in order to provide the necessary insight into the relative importance of contaminant layers in the catalysis of the electrochemical responses of redox proteins.

(a) Gold

Polycrystalline gold electrodes routinely-polished with 0.3μ alumina, followed by extensive sonication, showed no detectable direct electrochemistry of cytochrome c or plastocyanin. A simple surface modification to increase the activity of such electrodes (although not generally sonicated following polishing) is to dip for two minutes into a 1 mM solution of a suitable bifunctional base (8) followed by copious washing. In the context of this chapter the state of the 'bare'

surface, found to be inactive, is of interest.

In a previous study White and Drobek (9) examined alumina-polished, ultrasonicated polycrystalline gold samples by glancing-angle electron diffraction. Such surfaces showed a ´muddy´ or poorly developed Au diffraction pattern. Following high temperature treatment the same surfaces developed sharp Au, α-Al_2O_3 and trace γ-Al_2O_3 patterns, due to recrystallisation of Al_2O_3, originally smeared across the surface, into large aggregates, consequently revealing ´bare´ Au. In common with edge graphite and glassy carbon it is clear that mechanical polishing results in the retention of residual abrasive particles at gold surfaces.

Electrochemical studies of metal electrodes present the possibility of using H and O chemisorption as characteristic criteria for the cleanliness of a surface. The initial scan cyclic voltammogram for an alumina-polished polycrystalline gold electrode (pH 7.0) is shown in Figure 6.6(a). Cycling this electrode in the potential region between H_2 and O_2 evolution produces clear changes over 15 - 20 cycles (50 mVs^{-1}) until a typical steady-state response is reached (Figure 6.6(b)). The electrode processes corresponding to the peaks observed on this cyclic voltammogram are the formation of oxide layers on Au above +950 mV vs. NHE and a sharp single reduction of these layers at ca. +650 mV.

At the alumina-polished, sonicated surface the anodic charge due to O adsorption is significantly less than at the precycled surface (Figure 6.6) indicating that only a fraction of the surface is capable of chemisorbing oxygen and implying surface contamination by a significant concentration of

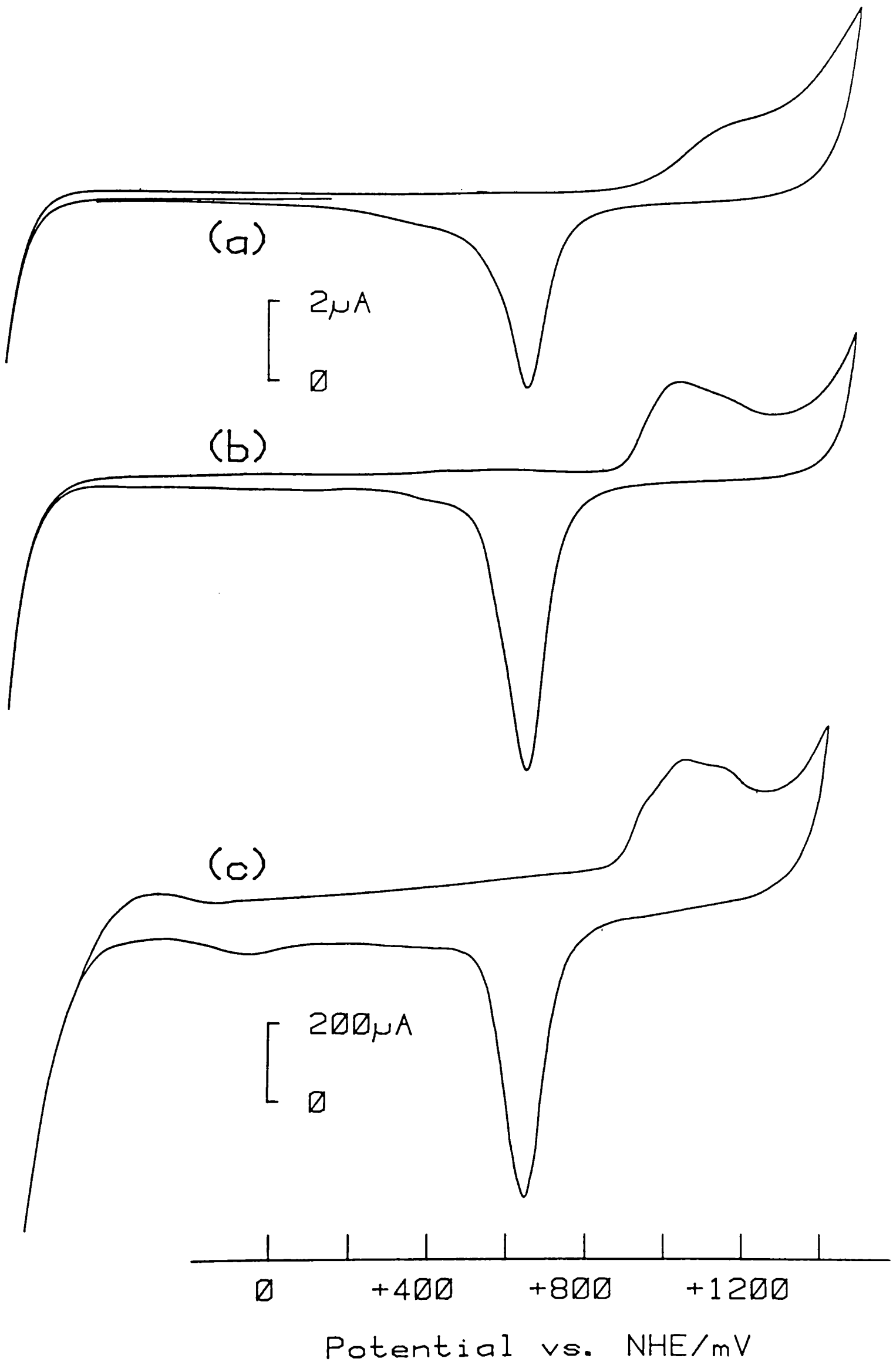

Figure 6.6: Cyclic voltammograms (50 mVs^{-1}) illustrating the pre-cycling of Au electrodes in 20 mM phosphate, 100 mM $NaClO_4$, pH 7.0. (a) Alumina-polished gold disc electrode (4 mm dia.), cycle 1; (b) as (a), steady-state response; (c) thin film Au electrode (area = 4 cm^2), cycle 1.

impurities. After pre-cycling to the steady-state the anodic charge increases due to oxidation and displacement of these contaminants. At a surface 'cleaned' in this way irreversible electron-transfer to cytochrome c may be evident but is still usually impersistent.

An alternative source of polycrystalline Au is thin films deposited on to a convenient substrate in vacuo. The oxide growth at a 1000 Å thin film, with no pre-treatment, shows only marginal changes over the first few cycles (Figure 6.6(c)). The behaviour of this surface implies that there is only a low level of intrinsic organic contamination or that the major impurity evident in Figure 6.6(a) is alumina. Electrochemical trials of cytochrome c at these thin film electrodes gave only a trace, impersistent response in all experiments (Figure 6.7) and near reversible electrochemistry on addition of 4,4'-bipyridylethylene to solution.

The initial (scan 1) voltammetric response of a detergent ('Micro') treated (thorough sonication or polishing with detergent followed by copious rinsing or sonication in H_2O) polycrystalline gold disc electrode is similar to that of a pre-cycled steady-state electrode (Figure 6.6(b)). However, the electrochemistry of cytochrome c is now significantly enhanced and more stable (Figure 6.7(b)) than at the other 'clean' surfaces, although the observed response (ΔE_p 85 [97] mV, i_p 0.054 [0.044] μA at 2 mVs^{-1}, cycle 2 [10]) is less reversible and less stable than is observed at the same surface following modification with 2-(pyridinyl-methylene)hydrazinecarbothioamide (ΔE_p 60mV, i_p 0.055 μA at 2 mVs^{-1}, steady-state). Simple dipping of a gold surface into the detergent, followed by rinsing with water prior to use, produced

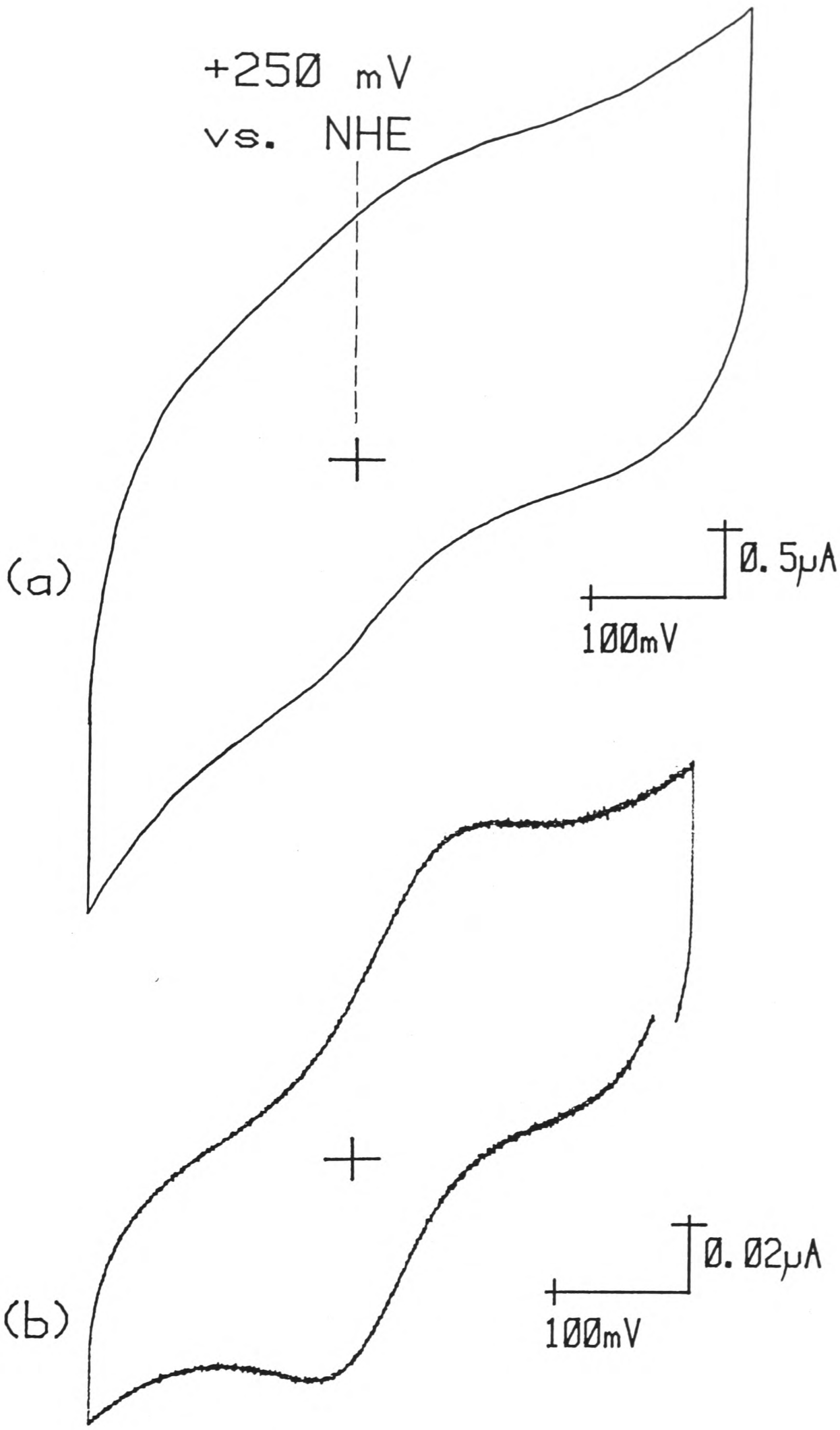

Figure 6.7: Cyclic voltammograms showing the faradaic response of cytochrome c (50 μM) in 5 mM Tricine, 100 mM NaCl, pH 8.0, at 'bare' Au electrodes. (a) Thin film gold electrode (area = 4 cm^2), cycle 4 at 20 mVs^{-1}; (b) detergent-treated Au disc electrode (4 mm dia.), cycle 6 at 2 mVs^{-1}.

no detectable direct electrochemistry whilst ESCA analysis of detergent ('Micro')- treated gold surfaces revealed no detectable residual contamination resulting from this pretreatment procedure. It seems that the detergent acts to remove residual contaminants from the gold surface. It is relevant to note that a similar treatment restores activity to inactive batches of thin film RuO_2 electrodes (10).

A similar investigation of the effects of electrode contamination was undertaken for the 2[4Fe-4S] ferredoxin. The electrochemical response at alumina-polished gold electrodes, in the presence or absence of multivalent cations, showed no detectable difference from the response in buffer alone (Figure 6.8(a)). The same electrode following thorough detergent ('Micro') treatment (as above) showed a poorly-defined yet reproducible faradaic response (Figure 6.8(b)). Addition of $Cr(NH_3)_6^{3+}$ to 4 mM promoted a reasonably stable faradaic response with ΔE_p <100 mV (Figure 6.8(c)). The corresponding response at edge graphite (ΔE_p 62.5 mV) is shown for comparison, Figure 6.8(d).

(b) Graphite

Several reports have described the ability of heat or electrochemical pretreatments following polishing to improve the reversibility of electrochemical responses observed at carbon electrodes (11,12). The effect of such procedures probably involves changes in the degree of functionalisation and removal of surface contaminants. Reductive and oxidative pre-treatments of a cleaved basal plane electrode (-1.5 V or +0.7 V vs. SCE for 10 mins.) had no observable effect on the electrochemical response of the 2[4Fe-4S] ferredoxin at pH 8.0. Similarly,

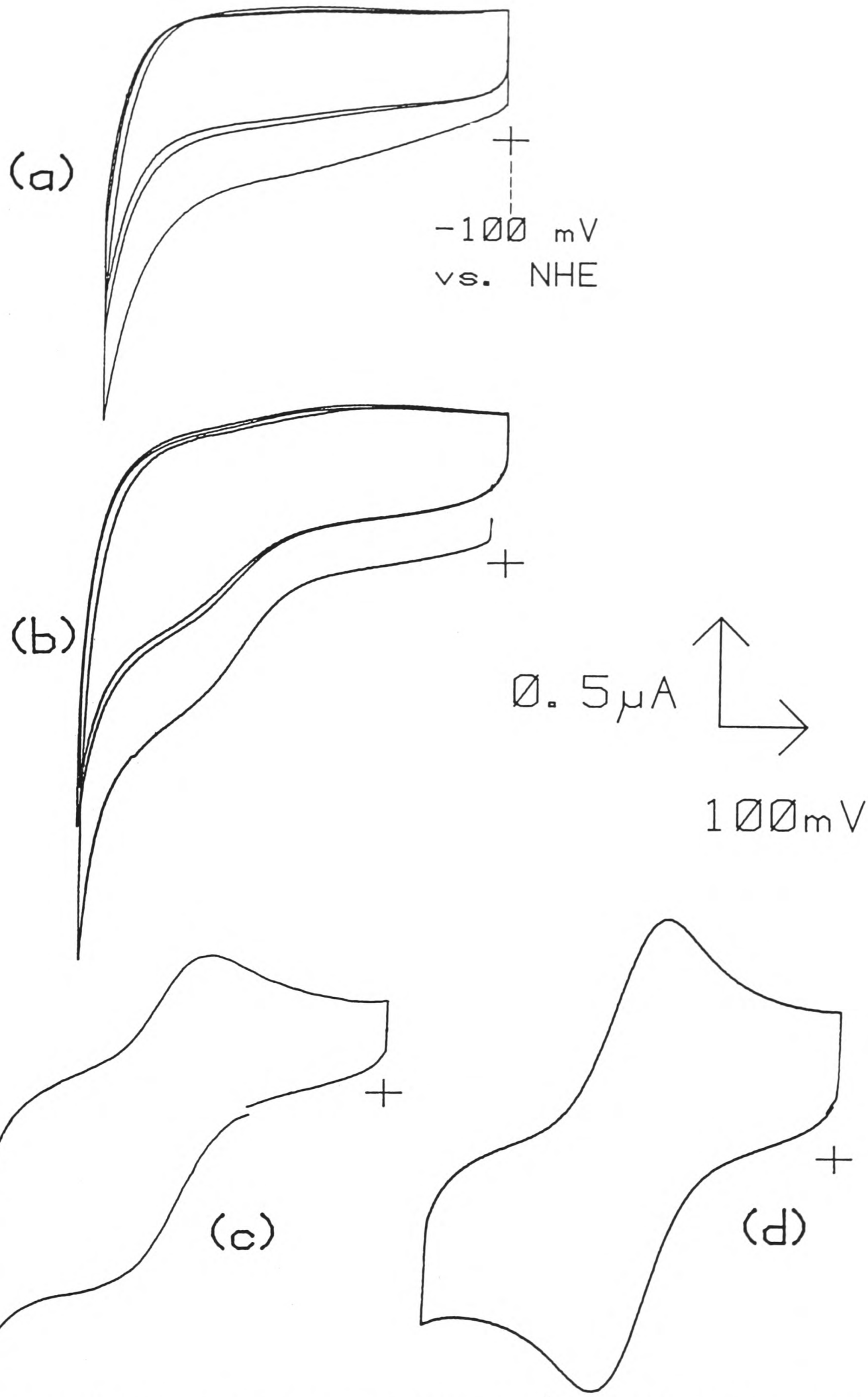

Figure 6.8: Cyclic voltammograms (20 mVs^{-1}) of 67 μM 2[4Fe-4S] ferredoxin (in 5 mM Tricine, 100 mM NaCl, pH 8.0) at 'bare' Au electrodes. (a) Alumina-polished Au disc electrode; (b) as (a), but following detergent-treatment of the electrode; (c) as (b), with the addition of 4 mM $Cr(NH_3)_6^{3+}$; (d) comparative response at edge plane graphite, conditions as (c). (a,b) voltammetric cycles 1-3 shown. (c,d) voltammetric cycle 4 shown.

sonication of edge and cleaved basal surfaces in detergent ('Micro') has no significant effect on the observed electrochemical responses.

6.7 Direct Electrochemical Studies at Ruthenium Dioxide Electrodes.

Exploratory studies of thin film ruthenium dioxide electrodes using the 2[4Fe-4S] ferredoxin revealed similar behaviour towards cation promotion effects to that seen at edge graphite. The addition of 12 mM $Cr(NH_3)_6^{3+}$ to solution is sufficient to promote a quasi-reversible, stable electrochemical response (ΔE_p <100 mV, 20 mVs^{-1}) superimposed on a background due to H_2 evolution and RuO_2 reduction (Figure 6.9)

6.8 Discussion.

Direct electrochemical studies at a 'bare' gold electrode show that faradaic responses are critically dependent upon the removal of surface contaminants. These are most likely dispersed alumina particles and hydrocarbon adsorbates. This suggests that the interaction between proteins and carbon electrodes may also be regulated by surface contaminants. However, electrochemical oxidation and reduction, detergent treatments and various polishing procedures do not affect the responses at edge and cleaved basal plane graphite electrodes. Thus, it appears that the important parameter in promoting direct electrochemical responses at pyrolytic graphite is the degree of oxidation of the carbon surface. Nevertheless, a picture of a clean, homogeneous edge surface is, clearly, an ideal and the presence of alumina and inevitably trace organic surface contaminants cannot be overlooked. It must also be remembered that a polished edge

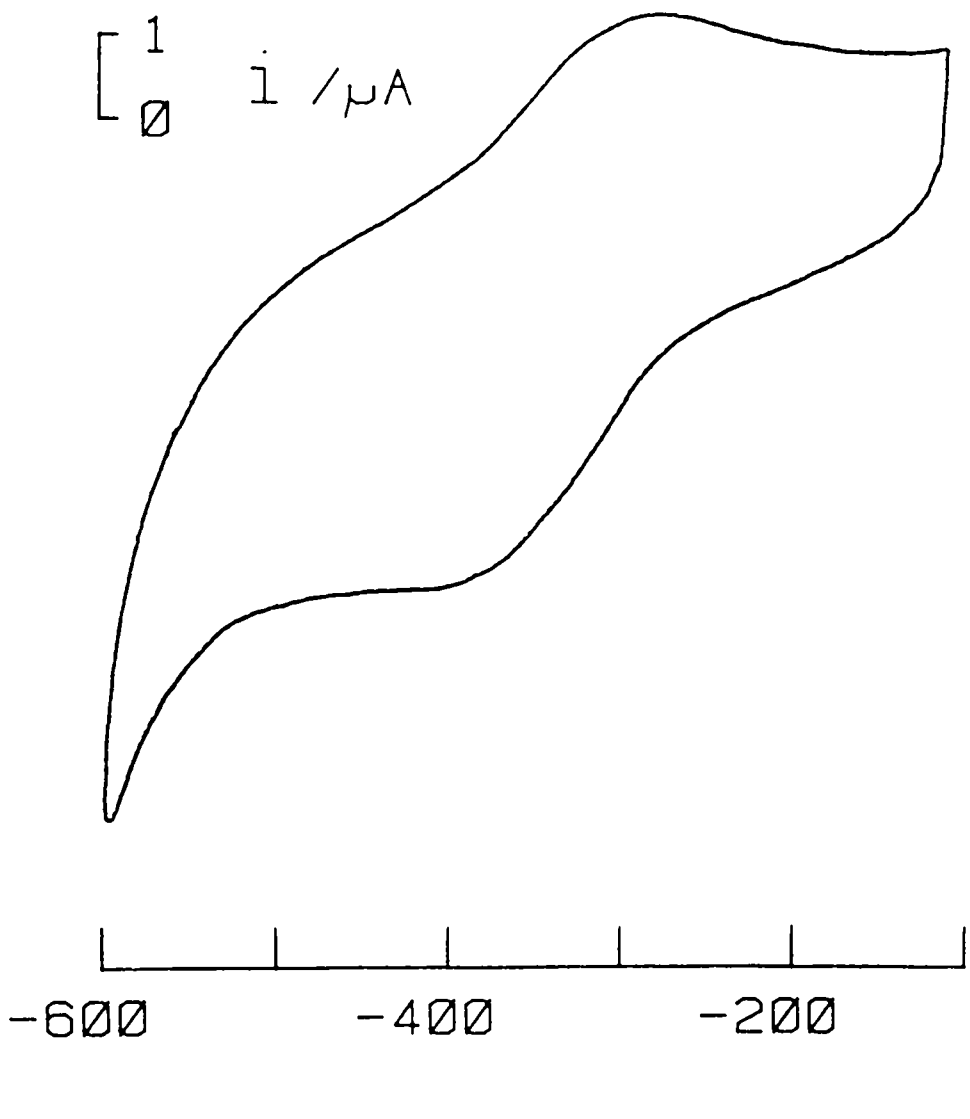

Figure 6.9: Cyclic voltammogram (20 mVs^{-1}, cycle 4) of 0.3 mM 2[4Fe-4S] ferredoxin (in 5 mM Tricine, 100 mM NaCl, pH 8.0) at a ruthenium dioxide electrode, following the addition of 12 mM $Cr(NH_3)_6^{3+}$.

electrode has a reflective finish similar to glassy carbon, and that the direct electrochemistry of cytochrome c is essentially identical at these two surfaces (see Chapter 4). A glassy carbon surface consists of random, tangled aromatic ribbons (13).

In view of the preceeding statements a model of a polished edge surface is shown in Figure 6.10. This model contains some of the groups detected chemically (14), including carboxyl groups and phenols. Also represented are surface 'disorder' regions with 'glassy' or folded over planes adjacent to pits or sites of alumina inclusion. These basal areas may provide sites for contaminant adsorption. Specific boundary zones at edge sites may have an 'arm-chair' or 'zig-zag' boundary. A key feature of any surface model is the degree to which 'hills' and 'valleys' are formed in the surface following polishing. Comparison of electrochemically-derived diffusion coefficients with calculated or literature values (Chapters 4 and 8) shows that the surface area accessible to redox proteins differs by no more than an order of magnitude from the geometric surface area.

In evaluating the role of edge-surface functionalisation the effect of pH on direct electrochemical responses provides clear evidence for the importance of charge interactions in the interfacial region. These effects are evident over a wide potential range (~800 mV). The direct electrochemistry of cytochrome c is "switched off" as the pH drops below 6. By contrast electron-transfer to ferredoxin, ferricyanide and plastocyanin (Chapter 8) is "switched on" by mild acidification.

An increase in the number of protons in the interfacial region will alter the potential of the reaction plane. Thus, one interpretation of the observed pH titrations is simply one of a

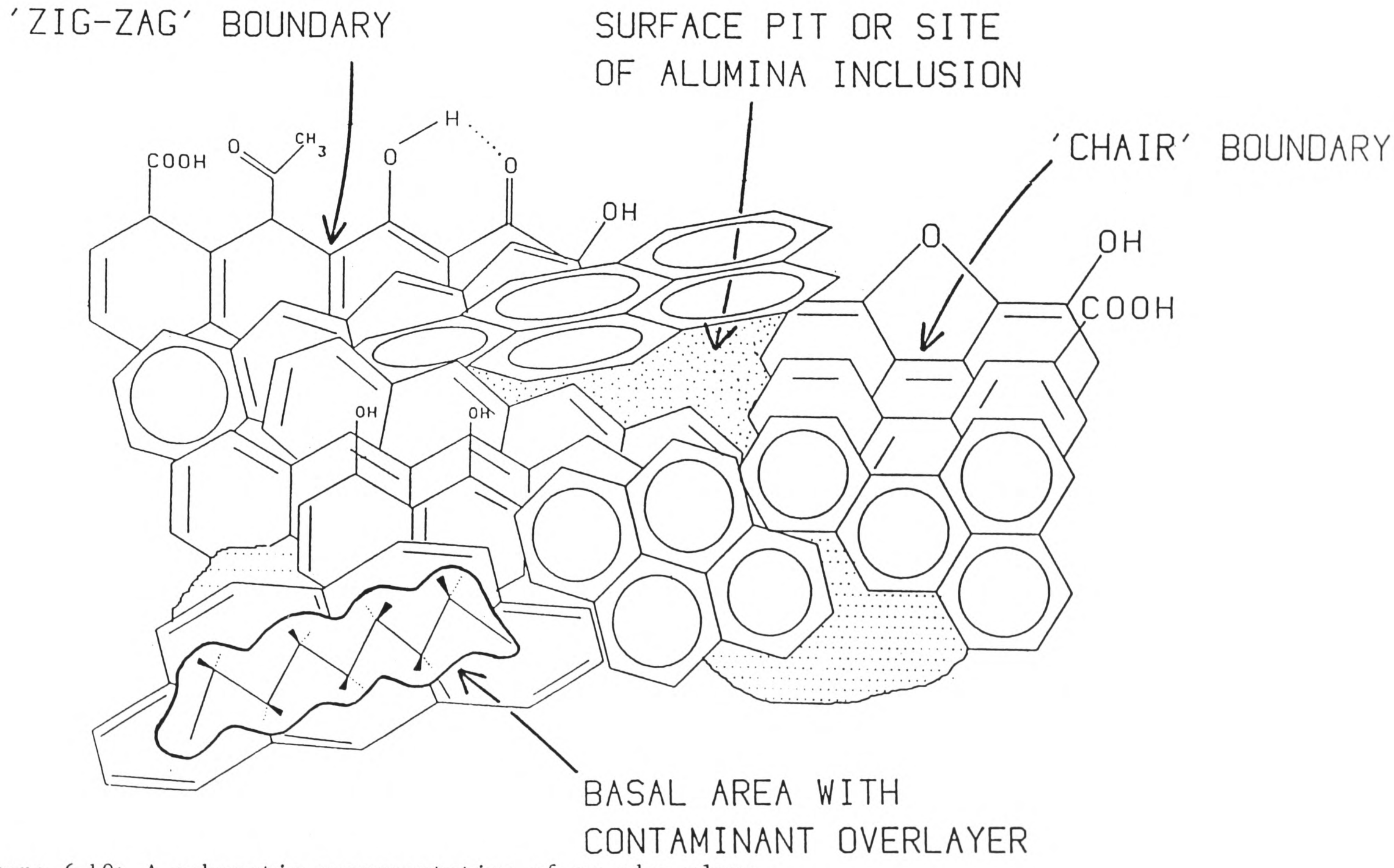

Figure 6.10: A schematic representation of an edge plane pyrolytic graphite electrode surface.

change in diffuse-layer characteristics leading to a relief of electrostatic repulsions at low (negatively-charged proteins or $Fe(CN)_6^{3-}$) or high (cytochrome c) pH. This may arise from protonation of electrode surface groups or perhaps of amino acids on the protein. Alternatively, the protonation of titratable groups may facilitate hydrogen-bonding interactions between electrode surface groups and negatively-charged protein molecules in the interfacial region. In the case of cytochrome c, a decrease in pH will remove the capacity for the formation of hydrogen bonds involving haem-face lysine residues, in accord with the decrease in faradaic current towards low pH. In view of the observation (4) that $IrCl_6^{2-}$ shows a similar pH profile to those described in this chapter, then it seems likely that the regulation of electrode processes through hydrogen-bonded interactions will only be of secondary importance. In addition, it is unlikely that dispersed alumina has a role in this effect as such behaviour is a general property of carbon electrodes (4) including carbon paste and glassy carbon which are both expected to carry oxidised C-O functionalities.

Ferricyanide exhibits no intrinsic protonation equilibria in the pH range 4 - 8. Thus, it may be concluded that the direct electrochemical responses are regulated by electrode surface protonation. Assuming that these protons associate with functional groups at the surface then an apparent surface pK for edge graphite is 5.5 - 5.8. This value lies above the range expected for a weak aromatic acid (benzoic acid- pK = 4.2; α-naphthoic acid- pK = 3.7) and below that for a phenolic group. However, at such a heterogeneous surface, the nature of the microenvironment will clearly be important in determining the

dissociation of charged functional groups. In particular, shifts of pK values from those expected in the bulk solution may occur due to hydrogen-bonding with neighbouring groups, or to a change in pH close to the electrode surface arising from the interplay of pK, local H^+ concentration, and surface potential (ψ_o) (15). In general, the dissociation constant is shifted according to (6.1):

$$pK = pK^B - (f/2.303).\psi_o \qquad (6.1)$$

pK = apparent pK.

pK^B = pK of species free in solution

f = F/RT

ψ_o = potential at the surface arising from a charge density σ

An example of a neighbouring group effect is the marked shift (>4pK units) of the pK of His-159 in papain attributed to a salt bridge His....Cys-25 (16). These effects complicate assignment of the surface pK to a particular acidic group as does the detection of both acidic and weakly basic groups on carbon surfaces (14).

In view of the complex functional chemistry expected at an edge surface, it seems likely that the observed pH dependence is not attributable to a single type of C-O group at the electrode but represents a complex function of the ionisation constants of a range of acidic and basic functional groups. In fact, analogy with biological macromolecules suggests that the pH dependence may represent a transition from a negatively-charged surface (pH >5.5) to a positively-charged surface (pH <5.5). If this is the case, then pK values derived from the Henderson-Hasselbach

analysis may be more truly described as isoelectric points (pI). In accord with this proposal, the electrochemistry of negatively-charged species is 'switched off' at low pH, whilst that of the positively-charged species, cytochrome c, is 'switched on'. These observations suggest that there is some positive charge character associated with the surface at low pH.

As part of the discussion of protonation equilibria interesting analogies may be drawn with the use of 'dimensionally-stable anode' electrodes such as RuO_2 thin films. It has already been seen that there is a close parallel with the behaviour at edge graphite in that ferredoxin undergoes cation-promoted direct electrochemistry at both surfaces. In a more comprehensive study (17), RuO_2 electrodes were found to display the same kind of trend towards H^+-promotional effects as that described for cytochrome c at edge graphite. The pH profile observed is consistent with a transition around pH 6.0. From a consideration of previously published values for the potential of zero zeta potential (pzzp) of RuO_2 (5.1 - 6.1), this transition has been ascribed (17) to a change in surface charge due to the amphoteric nature of surface hydroxyl groups. For cytochrome c similar changes have also been observed (18) at a gold electrode surface-modified with 4,4'-bipyridylethylene and ascribed to the protonation of pyridyl nitrogen.

It is apparent that a general feature of edge graphite, RuO_2 and surface-modified gold electrodes is acid-base protonation equilibria which may provide charged groups and the basis for electrostatic interactions with charged redox proteins. Indeed, mechanistic studies (19) on the near reversible electrochemistry of cytochrome c at a gold electrode surface-

modified with 4,4′-bipyridylethylene have shown that there is considerable adsorption of both reactant and product at the electrode. This may occur through H-bonding between lysine groups on the cytochrome and the free pyridyl N of the adsorbed promoter.

The major feature of edge graphite and RuO_2 is a hydrophilic surface associated with surface functionalisation. In the latter case the surface binds water under ambient conditions so forming an extensively hydroxylated surface. It is likely that this functionalisation can lead to specific electrostatic binding interactions with redox proteins similar to those detailed above for modified gold. These interactions may result from ion-ion, ion-dipole or more specific H-bonds with charged groups on the surface of redox proteins. By virtue of their solubility in water all redox proteins carry such groups on their surfaces. In the case of azurin, however, there is extensive charge pairing among side-chain residues. This is reflected in the lower selectivity seen for this protein at various electrodes (Chapter 4). In this particular case binding may occur through hydrophobic interactions between regions of basal plane character at the electrode and the hydrophobic surface close to the Cu site of azurin.

The hydrophobic contribution to association is dominated by the entropy gain which derives from a reduction in solvent accessible surface area (20). Such interactions involving large areas of surface are entirely non-specific leading to stronger and more permanent adsorption. Such is the case for azurin whose direct electrochemistry is complicated by adsorption at graphite surfaces. On the other hand, for electrostatic interactions, the difference between a protein-protein or protein-electrode

hydrogen-bond and the corresponding bonds made with water, by separated reactants, will only be small, implying weak adsorption and ready exchange with the bulk of solution. That such binding is weak and freely reversible is consistent with the observation of predominantly diffusion-controlled electrochemical responses. Perhaps weak binding also ensures a degree of lateral mobility so that the protein may 'roll' along the surface until a productive orientation is reached and the electron-transfer event occurs.The more complementary the two surfaces the stronger will be the binding. This key feature is also that which forms the basis for recognition in protein-protein electron-transfer (see Chapter 1). Given the heterogeneity of even 'modified' electrode surfaces it is unlikely that the degree of complementarity achieved will approach that found in protein-protein interactions and this may contribute to the weak binding observed at electrode surfaces. Nevertheless, the widespread, almost 'universal', success of polished graphite may be due to just such asymmetry in charge and site distribution, affording structural complementarity to any organised protein surface through the heterogeneity and random distribution in functional groups available at the surface. Taking this one step further, especially favourable interactions may arise as a result of the large diameter of a redox protein. Take cytochrome c, for example, with a diameter of 33 Å, approaching an edge graphite electrode surface with a monolayer coverage of C-O functionalities (as suggested by ESCA studies). In an orientation with the haem face proximal to the electrode surface, then there may be >100 C-O groups in the immediate vicinity of the haem face lysine residues.

The interfacial interactions between a charged protein molecule and a 'clean' or 'bare' gold surface are of interest in light of the previous discussions. Such surfaces may be charged, may even be hydrophilic but are not specifically functionalised as are edge graphite, RuO_2 or surface-modified gold surfaces.

It has been seen that direct electrochemistry of cytochrome c may, under certain conditions, be observed at gold electrodes in the absence of adsorbed promoters. The appearance of a faradaic response may be attributed to removal of contaminants from the surface. A similar improvement has also been reported (21) following exposure of a gold surface to an air plasma or a soft hydrogen flame. It may be that an additional role for modifiers such as 4,4'-bipyridylethylene is to displace less-specifically adsorbed contaminants from a gold surface or to provide defects ('hot spots') in an organic overlayer at which electron-transfer may proceed. These contaminants, whether polishing abrasives or organic adsorbates, are clearly present at significant levels at routinely used electrodes. It is evident that all 'cleaning' procedures lead to distinctly less-reversible electrochemistry than is seen at modified surfaces and also that modifiers are still active as promoters at specially cleaned surfaces. Clearly, modifiers have a specific effect and reversible adsorption of proteins through specific protein-electrode interactions is less favourable at a 'bare' surface.

The formal potential of cytochrome c lies close to the potential of zero charge (pzc) of polycrystalline Au (-40 mV vs. SCE in ClO_4^- (22)). There has been considerable controversy (23,24) in the literature over the degree of orientation of inner layer solvent dipoles, at polycrystalline Au substrates, in this

potential domain. The degree of hydrophobicity of the surface and, hence, the extent of orientation of inner layer solvent molecules is still not satisfactorily resolved. The impersistent faradaic response of cytochrome c observed at a 'clean' Au surface suggests that a durable contact is made through close approach of the protein to this boundary structure and that there is more than just free diffusion in the region of the outer Helmholtz plane (OHP). In a spectro-reflectance study, Parsons et. al. (25) found that cytochrome c, albeit unpurified, bound very strongly to 'clean' Au single crystal faces. Strong interactions may occur through hydrogen-bonding to suitably oriented solvent molecules, ion-pairing to specifically adsorbed anions or, more likely, through more permanent non-coulombic adsorption processes. The latter may occur at regions of organic contamination or by displacement of inner layer solvent molecules. Furthermore, there is no reason to expect a strong orienting influence upon the incoming cytochrome. This may lead to non-productive interactions with regions other than those adjacent to the haem edge.

At high negative charge densities (i.e. away from the pzc) inner layer solvent dipoles orient under the influence of the interfacial electric field gradient, with ordering propagated perpendicular to the surface through dipole-dipole interactions. Such will be the case at the formal potential of C. pasteurianum ferredoxin. The characteristics of the surface at these potentials - solvent ordering and excess negative charge density- are similar to those expected at edge graphite under the same conditions. Indeed, ferredoxin undergoes cation-promoted direct electrochemistry at both surfaces. However, a 'hydrophilic' surface and charge compensation are clearly not the only factors

determining the reversibility observed, as the response is less reversible and more impersistent at the bare Au surface. Evidently there is a need for specific functionalisation and perhaps non-discrete charge density to achieve an electrode with near optimal electron-transfer activity.

The importance of solvent structure to the conformational integrity of redox proteins is well documented (26,27,28). Changes in solvent structure in aqueous media can be observed close to phase boundaries. With reference to electrochemical studies, such a ´medium´ change may arise from the local order induced in a solvent by electric field gradients across the double layer, or by the chemical nature of the surface. On the basis of a wide range of experimental observations, Drost-Hansen (29) and Trasatti (30) have proposed models for the structure of water near polar and non-polar surfaces and discussed their relevance to biological phenomena. Surface ordering of water is a feature of polar surfaces and may extend to the formation of gel-like water structures at metal oxide electrodes. By contrast, the bulk structure of water may be enhanced near hydrophobic surfaces. Clearly, the extent of changes in the conformation of a protein at an electrode will depend upon the structural dissimilarity between interfacial (vicinal) and bulk water. From the current study it appears that redox proteins undergo reversible association with electrode surfaces which are predominantly hydrophilic (polar) in character.

A further likely effect of surface hydration is illustrated by studies (31) of the electrode reactions of the Cr(III)/Cr(II) couple. Thus, $Cr(H_2O)_6^{3+}$ undergoes reduction some 0.1 to 0.2 nm further from an electrode than $Cr(NH_3)_6^{3+}$. This is

consistent with the greater hydrated radii of the former and represents a strong 'surface hydrophilicity' effect. As most proteins are normally highly-aquated (26,32) then close approach to polar surfaces, such as RuO_2 and edge graphite, may also be 'hindered' by ordered water structure. The ability to prevent close approach of protein and electrode surfaces may prevent strong adsorption concomitant with denaturation. Similarly, a gold electrode with a surface-modifier in an 'upright' rather than a 'flat' orientation may successfully constrain an approaching macromolecule to a reversible binding site outside the OHP. The observed surface pK of 4,4'-bipyridylethylene, as measured by faradaic response titrations of cytochrome c (18), is the same as that observed for the promoter free in the bulk of solution. This suggests that the protein is held at, but not too close to, the electrode surface. The electrochemistry of azurin is most reversible at surface-modified Au surfaces whereas surfaces with aromatic character (graphite) show weak adsorption. The success of surface-modified gold electrodes may lie in preventing azurin from reaching hydrophobic surface regions.

The most stringent test of the efficiency of edge graphite, RuO_2 and surface-modified Au as electrodes for promoting biological electron-transfer activity is the viability of the redox proteins interacting with these artificial surfaces. That activity is successfully maintained is evident from spectro-electrochemical studies (33), and the coupling of electron-transfer to natural redox partners, in particular, the ability of cytochrome c to act as an exogeneous source of reducing equivalents to intact organelles of which it is an integral component (34).

References - Chapter 6

1) Dong, S. and Kuwana, T., J. Electrochem. Soc. 131, 813, (1984).

2) Zak, J. and Kuwana, T., J. Electroanal. Chem. 150, 645, (1983).

3) Blurton, K. F., Electrochim Acta 18, 869, (1973), and Britton, W. E., El-Hashash, M., El-Cady, M. and Assubaie, F., J. Electroanal. Chem. 172, 189, (1984), and references therein.

4) Deakin, M. R., Stutts, K. J. and Wightman, R. M., J. Electroanal. Chem. 182, 113, (1985).

5) Jordan, J. and Ewing, G. J., Inorg. Chem. 1, 587, (1962).

6) Greenwood, C. and Palmer, G., J. Biol. Chem. 240, 3660, (1965).

7) Osheroff, N., Borden, D., Koppenol, W. H. and Margoliash, E., J. Biol. Chem. 255, 1689, (1980).

8) Allen, P. M., Hill, H. A. O. and Walton, N. J., J. Electroanal. Chem. 178, 69, (1984).

9) White, M. L. and Drobek, J., J. Phys. Chem. 70, 3432, (1966).

10) Harmer, M. A., unpublished results.

11) Wightman, R. M., Deakin, M. R., Kovach, P. M., Kuhr, W. G. and Stutts, K. J., J. Electrochem. Soc. 131, 1578, (1984).

12) Engstrom, R. C. and Strasser, V. A., Anal. Chem. 56, 136, (1984).

13) Jenkins, G. M. and Kawamura, K., Nature 231, 175, (1971).

14) Boehm, H. P., Adv. in Catalysis 16, 198, (1966).

15) Barber, J., Biochim. Biophys. Acta 594, 253, (1980).

16) Johnson, F. A., Lewis, S. D. and Schafer, J. A., Biochemistry 20, 52, (1981).

17) Harmer, M. A. and Hill, H. A. O., J. Electroanal. Chem. 189, 229, (1985).

18) Eddowes, M. J. and Hill, H. A. O., J. Am. Chem. Soc. 101, 4461, (1979).

19) Albery, W. J., Eddowes, M. J., Hill, H. A. O. and Hillman, A. R., J. Am. Chem. Soc. 103, 3904, (1981).

20) Clothia, C. and Janin, J., Nature 256, 705, (1975).

21) Bowden, E. F., Hawkridge, F. M. and Blount, H. N., J. Electroanal. Chem. 161, 355, (1984).

22) Clavillier, J. and Nguyen Van Huong, C., J. Electroanal. Chem. 80, 101, (1977).

23) Trasatti, S., Adv. Electrochem. and Electrochem. Eng. 10, 213, (1977).

24) Gardner, J. R. and Woods, R., J. Electroanal. Chem. 81, 285, (1977).

25) Hinnen, C., Parsons, R. and Niki, K., J. Electroanal. Chem. 147, 329, (1983).

26) Franks, F. and Eagland, D., Critical Rev. Biochem. 3, 165, (1975).

27) Gekko, K. and Koga, S., Biochim. Biophys. Acta 786, 151, (1984).

28) Hill, C. L., Renaud, J., Holm, R. H. and Mortensen, L. E., J. Am. Chem. Soc. 99, 2549, (1977).

29) Drost-Hansen, W., Ind. Eng. Chem. 61, 10, (1969).

30) Trasatti, S., Electrochim. Acta 28, 1803, (1983).

31) Weaver, M. J. and Satterberg, T. L., J. Phys. Chem. 81, 1772, (1977).

32) Watenpaugh, K. D., Sieker, L. C. and Jensen, L. H., J. Mol. Biol. 131, 509, (1979).

33) Armstrong, F. A., Hill, H. A. O. and Walton, N. J., FEBS Lett. 145, 241, (1982).

34) Coleman, J. O. D., Hill, H. A. O., Walton, N. J. and Whatley, F. R., FEBS Lett. 154, 319, (1983).

CHAPTER 7

MULTIVALENT CATIONS AS PROMOTERS OF THE DIRECT ELECTROCHEMISTRY OF IRON-SULPHUR PROTEINS

7.1 Introduction.

Carbon electrodes are frequently used in electroanalytical studies. However, for many low molecular weight compounds, heterogeneous charge-transfer rates at these electrodes are very slow and far from the expected diffusion-controlled behaviour. The factors affecting these electron-transfer rates are still, in general, poorly understood, despite several recent studies directed at providing a more complete understanding of the behaviour of these electrodes in aqueous systems. Nevertheless, a 'catalogue' of methods for improving electrochemical reversibility at carbon electrodes is developing in the literature. Factors evaluated include electrode fabrication techniques, solution pH, polishing procedures and thermal, chemical or electrochemical pretreatments. At carbon paste electrodes, a decrease in electrochemical reversibility has been correlated with an increase in the concentration of pasting liquid (1), whilst electrochemical responses at glassy carbon appear particularly sensitive to dispersed polishing agents (2) and the degree to which the surface is exposed to air (3). Wightman et. al. (4) have suggested that an important step in improving responses at graphitic electrodes is to increase the availability of edge orientation.

The initial observations of redox protein electrochemistry implicate the importance of multivalent cations as regulators of electrochemical reversibility at polished graphite electrodes. In

the case of negatively-charged redox proteins, such as the Fe-S proteins, the addition of multivalent cations is sufficient to effect a transition from no detectable to a quasi-reversible faradaic response, corresponding to an increase in the heterogeneous rate constant, k_s, of several orders of magnitude. The efficiency of a particular cationic promoter is a function of charge, $M^{3+} > M^{2+} > M^{+}$, in accord with a predominantly electrostatic interaction. It is the aim of this chapter to provide a more detailed exploration of the fundamental role of multivalent cations in the interaction between negatively-charged redox proteins and graphite electrodes. Clearly, there is a need to recognise that specific electrostatic effects upon the rates of heterogeneous electron-transfer at graphite electrodes may be determined by the nature of **protein charge, electrode charge** and **cationic charge.**

The work of Frumkin's school provides the starting point for interpreting the role of cations. Correction for simple, non-specific, double-layer effects, as described by classical Frumkin theory (5), in which the only influence is that of coulombic effects on electrode reaction rates, can be made assuming an exponential dependence of reaction rate on the average electrostatic potential at the reaction plane (usually defined as the outer Helmholtz plane (OHP)). Such corrections, when applied to inorganic couples, such as $Fe(C_2O_4)_3^{3-}$ and $Fe(CN)_6^{3-}$, yield corrected rate constants at solid metal surfaces which are largely independent of the electrode material (6). This also appears to be a feature of graphite surfaces in that the rate of electron-transfer to $Ru(NH_3)_6^{3+}$ is identical at edge or cleaved basal plane electrodes. In the case of $Fe(CN)_6^{3-}$, faradaic

responses indicate a small edge-basal surface selectivity, but responses are promoted by multivalent cations at **both** edge and cleaved basal surfaces. However, for all the redox proteins examined in Chapter 4 there is a marked surface-selectivity distinguishing edge and cleaved basal electrodes, and cation promotion is only observed at edge but not cleaved basal surfaces. Clearly, in the case of redox proteins, there are factors more selective than simple double layer effects operating.

One of the properties of an electrical double layer that can be tested experimentally is the differential capacitance and its dependence on electrolyte type and concentration. However, the main drawback of using edge graphite electrodes is the complete lack of unambiguous differential capacitance-potential data, so that values of surface potential and charge density are not available and simple double-layer effects cannot be corrected for. Nevertheless, specific cation promotion effects at this surface may be probed through variations in the ionic strength (through which the extent of the diffuse layer, as given by the Debye length, may be controlled), variations in the charge and coordination environment of the cation, and through comparative studies of a series of negatively-charged proteins (e.g. the Fe-S proteins) of varying redox potential and structure.

In view of the introductory statement, any comparative study of specific cation effects upon individual redox proteins will be restricted by the activity and reproducibility of the type of carbon electrode used. It is apparent that the surface providing the most favourable and reproducible interface for a wide range of redox proteins is edge-oriented pyrolytic graphite.

Additionally, an extensive spectroscopic and electrochemical investigation (Chapters 5 and 6) has gone some way towards characterising the specific surface chemistry associated with this surface. This electrode may then be used as a reliable basis for defining more closely the relation between protein, cation and electrode surface.

7.2 Experimental Details.

(a) **Preparation of titrant solutions.**

Hexa-ammine chromium(III) chloride hydrate [$Cr(NH_3)_6Cl_3 \cdot H_2O$], tris(1,2-diaminoethane) chromium(III) chloride [$Cr(en)_3Cl_3$], tris(trans-1,2-diaminocyclohexane) chromium(III) chloride [$Cr(chxn)_3Cl_3$] and tris(phenanthroline) iron(II) perchlorate [$Fe(phen)_3(ClO_4)_2$] were synthesised by V. J. Lowe according to literature procedures (7). Purities were established by chemical analysis and spectrometry. The perchlorate salt of $Fe(phen)_3^{2+}$ was converted into the more soluble chloride form by anion exchange. Hexamethonium chloride, $HMCl_2$ [$Me_3N(CH_2)_6NMe_3 \cdot Cl_2$] and decamethonium bromide, $DMBr_2$ [$Me_3N(CH_2)_{10}NMe_3 \cdot Br_2$] (Fluka AG, Switzerland) were recrystallised from aqueous solution by the addition of acetone, to remove yellow contaminants, and stored over silica. Solutions of all the above reagents were made up immediately prior to use. Ammine complexes of Cr(III) are photosensitive (8) and were protected from light by storing in containers covered with aluminium foil. In addition, neutral solutions of these Cr(III) complexes decompose slowly at room temperature. Consequently, experiments with these complexes were conducted under subdued light conditions and titrant solutions were stored in the dark at $0^{\circ}C$ during experiments.

Stock solutions of $MgCl_2$ and $BaCl_2$ (typically 2.5 M) were prepared using AnalaR (BDH, U.K.) grade reagents. The solids NaCl, KCl and CsCl were of AnalaR or AristaR grade.

(b) **Titration procedures.**

Stock solutions of salts were prepared so that the addition of 2 μL of stock solution to ca. 500 μL of test solution gave the desired increase in cation concentration. All additions were made with a 25 μL Hamilton syringe (Phase Separations, U.K.). In general, no more than 30 μL of stock solution were added so that dilution errors were restricted to 6%. Solutions were stirred briefly, after addition of titrant, with a teflon-coated 'micro' stirring-flea.

For titrations with the halide salts of Group IA cations, it was not possible to prepare sufficiently concentrated stock solutions. Consequently, all titrations were performed by adding accurately weighed amounts of solid through a small funnel.

Cation titrations of the 8Fe ferredoxin at a fixed potential, rotating, edge graphite electrode were performed using deoxygenated titrant solutions and a gas-tight Hamilton syringe.

(c) **Electrochemical methods.**

Cyclic voltammetry (Oxford Electrodes potentiostat) and rotating-disc electrochemistry (380-Z microprocesor-based instrumentation) were performed as previously described (Chapters 4 and 6). All electrochemical measurements were carried out at 25°C. The reference electrode was a saturated calomel electrode (SCE). The graphite working electrodes (5 mm diameter discs) were polished using 0.3μ alumina (Banner Scientific, U.K.) and

sonicated in distilled water for at least 10 secs. prior to use. The working electrode was reproducibly held in place in the electrochemical cell ca. 2 mm from the Luggin tip by a screw fitting. Faradaic measurements (typically at 20 mVs^{-1}) were initiated within 5 secs. of connecting the working electrode. Faradaic peak currents were measured using baselines drawn by extrapolation of the slope at the commencement of the sweep.

The reference arm of the electrochemical cell typically contained the same concentration of buffer and supporting electrolyte as the working compartment. However, for experiments at high (>0.3 mM) protein concentrations or with high concentrations of multivalent cations (e.g. >0.3 M M^{+}), diffusion through the capillary and junction potentials at the Luggin tip, respectively, necessitated special consideration of the reference medium. For work with high protein concentrations, the reference arm of the cell was also filled with a solution containing protein at the same concentration. Similarly, in anticipation of high titrant concentrations, the reference arm was filled with a solution of high ionic strength.

7.3 Direct Electrochemical Studies of C. pasteurianum 8Fe Ferredoxin at Edge Graphite.

In this section, general features of cation promotion will be assessed in a comprehensive study of cation effects upon the electrochemistry of a readily available redox protein - Clostridial 8Fe ferredoxin - at edge graphite.

7.3.1 Promotion-stabilisation profiles.

7.3.1a The role of cation concentraton.

For an initial evaluation of electrostatic effects, cation promotion responses were studied in the presence of two levels of background electrolyte (1 and 100 mM NaCl), with the buffer concentration typically restricted to 5 mM (Tricine, pH 8). Faradaic responses were found to be independent of buffer concentration. Buffering action at this low concentration was found to be adequate with < 0.5 pH unit change for the addition of >10 mM $MgCl_2$.

The effect of successive addditions of $Cr(NH_3)_6^{3+}$ to the 2[4Fe-4S] ferredoxin, with a minimum of background electrolyte (1 mM NaCl, in which there is no faradaic response), is illustrated in Figure 7.1. The addition of only 60 μM $Cr(NH_3)_6^{3+}$ is sufficient to stimulate an initial (scan 1) faradaic response which then decays over the first few cycles. This time dependent deterioration of response or ´impersistence´, apparent as a decrease in peak current and an increase in peak separation on successive cycles, is less pronounced at higher cation levels. At these higher cation levels there is also an increase in the maximum faradaic current recorded. Thus, increasing the titrant concentration both promotes and stabilizes the faradaic response

FIGURE LEGEND

Figure 7.1

Cyclic voltammograms of 67 μM C. pasteurianum 2[4Fe-4S] ferredoxin (in 5 mM Tricine, 1 mM NaCl, pH 8.0) showing the effect of successive additions of $Cr(NH_3)_6^{3+}$ to an edge graphite electrode in the presence of 1 mM or 100 mM NaCl background electrolyte. The cyclic voltammograms show consecutive cycles (20 mVs^{-1}) recorded after initiating the scan. Potential scan limits are -415 mV to -845 mV vs. SCE (1 mM NaCl) and -365 mV to -820 mV (100 mM NaCl). Also shown is the response at a polished basal plane pyrolytic graphite electrode in 3 mM $Cr(NH_3)_6^{3+}$, 100 mM NaCl, pH 8.0 (-365 mV to -820 mV).

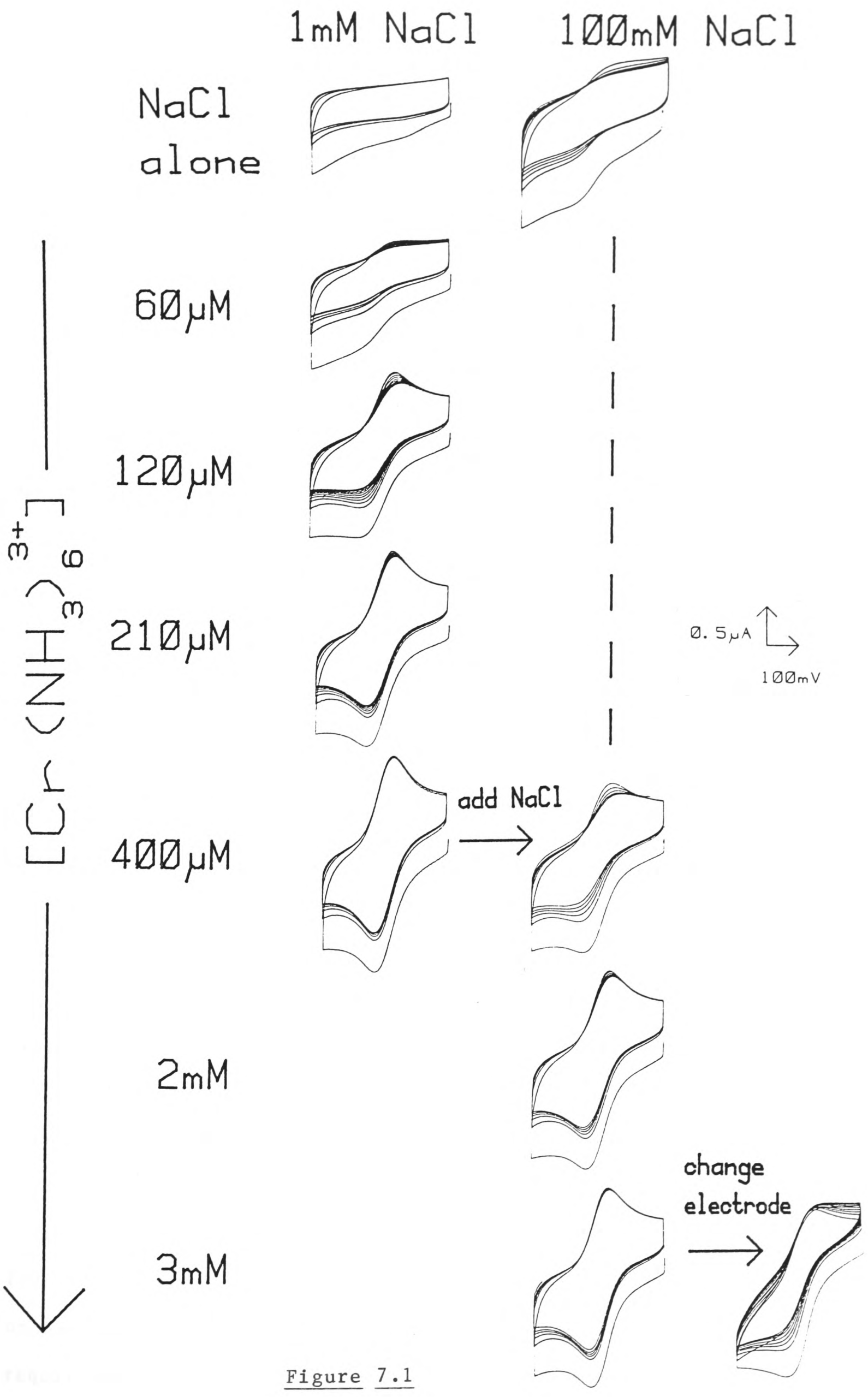
1mM NaCl
100mM NaCl
NaCl alone
60μM
120μM
210μM
400μM
2mM
3mM
$[Co(NH_3)_6]^{3+}$
$[Cl^-]$
0.5μA
100mV
add NaCl
change electrode

Figure 7.1

up to an optimal level reached above 250 μM $Cr(NH_3)_6^{3+}$, Figure 7.2. Addition of solid NaCl to a final concentration of 100 mM, at this point, inhibits the faradaic response, causing both a depromotion of the faradaic peak current and a destabilisation of the response - impersistence is again evident, Figure 7.1. However, a qualitatively similar promotion characteristic to that observed in 1 mM NaCl, may be observed at this higher background level, by the addition of further $Cr(NH_3)_6^{3+}$. Promotion and stabilisation of the faradaic response is now observed up to an optimum at 2 - 3 mM $Cr(NH_3)_6^{3+}$, Figure 7.2. There is initially a small, impersistent response in 100 mM NaCl alone. Comparison of the response at a polished basal plane electrode, with that at the edge surface, in 3 mM $Cr(NH_3)_6^{3+}$, emphasizes the higher cation levels required to optimise faradaic responses at the polished basal surface.

Similar promotion-stabilisation characteristics are observed for the addition of Mg^{2+} to ferredoxin at an edge surface.

7.3.1b The role of protein concentration.

The promotion and stabilisation of electrochemical response, and the levels of cation required to optimise electron-transfer rates, also depend quite markedly on protein concentration. This is illustrated in Figure 7.3 for the $Cr(NH_3)_6^{3+}$-promoted electrochemistry of C. pasteurianum ferredoxin in 100 mM NaCl (at this higher background electrolyte level, measurements of ΔE_p are not complicated by errors due to uncompensated resistance). At low protein concentrations, cation requirements are low and ageing is minimal. At high (>150 μM)

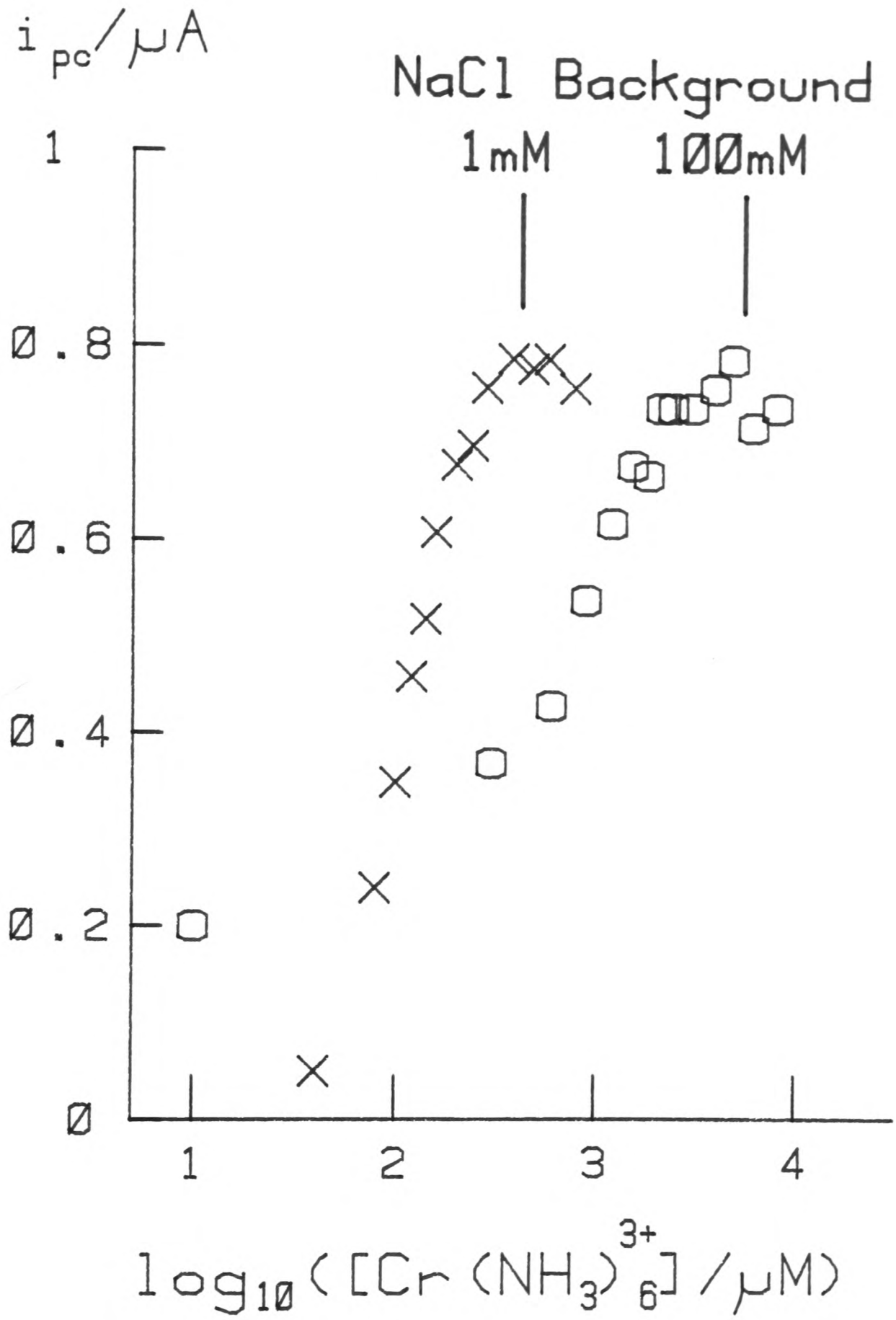

Figure 7.2: The variation of cathodic peak current (cyclic voltammetry) with the concentration of $Cr(NH_3)_6^{3+}$ for 67 μM C. pasteurianum 2[4Fe-4S] ferredoxin in 1 mM (x) and 100 mM (o) NaCl background electrolyte. Scan rate 20 mVs^{-1}, 5 mM Tricine, pH 8.0. Measurements taken on the 4th voltammetric scan at an edge graphite electrode surface.

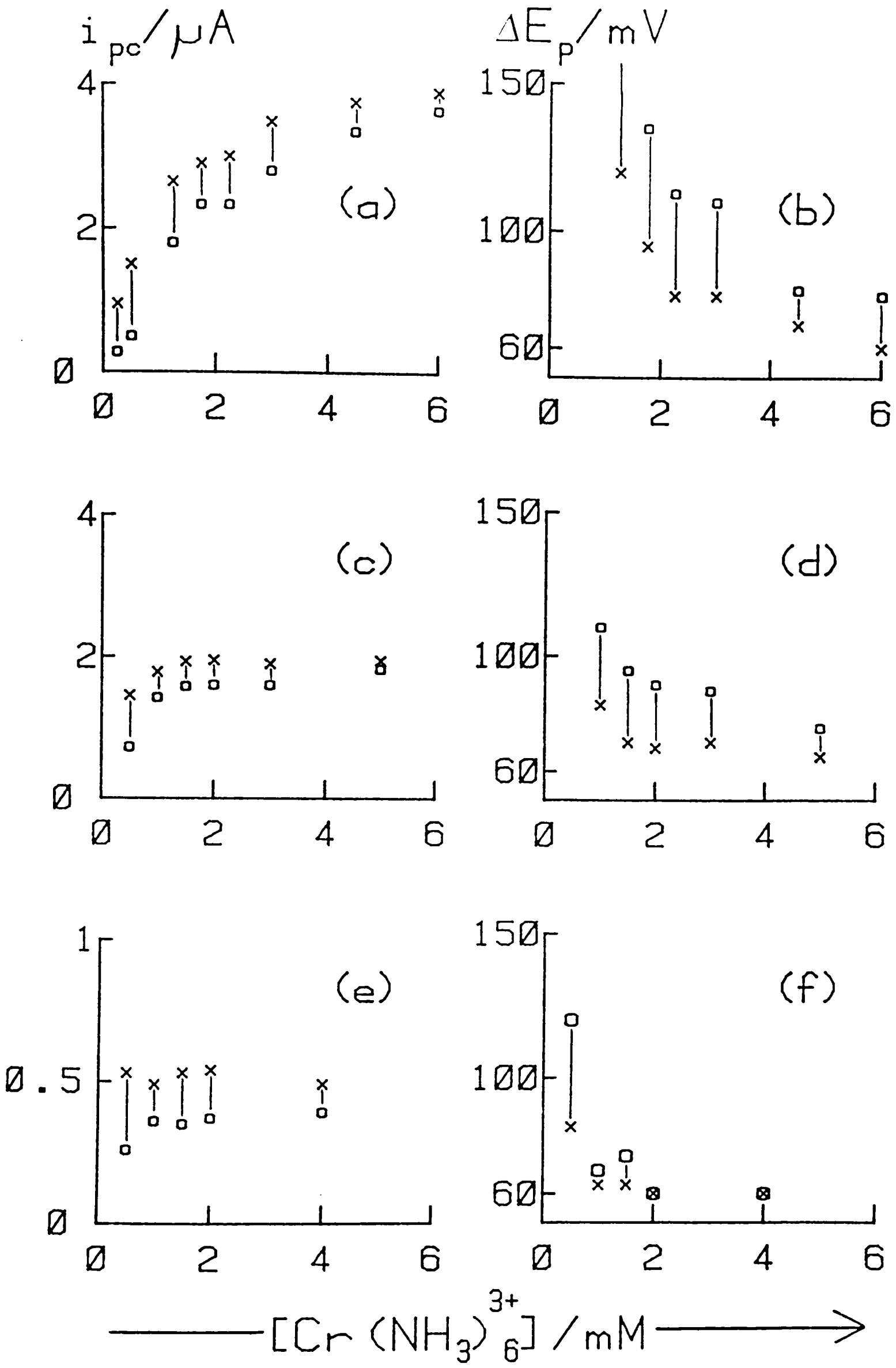

Figure 7.3: The variation of the cyclic voltammetric response of 2[4Fe-4S] ferredoxin as a function of protein concentration and $Cr(NH_3)_6^{3+}$ concentration (100mM NaCl). The plots show measurements of peak current and peak separation taken on the 1st (x) and 4th (o) voltammetric cycles (20 mVs^{-1}) at edge graphite. Protein concentrations are 0.3 mM (a,b), 0.11 mM (c,d) and 0.03 mM (e,f).

protein levels, saturation of the current-cation isotherm is not observed, faradaic responses are less reversible, there is a higher cation requirement, and faradaic responses are less readily stabilised. A marked dependence of faradaic response on protein concentration is a common feature of the electrochemical response of **all** redox proteins at edge graphite electrode surfaces. Further examples can be seen in the $Cr(NH_3)_6^{3+}$-promoted direct electrochemistry of Spinach 2Fe ferredoxin (section 7.6) and the direct electrochemistry of cytochrome c in the absence of multivalent cations (Chapter 9).

7.3.2 An investigation of 'impersistence'.

It is apparent that 'impersistence' or 'ageing' of faradaic responses is a key feature in the overall mechanism of the direct electrochemistry of redox proteins at graphite surfaces. In order to ascertain the origin of this instability, complementary studies were carried out on the hexacyanoferrate (II/III) couple. The electrochemistry of this negatively-charged complex is similar to that of negatively-charged redox proteins in that electrochemistry at edge graphite is promoted by the addition of multivalent cations, as shown in Figure 7.4. Interestingly, $Fe(CN)_6^{3-}$ shows no ageing effects at edge electrodes even at sub-optimal cation levels (see cyclic voltammograms, Figure 7.4). From this it is clear that impersistence of electrochemical response is only a feature of protein studies. An initial conclusion is that impersistence is a manifestation of bulk denaturation of redox proteins under the conditions used. However, ageing effects are not just restricted to those proteins which are normally regarded as being unstable

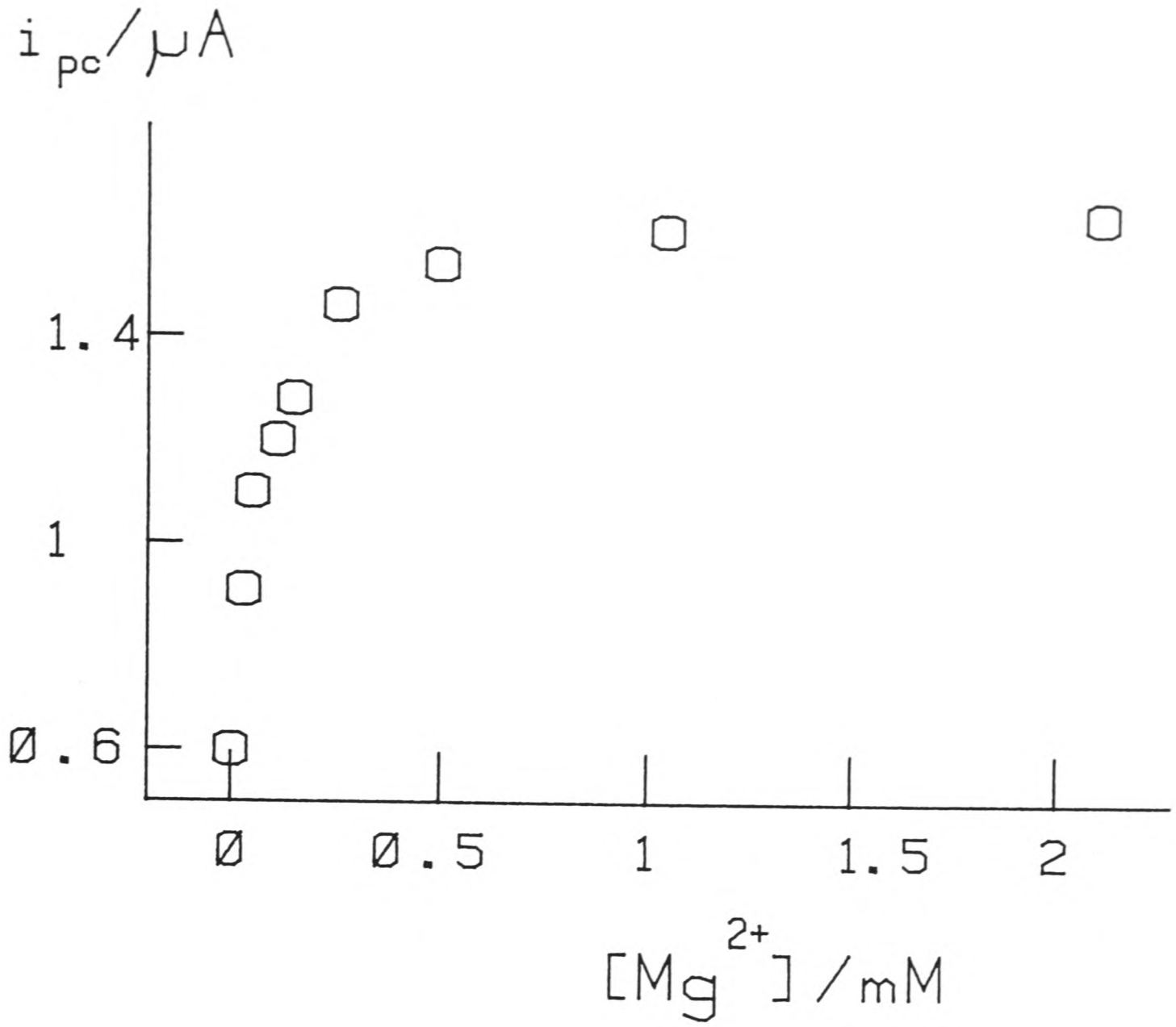

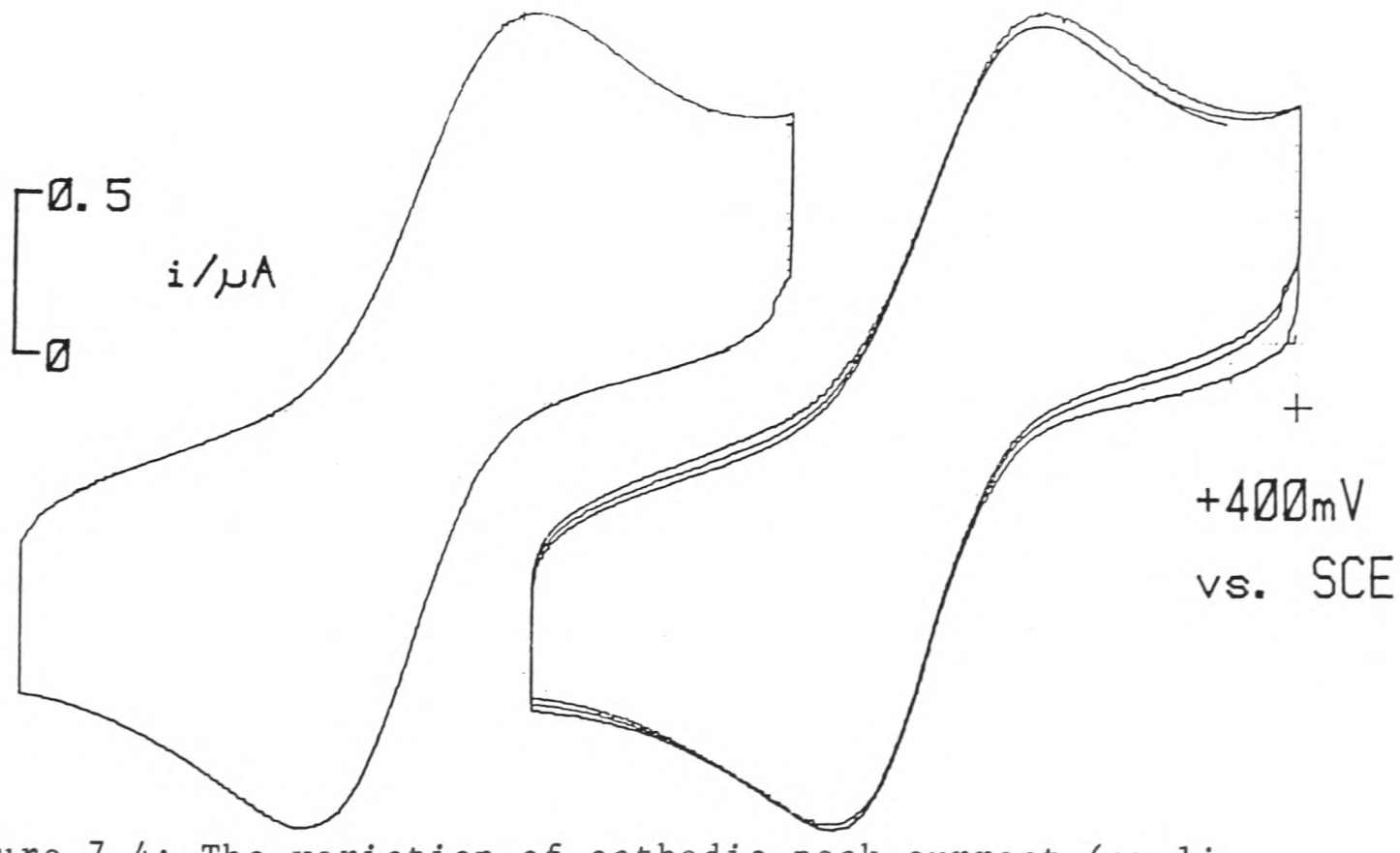

Figure 7.4: The variation of cathodic peak current (cyclic voltammetry) with the concentration of Mg^{2+} for 0.1 mM $K_3Fe(CN)_6$ in 5 mM Tricine, 1 mM NaCl, pH 8.0. Measurements taken on the 4th voltammetric cycle (20 mVs^{-1}) at an edge graphite electrode. Also shown are the cyclic voltammograms [voltammetric cycles 1 - 3, and steady-state cycle (shown separately)] for 54 μM Mg^{2+} (other conditions as given above).

when isolated, and are a feature of even the most 'robust' proteins (e.g. cytochrome c: see Chapter 9). The 8Fe Clostridial ferredoxin is notoriously unstable in the presence of dioxygen. However, no significant bleaching of the protein, as measured by a decrease in the absorbance ratio (A_{490}/A_{280}), was evident for this protein over a period of 2 - 3 hours under the anaerobic conditions established in an electrochemical cell. Similarly, bulk spectro-electrochemical reduction and re-oxidation of a ferredoxin solution recovers >99% of the initial absorbance of the oxidised protein (9). Apparently, the observed impersistence is associated with changes occurring at or close to the electrode surface. These may be due to time-dependent changes in the electrode surface itself or denaturation of only those protein molecules within the diffusion layer.

7.3.2a Cyclic voltammetric studies.

Preliminary investigations of impersistence were made by cyclic voltammetric studies on C. pasteurianum ferredoxin (67 μM) in the presence of $Cr(NH_3)_6^{3+}$. At a sub-optimal level of promoter (120 μM) the deterioration of faradaic response is clearly evident, Figure 7.5(b-d). Precycling a polished, sonicated electrode in buffer alone for 15 mins., using the same sweep amplitude as that used in protein studies (typically -153 to -553 mV vs. NHE), had no significant effect on the initial (scan 1) response (Figure 7.5(b)) in the ferredoxin/12 μM $Cr(NH_3)_6^{3+}$ solution. However, cycling (-153 to -553 mV) or poising (-553 mV) the electrode for only 8 mins. in 67 μM ferredoxin/120 μM $Cr(NH_3)_6^{3+}$ produces a marked deterioration of the observed faradaic response. The extent of the deterioration observed is

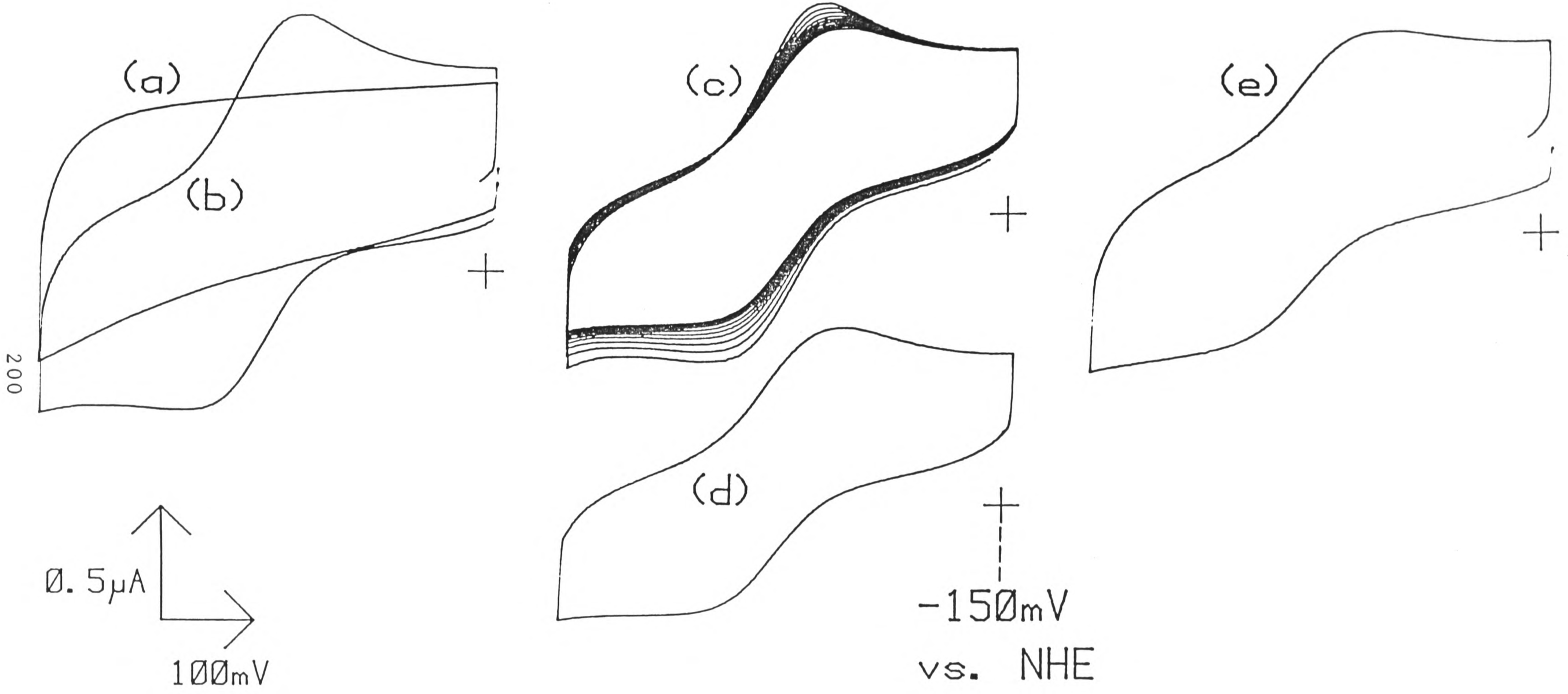

Figure 7.5.
Cyclic voltammograms (20 mVs^{-1}) of 67 μM 2[4Fe-4S] ferredoxin in 5 mM Tricine, 1 mM NaCl, pH 8.0. Edge graphite.
(a) response in 1 mM NaCl alone.
(b) after the addition of 120 μM $Cr(NH_3)_6^{3+}$. Electrode pre-cycled (15 minutes) in buffer prior to use.
(c) successive voltammetric cycles recorded following the initial scan (scan (b)).
(d) the residual response after 8 minutes cycling in protein.
(e) after sonicating (1 minute) the electrode as in (d).

not significantly influenced by the sweep amplitude. After 'ageing' of the electrode, the initial (scan 1) faradaic response can only be renewed by repolishing the electrode surface. The response cannot be regenerated by copious washing, stirring in buffer or sonication of the electrode surface, Figure 7.5(e). However, this result should be treated with caution as perturbation of the double layer on removing the electrode from solution and the subsequent medium change on washing or sonicating the surface may have affected the nature of the protein-surface interaction. Finally, a repolished, sonicated electrode was pre-treated by immersing the electrode in 67 μM ferredoxin/120 μM $Cr(NH_3)_6^{3+}$ for 8 mins., at open circuit potential, prior to initiating faradaic measurements. The initial (scan 1) response showed an obvious deterioration of faradaic response compared to that of an electrode with no prior immersion.

7.3.2b Rotating-Disc Studies.

Rotating-disc techniques provide a convenient approach to the study of the dynamics of electrode processes in the absence of complications due to charging currents. In addition the motion of the electrode itself provides an efficent means of mixing injected titrant into the test solution, without the need for removing the electrode. This technique was used to probe further into the nature of the ageing process.

Figure 7.6(a) illustrates the current response at a rotating edge graphite electrode (ω = 20 Hz., E = -553 mV vs. NHE) for 20 μM 2[4Fe-4S] ferredoxin under saturating cation conditions (1 mM $Cr(NH_3)_6^{3+}$, pH 8.0). The initial sharp decay in current,

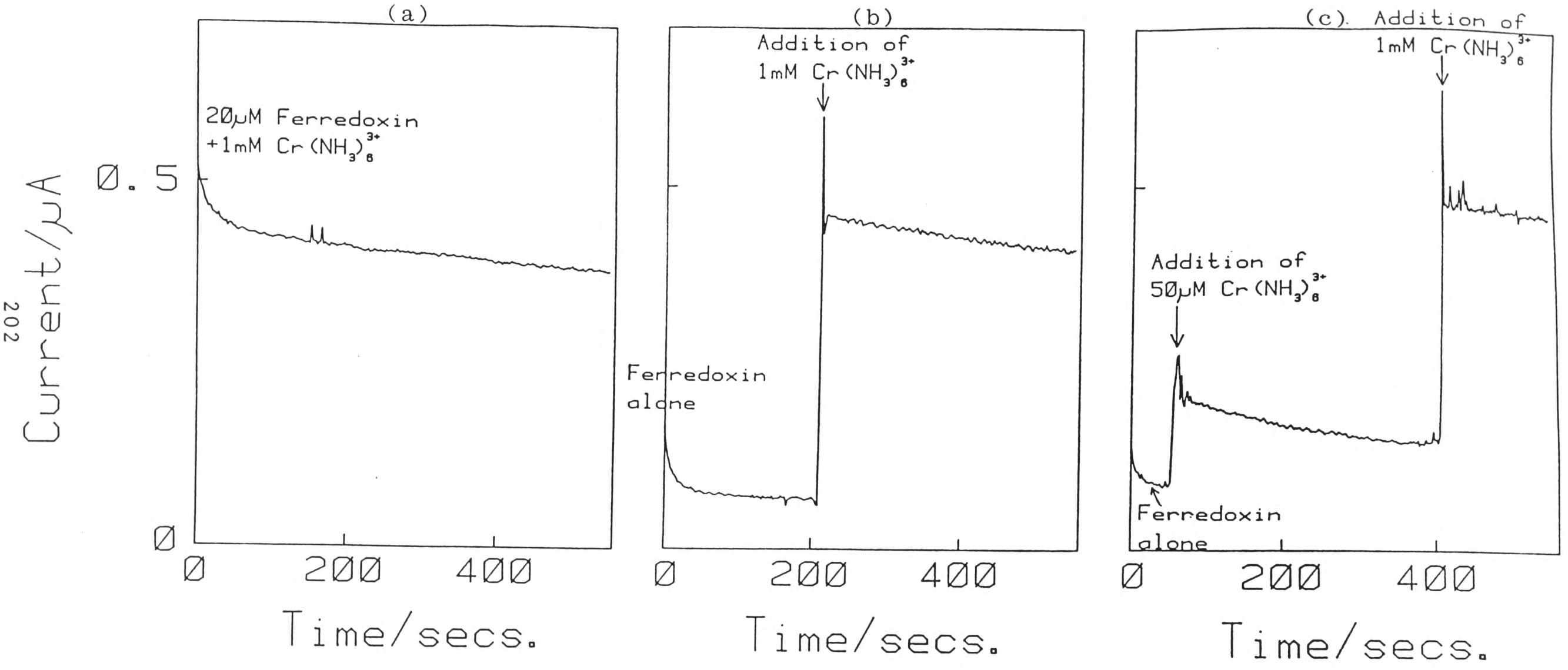

Figure 7.6: Current-time responses at a rotating edge graphite electrode, for 20 μM *C. pasteurianum* 2[4Fe-4S] ferredoxin in 5 mM Tricine, 1 mM NaCl, pH 8.0. Rotation speed 20 Hz, electrode potential -553 mV vs. NHE.

also detectable in buffer alone, is due to trace dioxygen. This is followed by a slow decrease in current with time (14% decrease in 9 mins.). A complementary cyclic voltammetric study, under identical conditions, confirmed the observed faradaic response to be stable with **no ageing** (ΔE_p 62.5 mV at steady-state scan). The slow decrease in current with time observed in the rotating-disc study must then arise from bulk reduction of ferredoxin (estimated to contribute 40% of the observed decay) together with reduction of residual dioxygen or background faradaic processes.

In separate experiments, the faradaic response was initially monitored in (i) 20 μM ferredoxin alone (Figure 7.6(b)), in (ii) 20 μM ferredoxin after injecting de-oxygenated buffer solution and, in (iii) 20 μM ferredoxin after injection of $Cr(NH_3)_6^{3+}$ to a final concentration of 50 μM during the run (Figure 7.6(c)). No time dependent changes in the faradaic response were observed in (i) or (ii). However, in accordance with cyclic voltammetric studies, a ca. 50% decrease of the current was observed over a 6 minute period in (iii), due to 'ageing' at this sub-optimal cation concentration (the observation of 'ageing', under these conditions, was confirmed in a complementary study by cyclic voltammetry). In both (i) and (iii) the injection of $Cr(NH_3)_6^{3+}$ to saturating levels (1mM) during the run, generates the faradaic response observed for the system at saturating cation concentration but with no prior 'ageing'.

A complementary study by cyclic voltammetry in a quiescent solution confirmed the observation that addition of cations to saturating levels restores maximal faradaic activity ($\Delta E_p < 65$ mV) at an aged electrode. An initial hypothesis based on these

observations is that the restoration of optimal faradaic activity upon addition of cations is due to the reversal of ageing processes, i.e cations may be able to displace impurities which are blocking surface sites. This hypothesis was tested by further cyclic voltammetric studies. An electrode 'aged' in 20 μM ferredoxin, 50 μM $Cr(NH_3)_6^{3+}$ (-153 to -553 mV vs. NHE) was subsequently treated by cycling (-153 to -553 mV, 5mins.) in a second electrochemical cell containing (a) buffer alone and (b) buffer containing a saturating level of $Cr(NH_3)_6^{3+}$ (1 mM). The electrode was then returned to the initial ferredoxin solution, containing no additional cations. The electrochemical response of the 'aged' electrode showed no restoration of faradaic activity following treatments (a) or (b). Clearly, cations alone do not **reverse** the ageing process but in some way **overcome** the effects of ageing. In view of these results, it is not clear whether the apparent 'lack' of a faradaic response in a system containing no multivalent cations (1 mM NaCl), Figure 7.5(a), implies rapid impersistence which may then be overcome by cation addition to the ferredoxin solution, or that protein molecules are unable to approach (and foul) the electrode surface under these conditions.

7.3.3 Discussion of ageing.

A time dependent deterioration of faradaic response, represented by a decrease in faradaic peak current and an increase in peak separation, is evident only in direct electrochemical studies of redox proteins. The decrease in reversibility is not related to alterations in the electrode surface (e.g. formation or reduction of surface oxide) induced by large amplitude potential sweeps. The ageing effect is then,

apparently, protein-related and in accord with this statement is most evident at higher protein concentrations. However, the effect is not a bulk process and is confined to changes occurring at or close to the electrode surface.

A reasonable initial conclusion is that the electrode surface becomes covered by impurities which block or slow down the rate of electron-transfer. These impurities may be intact protein molecules irreversibly bound at the electrode surface or may be the result of denaturation close to the surface. Strong adsorption at interfaces is a general feature of polymer and protein chemistry. For example, Norde and Lyklema (10-12) have shown that the adsorption of a negatively-charged protein, human plasma albumin, at negatively-charged polystyrene latex particles, is highly irreversible towards dilution and is accompanied by substantial structural rearrangements. In view of the observation, described in the previous section, that only polishing the surface restores the activity of an electrode, then surface contaminants must be very strongly adsorbed at the electrode surface. There are four possible models based upon blocking of the surface:

1) A stack of inhibiting layers completely covers the electrode surface, or those sites at which the electron-transfer event occurs. Any subsequent electron-transfer must necessarily occur through these layers and so the resulting increase in protein-electrode electron-transfer distance leads to a decrease in the rate of heterogeneous electron-transfer. A gradual increase in the thickness of these layers will lead to a gradual decrease in reversibility. In effect, the coating on the electrode surface builds up into an insulating layer.

2) The 'active' surface becomes only partially covered by an inhibiting layer. There is now electron-transfer activity only at the 'bare' sites with the 'covered' sites being totally ineffective towards electron-transfer. Theoretical approaches to cyclic voltammetric responses at partially active electrodes (13) leads one to expect changes in the electrochemical response away from the usual characteristic features associated with uniformly active electrodes of ordinary dimensions, arising from semi-infinite linear diffusion. Most notably, faradaic responses may be governed by non-linear diffusion resulting in 'steady-state' currents and greater sensitivity to electron-transfer rates. However, the type of electrochemical behaviour observed appears to be a complex function of 'active' site radius, intersite distance, the fractional coverage by impurities and the time scale of experiment. Clearly, a detailed 'map' of the distribution of electrochemical activity on an edge electrode surface would be needed to interpret 'ageing' phenomena in terms of a change in diffusion characteristics. However, experimental approaches to these theoretical problems, through the construction of arrays of small voltammetric electrodes, may be of significance to this discussion. Sleszynski (14) and Engstrom (15) have recently examined the electrochemical behaviour of carbon-epoxy composite electrodes. These surfaces show a spatial variation of electrochemical activity and demonstrate that non-linear diffusion is the predominant mode of mass transport to the surface on the time scale of seconds. At a graphite-epoxy surface, where the two-dimensional distribution of electrochemical activity is highly heterogeneous, faradaic responses more closely ressemble plateaus than peaks and

voltammograms are noticeable less reversible than at a glassy carbon disc electrode under the same experimental conditions. The contrast in behaviour between an ordinary disc electrode and a composite (or partially-blocked) electrode, is reminiscent of the transition in behaviour between an initial faradaic response and an 'aged' faradaic response, observed in direct electrochemical studies.

3) The electrode surface is heterogeneous and there are two or more different sites at the surface at which there is protein-electrode electron-transfer activity. A change in the reversibility of faradaic response with time reflects a change in the relative population of individual sites at which there is electron-transfer activity. Such a change might be influenced by selective blocking of one site through irreversible binding or denaturation of proteins at that site.

4) The final proposal, which is consistent with the nature of the observed ageing process, is that at sub-optimal cation levels, negatively-charged protein molecules irreversibly adsorb at the electrode surface and so increase the effective negative surface charge density of the surface. Alternatively, adsorbed molecules may unfold across the surface so effectively 'modifying' the edge surface with a polymer (polypeptide) bearing negatively-charged residues. In accord with simple electrostatic considerations (see section 7.8.2) this would hinder close approach to the surface of further negatively-charged protein molecules. As adsorption proceeds there will be a slow decrease in reversibility as charge constraints become progressively more severe.

An important role of added multivalent cations is to

modulate the extent of impersistence. At sub-optimal cation levels, electrostatic repulsion at negatively-charged functional sites may force the protein to adopt unfavourable orientations or to populate sites of lower negative surface charge density, in order to minimise electrostatic effects. These sites may be predominantly hydrophobic in character, with no C-O functionalisation. Adsorption at these sites through strong protein-electrode hydrophobic interactions, may lead to irreversible binding, accompanied by deformation or unfolding of the protein in order to maximise hydrophobic contacts and exclude hydrophilic residues from the contact zone. As a result these sites become 'blocked' to further electron-transfer, as discussed previously. At optimal cation levels, electron-transfer may be concentrated at suitably 'screened' (see section 7.8.3) functional sites bearing a discrete negative charge where there is only weak binding and no blocking of the surface. As a consequence, ageing effects are minimised. Alternatively, the cation itself may bind at or close to strong surface binding sites so blocking these sites and displacing protein molecules onto weaker binding sites. The impersistence observed in the early stages of cation titrations restricts any attempt at numerical analysis of promotion profiles.

The observation that cation addition may restore the activity of an 'aged' electrode is consistent with the proposal that different binding sites may be populated at different stages of a faradaic response titration. Thus, sites blocked at low cation levels are <u>not</u> those sites utilised at optimal cation levels. A plot of the maximum observed faradaic peak current in $Cr(NH_3)_6^{3+}$ promotions of ferredoxin electrochemistry, is linear

up to at least 150 μM ferredoxin. This suggests that binding sites at the surface do remain largely unoccupied up to this concentration and that discussions of site selectivity are reasonable initial proposals. However, the ability of cations to restore activity, by a simple step in cation level, is also consistent with an ageing process in which there is a general electrostatic ´blocking´ of the surface (deposition of negatively-charged polypeptide has been suggested as a possible cause of ´ageing´). Cation addition could simply overcome this electrostatic barrier by charge neutralisation or ´screening´, so restoring activity to an ´aged´ surface. It would be expected that the cation promotion profile of an ´aged´ surface, at which there is adsorbed polypeptide, would differ from that of the ´native´ polished edge surface. However, it is apparent from $Cr(NH_3)_6^{3+}$ titrations of 20 μM ferredoxin (see section 7.4.4) that this cation was added to excess in the rotating-disc study of ageing and so any change in cation requirement is not immediately evident.

A preliminary test of the ´nature´ of an aged electrode surface was made by comparing the electrochemical responses of small inorganic redox couples (e.g. ferrocene boronic acid, ferrocene mono-carboxylic acid) at an edge surface, both before and after exposure of the electrode to a ferredoxin solution (67 μM) containing a sub-optimal level of $Cr(NH_3)_6^{3+}$ (50 μM). No significant changes in the faradaic responses of these couples were noted after ´ageing´ of the surface and, yet, the aged surface remained inactive towards ferredoxin when returned to the ferredoxin solution. This result suggests that only a small fraction of the accessible surface area becomes ´blocked´ during

the ageing process.

The final point to be considered of relevance to ageing is the noticeably lower stability of electrochemical responses and the higher cation levels required to achieve optimal responses at high (ca. 0.3 mM) protein concentrations. This may be a direct consequence (10,11) of lateral interactions at the surface and a low surface coverage of productive binding sites. Thus, the resultant effects may be (i) protein molecules are forced to populate unproductive binding sites, (ii) protein-protein interactions arise from severe crowding of protein molecules around preferred sites for electron-transfer or (iii) there is protein-protein electron-transfer. The higher cation requirements may reflect the need to facilitate interactions between adjacent, highly-charged protein molecules. Protein-protein interactions may be particularly susceptible to the formation of tight protein-protein complexes in orientations unproductive towards rapid electron-transfer. This would break electron-transfer chains and so slow the overall rate of electron-transfer.

The results of studies on impersistence emphasize the need to conduct experiments, at edge graphite, at as low a protein concentration as possible in order to minimise this problem and maximise stability and electron-transfer kinetics. It is interesting to speculate whether, upon continued dilution of ferredoxin below the levels used in this chapter, a limiting protein concentration will be reached, below which there are highly persistent responses and no further decrease in cation requirement. This may then reflect the occurrence of only protein-electrode interactions uncomplicated by protein-protein effects.

7.4 Systematic studies of a range of cations of varying charge and ligand environment.

Comparative studies of the effectiveness of a range of cation are subject to several preliminary requirements. Firstly, the concentration of the protein used should be sufficient to facilitate accurate measurements of faradaic peak currents, while being sufficiently low to minimise stabilisation problems. The most readily available protein, 8Fe ferredoxin, was typically used at a **constant** concentration of 150 μM. Secondly, in order to cover a wide range of cation charge with minimal problems from simple ion-pairing or precipitation, it was decided to use chloride salts, despite anticipated numerical complications arising from the use of non-symmetrical electrolytes. Finally, most experiments were conducted in 5 mM Tricine, pH 8.0 with a background electrolyte of 1 mM NaCl; this avoided the pronounced, but unstable, response evident when using 100 mM NaCl background electrolyte. For experiments conducted at these low levels of electrolyte, errors attributable to uncompensated resistance may be evident in measurements of peak separations. The peak separation (90 mV) observed for ferrocene monocarboxylic acid in 1 mM NaCl, 5 mM Tricine, at a concentration giving comparable, maximal peak currents to those observed with 150 μM ferredoxin, suggests that measurements of peak current will more faithfully reflect the progress of cation titrations in 1 mM NaCl than will measurements of peak separations.

In the cases where the electrochemistry was rather irreversible and impersistent, i.e. in the early stages of cation promotion titrations, distortions of cyclic voltammograms made it feasible to measure only cathodic peak currents. These were

typically measured on the 4th voltammetric scan (20 mVs^{-1}) to allow charging and background processes to decay.

7.4.1 Divalent cation titrations - 150 μM ferredoxin.

Ba^{2+}, Mg^{2+} and organic di-cations.

Figures 7.7 and 7.8 show faradaic response titrations, expressed as peak separations (ΔE_p, scan 4) and cathodic peak currents (scan 4), versus cation concentration, for the Group IIA cations, Ba^{2+} and Mg^{2+}, and two organic divalent cations, $^{+}Me_3N-(CH_2)_n-NMe_3^{+}$ (where n=6 [hexamethonium] and n=10 [decamethonium]). Comparison of Ba^{2+} and Mg^{2+} titrations (5 mM Tricine, pH 8.0) reveals a marked difference in the promotion characteristics. Optimal faradaic responses were achieved with ca. 15 mM Ba^{2+} (ΔE_p 85 mV, $i_{pc,max}$ 2 μA) and ca. 30 mM $MgCl_2$ (ΔE_p 100 mV, $i_{pc,max}$ 1.8 μA). This difference was reproducibly obtained on at least three separate occasions. Experiments with Ca^{2+} reported elsewhere (7), reveal promotion characteristics similar to Ba^{2+}.

The two organic di-cations promote optimal faradaic responses at levels of promoter <15 mM. The cation HM^{2+} effects optimal faradaic responses at a concentration of ca. 15 mM (ΔE_p 100 mV, $i_{pc,max}$ 1.8 - 1.9 μA). The cation DM^{2+} appears to be the most efficient promoter of the four divalent cations in that optimal faradaic responses (ΔE_p 75 - 85 mV, $i_{pc,max}$ 1.8 μA) are achieved at a concentration of ca. 7 mM.

For all cations, faradaic responses under optimal cation concentrations were symmetrical with $i_{pa} \simeq i_{pc}$, suggesting that values of the electrochemical charge transfer coefficient, α, were close to 0.5.

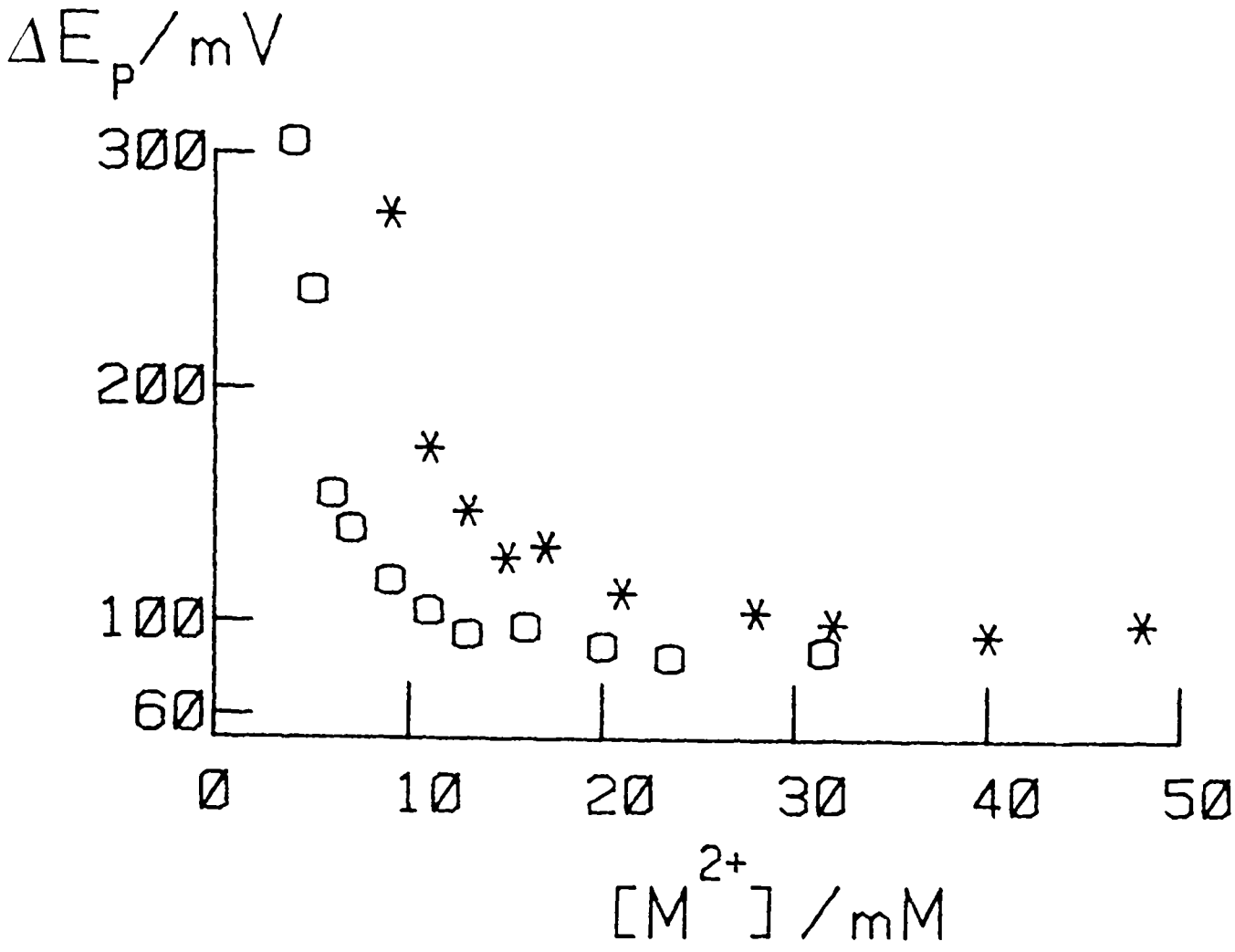

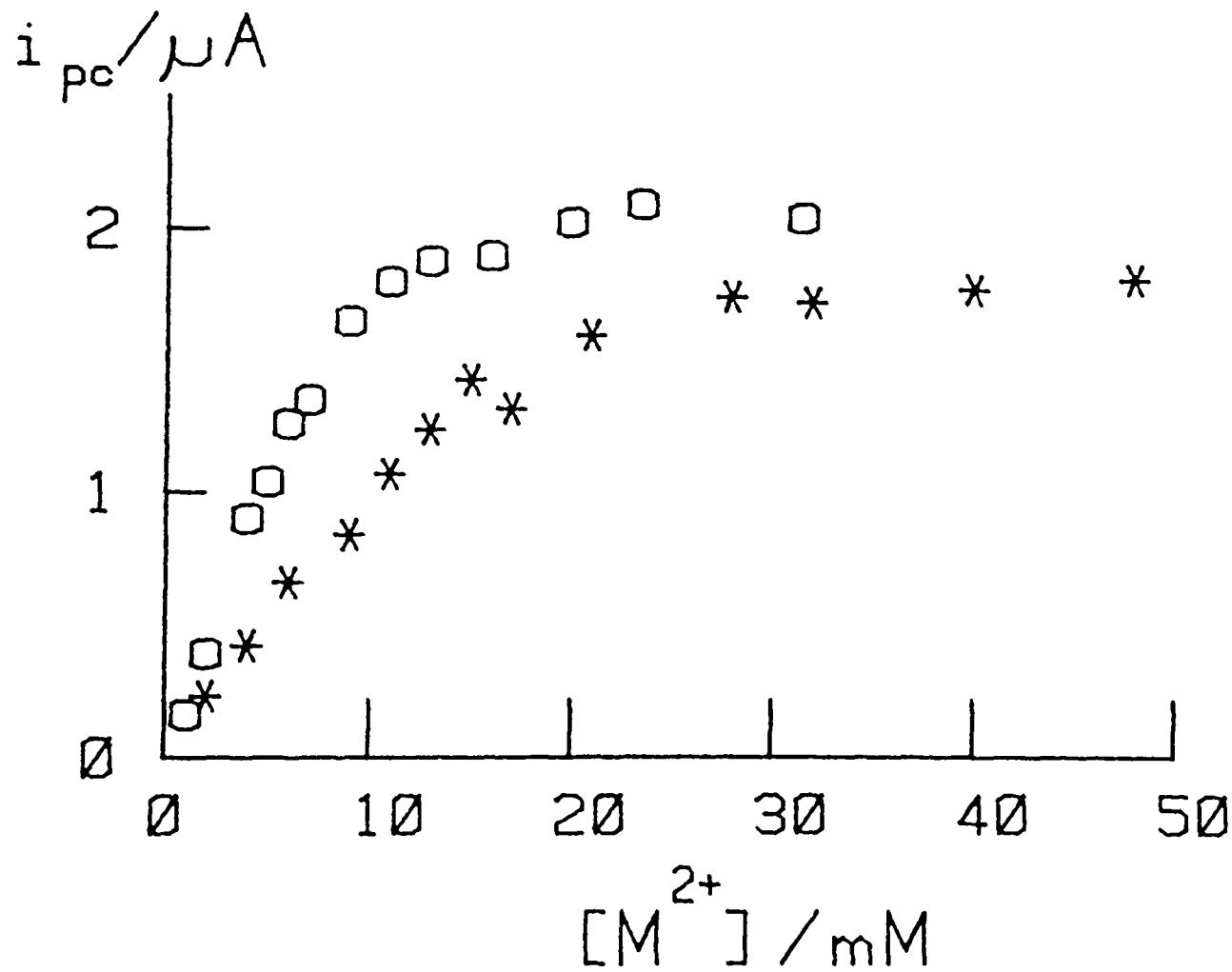

Figure 7.7: The variation of cathodic peak current and peak separation (cyclic voltammetry) with cation concentration for the addition of $MgCl_2$ (*) and $BaCl_2$ (o) to 150 μM 2[4Fe-4S] ferredoxin in 5 mM Tricine, 1mM NaCl, pH 8.0. Measurements taken on the 4th voltammetric cycle (20 mVs^{-1}) at an edge graphite electrode.

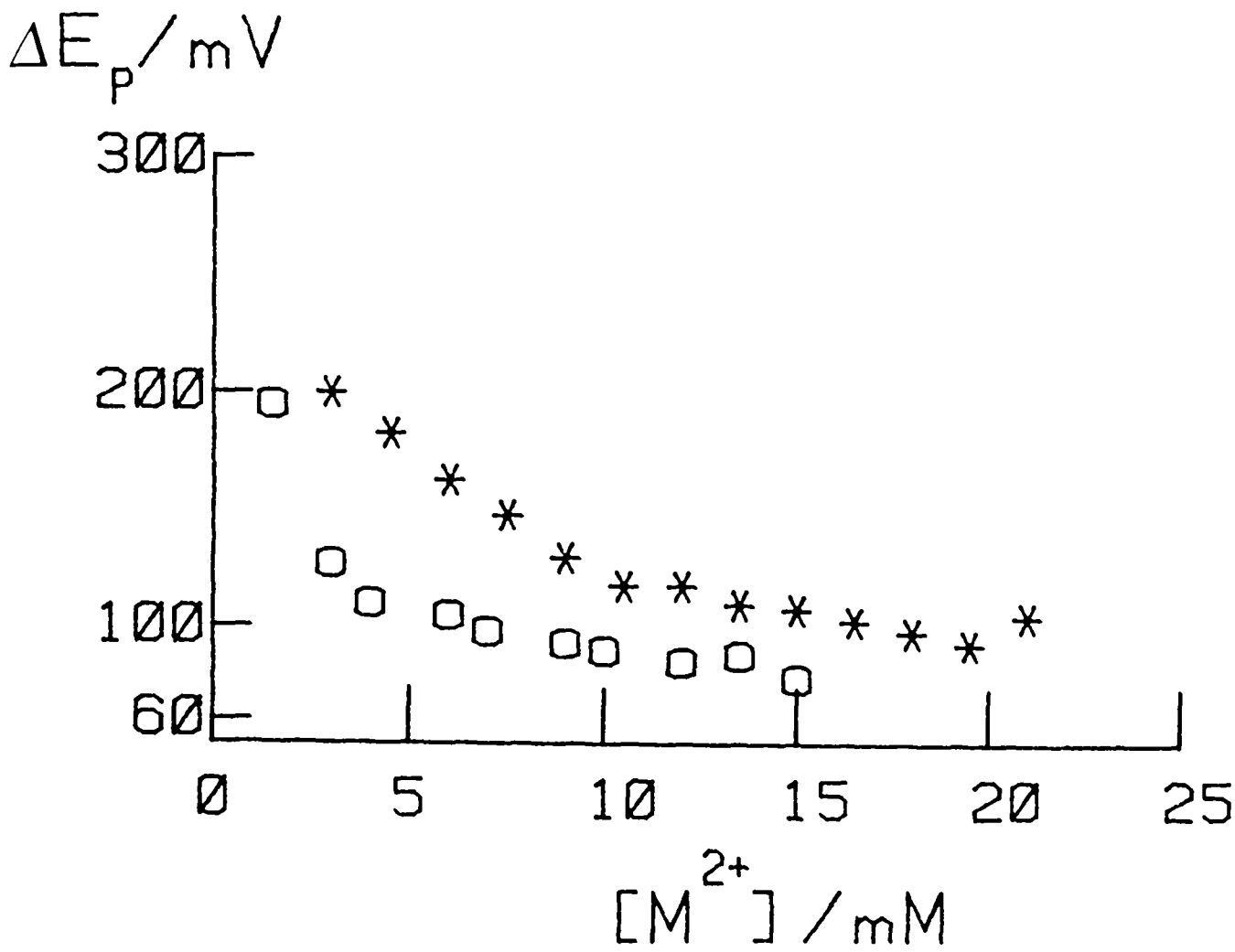

Figure 7.8: The variation of cathodic peak current and peak separation (cyclic voltammetry) with cation concentration for the addition of the organic di-cations ($^{+}Me_3N-(CH_2)_x-NMe_3^{+}$) decamethonium bromide [x=10: (o)] and hexamethonium chloride [x=6: (*)] to ferredoxin. Conditions given in Figure 7.7.

$Fe(phen)_3^{2+}$.

In a previous study (7), it has been found that the divalent cation $Fe(phen)_3^{2+}$ is by far the most efficient divalent cationic promoter of ferredoxin electrochemistry. A faradaic response titration performed under identical conditions to those adopted in this section (150 μM protein, 5 mM Tricine, 1 mM NaCl, pH 8.0) is reproduced in Figure 7.9(a). The cation is clearly seen to promote optimal faradaic responses ($i_{pc,max}$ ca. 1.6 μA, ΔE_p 75 - 85 mV) at a concentration of only 2 - 3 mM. However, prolonged voltammetric cycling at saturating cation levels (>5 mM) revealed a marked impersistence of the faradaic response.

The study of $Fe(phen)_3^{2+}$ as a promoter, through faradaic response titrations, was followed up in the current study by experiments designed to test for irreversible adsorption of this cation at graphite surfaces. A polished edge graphite surface was exposed to a solution of $Fe(phen)_3^{2+}$ (27 mM, in 5 mM Tricine, 1 mM NaCl pH 8.0) for 10 mins. The electrode was then rinsed and stirred vigorously in water (2 changes) for at least 1 minute. Subsequent, electrochemical tests with the 8Fe ferredoxin (22 μM ferredoxin, in 5 mM Tricine, 100 mM NaCl pH 8.0), Figure 7.9(b), revealed a symmetrical, quasi-reversible faradaic response with a redox potential ($E_{1/2}$ = -349 mV vs. NHE) close to that expected for ferredoxin. Successive voltammetric cycles showed the response to be slightly impersistent ($i_{pc}/\mu A$, $\Delta E_p/mV$ [20 mVs^{-1}]: 0.25, 85 (Scan 2); 0.22, 95 (Scan 4)). Similar experiments with cleaved basal plane and glassy carbon surfaces revealed no detectable faradaic responses, in the potential region of interest, after exposure to the same solution of $Fe(phen)_3^{2+}$.

Clearly, the cation, $Fe(phen)_3^{2+}$ is irreversibly adsorbed

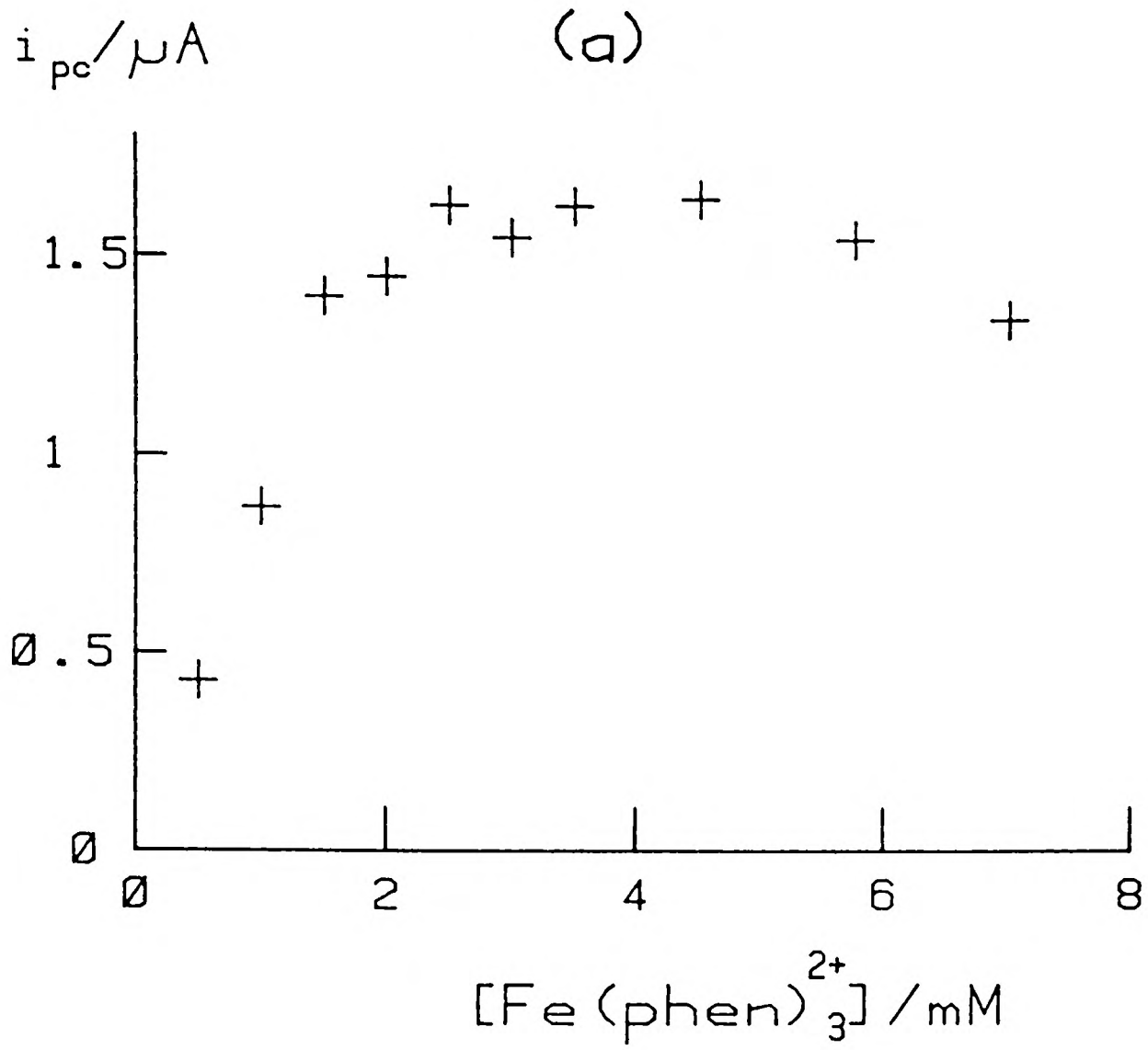

Figure 7.9: **(a)** The variation of cathodic peak current with the concentration of $Fe(phen)_3^{2+}$ for 150 μM *C. pasteurianum* 2[4Fe-4S] ferredoxin in 5 mM Tricine, 1 mM NaCl, pH 8.0. Measurements taken on the 4th voltammetric cycle (20 mVs^{-1}) at an edge graphite electrode surface. Reproduced from reference 7;
(b) Cyclic voltammograms [voltammetric cycles 1 - 3, and cycle 4 (shown separately)] recorded at an edge graphite electrode modified with $Fe(phen)_3^{2+}$. 22 μM ferredoxin in 5 mM Tricine, 100 mM NaCl, pH 8.0, 20 mVs^{-1}.

only at graphite electrodes with an edge plane orientation. Edge surfaces exposed to stock solutions of Mg^{2+}, Ba^{2+} and organic di-cations provided no evidence for significant irreversible adsorption of these cations.

7.4.2 Trivalent cation titrations - 150 μM ferredoxin.

Figure 7.10 shows faradaic response titrations carried out with the cations $Cr(NH_3)_6^{3+}$ and $Cr(en)_3^{3+}$ (5 mM Tricine, 1 mM NaCl, pH 8.0). A titration carried out under comparable conditions with the trivalent cation $Cr(chxn)_3^{3+}$ (7) is also reproduced in Figure 7.10 for comparative purposes. All three cations show remarkably similar promotion characteristics, with saturation achieved close to 0.5 mM added cation. Optimal faradaic peak currents and peak separations ($i_{pc,max}/\mu A$, $\Delta E_p/mV$) were $Cr(NH_3)_6^{3+}$ (2,65), $Cr(en)_3^{3+}$ (1.9,70) and $Cr(chxn)_3^{3+}$ (1.8 - 1.9, 60 - 65). Faradaic responses at optimal levels of $Cr(NH_3)_6^{3+}$ and $Cr(en)_3^{3+}$ were symmetrical with $i_{pc} \simeq i_{pa}$. However, cyclic voltammograms recorded with the cation $Cr(chxn)_3^{3+}$ show a marked enhancement of the anodic peak current at levels of promoter >0.5 mM.

7.4.3 Monovalent cations titrations - 150 μM ferredoxin.

The monovalent cations Na^+, K^+ and Cs^+ are noticeably less effective as promoters of direct electrochemistry when compared to the divalent and trivalent cations., Figure 7.11. In particular, optimal peak currents with the monovalent cations are reproducibly lower than those recorded with higher valent cations.

Faradaic response titrations recorded with the three

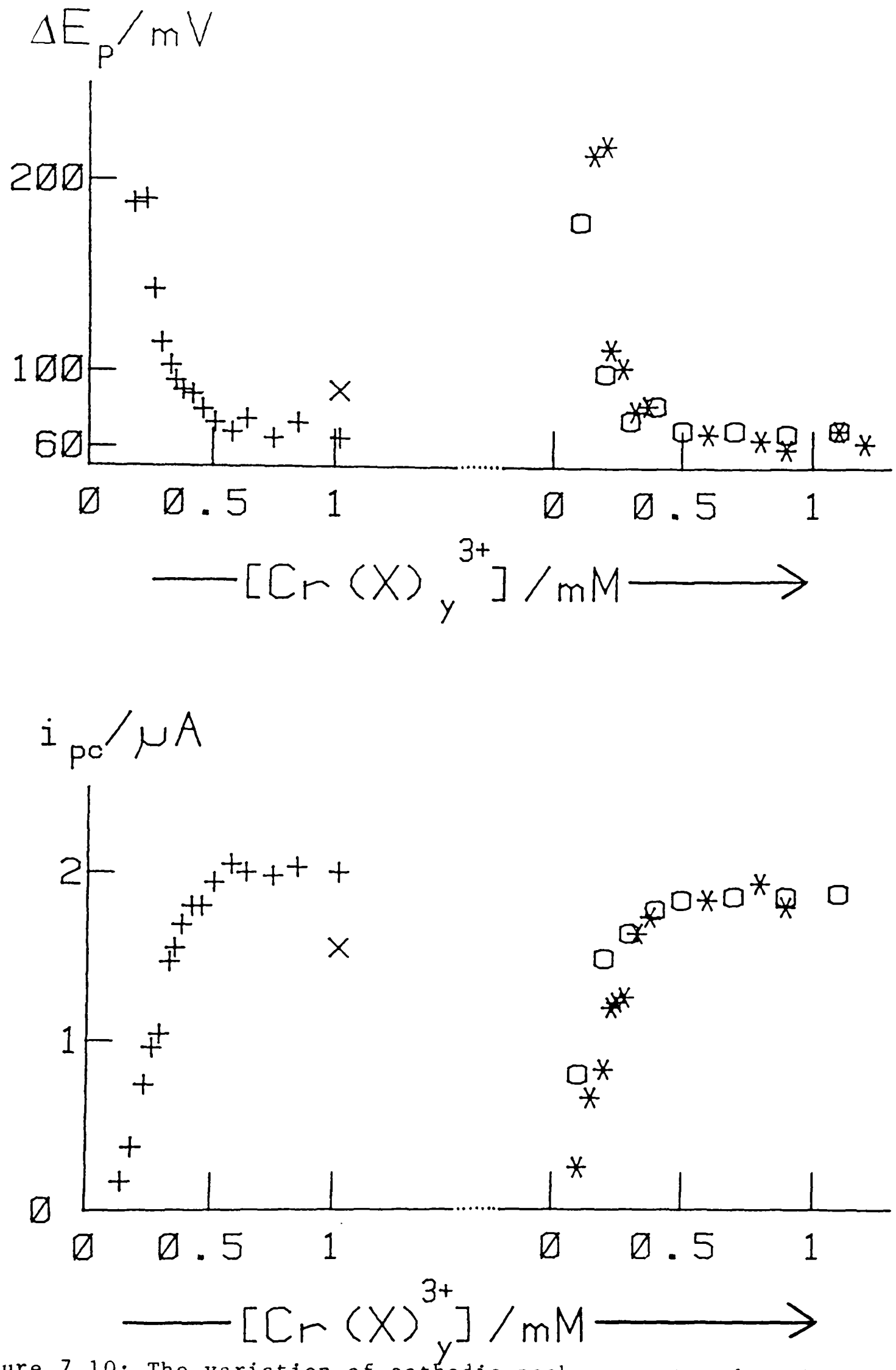

Figure 7.10: The variation of cathodic peak current and peak separation (cyclic voltammetry) with the concentration of trivalent cations for 2[4Fe-4S] ferredoxin. Conditions as in Figure 7.7.
(+) $Cr(NH_3)_6^{3+}$: 1mM NaCl background electrolyte.
(x) as (+), with the addition of 100 mM NaCl
(o) $Cr(ethylenediamine)_3^{3+}$: 1 mM NaCl.
(*) $Cr(cyclohexanediamine)_3^{3+}$: 1 mM NaCl.

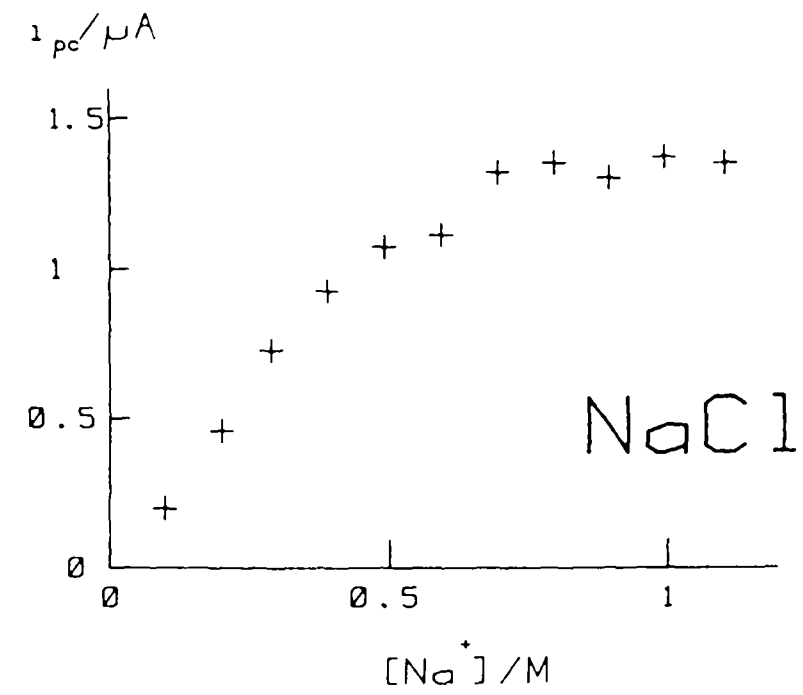

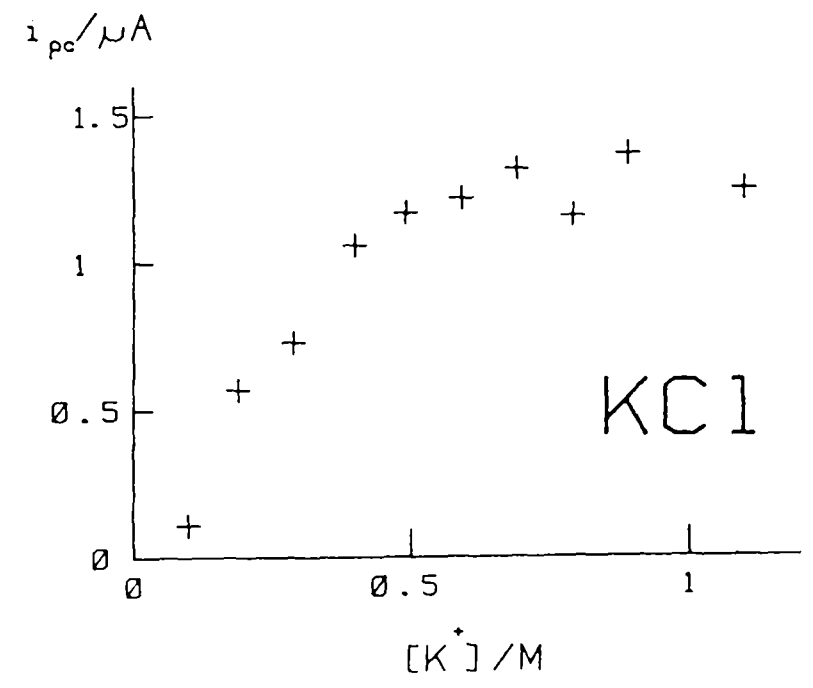

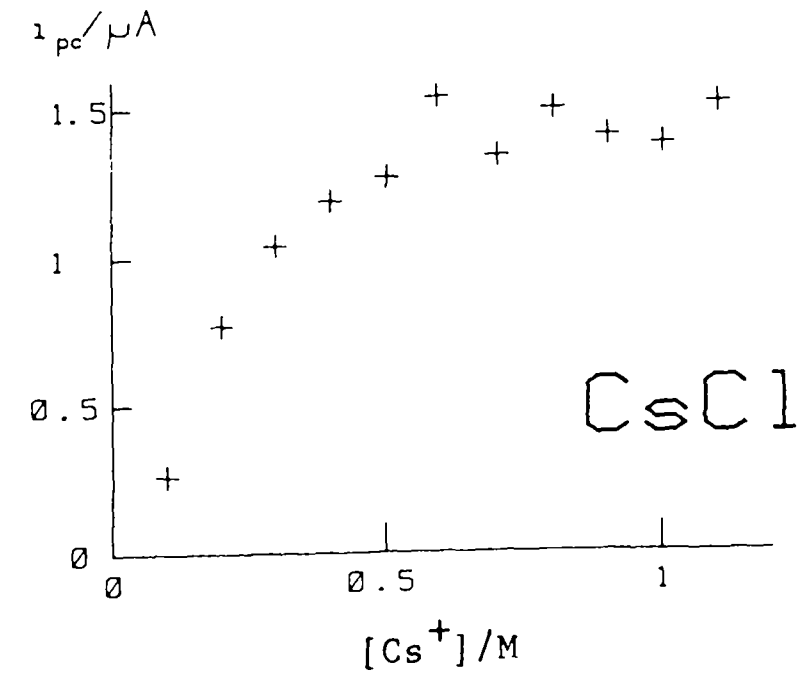

Figure 7.11: The variation of cathodic peak current and peak separation (cyclic voltammetry) with monovalent cation concentration for the addition of NaCl, KCl, and CsCl (as indicated) to the 2[4Fe-4S] ferredoxin. Conditions given in Figure 7.7.

cations are remarkably similar. Optimal faradaic responses ($i_{pc,max}/\mu A$, $\Delta E_p/mV$), achieved at cation levels of ca. 500 mM M^+, are Na^+ (1.3, 90), K^+ (1.2 - 1.3, 100) and Cs^+ (1.3 - 1.5, 85 - 95). In each case, optimal voltammetric responses are symmetrical with $i_{pc} \simeq i_{pa}$.

7.4.4 Faradaic response titrations at low (28 μM) protein concentrations.

Comparative titrations of representative cations ($Cr(NH_3)_6^{3+}$, Ba^{2+} and Na^+) were carried out following a ca. 5 - fold reduction in protein concentration (28 μM ferredoxin in 5 mM Tricine, 1 mM NaCl, pH 8.0), Figure 7.12. In accord with the results obtained at high protein concentrations, the cation concentrations required to achieve optimal faradaic responses (250 mM Na^+, 4 mM Ba^{2+}, 200 - 300 M $Cr(NH_3)_6^{3+}$) show a marked dependence on valence type, $M^+ > M^{2+} > M^{3+}$. However, at this low protein concentration, the optimal faradaic response ($i_{pc,max}/\mu A$ ca. 0.3 μA, ΔE_p 65 - 75 mV) is independent of valence type. Faradaic responses in the presence of Ba^{2+} and K^+ were noticeably more reversible (i.e. ΔE_p 20 - 30 mV lower) than at high (150 μM) protein concentrations.

7.5 ^{1}H-NMR Studies of C. Pasteurianum 8Fe Ferredoxin.

Paramagnetic cations such as $Cr(NH_3)_6^{3+}$, may be used to probe site-specific interactions between redox proteins and inorganic complexes by following the specific broadenings of assigned proton resonances in the ^{1}H-NMR spectrum.

The 300 MHz ^{1}H-NMR spectrum (Figure 7.13(a)) of a 3mM sample of oxidised C. pasteurianum 2[4Fe-4S] ferredoxin in

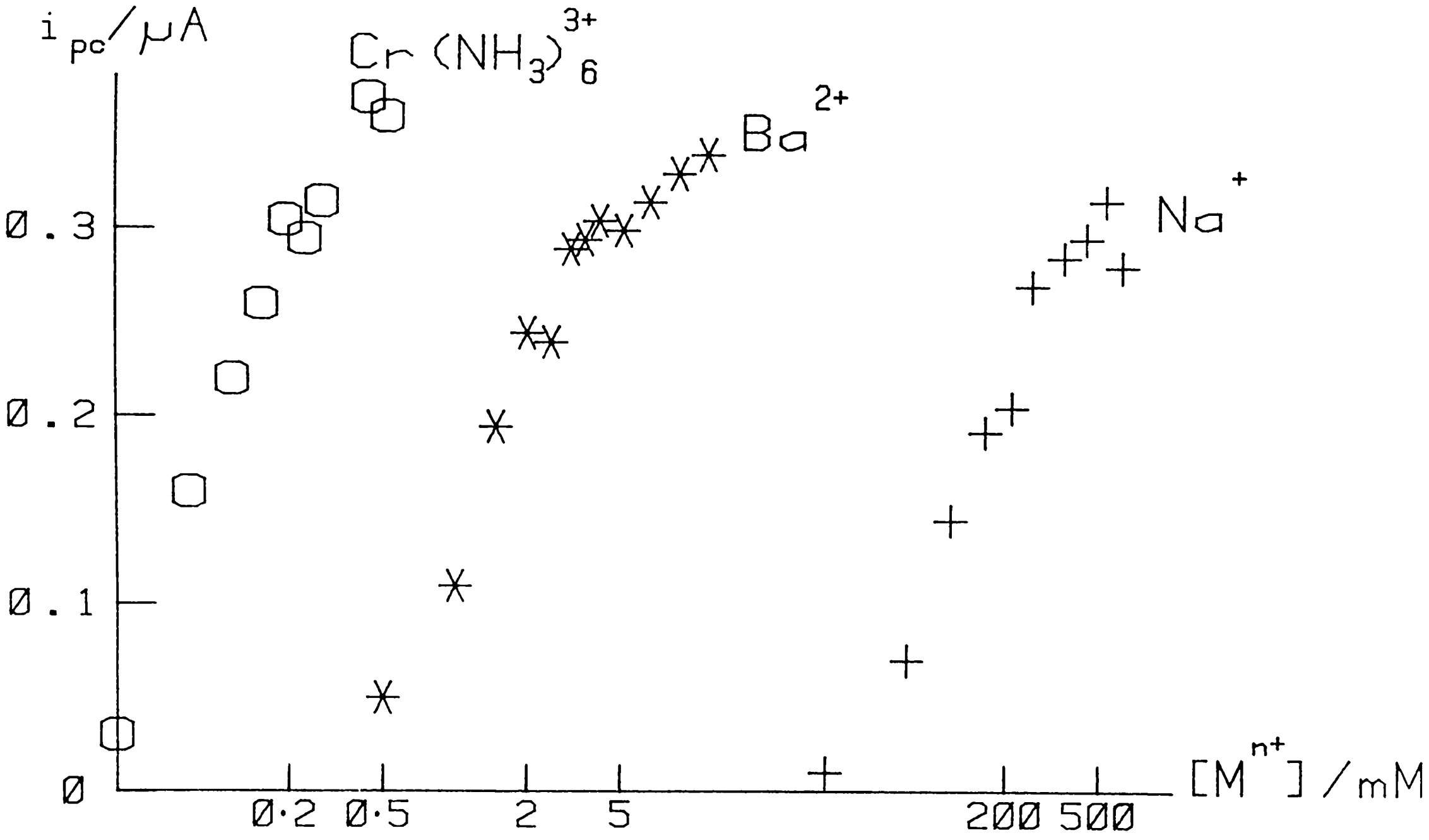

Figure 7.12: The variation of cathodic peak current (cyclic voltammetry) with cation concentration for the addition of $Cr(NH_3)_6^{3+}$ (o), Ba^{2+} (*) and Na^+ (+), to 28 μM 2[4Fe-4S] ferredoxin. Conditions given in Figure 7.7.

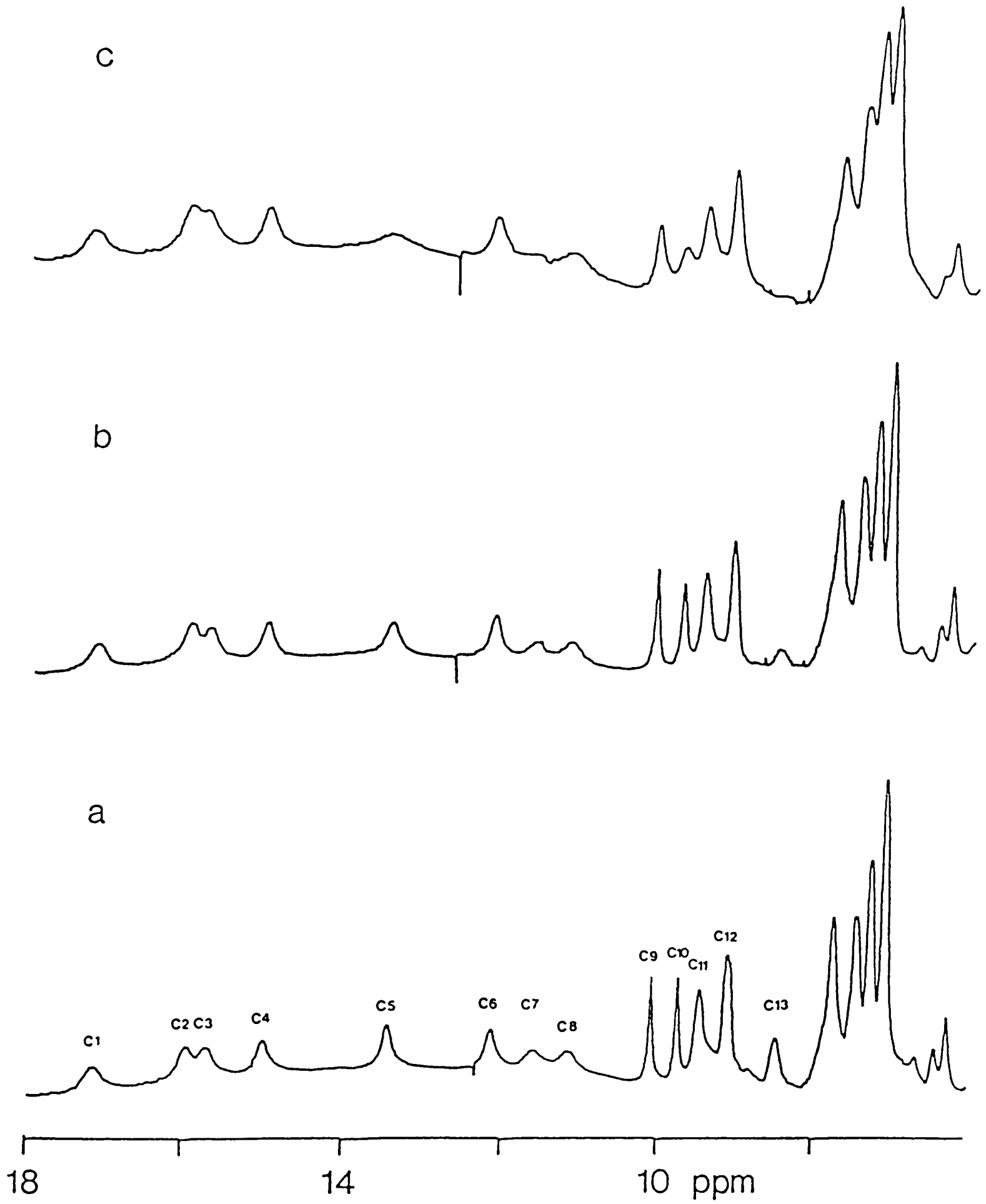

Figure 7.13: The effects of the addition of $Cr(NH_3)_6^{3+}$ on the 300 MHz ^{1}H-NMR spectrum of 3 mM oxidised 2[4Fe-4S] ferredoxin, 23°C, pH* = 7.6, 12 mM Tris-HCl, 0.1 M NaCl in D_2O.
(a) conventional spectrum of oxidised ferredoxin.
(c) (a) + 5 mM $Cr(NH_3)_6^{3+}$.
(b) (a) + 5 mM $Cr(NH_3)_6^{3+}$ + 1 M NaCl.

12 mM Tris (D_2O), pH^* = 7.6, 0.1 M NaCl, shows eight one-proton resonances shifted downfield in the region 11 ppm - 18 ppm. These are consistent with similar resonances observed in published spectra of Clostridial-type ferredoxins (16,17) and assigned to eight of the sixteen β-CHs of the ligand cysteines.

Addition of $Cr(NH_3)_6^{3+}$ to the oxidised ferredoxin causes several marked changes in the spectrum as shown in Figure 7.13(c). For resonances in the region 8 ppm - 18 ppm (labelled as C_1-C_{13}) it is possible to measure their line-broadenings as a function of the amount of $Cr(NH_3)_6^{3+}$ added, and these are plotted, for resonances arising from single protons, in Figure 7.14. Three resonances are clearly broadened more quickly than any of the others. Similarly, in the aliphatic region, three resonances (at 4.28 ppm, 2.71 ppm and 1.7 ppm) broaden before neighbouring resonances, upon $Cr(NH_3)_6^{3+}$ additions. An increase in ionic strength effects a partial reversal of the observed line broadenings, as illustrated in Figure 7.14(b).

In a parallel study, the paramagnetic divalent cation Mn^{2+} was used to probe specific divalent cation - protein interactions. This cation has been previously shown to promote rapid direct electrochemistry of C. pasteurianum 8Fe ferredoxin (9). However, little or no significant changes were observed in the ^1H-NMR spectrum of oxidised ferredoxin upon the successive addition of aliquots (1 mM) of a Mn^{2+} stock solution.

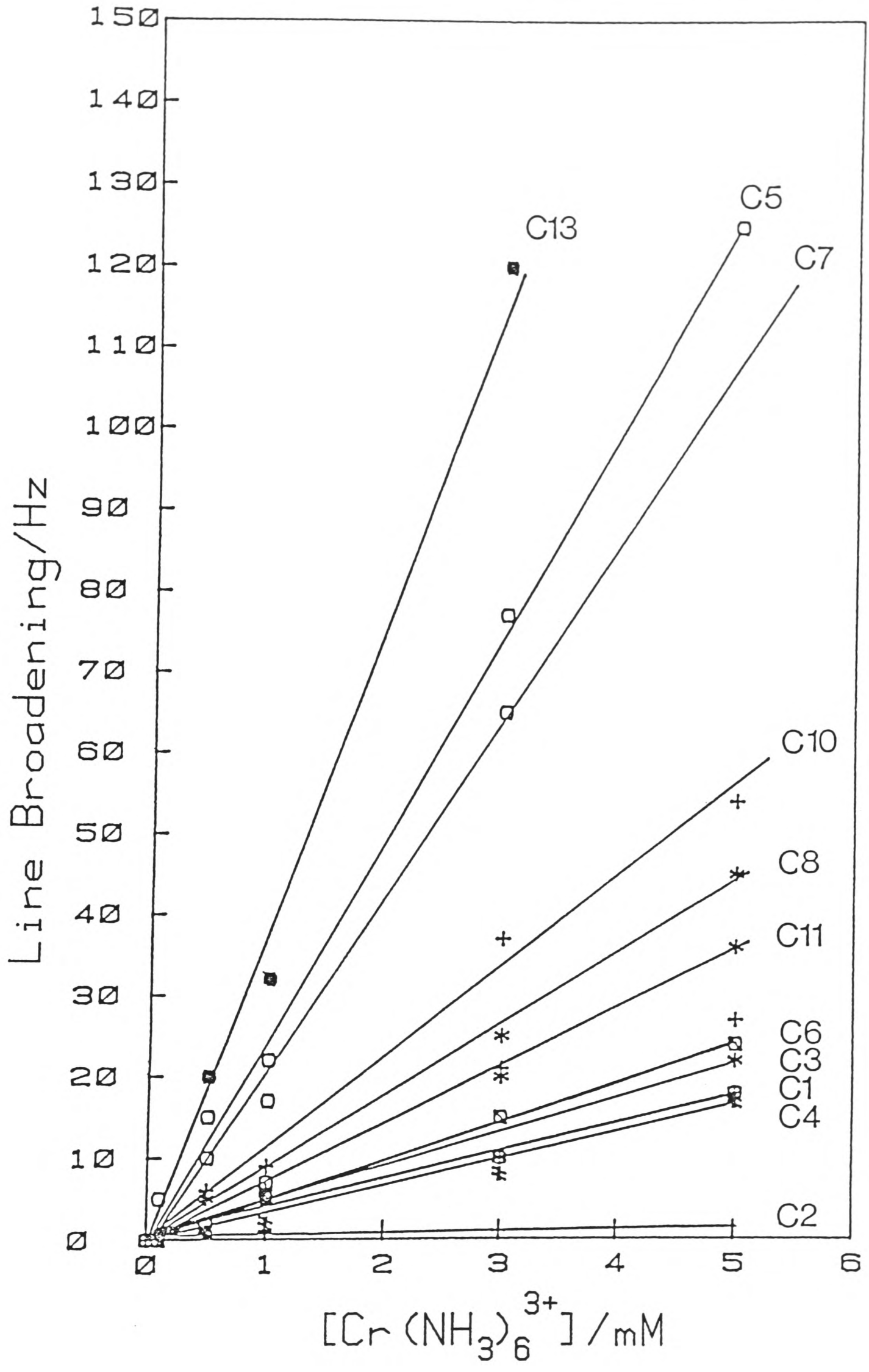

Figure 7.14: Line broadenings of the contact-shifted resonances in oxidised C. pasteurianum ferredoxin as a function of the concentration of $Cr(NH_3)_6^{3+}$ added. Resonance labels are as defined in Figure 7.13.

7.6 Comparative Direct Electrochemical Studies of the Fe-S Proteins, Rubredoxin, 8Fe Ferredoxin and Spinach (2Fe) Ferredoxin.

Figures 7.15 and 7.16 illustrate features of the cation-promoted direct electrochemistry of Spinach 2Fe-2S ferredoxin, and Clostridium pasteurianum 8Fe ferredoxin and rubredoxin (all 67 μM protein in 5 mM Tricine, 1 mM NaCl at pH 8.0).

Spinach Ferredoxin.

K^+, Mg^{2+} and $Cr(NH_3)_6^{3+}$ additions to Spinach ferredoxin reveal features in common with those previously described for the 8Fe ferredoxin. In particular, cation effectiveness follows the order $M^{3+} > M^{2+} > M^+$; cation requirements increase with increasing protein concentration; the faradaic response is markedly destabilised by increasing the protein concentration (250 μM vs. 82 μM ferredoxin, Figure 7.16) and the addition of NaCl to a final concentration of 100 mM, at saturating $Cr(NH_3)_6^{3+}$ levels (1 mM NaCl), markedly de-promotes the faradaic reponse (1.5 mM $Cr(NH_3)_6^{3+}$, 1 mM NaCl: ΔE_p 67 mV, i_p 0.34 μA [SCAN 4]; 1.5 mM $Cr(NH_3)_6^{3+}$, 100 mM NaCl: ΔE_p >150 mV, i_p 0.16 μA [SCAN 4]; Figure 7.15). However, the $Cr(NH_3)_6^{3+}$ levels required to optimise the faradaic response are ca. two-fold higher and optimal faradaic peak currents ca. two-fold lower for the 2Fe ferredoxin when compared with the 8Fe protein. A change in cation requirement is also emphasised by the inability of Mg^{2+} additions (to > 160 mM) to stabilise the observed faradaic response (Figure 7.15). Furthermore, unlike the 8Fe protein, a trace faradaic response is no longer observed in 100mM NaCl alone.

FIGURE LEGENDS

Figure 7.15

Cation-promoted direct electrochemistry of iron-sulphur proteins (67 μM protein in 5 mM Tricine, pH 8.0).
TOP: [2Fe-2S] ferredoxin (spinach). Plot of the variation of cathodic peak current (cyclic voltammetry) with the concentration of added $Cr(NH_3)_6^{3+}$, (+) 1 mM NaCl background electrolyte; (x) with the addition of 100 mM NaCl. Also shown are cyclic voltammograms (20 mVs^{-1}) recorded in 162 mM $MgCl_2$, 1 mM NaCl (1eft), and 1.5 mM $Cr(NH_3)_6^{3+}$ (right) before and after the addition of 100 mM NaCl.
MIDDLE: 2[4Fe-4S] ferredoxin (C. pasteurianum). Plot of the variation of cathodic peak current with the concentration of added $Cr(NH_3)_6^{3+}$, (+) 1 mM NaCl; (x) with the addition of 100 mM NaCl. Also shown is the cyclic voltammetric response (20 mVs^{-1}) in 100 mM NaCl alone.
BOTTOM: Rubredoxin. Conditions as given for the 2[4Fe-4S] ferredoxin.

Figure 7.16

The variation of the cyclic voltammetric response of spinach [2Fe-2S] ferredoxin as a function of protein concentration and the level of added $Cr(NH_3)_6^{3+}$. The plots show measurements of cathodic peak current and peak separation taken on the 1st (x), 2nd (*) and 4th (o) voltammetric cycles (20 mVs^{-1}) at an edge graphite electrode. Protein concentrations are 82 μM (....) and 250 μM (———).

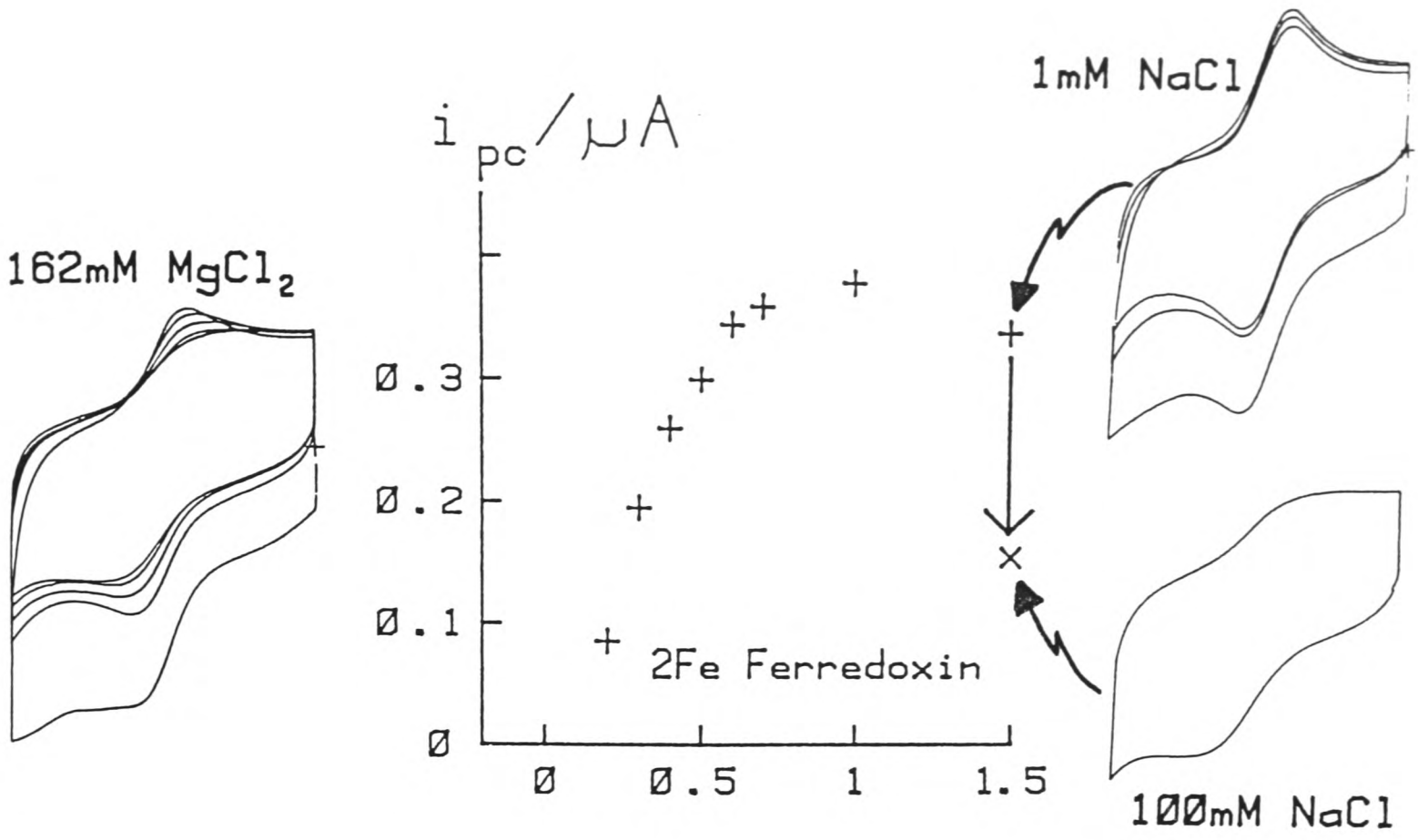
162mM $MgCl_2$
$i_{pc}/\mu A$
1mM NaCl
100mM NaCl
2Fe Ferredoxin
Ø
Ø.1
Ø.2
Ø.3
Ø
Ø.5
1
1.5

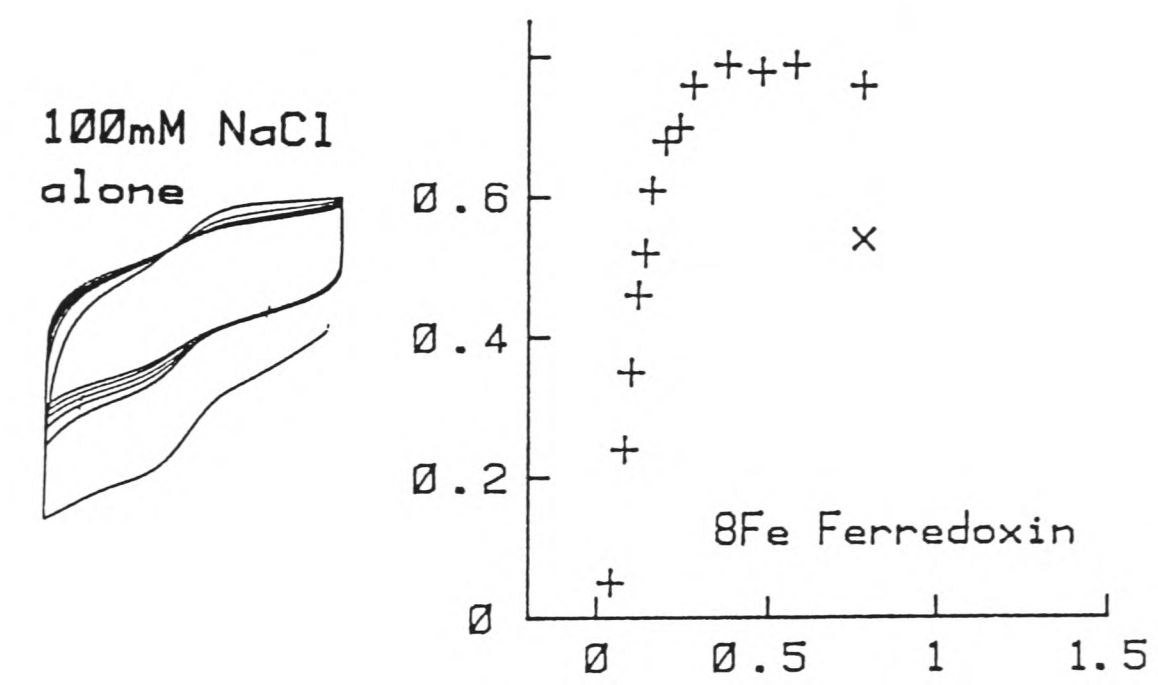
100mM NaCl
alone
8Fe Ferredoxin
Ø
Ø.2
Ø.4
Ø.6
Ø
Ø.5
1
1.5

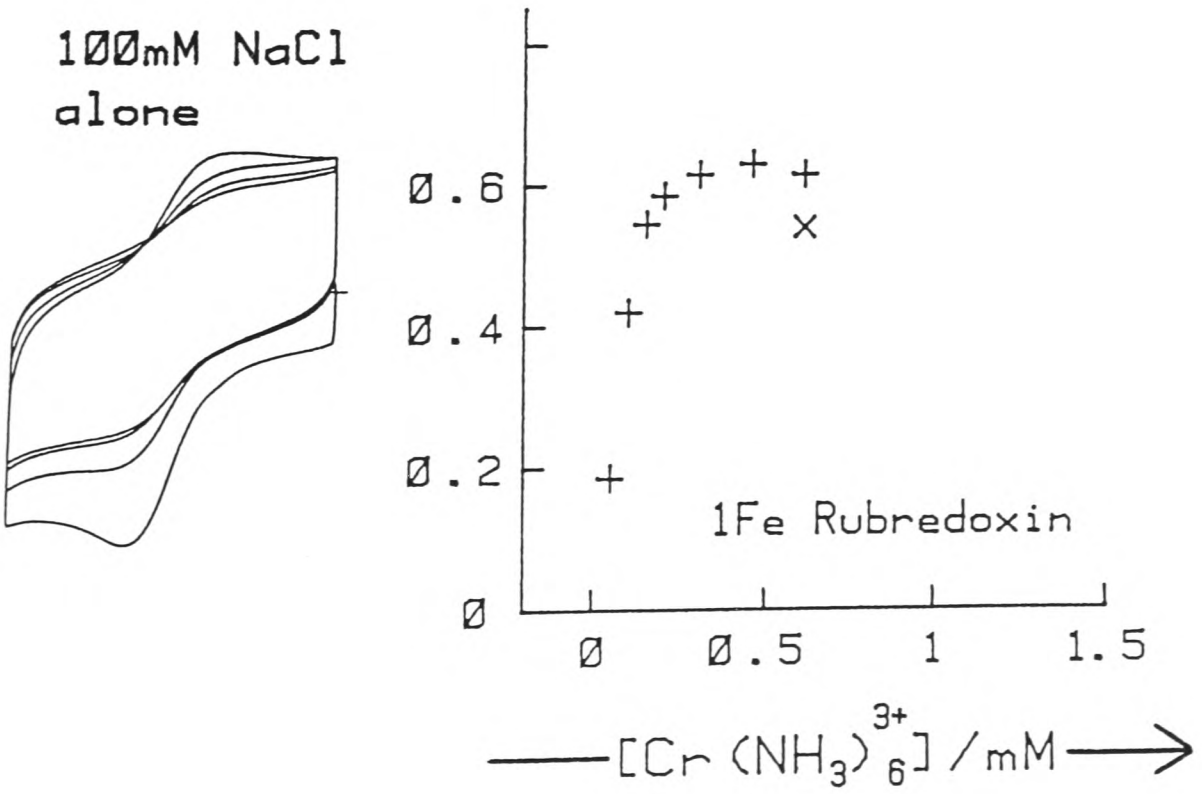
100mM NaCl
alone
1Fe Rubredoxin
Ø
Ø.2
Ø.4
Ø.6
Ø
Ø.5
1
1.5
$[Cr(NH_3)_6^{3+}]$ /mM

Figure 7.15

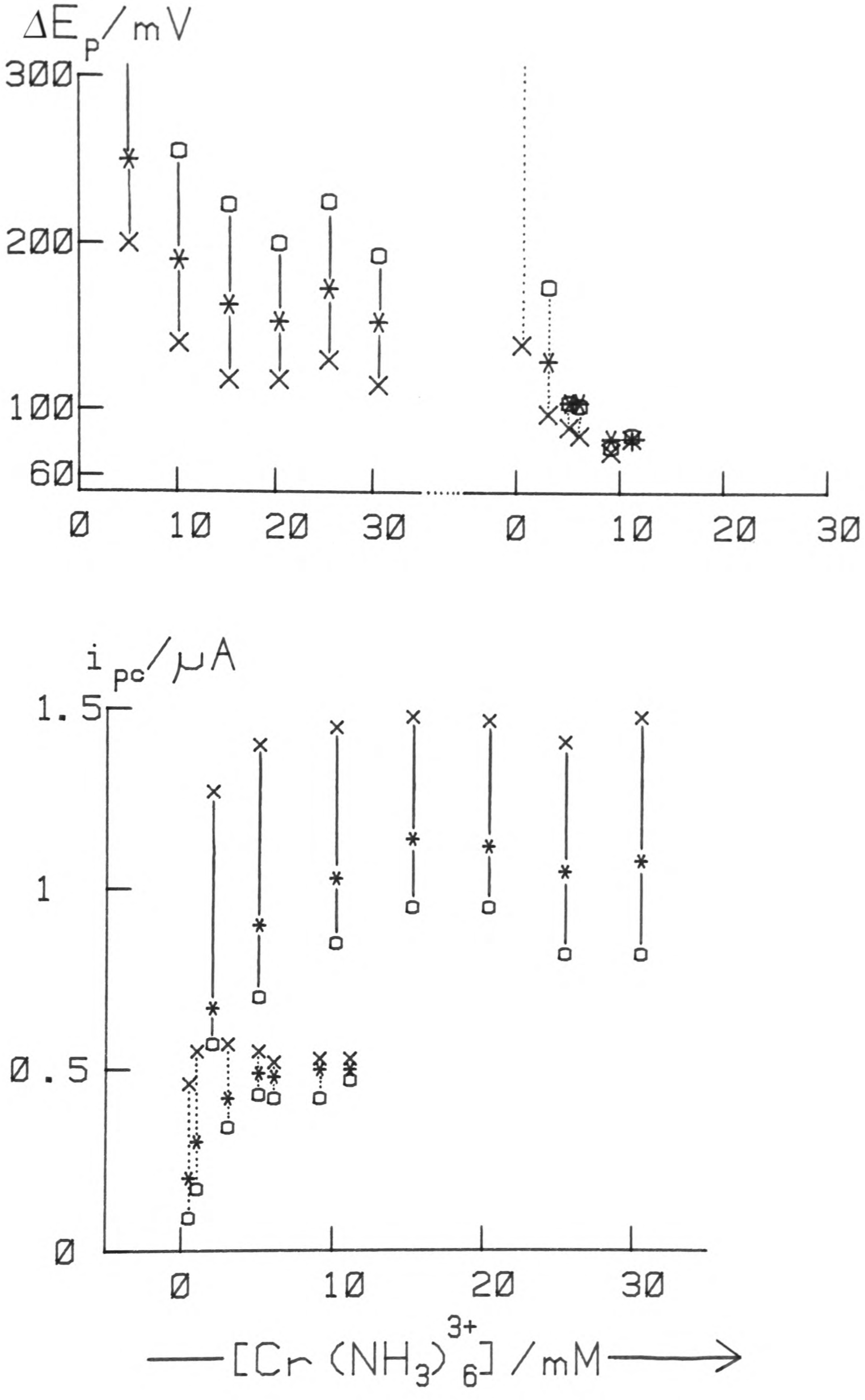
ΔE_p / mV
300
200
100
60
0
10
20
30
0
10
20
30
i_pc / μA
1.5
1
0.5
0
0
10
20
30
[Cr(NH3)6]3+ / mM

Figure 7.16

Rubredoxin.

As for the other negatively-charged Fe-S proteins, cation effectiveness follows the order $M^{3+} > M^{2+} > M^{+}$ and cation requirement increases with increasing protein concentration. However, comparison with the negatively-charged ferredoxins shows that rubredoxin is the least cation-sensitive of the three proteins. In particular, there is now a marked, although highly impersistent response in 100 mM NaCl alone. The requirements for $Cr(NH_3)_6^{3+}$ (1 mM NaCl) are similar to those for the 8Fe ferredoxin, although optimal faradaic peak currents appear lower. Further experiments with rubredoxin are needed to confirm the relative magnitude of optimal peak currents obtained for rubredoxin and ferredoxin (8Fe) under comparable conditions. In contrast to the two ferredoxins, a step in the ionic strength (1 - 100mM NaCl) has little or no effect upon optimal faradaic responses in the presence of $Cr(NH_3)_6^{3+}$ (Figure 7.16).

7.7 Summary Of Cation Promotion Effects.

For the negatively-charged iron-sulphur redox proteins, the salient features of cation **promotion** effects in direct electrochemical studies, may be summarised as below:

1) The addition of multivalent cations to a solution at low (1 mM NaCl) and high (100 mM NaCl) ionic strength effects a promotion of faradaic response evident as an increase in peak current and a decrease in peak separation with increasing cation concentration.

2) In parallel with promotion of direct electrochemistry, increasing multivalent cation concentration stabilizes the observed electrochemistry, by retarding a time-dependent deterioration of response.

3) The ability of cations to act as promoters follow the general trend $M^{3+} > M^{2+} > M^{+}$.

4) No significant differences are observed between the effectiveness of various monovalent or trivalent cations as promoters.

5) The divalent cations display marked departures from uniformity. $Fe(phen)_3^{2+}$, the most effective divalent cation, is the only cation irreversibly adsorbed at edge graphite. Mg^{2+} is the least effective divalent cation.

6) Increasing protein concentration increases the level of cations required to optimise electron-transfer rates.

7) At higher protein concentrations (ca. 0.3 mM) successive cation additions are less effective at achieving optimal and stable faradaic responses.

8) $Cr(NH_3)_6^{3+}$ causes the selective broadening of resonances assigned to the β-CH protons of ligand cysteines, in the ^{1}H-NMR spectrum of C. pasteurianum 8Fe ferredoxin.

7.8 Discussion of cation promotion effects.

7.8.1 General Features.

It is apparent that the electrochemical characteristics of all three negatively-charged Fe-S proteins reflect the same **general** features. This emphasises that the same basic constraint is operating in each case. However, the three proteins differ markedly in the **relative** cation levels (M^{3+} vs. M^{2+} vs. M^{+}) required to stabilise and optimise faradaic responses. This shows that there are specific features relevant to each individual protein.

In the absence of multivalent cations (1 mM NaCl alone) there are no detectable faradaic responses, attributable to the Fe-S proteins, evident at an edge-oriented graphite electrode. This may imply that there is no significant population of protein molecules retained within the interfacial region. Alternatively, protein molecules may be at, or close to, the electrode surface but in an unfavourable orientation for rapid protein-electrode transfer to occur. An unfavourable orientation at the surface may be accompanied by strong protein-electrode binding. Thus, a third possibility is that there is total 'ageing', with no response detectable on the cyclic voltammetric time scale. The latter can not be ruled out on the evidence available from rotating-disc studies of ageing effects. The first proposal is in accord with elementary electrostatic considerations. It is expected that the edge graphite surface carries a net negative surface charge density in the potential region of interest (+170 to -350 mV vs. NHE). This will comprise excess electronic charge density at the

lower potentials and also discrete charge arising from acidic surface oxides. The ensuing negative surface potential will repel the highly negatively-charged protein molecules from the surface of the electrode, so ensuring a negative surface excess of protein. Since it is the protein concentration at the surface which is effective in electron-exchange then no electron-transfer event will be observed. Alternatively, since most metalloproteins have an irregular shape with a non-uniform distribution of charged amino acid groups, then protein molecules may approach the surface in an orientation which minimises unfavourable charge interactions. This orientation may be unfavourable for rapid electron-transfer. Thus, the initial postulate of cation action is that the role of cationic promoters is to facilitate close approach to the electrode surface, in a favourable orientation for electron-transfer to occur, by relieving unfavourable charge interactions.

At least three factors may be important in determining the relative electrochemical behaviour of the three Fe-S proteins: protein size, protein charge and its distribution, and redox potential. Initially, attention may be focussed on the distribution of charged residues at the surface of rubredoxin. The crystal structure of this protein reveals that the Fe-S cluster lies close (ca. 5 Å) to the surface of the protein. The surface region in the vicinity of the Fe-S centre is distinguished by the presence of hydrophobic groups and a total lack of hydrophilic groups. In fact, rubredoxin is essentially a dipolar molecule with almost half the acidic groups spread in a band across the lower face of the molecule (Chapter 1). An orientation with the cluster held in close proximity to the

surface may then hold charged groups directed away from the elecrode surface. This will decrease unfavourable electrostatic interactions. This is in accord with the lower cation requirements of rubredoxin, in particular, the marked response in 100 mM NaCl alone.

Secondly, it must be recalled that the 2Fe ferredoxin is the largest of the three proteins (RMM 10660) and may carry a significantly larger overall net negative charge (Table 4.1). An increase in cation requirements, lower peak currents and a decrease in stability at higher protein concentrations, relative to the 8Fe ferredoxin, would be fully consistent with the additional charge and size constraints imposed upon the 'packing' of larger protein molecules into the interfacial region at the electrode surface. Similar interfacial restrictions may be expected to operate in the case of the highly negatively-charged redox protein flavodoxin (RMM ca. 16000). Indeed, cation-promoted direct electrochemical studies (18) of this protein at edge graphite electrodes have highlighted features similar to those seen with the 2Fe ferredoxin. Thus, $Cr(NH_3)_6^{3+}$ can efficiently stabilise faradaic responses, whereas Mg^{2+} and Na^{+} are ineffective at levels >150 mM. It should be noted that the effect of increased molecular weight upon the diffusion coefficient and, hence, the faradaic peak current ($i_p \propto D_o^{1/2}$), is insufficient to account for the observed change in the magnitude of the faradaic response between the 8Fe and 2Fe ferredoxins.

The redox potential at which electron-transfer activity is observed may be important in determining the charge distribution and potential profiles near the electrode-solution interface. At increasingly positive electrode potentials, positive electronic

charge density may compensate for the negative surface dipoles and discrete charges arising from surface oxygen groups. In the case of the 2Fe (-397 mV vs. NHE) and 8Fe (-373 mV vs. NHE) ferredoxins the experimentally-determined redox potentials are sufficiently similar to suggest that the changes in cation requirement arise purely from differing structural characteristics of the protein concerned. In the case of rubredoxin, changes in cation requirements may also be a result of a redox potential (-79 mV vs. NHE) some 300 mV more positive than that of the 8Fe ferredoxin.

7.8.2 Diffuse-Layer Effects.

At low protein concentrations (as exemplified by studies with 28 μM 8Fe ferredoxin) the major aspect of cation promotion appears to be that the effect is largely a function of cation charge (z). The cations Na^+ (250 mM), Ba^{2+} (4 mM) and $Cr(NH_3)_6^{3+}$ (0.2 mM) are found to be equally effective in terms of the stability of the final response, the optimal peak current (0.3 μA) and the optimal peak separation (60 - 70 mV). With this in mind, it is appropriate, at the low supporting electrolyte concentrations employed in these relative cation studies, to focus attention upon Gouy-Chapman diffuse layer theory which provides the basis for analysing surface phenomena which are predominantly electrostatic in nature. The relevant equations for this approach are given in the Appendix to this chapter and for more extended theoretical discussion, reference may be made to several excellent reviews (19,20)

In terms of the Gouy-Chapman theory, the effect of a negative surface charge density (σ) at an edge graphite surface

will be to produce a negative surface potential (ψ_o) at the aqueous side of the electrode-solution interface. The magnitude of this surface potential depends on the salt concentration, as given by the Gouy equation (equation 7.5: Appendix). Similarly, the distance over which the potential decays perpendicular to the surface is also dependent on the salt concentration. The Debye length ($1/\kappa$), the distance from the surface at which the potential falls to 1/2.7 of its value at the surface, is about 100 Å when the concentration of monovalent ions is 10^{-3} M, Figure 7.17(a). Knowing the surface potential, the concentration of ions at any distance from the electrode may be calculated from the Boltzmann relation. Simple calculations based on a small negative surface potential of -16 mV yields the concentration profiles presented in Figure 7.17(b). The surface is seen to exert long range electrostatic forces which serve to produce an ionic atmosphere extending some 200 Å from the surface (the 'diffuse' layer). Within this diffuse layer there is a deficiency or negative surface excess of anions, which is particularly marked in the case of multiply-charged anionic species (e.g. M^{9-}), such as the Fe-S proteins.

7.8.3 The Relative Screening Ability of Cations and the Concept of Ionic Strength.

The theoretical curves in Figure 7.17(a), calculated from the Gouy equation for a surface potential of ψ_o = -16 mV, predict that 4 mM Ba^{2+} has a substantially larger effect on the diffuse layer than does 1 mM NaCl. The negative surface charge density is effectively 'screened', as indicated by a reduction in the surface potential (ψ_o) and a reduction in the Debye length ($1/\kappa$).

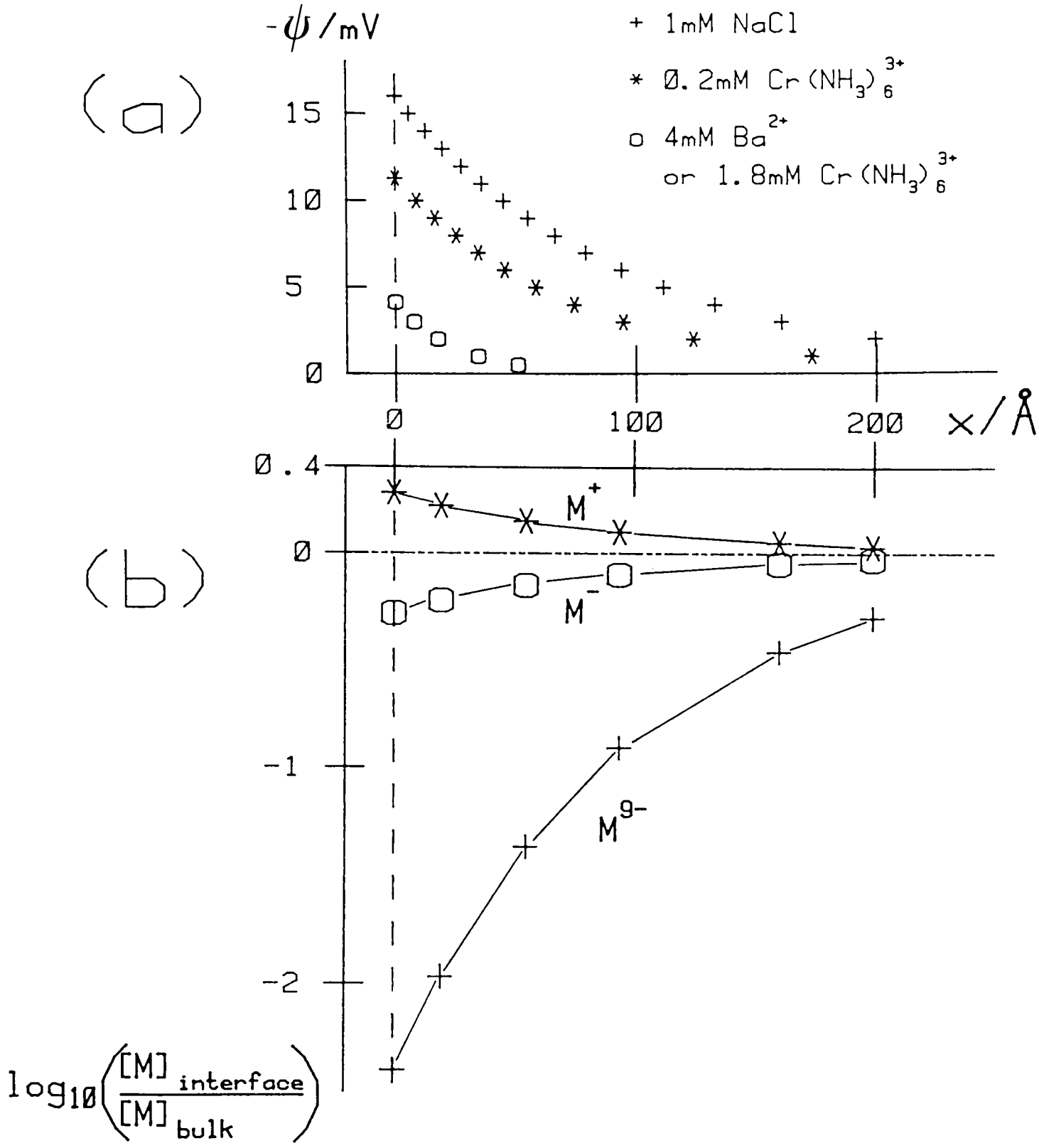

Figure 7.17: Potential (a) and concentration (b) profiles through the diffuse layer in the Gouy-Chapman model. Calculated for a surface potential of ψ_o = -16 mV and symmetrical z:z electrolytes. T = 25°C. (a) Cation concentrations as indicated in the figure. (b) Bulk ion (M) concentrations are 1 mM M^+ (*), 1 mM M^- (o) and 30 μM M^{9-} (+).

However, the divalent cation is only predicted to be a factor of four more potent than the monovalent cation, whereas in direct electrochemical studies of 28 μM ferredoxin (1 mM NaCl background), the addition of 4 mM Ba^{2+} produces a rate enhancement of several orders of magnitude. Even more striking is the 'screening' ability predicted for 0.2 mM $Cr(NH_3)_6^{3+}$, Figure 7.17(a). At a concentration of 0.2 mM, the trivalent cation is predicted to be markedly <u>less</u> effective than the divalent cation at screening diffuse layer interactions. However, electrochemically, 4 mM Ba^{2+} and 0.2 mM $Cr(NH_3)_6^{3+}$ are <u>equally</u> efficient as promoters. Clearly, the observed electrochemical cation requirements contradict the predictions of a simple diffuse layer argument. In fact, the Gouy equation predicts that 1.8 mM $Cr(NH_3)_6^{3+}$ would be required to produce a screening efficiency comparable to that of 4 mM Ba^{2+}.

The cation levels predicted to afford <u>equal screening efficiency</u> follow a z^2 dependence, in accord with the concept of ionic strength, $I=1/2 \sum_i c_i z_i^2$. However, the concept of ionic strength and the exponential ψ_o-x function (equation 7.7: Appendix) used to construct Figure 7.17(a), arise from the linearisation of the exponent in the Poisson-Boltzmann relation, an invalid assumption for surface potentials > 50/z mV. In addition, the Gouy equation is only applicable to <u>symmetrical</u>, <u>single</u> electrolytes, although the valence of the co-ion and the presence of 10^{-3} M 1:1 electrolyte are usually of little consequence to the final result (23).

A more general expression is the Grahame equation (equation 7.3: Appendix) which is applicable to unsymmetrical, mixed electrolytes with no restriction on the magnitude of the

surface potential. Numerical analysis of the observed cation requirements (28 μM ferredoxin, 1 mM NaCl) can be carried out by equating the surface charge density in an appropriate Grahame expression (e.g. for a 1:1 / 2:1 mixed electrolyte solution, see equation 7.4: Appendix) with the charge density as given by a Gouy equation for a monovalent titration alone (single, symmmetrical electrolyte). Substitution in these equations of the minimum cation levels observed to promote the optimal peak current of 0.3 μA (e.g. 4 mM $BaCl_2$, 1 mM NaCl in the Grahame equation; 250 mM NaCl in the Gouy equation) leads to a solution for the surface potential under these conditions. This potential may then be used to estimate the surface charge density and to predict the concentration of other multiply-charged cations, e.g. $Cr(NH_3)_6^{3+}$, which will produce the same reduction in surface potential. Finally, the calculated surface charge density may be used to calculate the potential profile in the diffuse layer in 1 mM NaCl alone.

The results of an analysis based on the Grahame equation are presented in Table 7.1. Computer-derived curves (based on Table 7.1 and equation 7.8: Appendix) for the predicted potential-distance profiles in the interfacial region, in the presence or absence of divalent cations, are shown in Figure 7.18. These support the hypothesis that the addition of multivalent cations to solution, under low salt conditions (1 mM NaCl), generates a high space charge density immediately adjacent to the surface. This serves to electrostatically 'screen' the negative surface charge density, by reducing the surface potential and dramatically decreasing the Debye length. This has important implications with respect to the interaction between

TABLE 7.1

ESTIMATED DIFFUSE LAYER CHARACTERISTICS

(28 μM 8Fe FERREDOXIN, 1 mM NaCl BACKGROUND ELECTROLYTE).

Calculation Based On	Surface Charge Density	Charge Distribution	Surface Potential	Predicted Cation Requirement	Debye Length
$BaCl_2$,4mM vs. NaCl,250mM	$-0.22 Cm^{-2}$	1 electronic charge every $2.2 nm^2$	-105mV	66 M M^{3+}	10 Å
$Cr(NH_3)_6^{3+}$,0.2mM vs. $BaCl_2$,4mM	$-0.07 Cm^{-2}$	1 electronic charge every $0.6 nm^2$	-77mV	89mM M^{+}	
1mM NaCl alone	$-0.22 Cm^{-2}$	-	-246mV	-	32 Å
1mM NaCl alone	$-0.07 Cm^{-2}$	-	-190mV	-	45 Å

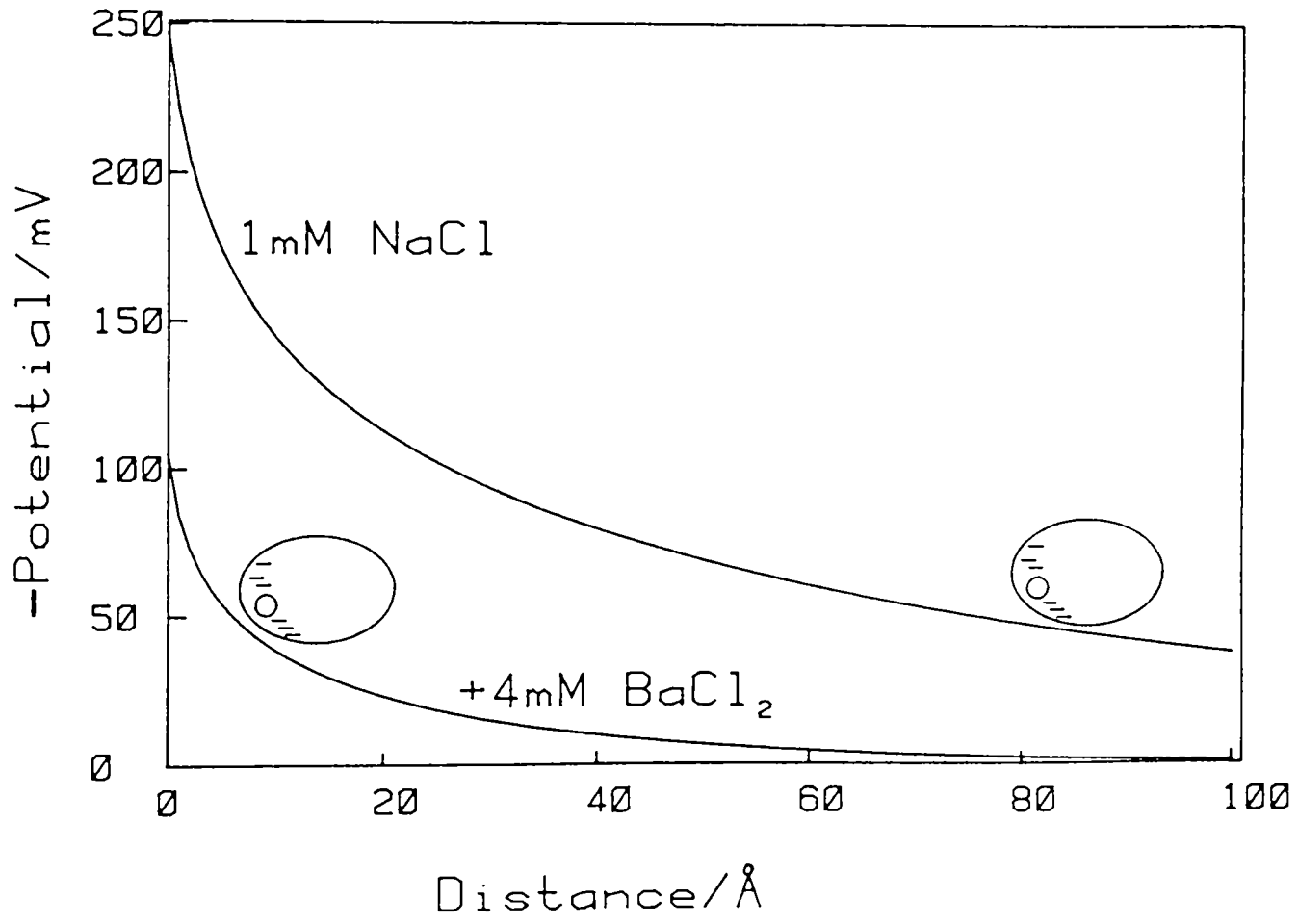

Figure 7.18: Potential profiles through the diffuse layer for a surface charge density of 0.22 Cm^{-2}. Calculated for a 1mM solution of a 1:1 electrolyte (eqn 7.6), and a solution containing, in addition, 4 mM 2:1 electrolyte ($BaCl_2$-type) (eqn. 7.8). Estimated diffuse layer characteristics taken from Table 7.1. T = 25°C.

this surface and a negatively-charged redox protein in that multivalent cations will alleviate electrostatic repulsion and facilitate close approach to the surface, as illustrated schematically in Figure 7.18.

It is apparent from Table 7.1 that a diffuse layer analysis of the experimental data presents no unique solution for the surface and diffuse layer characteristics of an edge graphite electrode. However, this analysis demonstrates that an approach using simple diffuse layer theory is capable of accounting for both the relative screening effects of monovalent vs. divalent and divalent vs. trivalent cations, if it is recognised that the electrode has a high negative surface charge density (one electronic charge per 0.6 to 2.2 nm^2). This negative surface charge density is considerably higher than the charge density on photosynthetic membrane surfaces, calculated to be in the region of one electronic charge per 15 - 20 nm^2 (24). The negative charge density at the electrode surface may arise in part from discrete structural charge at the functionalised edge surface. Assuming a regular, hexagonal edge layer structure (25) and monolayer oxide coverage (Chapter 4) then the estimated surface charge density predicts that < 5% of surface C atoms have an associated functional group carrying a discrete charge.

In considering the results of a simple diffuse layer analysis of cation promotion effects, it must be remembered that there are many assumptions inherent in the derivation of Gouy-Chapman theory and the Grahame equation (20). An investigation of the diffuse double layer in aqueous $KCl/MgCl_2$ mixtures gives experimental cation surface concentrations in adequate agreement with simple Gouy-Chapman theory (26). Nevertheless, this remains

the only experiment to specifically test the general applicability of diffuse layer theory. It seems likely that the most serious error in the present analysis is that the electrode is far from homogeneous and smooth and is unlikely to satisfy the requirements of transversely smeared surface charge density. The true significance of the derived surface charge density is also open to question. Although diffuse layer calculations were restricted to the results of cation titrations at low protein concentration, to minimise protein-protein interactions, any calculations must also recognise that the interface is composed of both a charged electrode surface and large charged macromolecules, in an ionic bathing medium. A charged macromolecule whose surface has multiple ionisable groups must also be recognised as the source of an external field and a corresponding Poisson-Boltzmann relation formulated for a system of small ions in this field. Bearing in mind the assumptions of diffuse layer theory and the complexity of the electrostatic interactions between two intrinsically charged surfaces, it is premature to derive any serious conclusions from the results in Table 7.1.

7.8.4 The Nature of Surface Charge.

Spectroscopic and electrochemical studies of edge surfaces, described in Chapters 5 and 6, suggest that detailed knowledge of the microstructure of this surface may reveal a disordered surface with a low surface concentration of individual functional groups. If this is the case, then the discrete nature of chemical charges and the lateral intercharge spacing may need to be considered in quantitative attempts to analyse surface charge phenomena. Indeed, as suggested by 'impersistence'

studies, the electrode may have a range of active surface sites with a non-uniform distribution of distinct hydrophilic and hydrophobic regions. Within the hydrophilic surface zones there may also be heterogeneity with random arrays and clusters of neutral, polar and dipolar functional groups.

At distances closer to the electrode surface than the Debye screening length, the field strength ($d\psi/dx$), at any point in solution, arising from an array of point charges will differ significantly from that predicted by the smeared charge model and the electrostatic surface potential will depend critically on the local surface structure (20). Similarly, the concentration of counterions in the ionic atmosphere of the surface will be greatest directly over charged zones and smallest between the charged zones or over hydrophobic regions. This prediction is confirmed by calculations based on a two-dimensional periodic lattice array of surface charges (27). Thus, a non-uniform distribution of ions will build up throughout a protein faradaic response titration and can be expected to influence the flux of protein molecules **towards** and **across** the electrode surface. Different surface regions with varying charge characteristics and cation populations may then be populated by protein molecules at different stages of a cation promotion profile, so influencing the extent of ageing and stabilisation throughout a profile, as discussed previously.

In the absence of multivalent cations, at low ionic strength, the smeared charge and point charge models may be approximately equivalent, with a uniform field strength across the interfacial region, at large distances from the surface. In this instance, all of the surface may be electrostatically

'unavailable' for approach by negatively-charged protein molecules, consistent with the absence of a faradaic response under such conditions.

For a surface with discrete structural charge, an assumption of a fixed surface charge density which is independent of ionic conditions, as invoked in the application of the Grahame and Gouy equations, is now a poor assumption. Instead, the density of ionisable groups (S_i) and their **intrinsic** dissociation characteristics (a_i) should be specified, from which will follow local values of σ (and ψ_o) as given by:

$$\sigma_i = -ea_i/S_i \qquad (7.1)$$

The effect of the local surface charge density will be to produce a local surface potential, the magnitude of which will depend upon the ionic constitution of the bathing medium. The local surface potential is implicated in the local surface pH as given by equation (7.2). The local surface pH directly influences the fraction of ionised groups.

$$[H^+]_o = [H^+]_{bulk} \exp(-A\psi_o) \qquad (7.2)$$

where $[H^+]_{bulk}$ = reservoir pH

A = constant

7.8.5 The Relation Between Promotion Characteristics And Ionic Strength - The Involvement Of Ion-Binding.

Saturation limits measured for $Cr(NH_3)_6^{3+}$ promotion profiles of the 8Fe ferredoxin, with 100 mM NaCl as the supporting

electrolyte, are ca. seven-fold higher than those in 1 mM NaCl (300 μM vs. 2 mM $Cr(NH_3)_6^{3+}$). The increase in cation requirement with increasing ionic strength is inconsistent with simple diffuse layer theory. In addition, at the higher ionic strength, the Debye screening length ($1/\kappa$ < 10 Å) indicates that the surface potential will decay almost entirely across the Stern layer and so a protein molecule approaching the electrode surface will no longer have to migrate through a diffuse layer. This emphasizes the importance of cations in a compact layer at the electrode surface, under conditions of high ionic strength. The observed ionic strength dependence implicates binding, which is electrostatic in nature, in the activity of $Cr(NH_3)_6^{3+}$ as a promoter of the direct electrochemistry of the 8Fe ferredoxin. Similarly, the faradaic response of spinach ferredoxin (1.5 mM $Cr(NH_3)_6^{3+}$, 1 mM NaCl) is profoundly inhibited by an increase in ionic strength (1 - 100 mM monovalent salt). This result demonstrates that the interaction between the 2Fe ferredoxin and the electrode, in the presence of $Cr(NH_3)_6^{3+}$, is also dominated by an electrostatic binding interaction.

7.8.6 Specific Ionic Adsorption.

The pure 'screening' approach deduced from the Grahame equation takes no account of binding or ion-pairing between cations and negative sites on the electrode surface. However, adsorption of cations at electrodes is well documented for a range of surfaces including Hg (28,29), carbon (30) and oxide surfaces (31). In the current study, the divalent cation $Fe(phen)_3^{2+}$ provides clear evidence for the importance of irreversible cation adsorption in the promotion of electrochemical

responses. Similarly, an edge electrode covalently-modified with cationic Cr(III) complexes permits rapid, reversible and persistent direct electrochemistry of negatively-charged redox proteins (Chapter 11). This conclusively demonstrates the importance of cations bound in the Stern layer at the electrode surface.

At a functionalised edge graphite surface, surface C-O groups may effectively 'solvate' cations in the compact layer at the electrode surface. This may take the form of inner sphere binding (Mg^{2+} , Ba^{2+}) or outer sphere electrostatic binding to substitution-inert Cr(III) complexes. The latter may arise from ion-pair formation or charge-dipole complexes. In contrast to diffuse-layer 'screening' effects, cation-binding effectively neutralizes negative surface charge density and, at high surface coverages, bound cations may invert the surface potential. Comparative studies of various divalent cations indicate varying degrees of effectiveness which may be consistent with cation-binding at the surface. Of the divalent cations studied, Mg^{2+} is by far the least effective promoter. It is conceivable that this is due to hydrolysis of the solvated cation (pK_1 [I=0]: Mg^{2+} 11.4; Ba^{2+} 13.3 (32)) at pH8.0 leading to a decrease in effective charge ($MgOH^{+}$) or perhaps precipitation of $Mg(OH)_2$ at the electrode surface ($Mg(OH)_2$ is three orders of magnitude less soluble than $Ba(OH)_2$ (33)). However, control experiments carried out at pH 7.0 (34), revealed a similar discrepancy in Mg^{2+} - Ba^{2+} promotion characteristics to that observed at pH 8.0.

In order for an ion to adsorb, a 'hole' must be created in the Stern layer (at highly-charged or polar surfaces, oriented water molecules must be displaced) and the solvent sheath of the

ion must be distorted or displaced. Thus, cations with extensive primary hydration undergo little specific adsorption (28). Similarly, electrochemical rate parameters for $Cr(NH_3)_6^{3+}$ and $Cr(H_2O)_6^{3+}$ suggest (35) that the latter undergoes reduction some 0.1 to 0.2 nm. further from a Hg electrode surface, in accord with the extensive primary and secondary hydration of the hexa-aquo complex. Hence, the inefficiency of Mg^{2+} relative to Ba^{2+} may then simply reflect the more extensive primary and secondary hydration of Mg^{2+} (32) leading to a less favourable change in solvation energies accompanying adsorption, than with Ba^{2+}.

The pronounced efficiency of $Fe(phen)_3^{2+}$ as a promoter may imply involvement of the aromatic ligands in hydrophobic interactions leading to a protein-cation-electrode bridge, Figure 7.19. It is well-known that molecules bearing aromatic centres are strongly adsorbed on graphite surfaces. For example, the 1,10 phenanthroline ligands of the cation, $Cu(phen)_2^{2+/1+}$, are responsible for the adsorption of this complex at basal plane pyrolytic graphite (36). Adsorption of $Fe(phen)_3^{2+}$ at graphite electrodes is observed at edge, but not cleaved basal (or glassy carbon), surfaces. This suggests insertion of one of the octahedrally-disposed aromatic ligands into the edge lattice structure. A second phenanthroline ligand of the adsorbed $Fe(phen)_3^{2+}$ may be suitably disposed to bind the 8Fe ferredoxin in the interfacial region by penetrating the hydrophobic interior of the protein. This is in accord with homogeneous kinetic studies on the interaction between redox proteins and $Fe(phen)_3^{2+}$. The crystal structure of C. vinosum HIPIP (High Potential Iron Protein) reveals an Fe-S cluster buried 6 Å below the surface of the protein. The efficiency of electron-transfer

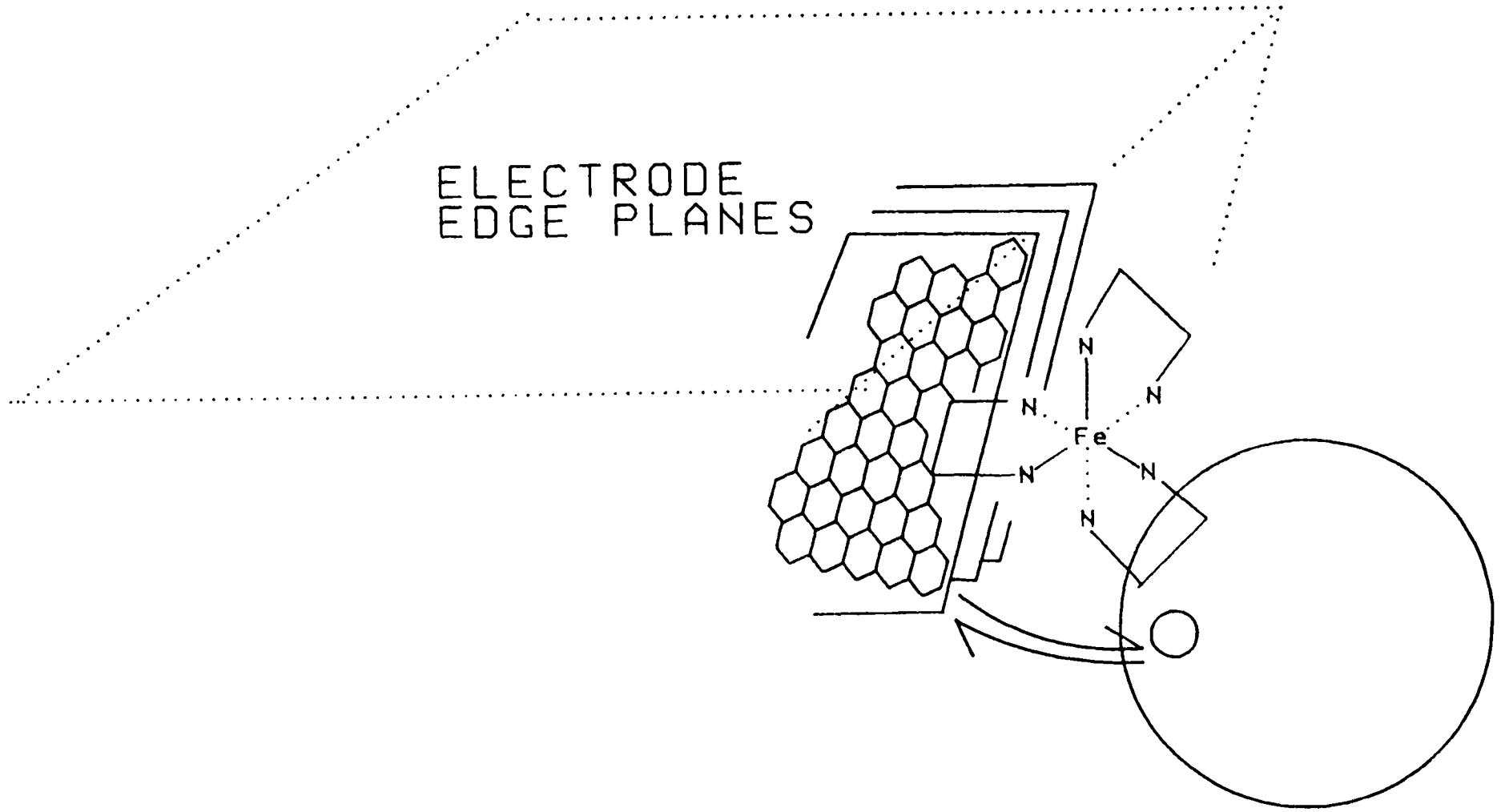

Figure 7.19: Schematic representation of the adsorption of $Fe(phen)_3^{2+}$ at an edge-oriented graphite electrode surface, and a resulting protein-electrode interaction 'bridged' by the adsorbed cation.

between HIPIP and various inorganic oxidants and reductants appears (37) to reflect accessibility to the cluster through penetration of the polypeptide structure. Thus, reagents with hydrophobic ligands yield electrostatically-corrected self-exchange rate constants several orders of magnitude larger than for hydrophilic reagents (k_{11} [$M^{-1}s^{-1}$]: $Co(phen)_3^{3+}$ 1.4 x 10^4 ; $Ru(NH_3)_6^{3+}$ 2.3). Strong adduct formation between $Fe(phen)_3^{2+}$ and ferredoxin, in direct electrochemical studies, is indicated by a marked deterioration in faradaic response upon prolonged cycling at optimal cation levels (34).

Small cations may also be included within the edge graphite lattice structure. However, the observation of cation promotion effects at both edge graphite and glassy carbon surfaces shows that inclusion of cations is unlikely to provide a major contribution to the observed electrochemical responses. Intercalation of cations (with charge transfer from the host lattice) can also be ruled out on the basis that intercalation compounds spontaneously decompose in aqueous solution.

The organic di-cations, hexa- and decamethonium, which are bifunctional with two spatially-separated monovalent charges, give promotional characteristics comparable to those of Ba^{2+}. The relative activity of these cations appear to follow the order $DM^{2+} > Ba^{2+} > HM^{2+}$. The properties of the organic di-cations which may account for their activity as promoters are:

(i) bifunctionality: a bifunctional cation could aid close apposition of redox protein and electrode surfaces by providing a link between the protein and electrode. Thus, each headgroup may bind to a charged group on the two opposing surfaces.

(ii) distance: a bifunctional cation which serves to reduce the

surface potential on two opposing surfaces, through binding or 'screening' effects, may also control the protein-electrode electron transfer distance through the length of the aliphatic chain separating the charged head groups.

(iii) flexibility: the conformational flexibility of the di-cations would permit both headgroups to adsorb at the electrode surface, so providing both a reduction in surface potential and a hydrophobic surface domain.

(iv) hydrophobicity: the hydrophobic domain between the charged headgroups may be advantageous in disrupting structured water at the hydrophobic edge surface.

Although differences are evident between the two organic di-cations, it is not possible to identify the relevant properties of these molecules from the limited data available. In a survey (38) of 54 surface-modifiers for the promotion of the direct electrochemistry of cytochrome c at Au electrodes, Allen et. al. suggested that neither the length of the molecule nor the presence of a hydrophobic zone were necessary for the successful promotion of electrochemistry at this surface.

To explore further the role of size and hydrophobicity in cation-promoted direct electrochemistry at edge graphite, various Cr(III) ammine complexes were tested as possible cationic promoters (7). Cyclohexanediamine (chxn) and ammonia ligands were chosen to provide more 'hydrophobic' and 'hydrophilic' solvation environments respectively. In addition the larger size of the ethylenediamine and cyclohexanediamine ligands would be expected to influence the distance of closest approach of the various trivalent promoters to the electrode surface (Stokes' radius/Å): $Cr(NH_3)_6^{3+}$ 2.8; $Cr(en)_3^{3+}$ 3.75). Similarly, if specific

adsorption at the surface is a dominant factor in the mechanism of cation-promotion, then the size of a cation will influence its packing density within the inner layer.

The similarity of the resultant faradaic response titrations for all three Cr(III) complexes supports a general conclusion that cation charge is the single most important factor in cation activity. A similar conclusion is suggested by the closely equivalent promotion characteristics observed for the various monovalent cations. In the particular case of cations with extensive hydrogen-bonded secondary solvation (Mg^{2+}), binding in the inner layer is energetically destabilised at the hydrophilic edge surface. However, in the absence of such secondary solvation, as with Cr(III) ammines (35), hydrophobicity and the finite size of individual cations apparently exert only minor influences on cation activity. It is worth noting that faradaic response titrations using the cyclohexanediamine complex revealed assymetric voltammograms, with an enhancement of the anodic peak current, as the level of promoter was increased above that required to saturate the faradaic peak current. This is consistent with disruption of inner layer water structure at the electrode surface by the adsorbed hydrophobic cation, accompanied by weak protein adsorption.

7.8.7 Protein-Cation Binding.

The efficiency of $Fe(phen)_3^{2+}$ and organic di-cations as promoters of direct electrochemistry suggests the possibility that cations may alleviate unfavourable charge interactions by binding at the surface of the protein in addition to binding at the electrode surface.

^{1}H-NMR studies of the Clostridial ferredoxin show a specific differential broadening of some of the β-CH cysteine protons in the presence of $Cr(NH_3)_6^{3+}$. This clearly indicates that there is binding of this cation to the surface of the protein, close to one or both of the Fe-S clusters. This may involve direct interaction with the one cysteine residue of each cluster which is exposed at or near the surface of the protein (39). Tentative assigment of the resonances broadened in the aliphatic region (40) suggests that there is also binding at or close to an acidic aspartate or glutamate residue. This proposal is supported by the observation that the addition of NaCl can sharpen peaks previously broadened by $Cr(NH_3)_6^{3+}$, indicative of the dissociation of $Cr(NH_3)_6^{3+}$ from an electrostatic binding interaction. Examination of the primary structure of C. pasteurianum ferredoxin reveals five negatively-charged residues at positions 6, 17, 33, 35, 39 lying in the vicinity of cysteines 8, 18, 37, and 40 which are incorporated in the co-ordination spheres of both Fe-S clusters. Clearly, cation binding sites may be close to the 'exposed' Fe-S clusters in this protein. A more complete description of the binding interaction is not possible in the absence of specific assignments for the observed resonances. In contrast to the result for $Cr(NH_3)_6^{3+}$, there is no evidence from ^{1}H-NMR for the specific binding of Mn^{2+} to the oxidised ferredoxin.

A study by ^{1}H-NMR (41) has also confirmed site-specific binding of $Cr(NH_3)_6^{3+}$ to the 2Fe ferredoxin and identified that three of the invariant or semi-variant aspartate residues close to the Fe-S centre may interact directly with $Cr(NH_3)_6^{3+}$. In this protein the 2Fe-2S cluster is located in a hydrophobic crevice

close to (<5 Å) the surface of the protein. Further investigations (41) by ^{1}H-NMR involving the interaction of spinach ferredoxin with its physiological partner spinach ferredoxin-NADP-reductase (FNR) suggested that $Cr(NH_3)_6^{3+}$ and FNR bind to the same general region of the molecule. Therefore, it appears that both the cation-binding site and the physiological electron-transfer site are close to the exposed 2Fe-2S cluster.

It is interesting to note that for P. aeruginosa azurin, no specific binding sites were observed by ^{1}H-NMR for any of the complexes $Cr(C_2O_4)_3^{3-}$, $Cr(EDTA)^-$ or $Cr(phen)_3^{3+}$ (40). This is in accord with the lack of charged patches on the surface of the protein, and the insensitivity of direct electrochemistry at edge graphite to cation addition, at pH 8.0 and pH 5.0.

Observations of protein-cation binding are also well documented through extensive kinetic studies. Homogeneous kinetic studies (42) of the oxidation of reduced Clostridial 8Fe ferredoxin by positively-charged Co and Pt complexes, have been interpreted in terms of protein-cation adduct formation prior to electron transfer. Similarly, competition studies (43) between these oxidants and redox-inert Cr(III) analogues have demonstrated that complexes such as $Cr(NH_3)_6^{3+}$ inhibit oxidation presumably by binding at a common surface site. Calculations of K_{ass} (association constant), ΔH^o and ΔS^o for protein (8Fe ferredoxin)-cation association gave similar values for $Co(NH_3)_6^{3+}$ and $Co(en)_3^{3+}$ (42). Clearly, specific H-bonding ($Co(NH_3)_6^{3+}$) and hydrophobic ($Co(en)_3^{3+}$) interactions are not utilised and association is dominated by electrostatic interactions. Similarly, the variations in K_{ass} in going from $Cr(NH_3)_6^{3+}$ (212 M^{-1}) to $Cr(en)_3^{3+}$ (318 M^{-1}) 'blocking' reagents (43) are

mild, in accord with a predominantly electrostatic interaction.

Similar conclusions have been reached as a result of homogeneous kinetic studies of the interaction between chloroplast ferredoxins (spinach and parsley) and Co(III) and Cr(III) cationic complexes (44). In the former case an association step prior to electron-transfer is proposed which may be blocked by binding a single $Cr(NH_3)_6^{3+}$ at the same site (K_{cr} 464 M^{-1}). Values of ΔH^o and ΔS^o suggest a predominantly electrostatic interaction, with little evidence for differences between individual trivalent cations. Complexes of lower charge gave no direct evidence for an association step prior to electron transfer.

The close similarity between the calculated binding constants for the various Co(III) and Cr(III) ammine-ferredoxin adducts makes a striking analogy with the similarity of Cr(III) ammine complexes as promoters of the electrochemistry of the same protein. These observations strongly suggest that the dominant role of various Cr(III) ammines complexes, as promoters of the direct electrochemistry of the 8Fe and 2Fe ferredoxins, is to quench negative surface charge density on ferredoxin by electrostatically binding to acidic residues close to the Fe-S clusters of these proteins. ´Ion-pair´ formation, in this way, will ease adverse electrostatic interactions at electrode surface sites of negative charge density. In the case of rubredoxin there are few reports of kinetic or spectroscopic studies to support a similar claim. In addition, increased ionic strength does not markedly perturb the optimal faradaic responses of this protein, in accord with only weak electrostatic association.

The association constant for $Cr(NH_3)_6^{3+}$-reduced ferredoxin adduct formation can be used to estimate the percentage of

ferredoxin bound with $Cr(NH_3)_6^{3+}$ in electrochemical studies. On the basis of the association constant for fully-reduced 8Fe ferredoxin (212 M^{-1}, 0.1 M NaCl), there is ca 40% protein-cation complexation as the optimal faradaic peak current is reached in $Cr(NH_3)_6^{3+}$ titrations of 67 μM ferredoxin (0.1 M NaCl). In view of the fact that cyclic voltammetry is a bulk diffusional process, then <100% Fd-$Cr(NH_3)_6^{3+}$ complexation suggests that there may be prior electrostatic association of $Cr(NH_3)_6^{3+}$ with the electrode surface. This would then provide a site(s) with an affinity for transiently binding to the surface those protein molecules within the diffusion layer at the electrode surface. An electrode-cation-protein ternary 'bridge' interaction of this type has also been suggested as a mechanism by which bifunctional cations (e.g. HM^{2+} and DM^{2+}) and $Fe(phen)_3^{2+}$ facilitate direct electron-transfer. The role of cations as promoters of the electroreduction rate of anions of the type $S_2O_8^{2-}$ and $Fe(CN)_6^{3-}$ at a mercury electrode, has been proposed to involve similar cationic bridges between the anion and the negatively-charged surface (45).

Interestingly, pH titrations (12) of the negatively-charged protein, human plasma albumin, adsorbed at a negatively-charged polystyrene latex, suggest that, in the presence of cations, the carboxyl groups of the adsorbed protein are directed towards the sulphonate groups of the latex, an arrangement suitable for the formation of 'bridged' interactions. It is also relevant to note that direct electrochemistry of the 8Fe ferredoxin may be observed (see Chapter 11), in the absence of mobile multivalent cations, at an edge electrode bearing surface-bound cationic Cr(III) complexes.

APPENDIX

Relevant Equations from Diffuse Layer Theory

The Grahame equation (eqn. 7.3) is a general relation for the electrostatic potential $\psi(x)$ at a distance x from a plane of surface charge density, σ. This equation applies to mixed unsymmetrical electrolytes of any valence type (21).

$$\sigma_E = \pm [(2RT\epsilon\epsilon_o) \Sigma C_i^b.(e^{-z_i F\psi(x)/RT} - 1)]^{1/2} \qquad (7.3)$$

$$= \pm A.[\Sigma_i C_i^b.(e^{-z_i F\psi(x)/RT} - 1)]^{1/2}$$

$$\text{where } A = (2RT\epsilon\epsilon_o)^{1/2}$$

For a mixture of a 1:1 (NaCl-type) electrolyte (concentration C_b') and 2:1 ($BaCl_2$-type) electrolyte (concentration C_b''), equation (7.3) becomes:

$$\frac{\sigma^2}{A^2} = C_b''.(e^{-2X} + 2.e^{X} - 3) + C_b'.(2.\cosh(X) - 2) \qquad (7.4)$$

$$\text{where } X = F\psi_o/RT$$

For a single symmetrical (z:z) electrolyte, (7.4) becomes the Gouy expression:

$$\sigma_E = 2AC_b^{1/2}.\sinh(zF\psi_o/2RT) \qquad (7.5)$$

The manner in which ψ varies with x can be obtained by combining the Poisson equation and the Gouy expression, followed by integration (19) to give the expression below.

$$x = -\left[\frac{RT\epsilon_r\epsilon_o}{2z^2F^2C_b}\right]^{1/2} \ln \frac{\tanh(zF\psi(x)/4RT)}{\tanh(zF\psi_o/4RT)}$$

$$\underline{\text{or}} \quad e^{-\kappa x} = \frac{\tanh(zF\psi(x)/4RT)}{\tanh(zF\psi_o/4RT)} \quad \text{where } \kappa = \left[\frac{z^2F^2C_b}{RT\epsilon_r\epsilon_o}\right]^{1/2}$$

This finally yields:

$$\psi = \psi_o.(\tanh^{-1}.e^{-\kappa x}) \qquad (7.6)$$

Equation (7.6) is valid for <u>any</u> surface potential. However, if ψ_o is sufficiently low that $\psi_o < 50/z$ mV at 25°C then tanh(X) ~ X everywhere and $\psi = \psi_o.e^{-\kappa x}$ (7.7).

Equations (7.6) and (7.7) apply only to single symmetrical electrolytes. The corresponding equation for the ψ - x dependence in an electrolyte mixture of valence type: (z^+/z^-, z^{2+}/z^{2-}), has been derived by Barber <u>et. al.</u> (22) from the full non-linear Poisson-Boltzmann equation. The resulting expression is conveniently written as:

$$-\psi(x) = \frac{RT}{F} \ln\{[\gamma\tanh^2(\varphi_o + \kappa x) - C_2^o]/(C_1^o + C_2^o)\} \qquad (7.8)$$

where $\varphi_o = \tanh^{-1}(v_o/\sqrt{\gamma})$

$v_o = [C_2^o + (C_1^o + 2C_2^o).e^{-F\psi_o/RT}]^{1/2}$

$\gamma = C_1^o + 3C_2^o$

C_i^o = bulk concentration of the ith ion.

References - Chapter 7

1) Rice, M. E., Galus, Z. and Adams, R. N., J. Electroanal. Chem. 143, 89, (1983).

2) Dong, S. and Kuwana, T., J. Electrochem. Soc., 131, 813, (1984).

3) Rusling, J. F., Anal. Chem. 56, 575, (1984).

4) Wightman, R. M., Deakin, M. R., Kovach, P. M., Kuhr, W. G. and Stutts, K. J., J. Electrochem. Soc. 131, 1578, (1984).

5) Bard, A. J. and Faulkner, L. R. Electrochemical Methods. New York: Wiley. 541, (1980).

6) Trasatti, S., Adv. Electrochem. Electrochem. Eng. 10, 213, (1977).

7) Lowe, V. J., Part II Thesis. Oxford (1984).

8) Oppegard, A. L. and Bailar, J. C. in: Inorg. Syntheses, Audrieth, L. F. ed. New York: McGraw-Hill 3, 153, (1950).

9) Armstrong, F. A., Hill, H. A. O. and Walton, N. J., FEBS Lett. 145, 241, (1982).

10) Lyklema, J., Colloids and Surfaces 10, 33, (1984).

11) Norde, W. and Lyklema J., J. Coll. Interf. Sci. 66, 257, (1978).

12) Norde, W. and Lyklema, J., J. Coll. Interf. Sci. 66, 206, (1978).

13) Amatore, C., Saveant, J. M. and Tessier, D., J. Electroanal. Chem. 147, 39, (1983).

14) Sleszynski, N., Oysteryoung, J. and Carter, M., Anal. Chem. 56, 130, (1984).

15) Engstrom, R. C., Weber, M. and Werth, J., Anal. Chem. 57, 933, (1985).

16) Phillips, W. D. and Poe, M., in: Iron-Sulphur Proteins. Lovenberg, W., ed. New York: Academic Press. 2, 255, (1973).

17) Sweeney, W. V. and Rabinowitz, J. C., Ann. Rev. Biochem. 49, 139, (1980).

18) Armstrong, F. A. unpublished result.

19) Grahame, D. C., Chem. Rev. 41, 441, (1947).

20) McLaughlin, S. G. A., in: Current Topics in Membranes and Transport. Bronner, F. and Kleinzeller, A. eds. New York: Academic Press. 9, (1977).

21) Grahame, D. C., J. Chem. Phys. 21, 1054, (1953).

22) Barber, J. and Rubin, B. T., Biochim. Biophys. Acta 592, 87, (1980).

23) McLaughlin, S. G. A., Szabo, G., Eisenman, G. and Ciani, S. M., Proc. Natl. Acad. Sci. U. S. A. 67, 1268, (1970).

24) Nakatani, H. Y., Barber, J. and Forrester, J. A., Biochim. Biophys. Acta. 504, 215, (1978).

25) Cotton, F. A. and Wilkinson, G. Advanced Inorganic Chemistry. New York: Wiley (1980).

26) Parsons, R. and Trasatti, S., Trans. Faraday Soc. 65, 3314, (1969).

27) Nelson, A. P. and McQuarrie, D. A., J. Theor. Biol. 55, 13, (1975).

28) Andersen, J. M. and Bockris, J. O. M., Electrochim. Acta 9, 347, (1964).

29) Damaskin, B. B., J. Electroanal. Chem. 65, 79, (1975).

30) Koresh, J. and Soffer, A., J. Electroanal. Chem., 147, 223, (1983).

31) Wiese, G. R., James, R. O. and Healy, T. W., Disc. Faraday Soc. 52, 302, (1971).

32) Burgess, J. Metal Ions in Solution. Chichester: Horwood (1978).

33) Handbook of Chemistry and Physics. Cleveland: Chemical Rubber Publishing Co. (1984).

34) Lowe, V. J. unpublished result.

35) Weaver, M. J. and Satterberg, T. L., J. Phys. Chem. 81, 1772, (1977).

36) Lee, C.-W. and Anson, F. C., Inorg. Chem. 23, 837, (1984).

37) Cummins, D. and Gray, H. B., J. Am. Chem. Soc. 99, 5158, (1977), and Rawlings, J., Wherland, S., and Gray, H. B., J. Am. Chem. Soc. 98, 2177, (1976).

38) Allen, P. M., Hill, H. A. O. and Walton, N. J., J. Electroanal. Chem. 178, 69, (1984).

39) Adman, E. T., Sieker, L. C. and Jensen, L. H., J. Biol. Chem. 248, 3987, (1973).

40) Kitchen, N. A., D. Phil. Thesis. Oxford (1984).

41) Chan, T.-M., Ulrich, E. L. and Markley, J. L., Biochemistry 22, 6002, (1983).

42) Armstrong, F. A., Henderson, R. A. and Sykes, A. G., J. Am. Chem. Soc. 102, 6545, (1980).

43) Armstrong, F. A., Henderson, R. A., Ong Wah Kim, H. and Sykes, A. G., Biochim. Biophys. Acta 681, 161, (1982).

44) Armstrong, F. A. and Sykes, A. G., J. Am. Chem. Soc. 100, 7710, (1978), and Armstrong, F. A., Henderson, R. A. and Sykes, A. G., J. Am. Chem. Soc. 101, 6912, (1979).

44) Frumkin, A. N., Trans. Faraday Soc. 55, 156, (1959).

CHAPTER 8

DIRECT ELECTROCHEMISTRY OF THE BLUE COPPER PROTEIN PLASTOCYANIN

8.1 Introduction.

Plastocyanin (Pc) is a small (RMM 10500) copper protein found in all higher plants, in many green algae and in some blue-green algae. It is now well established (1), partly from the use of Pc-specific antibodies, that, in higher plants, this protein is exclusively located in the intrathylakoid space of green photosynthetic tissues. Furthermore, a number of studies (2) have indicated a well-defined function for Pc, *in vivo*, as an electron-shuttle between cytochrome *f* (electron donor) of Photosystem II, and the Photosystem I (PSI) reaction centre (electron acceptor), a double chlorophyll pigment (P700-Chlorophyll a). Both of these redox partners are integral components of the highly-convoluted thylakoid membrane. Cytochrome *f* is part of a larger complex (3) including a Rieske high-potential iron-sulphur centre, two cytochromes b_6 and a cytochrome *f* molecule. Plastocyanin, itself, does not appear to be bound to the lamella membrane.

The crystal structure of Cu(II) poplar plastocyanin (Chapter 1) reveals a striking imbalance in the distribution of charged residues, and the existence of two surface regions which may have functional significance as recognition or binding sites. These are the highly-conserved hydrophobic patch at the 'northern end of the molecule and the elongated acidic patch (highly-conserved only in higher plants) on the 'eastern' face. In the former case, only the imidazole ring of the Cu ligand, His 87, lies between the Cu atom and the molecular surface. The Cu is closest (6 Å) to the surface at this point. In contrast, residues

42 - 45 of the acidic patch are 10 - 15 Å from the copper centre. However, the intervening region contains an array of highly-invariant aromatic residues which may facilitate electron-transport through the protein.

On the basis of these structural results, the question has arisen (4) whether or not plastocyanin utilizes two separate electron-transfer sites in its role as an electron shuttle, one of which functions in electron uptake and the other in electron delivery. Several methods have been used in an attempt to resolve the binding site or sites on plastocyanin for its physiological redox partners.

Both spinach plastocyanin (pI ca 4.0) and the thylakoid membrane are negatively-charged at neutral pH. In the latter case, the negative charge is thought (5) to arise from integral membrane protein complexes (cytochrome f, pI = 5.5 (6); PSI-enriched sub-chloroplast particles, pI = 5.0 (7)). At near neutral pH, there is an absolute requirement for cations to stimulate electron donation from plastocyanin to $P700^+$ located in broken chloroplasts (8) or isolated PSI particles (9). Chemically-modified plastocyanin (10,11) and PSI particles (7) have been prepared by the conversion of protein carboxyl residues into positively-charged amino groups, through reaction with a water-soluble carbodiimide and ethylenediamine. The use of either a cationic PSI preparation (pI 9.5) or plastocyanin carrying a net positive charge (+3) abolishes the requirement for cations in the reaction of plastocyanin and $P700^+$. Clearly, the Pc-P700 interaction is primarily electrostatic in nature. Following experiments using plastocyanin modified at the 'eastern' acidic patch, by attachment of Cr(III), Farver et. al. (12) suggested

that there is association of $P700^+$ at this site. However, the results of studies (10) using ethylenediamine-modified Pc are not in agreement with this proposal.

The amino acid sequence of cytochrome *f* suggests (13) a trans-membrane arrangement of this protein with a highly-charged (22% of total residues) haem-containing section (residues 1 - 250) extending into the intra-thylakoid space. The interaction between isolated cytochrome *f* and plastocyanin is poorly understood, mainly because of the difficulty in obtaining highly-purified, intact cytochrome *f*. However, recent reports have described the successful isolation of cytochrome b_6-*f* complexes from spinach (14) and *A. variabilis* (15). The complex from spinach gives the highest activity with chloroplast plastocyanin, but also reduces algal cytochromes *c*, which are all acidic proteins, at a reasonable rate (14). It is almost inert towards mammalian cytochrome *c*, which is a basic protein. In cyanobacteria, both a cytochrome c_{553} and plastocyanin occur, and can replace each other functionally, depending on growth conditions (16). Both are basic proteins and, together with mammalian cytochrome *c*, they show the highest affinity for the b_6-*f* complex from *A. variabilis*. Acidic cytochromes *c* or acidic plastocyanin from spinach are rather inefficient electron acceptors (15). Thus, the charge of the electron-accepting protein contributes to the specificity of the cytochrome b_6-*f* complex.

The reactivity (11,17) of a cytochrome *f* fragment (1 - 250 section) with native and chemically-modified plastocyanin, also suggests that the reaction of plastocyanin with cytochrome *f* is predominantly electrostatic in nature. In addition, a specific interaction between a positive patch on cytochrome *f* and the

'eastern' acidic patch of plastocyanin has been proposed (17). The importance of local positive charges on isolated cytochrome f has also been established through studies (18) of chemically-modified cytochrome f.

The light-driven electron-transport chain of photosynthesis is linked to the generation of a proton gradient across the thylakoid membrane. A direct consequence of proton transport in illuminated chloroplasts is that the pH inside the thylakoid decreases to about pH 5.0 (19) upon illumination, and that the proton influx is balanced by an efflux of Mg^{2+} and K^{+} into the stromal space (20). In view of the importance of electrostatic effects in the association of plastocyanin with its natural partners, it appears that ion fluxes in the illuminated chloroplast may be of significance in regard to the regulation of electron flow between photosystems I and II, via plastocyanin. In addition there is evidence for a structural perturbation of the active site of plastocyanin at these low pHs. This follows from the observation of a pH-dependent increase in the redox potential of plastocyanin below pH 5.5 (21,22). A suggestion that the E_o-pH behaviour is consistent with the protonation and subsequent disssociation of an imidazole group bound to the Cu centre was made in 1964 (23).

In a crystallographic study of PcCu(I) and PcCu(II) (24), diffraction data were collected at a series of pH values ranging from pH 7.0 to pH 3.8. The overall structure of the Cu(II) protein and the geometry of the Cu(II) site were found to be essentially identical at low (pH 4.0) and high (pH 6.0) pH. Similarly, there were no significant differences between the structures of the reduced protein at pHs in the range 3.8 - 7.0,

or between them and the structure of the oxidised protein, except at the Cu site. In Cu(I) plastocyanin, the average Cu(I)-N(His 87) bond length increases (2.3 - 3.4 Å) on decreasing the pH from 7.0 - 3.8. This distance is sufficient to accomodate a proton. Accordingly, Freeman proposed a proton-induced dissociation of the solvent-exposed His-imidazole ring from the Cu atom. In parallel with this dissociation the Cu centre becomes three-coordinate and planar. The stabilisation of PcCu(I) under these conditions is consistent with the observed E^{o}-pH behaviour. On the basis of these observations, Freeman suggested that the large change in the dimensions of the Cu site, upon reduction of plastocyanin at low pH, will lead to a large Franck-Condon reorganisation barrier for electron-transfer, sufficient to make PcCu(I) redox-inactive. At high pH, the Cu-ligand bond distances are suggested to be only 0 - 0.2 Å larger in PcCu(I) than in Pc Cu(II). These small differences are compatible with the rapid outer-sphere electron-transfer reactions of plastocyanin at pH8.0 (PcCu(I) is redox-active).

Kinetic manifestation of the resulting high reorganisation barrier at low pH has been established by Sykes and co-workers (22,25) in the study of pH effects on the bimolecular oxidation of parsley plastocyanin by small inorganic redox probes. Thus, the rate constants for the $Fe(CN)_6^{3-}$ oxidation of Pc Cu(I) decrease from 7.9×10^4 $M^{-1}s^{-1}$ at pH 7.9 to zero at pH <5. For Pc Cu(II) there is only a mild increase in rate between pH 7.0 and pH 5.0.

Observations of a redox active-inactive conversion in reduced plastocyanin may be of significance in the control of electron-transport linked proton-translocation in photosynthesis.

At the pH inside the illuminated thylakoid the redox-inactive form of plastocyanin will represent a significant proportion of the reduced plastocyanin molecules and so will act to control the flow of electrons from PSI to PSII.

This chapter describes direct electrochemical studies of plastocyanin and probes the heterogeneous electron-transfer activity of this protein at low pH.

8.2 Experimental Details.

Faradaic response titrations of plastocyanin were carried out by cyclic voltammetry according to the procedures described in Chapter 7. All reagents were of AnalaR or AristaR grade and doubly-deionised water was used throughout the studies. Solutions for electrochemistry were made up to include 5 mM buffer-1 mM KCl as the basis support medium. Buffers used were as follows: acetate, pH 4.0 - 5.5; MES (2-[N-morpholino]ethanesulphonate), pH 6.0 - 6.3; HEPES (N-2-[hydroxyethyl]piperazine-N'-2-ethanesulphonate), pH 7.0; Tricine (N-[tris(hydroxymethyl)methyl]glycine), pH 8.0. All pH standardisations were made at room temperature, and stock buffer adjustments were made with KOH or HCl. $Pt(NH_3)_6Cl_4$ was prepared according to a literature procedure (26) by V.J. Lowe.

Electrochemical experiments were carried out by thermostatting the cell at either 25°C or 3°C. From a graph of values for the saturated calomel electrode (SCE) potential at various temperatures (27), a value of E (SCE) = +258 mV vs. NHE was adopted in experiments at 3°C. In cyclic voltammetric experiments, current responses at high scan rates ($\upsilon > 500$ mVs^{-1}) were limited by the response of the y-t recorder. To overcome this problem, microprocessor-controlled cyclic staircase

voltammetry, with data acquisition and storage in a digital form, was carried out. This enabled scan rates up to at least 4 Vs^{-1} to be used in voltammetric measurements. The electrochemical rack system used in digital experiments has been described in more detail in Chapters 4 and 6.

Experimental Results.

8.3 Surface Selectivity in the Direct Electrochemistry of Plastocyanin.

In order to establish the basis for electrochemical studies of plastocyanin, a range of electrode surfaces were tested for electrochemical activity, using 0.1 mM plastocyanin in 20 mM Tricine, 100 mM KCl, pH 8 at 25°C. The results are summarised below:

SURFACE	MULTIVALENT CATIONS ADDED TO SOLUTION[a]	ELECTROCHEMISTRY OBSERVED[b]
Graphite - Edge	NO	NO
	YES	YES
- Basal	NO	NO
	YES	NO
Au- Alumina polish only	NO	NO
-bis(4-pyridine)bisulphide[c]	NO	NO
$-(SCH_2CO_2H)_2$[c]	NO	NO
	YES	YES

a. 5mM $Cr(NH_3)_6^{3+}$ or 50mM Mg^{2+}

b. Faradaic response at or close to +370 mV vs. NHE (21).

c. 1 minute dip into a 1 mM solution of the modifier, followed by extensive rinsing with de-ionised water.

The observation of a faradaic response only at those surfaces carrying acidic (carboxylate) residues (edge graphite, modified Au), together with the additional requirement for multivalent cationic promoters, is consistent (see, for example Chapter 7) with (a) the importance of electrostatic effects and (b) the significant overall (and conservatively-localised) negative charge of spinach plastocyanin (pI = 4.0). It is interesting to note that the direct electrochemistry of plastocyanin has been recently reported (28) at Au electrodes surface-modified with positively-charged organic compounds (e.g. $HS-CH_2-CH_2-NH_3^+$) or with surface-modifiers able to form hydrogen bonds to acidic residues on plastocyanin.

8.4 The Effect of Temperature: Divalent Cation Promoters.

At edge-oriented pyrolytic graphite surfaces, in the presence of Mg^{2+}, responses attributable to plastocyanin (100 μM) were impersistent with a large deterioration in the faradaic response over the first few cycles (20 mVs^{-1}). In an attempt to overcome this problem, dilute plastocyanin solutions (25 μM) were used, in accordance with studies on 'impersistence' in Chapter 7. However, initial Mg^{2+} titrations (5 mM Tricine, 1 mM KCl) showed that the faradaic response was still troubled by severe impersistence at room temperature, Figure 8.1, and was not stabilised by the addition of successive aliquots (additions to a final concentration of 5 mM) of $MgCl_2$. The problem of impersistence was largely overcome by using dilute plastocyanin (<50 μM) in an electrochemical cell thermostatted at **3°C.**

The stability of the electrochemistry of plastocyanin (50 μM) at 3°C is clearly evident in the series of steady-state

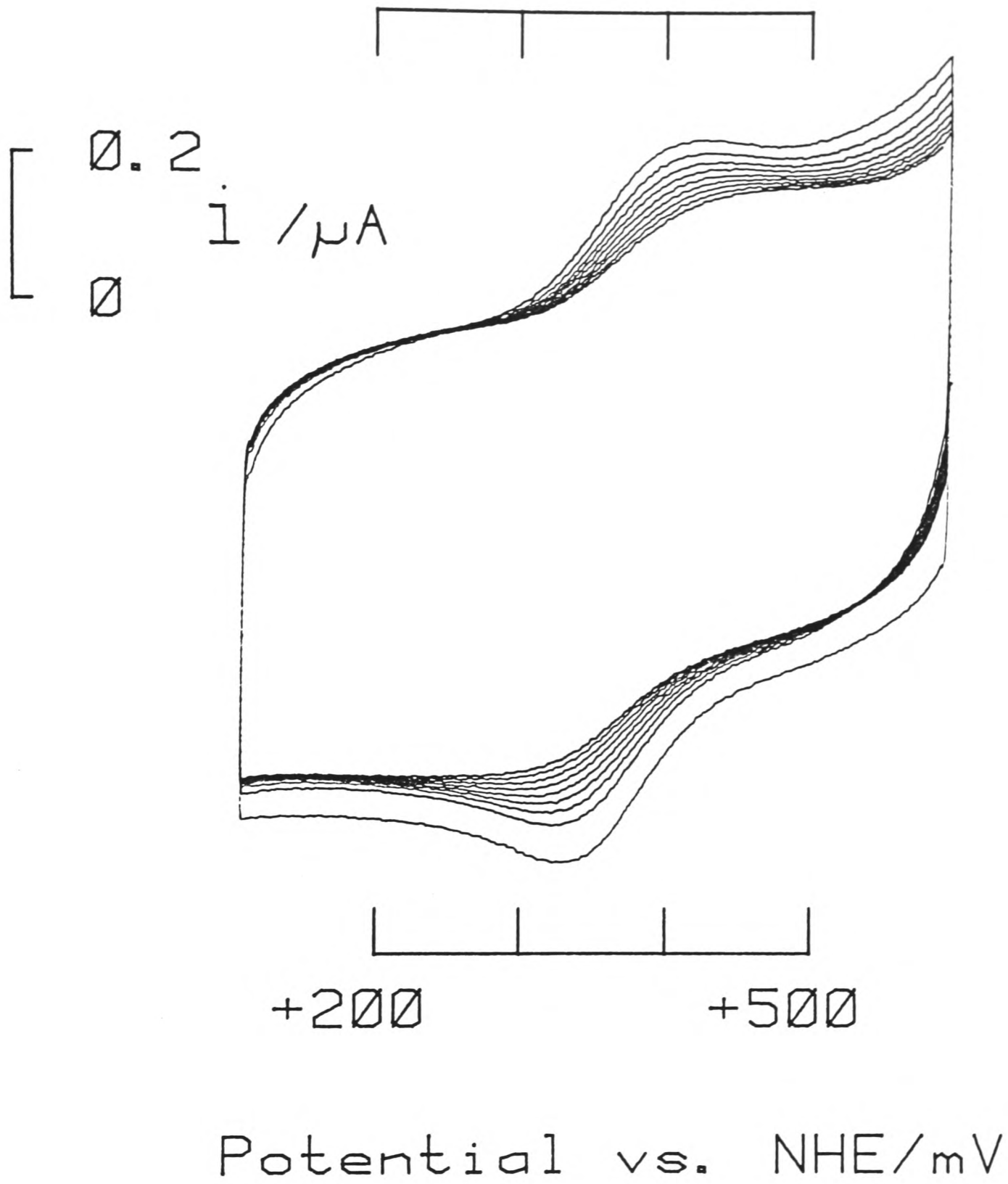

Figure 8.1: Cyclic voltammetric responses recorded for 25 μM plastocyanin at pH 8.0 (5 mM Tricine, 1 mM KCl), with the addition of 20 mM $MgCl_2$. The result shown is a series of consecutive cycles recorded at 20 mVs^{-1} after initiating the scan. Edge graphite electrode. T = 25°C.

cyclic voltammograms shown in Figure 8.2, obtained with the addition of 15 mM $MgCl_2$. For these measurements, voltammograms at different scan rates were recorded without intervening repolishing of the electrode, typically on the 10th cycle at each scan rate. As indicated in the inset, plots of cathodic peak current against (scan rate)$^{1/2}$ are linear up to at least 200 mVs^{-1}, consistent with charge-transfer dominated by diffusion of plastocyanin to the electrode surface. The diffusion coefficient (D_o) estimated from the slope of this plot (5.0 x 10^{-7} cm^2s^{-1}) is in good agreement with a value (8.7 x 10^{-7} cm^2s^{-1}) calculated from the Stokes-Einstein equation (29):

$$D = \frac{kT}{6\eta}\left[\frac{4\pi N}{3M\bar{v}}\right]^{1/3}$$

where M is the molecular weight

$\bar{v}$ the partial specific volume

$= 0.74\ cm^3g^{-1}$ for most proteins (30)

$\eta(H_2O) = 8.9 \times 10^{-3}\ g.cm^{-1}s^{-1}$ (25°C)

N is Avogadros number

With the use of increased protein concentrations, i.e. above 100 μM, higher levels of Mg^{2+} (>100 mM) were required to promote faradaic activity at 3°C. However, faradaic responses were poor with severe impersistence after the initial scan recorded at 20 mVs^{-1}.

8.5 Tri- and Tetra-valent Cationic Promoters. (a) $Cr(NH_3)_6^{3+}$

The trivalent cation $Cr(NH_3)_6^{3+}$ was found to be an effective promoter of plastocyanin (25 μM) electrochemistry at room temperature (Table 8.1), although faradaic responses were still troubled by slight impersistence at this temperature.

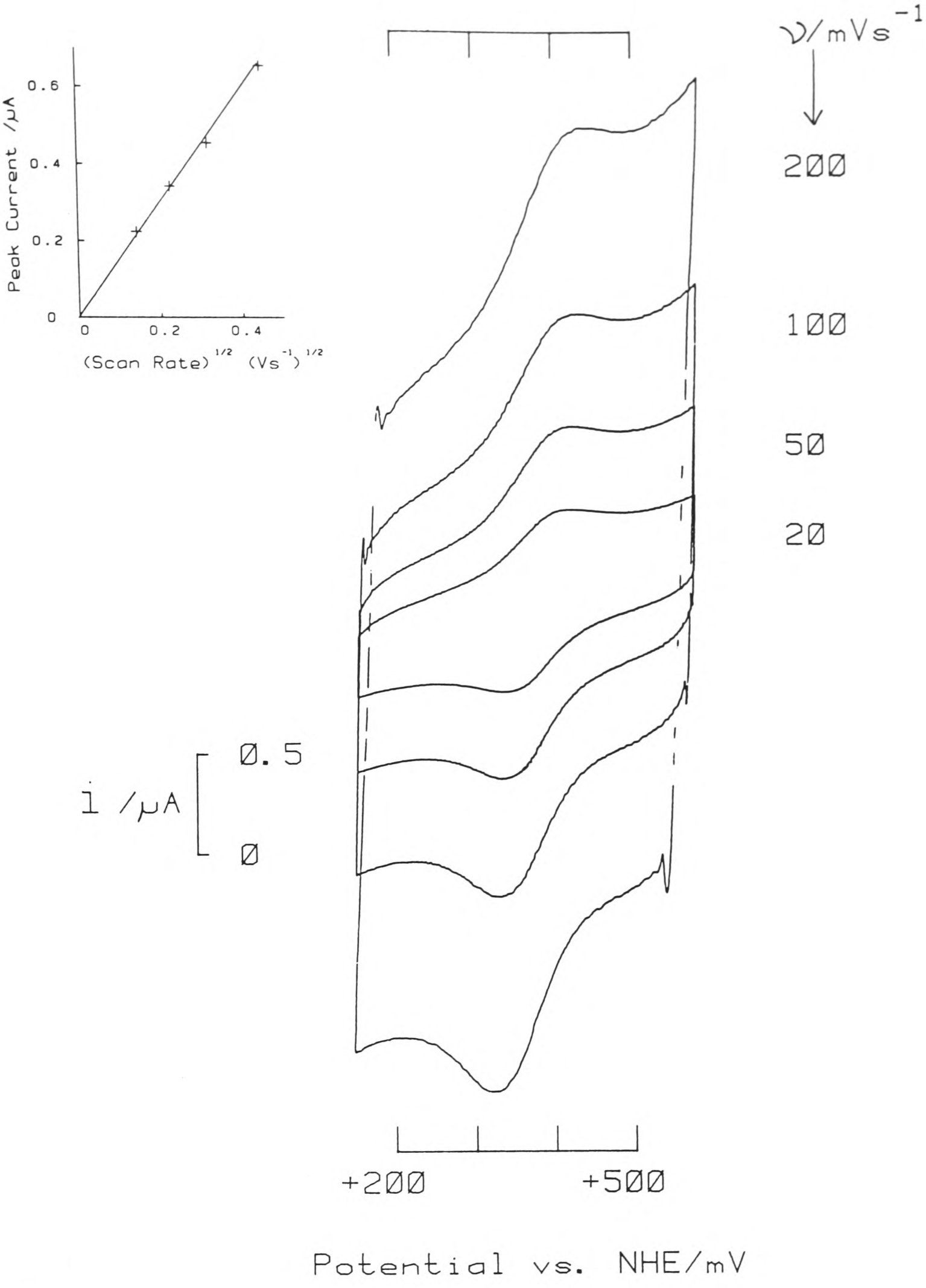

Figure 8.2: Steady-state cyclic voltammograms for plastocyanin (50 μM in 5 mM MES- 1 mM KCl, pH 6.3, with 15 mM $MgCl_2$) at various scan rates, 3°C. Inset shows plot of cathodic peak current vs. $(\text{scan rate})^{1/2}$. Scans were typically recorded on the 10th cycle. Edge graphite electrode.

TABLE 8.1

$Cr(NH_3)_6^{3+}$-Promoted Direct Electrochemistry[a] of Plastocyanin (25 μM), in 5 mM Tricine, 1 mM NaCl, pH 8.0

T = 25°C

$[Cr(NH_3)_6^{3+}]$/μM	$i_{pCATHODIC}$/μA		$i_{pANODIC}$/μA		ΔE_p/mV	
	SCAN 1	SCAN 4	SCAN 1	SCAN 4	SCAN 1	SCAN 4
20	n.d.		n.d.		n.d.	
55	0.12	n.d	0.12	n.d.	b	
70	0.15	<0.12	0.13	<0.1	130	b
90	0.18	<0.14	0.16	<0.14	110	b
110	0.2	<0.18	0.18	<0.15	98	b
145	0.22	0.20	0.21	0.21	70	85
180	0.22	0.19	0.2	0.19	72	82
250	0.23	0.17[c]	0.22	0.17[c]	60	98
350	0.24	0.2[c]	0.24	0.2[c]	60	88
350 + 100 mM NaCl	0.19	b	0.21	b	90	b

n.d not detected

a. all data taken from cyclic voltammograms recorded at 20 mVs^{-1}

b. accurate measurements restricted by background response.

c. after 10 minutes cycling

Nevertheless, this cation was more effective at stabilising the observed faradaic responses than the divalent cation Mg^{2+}. Additionally, the trivalent cation promoted optimal faradaic peak currents at sub-millimolar amounts, compared to a Mg^{2+} requirement of ca. 5 mM (25 μM Pc, 3°C). The monovalent electrolyte KCl is considerably less effective and concentrations around 200 mM and above are required for comparable promotion at pH 8.0 (3°C). The relative cation requirements are in accord with the importance of electrostatically-dominated protein-electrode interactions.

The addition of solid NaCl (to a final concentration of 100 mM) depromoted faradaic responses. This is consistent with similar observations in the direct electrochemistry of negatively-charged Fe-S proteins (Chapter 7).

b) $Pt(NH_3)_6^{4+}$

The tetravalent cation $Pt(NH_3)_6^{4+}$ is reduced at potentials negative of +100 mV vs NHE. This precludes its use with low potential Fe-S proteins. An additional problem with using this cation is base hydrolysis to lower charged species above pH 7.0 (31) (pK = 7.2 - 7.9). However, when used at pH 6.0, this cation is the most powerful promoter of the direct electrochemistry of plastocyanin. Cyclic voltammetric responses at room temperature (25 μM Pc) were symmetrical and stable with no impersistence at levels of promoter > 50 μM, Table 8.2. In addition, plots of peak current vs. (scan rate)$^{1/2}$ (Figure 8.3) were linear to at least 200 mVs^{-1}, with peak separations at the steady-state of 60 mV (up to 100 mVs^{-1}). The estimated diffusion coefficient, 1.1 x 10^{-6} cm^2s^{-1}, is in good agreement with a value calculated from the

TABLE 8.2

$Pt(NH_3)_6^{4+}$-Promoted Direct Electrochemistry[a] of Plastocyanin (25 μM), in 5 mM MES, 1 mM NaCl, pH 6.0

T = 25°C

$[Pt(NH_3)_6^{4+}]$/μM	$i_{pCATHODIC}$/μA		$i_{pANODIC}$/μA		ΔE_p/mV	
	SCAN 1	SCAN 4	SCAN 1	SCAN 4	SCAN 1	SCAN 4
10	0.07	0.06	b	b	b	b
15	0.09	0.08	0.05	b	b	b
30	0.15	0.15	0.12	0.09	105	115
40	0.19	0.19	0.15	0.13	92	82
50	0.2	0.18	0.17	0.16	78	78
60	0.2	0.2	0.2	0.21	60	65
80	0.22	0.22	0.22	0.2	60	60

a. All data taken from cyclic voltammograms recorded at 20 mVs^{-1}.

b. Accurate measurement restricted by background response.

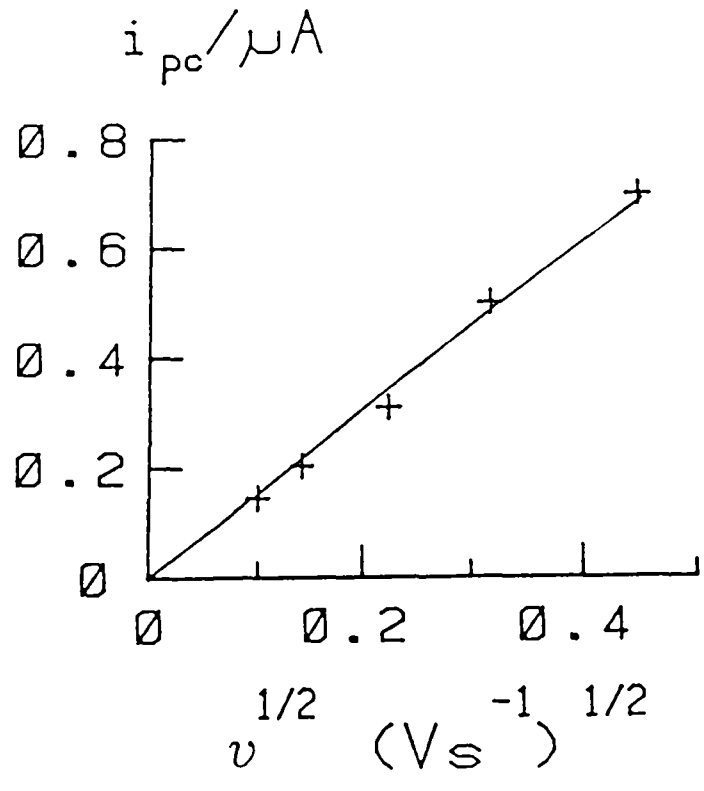

Figure 8.3: Plot of peak current vs. (scan rate)$^{1/2}$ for 25 μM plastocyanin in 5 mM MES, 1 mM KCl, pH 6.0, with 82 μM $Pt(NH_3)_6^{4+}$. 25°C.

Stokes-Einstein equation of 1.6×10^{-6} cm^2s^{-1} (25^oC).

At higher levels of plastocyanin (200 μM), the tetravalent cation is also a powerful promoter of direct electrochemistry at room temperature. A typical cyclic voltammetric response (Figure 8.4) shows only a slight deterioration of the initial faradaic response (ΔE_p, 20 mVs^{-1}) after 10 minutes cycling (ca. 10% decrease in faradaic peak current; ca 5 mV increase in peak separation). However, a plot of cathodic peak current vs. (scan rate)$^{1/2}$ showed deviations from linearity above $50mVs^{-1}$, consistent with less reversible electrochemical processes at this higher protein concentration. The estimated diffusion coefficient (25^oC), 6×10^{-7} cm^2s^{-1}, was lower than the calculated value.

8.6 The Effect of pH.

Changing the pH has a dramatic effect on the direct electrochemistry of plastocyanin at an edge graphite electrode, as illustrated by the set of cyclic voltammograms shown in Figure 8.5. Measurements correspond to initial scans at 20 mVs^{-1}, 3^oC with 25 μM plastocyanin in an initial background medium of 5 mM buffer- 1 mM KCl. Well-defined cathodic and anodic waves (with peak separations $\Delta E_p < 60$ mV) are generated upon mild acidification or the addition of millimolar amounts of $MgCl_2$. Similar behaviour was observed with the use of higher (25 mM) buffer concentrations. Further measurements, intended to define more closely the pH and Mg^{2+} requirements for faradaic response, yielded the numerical data as compiled in Appendix 8.3. The resulting profile is outlined in Figure 8.6, as initial-scan cathodic peak current densities based upon geometric electrode surface area. There is a clear transition from pH-promoted (pH 4)

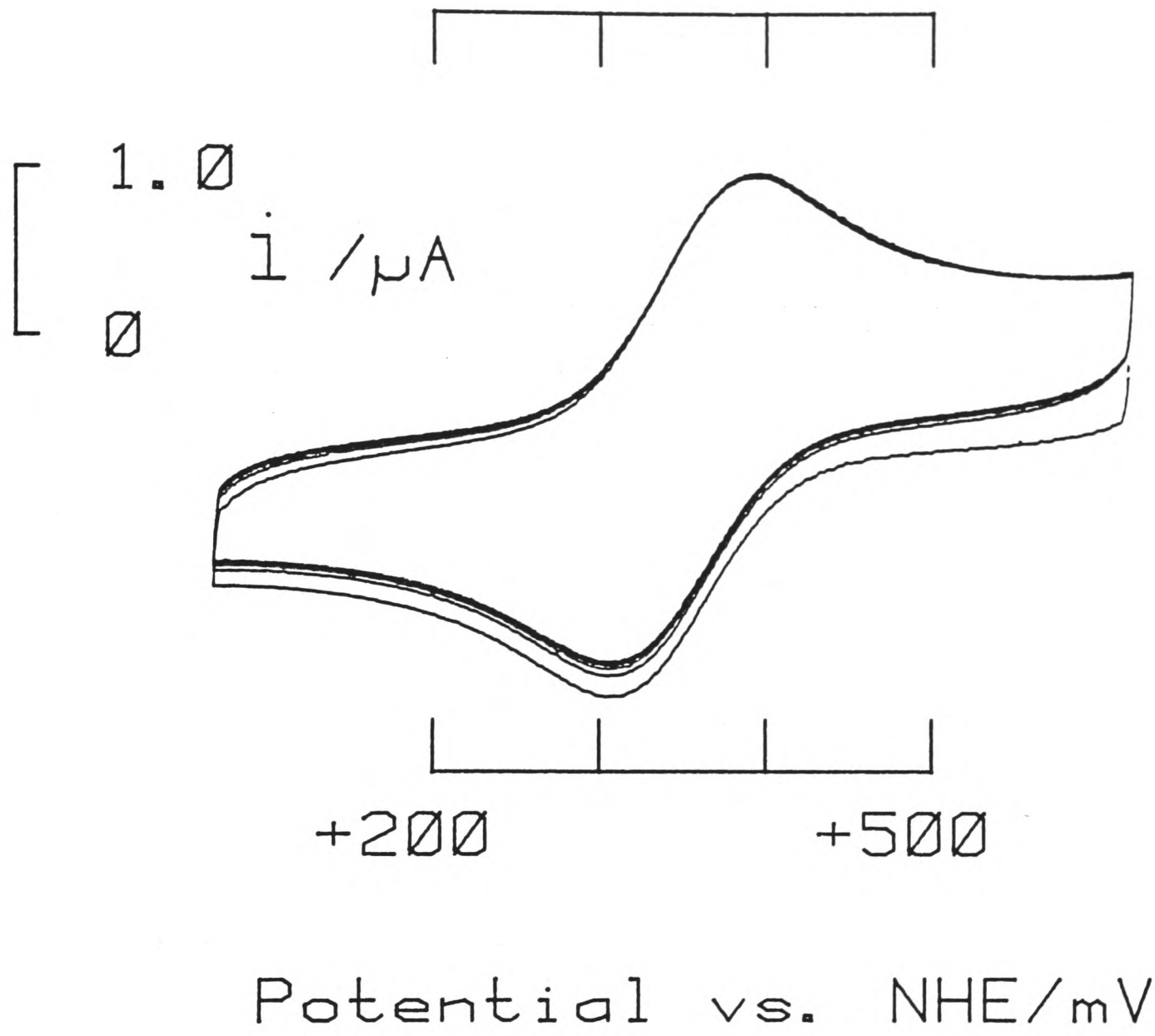

Figure 8.4: Cyclic voltammograms illustrating the stability of the electrochemical response for 0.2 mM plastocyanin, at pH 6.0 (10 mM MES, 1 mM KCl) following the addition of 0.5 mM $Pt(NH_3)_6^{4+}$. The result shown is a series of ten consecutive cycles (20 mVs^{-1}) recorded at 25°C. Edge graphite electrode.

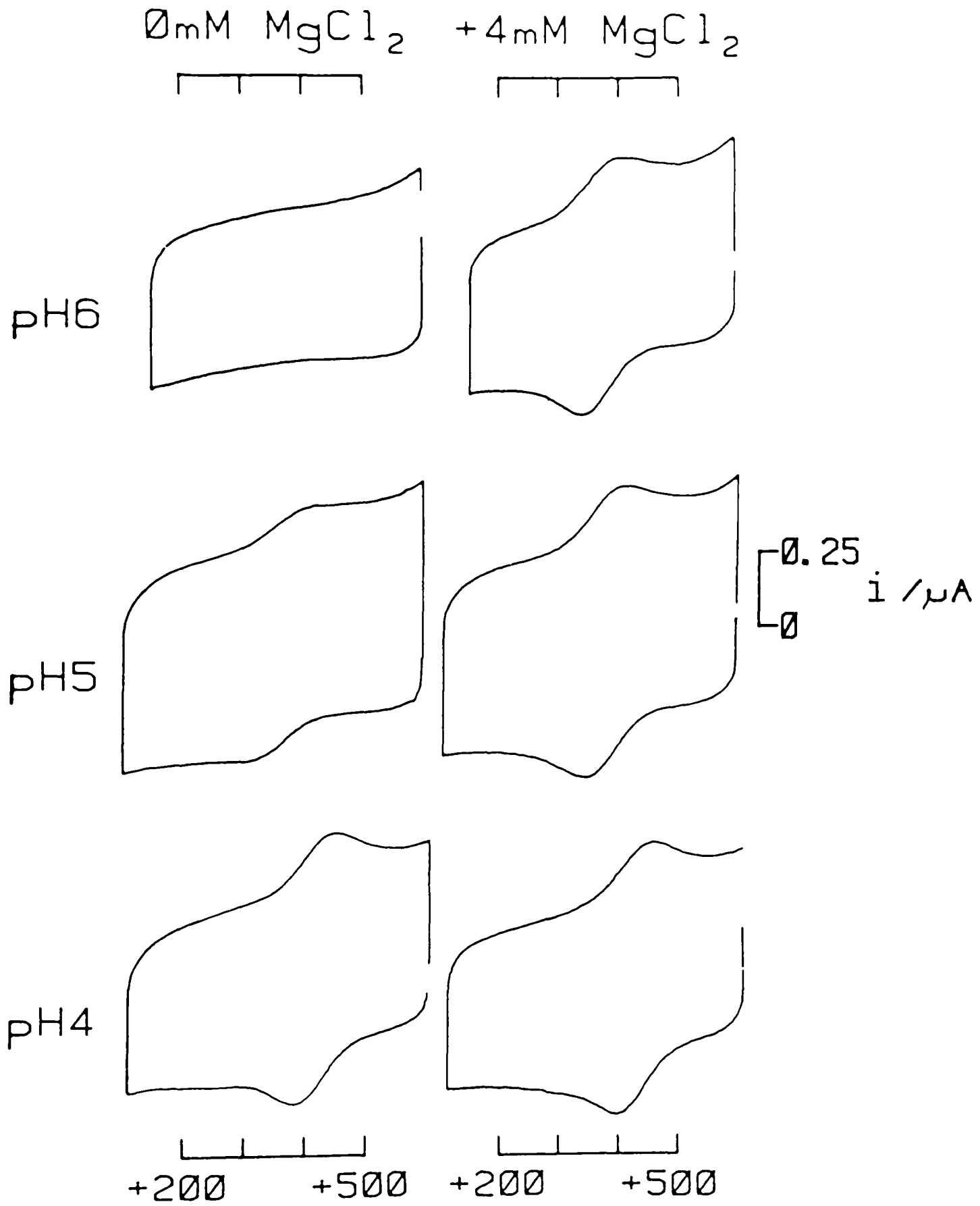

Figure 8.5: Cyclic voltammograms for plastocyanin (25 μM) at a polished edge-oriented graphite electrode, showing the effects of pH and addition of $MgCl_2$: (a) pH 6.0, 5 mM MES- 1 mM KCl as background electrolyte; (b) pH 5.0, 5 mM acetate- 1 mM KCl; (c) pH 4.0, 5 mM acetate- 1 mM KCl. Results shown are for initial scans at 20 mVs^{-1}. T = 3°C. A faint broad feature frequently appearing at ca. +200 mV on the cathodic scan at pH 4.0 could be identified as the reduction of trace amounts of Cu(II). The wave could be removed by the addition of 1 μM EDTA without affecting the faradaic response due to plastocyanin.

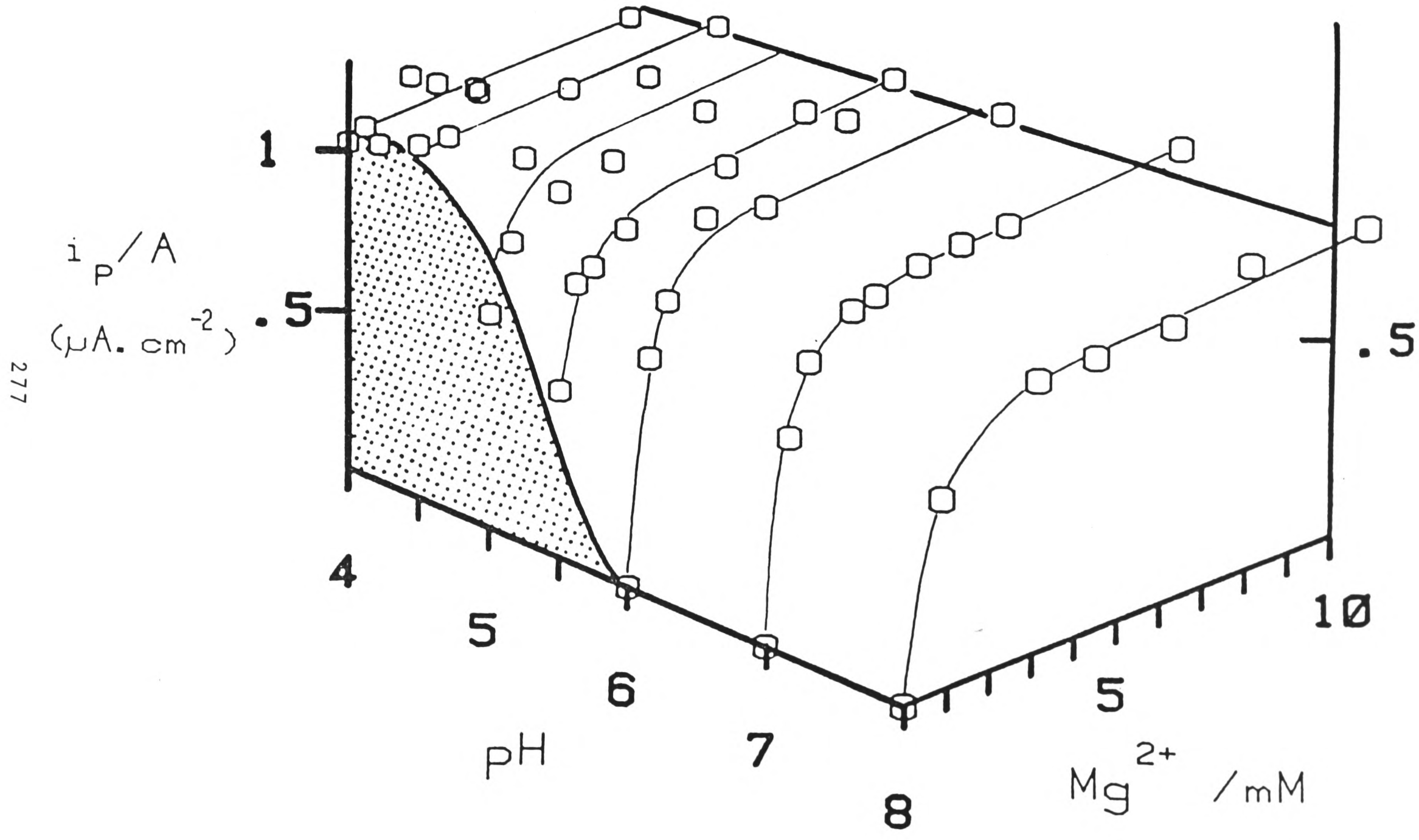

Figure 8.6: 3-D representation of the data tabulated in Appendix 8.3., illustrating the effects of pH and Mg^{2+} concentration upon observed (initial scan, 20 mVs^{-1}) peak current densities for plastocyanin, 25 μM in 5 mM buffer (acetate, MES, HEPES, Tricine), with 1mM KCl, at 3°C. Edge graphite electrode.

to Mg^{2+}-promoted (pH 6 - 8) electrochemistry. At low plastocyanin concentrations, i.e. 25 μM, saturation requirements for Mg^{2+} are <5 mM at pH 7. At the low pH limit, additions of Mg^{2+} do not markedly affect the observed current densities.

Inspection of the observed anodic and cathodic wave shapes and current amplitudes showed that voltammetric responses were symmetrical at all pH values, suggesting the electrochemical charge transfer coefficient, α , to be close to 0.5.

Comparison of faradaic responses, at pH 4, at 25°C and 3°C, showed the electrochemistry to be stable with no significant ageing at either temperature. However, cyclic voltammograms at 25°C (20 mVs^{-1}) were noticeably asymmetric with a broad anodic peak. This may indicate weak adsorption of plastocyanin at the higher temperature. Similarly, studies at high scan rates (1 - 4 Vs^{-1}) at 3°C indicated a transition from diffusion-controlled behaviour ($i_p \propto v^{1/2}$) to behaviour characteristic of an adsorbed redox couple ($i_p \propto v$). It has been proposed (32) that reversible binding of a redox protein at an electrode surface may be an essential prerequisite to direct electron-transfer. At higher scan rates (>1 Vs^{-1}) it appears that the time scale of the electrochemical experiment may be approaching the rate of the adsorption-desorption process occurring in the electrode reaction of plastocyanin.

Calculated diffusion coefficients, based upon geometric surface areas, show a decrease from 7 ± 1 x 10^{-7} cm^2s^{-1} at pH 4 to 4 ± 1 x 10^{-7} cm^2s^{-1} at pH 8. This may reflect some increase in hydrodynamic resistance due to higher levels of ion pairing or solvation or, possibly, diminishing effective surface area.

Rate constants for hetergeneous electron-transfer, as estimated from initial-scan cyclic voltammetric peak separations, at scan rates 20 - 100 mVs^{-1}, range from $10 \pm 5 \times 10^{-3}$ $cm.s^{-1}$ at pH 4 to $2 \pm 1 \times 10^{-3}$ $cm.s^{-1}$ at pH 8. It is most likely that the observed scatter arises from the reproducibility of polishing the electrode. Within the range of scan rates used, there were no marked trends towards larger rate constants at lower scan rates that would be indicative of effects due to uncompensated resistance in 1 mM KCl.

Values of $E_{1/2}$ increase below pH 5.5 with a limiting slope $-d(E_{1/2})/d(pH) \sim 55$ mV. At pH 7, the redox potential in the presence of 5 mM $MgCl_2$ is 375 ± 10 mV, whereas at pH 4, the corresponding value is 430 ± 10 mV.

8.7 Competition Studies.

A preliminary study was made on a mixture of the two negatively-charged redox proteins, plastocyanin and the 8Fe ferredoxin. At concentrations of 17 μM, in a solution containing 15 mM Mg^{2+} ($2^{o}C$), both proteins show persistent quasi-reversible responses when in separate solutions. In a mixture of the two proteins, under the same conditions, the response of plastocyanin is severely destabilised. By contrast, the response of ferredoxin is unperturbed. Clearly, these proteins are competing with each other in some way in the interfacial region, and may, perhaps, bind at the same surface sites.

8.8 Discussion of the Direct Electrochemistry of Plastocyanin.

Several important features are evident in the direct electrochemistry of plastocyanin. These are summarised below:

1) plastocyanin behaves as an effectively symmetrical ($i_{pc} \simeq i_{pa}$) redox couple throughout the pH range 4 - 8.

2) values of the redox potential for plastocyanin, derived from electrochemical data, indicate a pK of 5.5, in agreement with previous potentiometric and kinetic pH profiles (21,22).

3) direct electrochemistry of plastocyanin is promoted by pH or cationic reagents ($M^{4+} > M^{3+} > M^{2+} > M^{+}$).

4) cation-promoted direct electrochemistry of plastocyanin is stabilised by the use of low temperatures (3°C), or higher valent cations ($M^{4+} > M^{3+}$) at room temperature.

The promotion of direct electrochemistry by Mg^{2+} ions (<5 mM) or by mild acidification (pH 4 - 6) of the medium closely parallels regulatory characteristics observed for electron-transfer between plastocyanin and P700 in highly-purified PSI reaction centre complexes (9). In the latter, the rate of electron-transfer from plastocyanin to photo-oxidised P700 has been shown to be drastically accelerated by the addition of 10 mM $MgCl_2$ or by a decrease in the pH to values below pH 6, with a maximal rate at pH 4.3. However, in contrast to the absence of Mg^{2+} effects in direct electrochemical studies at low pH, the reduction of $P700^{+}$ by plastocyanin is inhibited by Mg^{2+} at low pH. This result is interesting in view of the efflux of Mg^{2+} from the intrathylakoid space which accompanies the acidification of this compartment upon illumination of the chloroplast. Apparently, plastocyanin may act in vitro as an efficient electron donor to $P700^{+}$, under illumination.

The role of cations in promoting electron-donation to $P700^+$ at neutral pH has been suggested (9) to be a result of a decrease in repulsive electrostatic interactions between plastocyanin and $P700^+$, both of which carry a high net negative charge density at this pH. The inhibition of $P700^+$ reduction by salts at pH 4 - 5 may simply be a consequence of the 'screening' of otherwise attractive interactions between the net negatively-charged plastocyanin and the net positively-charged PSI particle.

These observations suggest that the requirement for multivalent cationic promoters in direct electrochemical studies of plastocyanin at pH 8.0, may be a consequence of the 'screening' of otherwise repulsive electrostatic interactions between the net negative charge of plastocyanin (total protein charge at pH ca. 7 is estimated to be 9- : see Table 4.1) and a net negative charge density at the electrode surface. However, there may also be specific electrostatic interactions between sites of local negative charge density on the electrode and the acidic patch on plastocyanin. The case for predominantly electrostatic interactions, in direct electrochemical studies, is supported by the increased efficiency of higher valent cations ($Pt(NH_3)_6^{4+} > Cr(NH_3)_6^{3+} > Mg^{2+} > K^+$) as promoters.

The observations of multivalent cation promotion effects in the direct electrochemistry of plastocyanin are generally in accord with similar observations described for the negatively-charged, low potential Fe-S proteins (Chapter 7). More specifically, the relative cation requirements observed for comparable concentrations of the 8Fe ferredoxin (20 μM) and plastocyanin (25 μM) are remarkably similar, despite the ca. 1 volt difference in redox potential. This suggests that the

negative charge density at the electrode surface mainly arises from acidic functional groups at the electrode surface, rather than from excess electronic charge density ('smeared charge').

Promotion of electrochemistry by mild acidification may arise from protonation of electrode surface groups, leading to a relief of electrostatic repulsions. In view of the inhibitory effects of cations upon the plastocyanin-P700 interaction at low pH, the absence of cation effects in direct electrochemical studies at low pH suggests that the electrode (or localised binding zone for plastocyanin at the electrode) carries no net charge density at this pH. However, specific amino acid protonation equilibria, in addition to protonation at the Cu(I) active site, have also been detected (25) in kinetic studies at low pH, through a decrease in the association constant for the binding of plastocyanin to cationic complexes, such as $Pt(NH_3)_6^{4+}$ or $Cr(NH_3)_6^{3+}$. These effects were suggested to originate from protonation at the acidic patch. Consequently, protonation of amino acid residues may be mechanistically important in the promotion of electrochemistry at low pH. However, support for the suggestion that protonation equilibria at the electrode surface are <u>also</u> important stems from pH titration studies carried out with the hexacyanoferrate(II/III) system at low ionic strength, for which a similar 'cut-off' in faradaic response at pH > 6 is observed (Chapter 6). The reduction potential of hexacyanoferrate (+400 mV vs. NHE) is very similar to that of plastocyanin.

In addition to providing relief of unfavourable electrostatic interactions, protonation of acidic groups may also facilitate protein-electrode binding through the formation of hydrogen-bonds. More specifically, a carboxyl-carboxylate

interaction may lead to a protein($-CO_2^-$)...H^+...(^-O_2C)electrode 'bridge'. It has been reported previously (33) that hydrogen bonds between two carboxyl groups are an important stabilising force in protein-protein interactions at low pH.

A cation-binding domain, conserved in higher plant plastocyanins, has been identified in ^{1}H-NMR studies (34,35), from observations of the paramagnetic line broadening of assigned proton resonances by Cr(III) complexes. In particular, studies with $Cr(NH_3)_6^{3+}$ clearly indicate association at or close to Tyr-83. The side chain of this residue is surrounded by carboxylate groups of residues in the acidic patch. Clearly, a discrete protein-cation complex may be important in electrochemical studies. Indeed, a strong case can be made for the importance of an electrostatic association, since an increase in ionic strength de-promotes $Cr(NH_3)_6^{3+}$-promoted faradaic responses. A simple interpretation is that a positively-charged complex bound in the region of the acidic patch will influence specific local (or net) electrostatic forces in the interfacial region. More interestingly, perhaps, $Cr(NH_3)_6^{3+}$ may also undergo electrostatic association with acidic functional groups at the electrode surface, to form a transient protein-cation-electrode bridge. This will bind plastocyanin at the surface in a favourable orientation for electron-transfer, Figure 8.7(a). The construction of an edge surface bearing cationic Cr(III) complexes (Chapter 11) leads to rapid, reversible and sustained electron-transfer to plastocyanin. This highlights the importance of Cr(III) complexes bound at the electrode surface.

In further NMR studies (36,37), inorganic complexes have been used to probe self-exchange processes in mixtures of Cu(I)

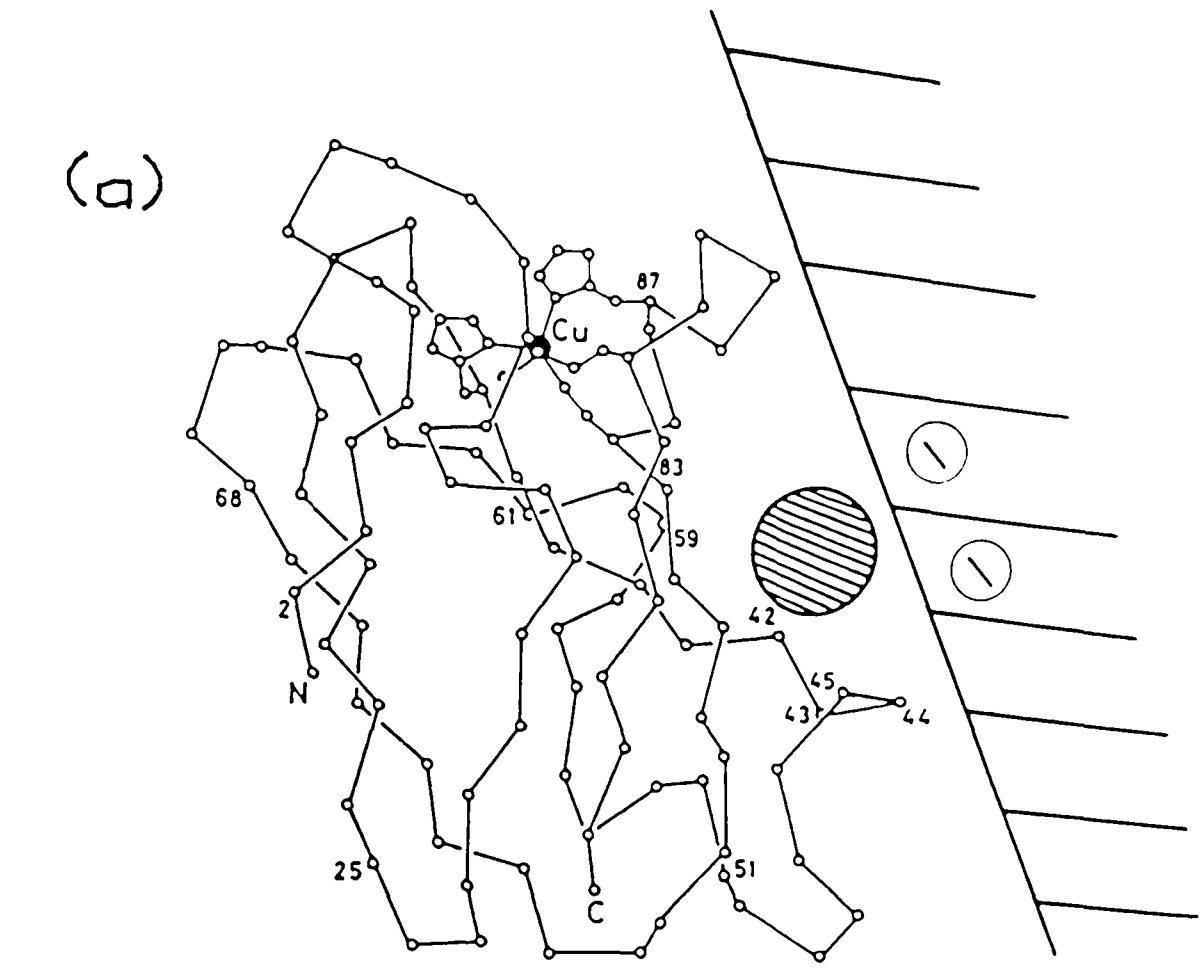

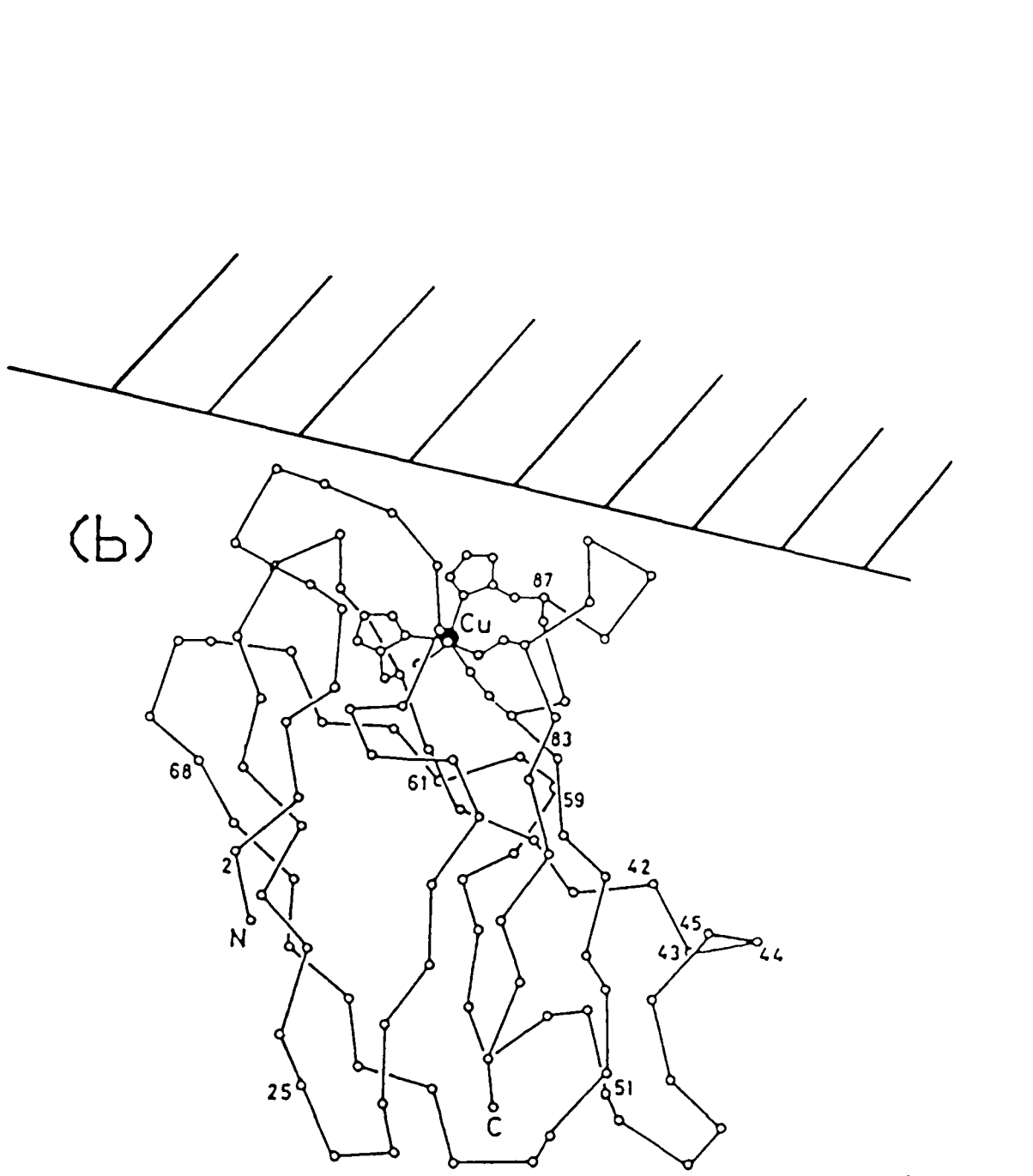

Figure 8.7: Schematic representations of plastocyanin-electrode interactions. (a) A cation-´bridge´ between the ´eastern´ acidic patch and acidic C-O functionalities at the electrode; (b) a hydrophobic interaction at the ´northern´ end of plastocyanin.

(diamagnetic) and Cu(II) (paramagnetic) plastocyanin. Recent studies in this laboratory (37), using a range of multivalent cations, have shown that addition of the diamagnetic complex $Co(NH_3)_6^{3+}$, but not K^+, results in appreciable broadening of resonances (in the aromatic region) close to the Cu centre (Figure 8.8). It follows that $Co(NH_3)_6^{3+}$, but not K^+, allows rapid (on the NMR time scale) electron exchange between Cu(I) and Cu(II) proteins. The tetravalent cation, $Pt(NH_3)_6^{4+}$, may be even more effective at promoting electron self-exchange. However, NMR studies have been limited by precipitation of plastocyanin in the presence of this cation. It appears that multivalent cations may facilitate protein-protein association, perhaps through the formation of protein-cation-protein electrostatic 'bridges'. However, the high charge density of $Pt(NH_3)_6^{4+}$ causes extensive aggregation leading to precipitation.

8.8.1 Stabilisation of Faradaic Responses.

A noticeable feature of the direct electrochemistry of plastocyanin is the marked problem of 'impersistence'. However, the cations $Cr(NH_3)_6^{3+}$ and, in particular, $Pt(NH_3)_6^{4+}$, are efficient at stabilising the 'impersistence' of plastocyanin electrochemistry at 25°C. This 'impersistence' may be due to irreversible protein binding at the electrode surface, leading to a progressive 'blocking' of electron-transfer sites (for further discussion see Chapter 7). At sub-optimal cation levels, irreversible binding to the electrode surface may be the result of strong hydrophobic interactions between the hydrophobic patch of plastocyanin and regions of basal plane character at the electrode surface, Figure 8.7(b). This explanation is in accord

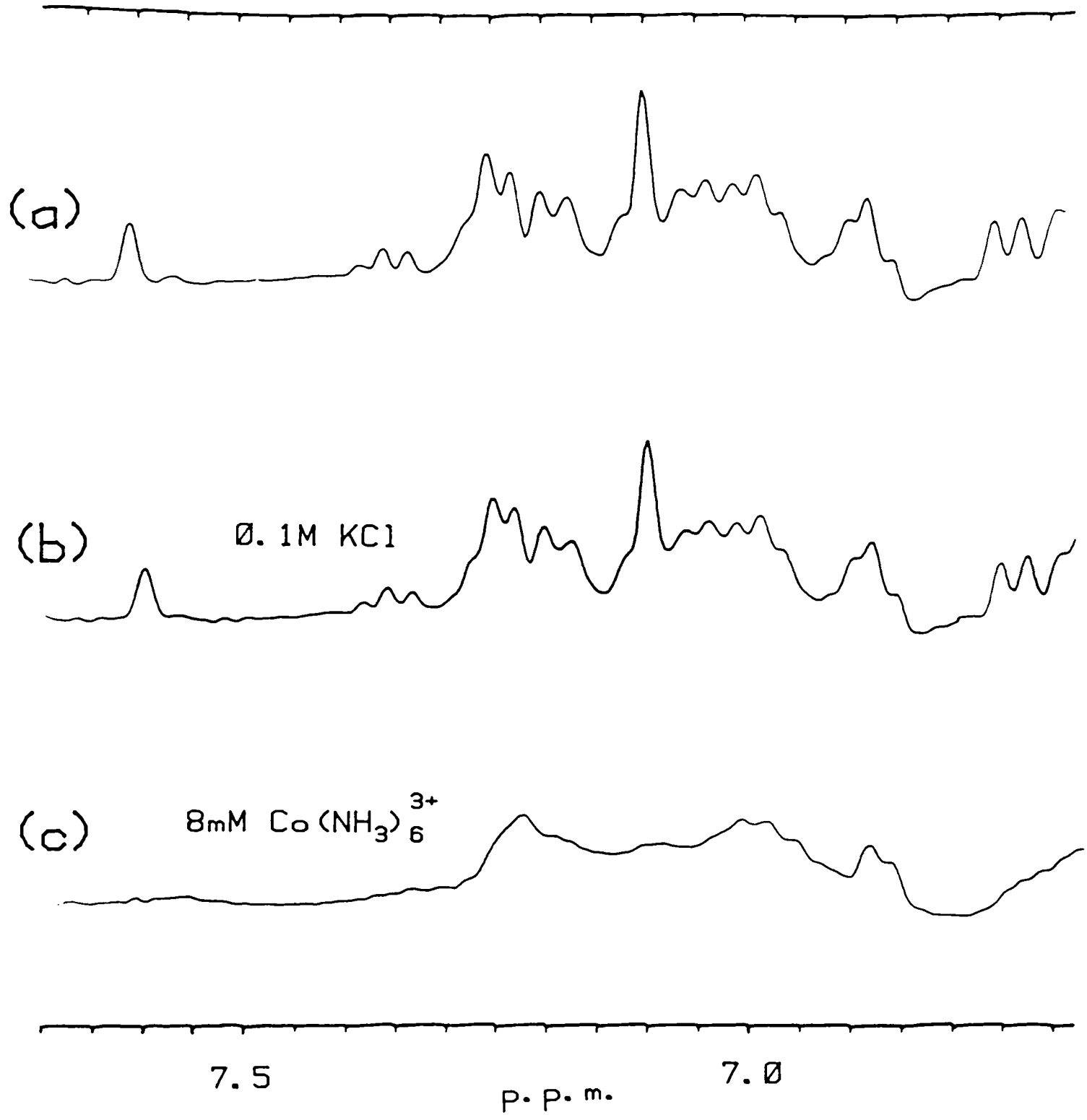

Figure 8.8: The effect of multivalent cations on a 1:1 mixture of PcCu(I) and PcCu(II) (total concentration 1.5 mM, pH 6.0). The aromatic region of the 300 MHz ^{1}H-NMR spectra of:
(a) PcCu(I) + PcCu(II), 1 mM KCl
(b) PcCu(I) + PcCu(II), 100 mM KCl
(c) PcCu(I) + PcCu(II), as (a) with the addition of 8 mM $Co(NH_3)_6^{3+}$

with studies on the oxidation of plastocyanin Cu(I) by the Co(III)-4,7-di(phenyl-4´-disulphonate)-1,10-phenanthroline complex [$Co(4\text{-}7\text{-}DPSphen)_3^{3-}$] (38). The extensive hydrophobic character of this ligand leads to the largest association constant ($K = 4600\ M^{-1}$) so far observed for reactions of inorganic complexes with blue copper proteins. It appears that strong hydrophobic protein-electrode interactions account for the particular problem of impersistence associated with plastocyanin. At optimal cation levels, electrostatic interactions dominated by a protein-cation-electrode ´bridge´ may lead to a more favourable orientation at the electrode surface, Figure 8.7(a), in which hydrophobic interactions are minimised and binding is more reversible.

The observations of impersistence may also reflect a tendency for contact with the electrode surface to be accompanied by structural rearrangements (reconformation) which ´spread´ the protein to maximise the area of hydrophobic contacts. Studies by Lyklema et. al (39-41) on the adsorption of a negatively-charged protein, human plasma albumin (HPA: pI = 4.2 - 5.0), at negatively-charged polystyrene latex particles have shown that irreversible adsorption increases with increasing temperature. The authors conclude that reconformation is endothermic and is driven by a gain in entropy (40). In accordance with this proposal, the Mg^{2+}-promoted electrochemical response of plastocyanin is stabilised at lower temperatures. Further studies (39,41) suggest that the net charge of a protein molecule contributes to its conformational stability at an absorbent. At the isoelectric point (pI) of the protein, this stability is maximal. However, at a pH different from the pI, reconformation

occurs during the adsorption process. The results in this chapter show that the electrochemistry of plastocyanin is quite stable at a pH (pH 4) close to the pI of this protein, in agreement with these observations. This may also explain why the addition of $Pt(NH_3)_6^{4+}$, at room temperature, stabilizes the observed electrochemical responses. The binding of one $Pt(NH_3)_6^{4+}$ at, or close to, residues 42 - 45 of plastocyanin is expected to neutralise the charge (4-) at this site.

The ease with which conformational changes occur will also depend upon the rigidity of the protein structure in solution. In the presence of $Pt(NH_3)_6^{4+}$, close interaction between plastocyanin and this cation will lead to contiguity between the hydration shells of the cation and the protein. The high charge density of $Pt(NH_3)_6^{4+}$ may then stiffen the water structure at the surface of plastocyanin. Similarly, as the temperature is lowered, the increase in the viscosity of water will lead to a more 'gel-like' water structure at the protein and electrode surfaces. These solvent effects will markedly reduce the mobility of the protein surface leading to a more rigid protein structure and improved interfacial stability. The role of 'ice-like' solvation shells in determining the reactions of proteins has been described in several previous reports (42,43).

At higher (>50 μM) protein concentrations, a combination of Mg^{2+} and reduced temperature (3°C) is no longer sufficient to stabilise faradaic responses. However, the use of $Pt(NH_3)_6^{4+}$, at 25°C, gives a faradaic response (0.2 mM Pc) which is essentially stable towards prolonged (>10 mins.) cycling. In the light of ^1H-NMR studies of electron self-exchange reactions, it appears that the particular potency of higher valent cations, such as

$Pt(NH_3)_6^{4+}$ (or $Cr(NH_3)_6^{3+}$), may be due to the ability to efficiently stabilise intermolecular interactions arising at high protein concentrations. It is possible that electron exchange through protein-protein interactions at, or close to, productive binding sites may remove the need to populate potentially less reversible binding sites. It is relevant to note that there is no evidence for precipitation in $Pt(NH_3)_6^{4+}$ studies of plastocyanin (25 μM or 0.2 mM) electrochemistry. However, the electrochemistry is less reversible, and electrochemical diffusion coefficients ca. two-fold lower, at the higher plastocyanin concentration. This may be consistent with the formation of molecular aggregates through $Pc\text{-}Pt(NH_3)_6^{4+}$ electrostatic bridges.

8.9 The Redox Inactivity of Plastocyanin Cu(I): Results and Discussion.

Cyclic voltammetric studies at edge graphite and modified Au (28) surfaces indicate that plastocyanin behaves as a quasi-reversible system uncomplicated by coupled chemical reactions throughout the pH range 4 - 8. Further investigations (44) showed that cyclic voltammograms at pH 4 were similar whether using oxidised or reduced plastocyanin solutions. These observations apparently contradict the evidence for the formation of a kinetically inactive protonated form of reduced plastocyanin. However, Sykes and co-workers have shown (22) that the kinetics of electron-transfer from Cu(I) plastocyanin to some inorganic oxidants are consistent with an equilibrium between a protonated form and an unprotonated form of the reduced protein. Thus, the system can be described as an E_rC_r reaction:

$$PcCu(II) + e^- \rightleftharpoons PcCu(I) \qquad \text{ELECTRODE}$$

$$PcCu(I) + H^+ \underset{k_b}{\overset{k_f'}{\rightleftharpoons}} HPcCu(I)$$

ACTIVE INACTIVE

$$K' = k_f'/k_b$$

$$k_f = k_f'[H^+]$$

$$K = K'[H^+]$$

Clearly, the perturbation that the coupled chemical reaction causes to the electrode reaction and, hence, the appearance of the cyclic voltammogram, will depend upon the protonation-deprotonation rate constants, as compared to the time required to perform the electrochemical experiment (i.e. the scan rate). Hence, the apparent quasi-reversible electron-transfer observed at pH 4 can be reconciled with evidence for a protonated, inactive form of plastocyanin if proton-transfer is rapid on the cyclic voltammetric time scale, and maintains an effective equilibrium between unprotonated and protonated forms of the reduced protein.

The electrochemical characteristics of an E_rC_r reaction have been considered by Nicholson and Shain (45). For initial scan cyclic voltammograms, the use of a working curve (Figure 2.5) showing the variation of the anodic-cathodic peak current ratio, i_{pa}/i_{pc}, with the function $\Psi(= K(nfv/[k_f+k_b])^{1/2})$, where v is the scan rate (Vs^{-1}) and k_f, k_b and K are as defined above, permits an estimate of the deprotonation rate constant to be made. As $\Psi \longrightarrow 0$, i.e. as (k_f+k_b) increases, the voltammetric response approaches the form expected for a normal uncoupled system with $E_{1/2}$ displaced by $(RT/F).\ln(1+K)$.

In order to estimate a lower limit for k_b, the electrochemistry of plastocyanin was examined at pH 4 at high scan rates (>500 mVs^{-1}). However, the accuracy of studies at high scan rates are limited by three considerations. Firstly, errors due to uncompensated resistance are likely to be significant at low electrolyte concentrations (1 mM KCl). An assessment of the magnitude of apparent increases in peak separation (ΔE_p), due to uncompensated resistance, was made by scanning a solution of ferrocene monocarboxylic acid (10 μM in 5 mM Tricine-1 mM KCl, pH 8.0). Under these conditions, currents obtained were similar to those in protein experiments. Typical results (ΔE_p) were; 60 mV (20 mVs^{-1}), 110 mV (200 mVs^{-1}). Addition of 4 mM $MgCl_2$ gave; 60mV (20 mVs^{-1}), 70 mV (200 mVs^{-1}), without increase in faradaic peak currents. At $MgCl_2$ concentrations above 4 mM, no further decreases in peak separation were evident. Consequently, all estimations of kinetic parameters for plastocyanin electrochemistry were carried out using data obtained with solutions containing 10 mM $MgCl_2$. Secondly, high charging currents and the necessarily low protein concentrations, which yield relatively small faradaic responses, restrict the upper limit in scan rate dependencies. Consequently, cyclic voltammetric measurements for kinetic purposes were restricted to 500 mVs^{-1}. Finally, as shown by Nicholson and Shain, the anodic portion of a cyclic voltammogram for an E_rC_r reaction is very sensitive to the kinetic parameters. In particular, the anodic peak height is a function of the switching potential, E_λ. Therefore, in order to construct the published working curve (Figure 2.5), an arbitrary switching potential of $(E_\lambda - E_{1/2}) - (RT/F)\ln(1+K)$ equal to -90 mV was assumed. However, experimental tests showed that general faradaic

wave shapes and anodic peak currents did not change significantly for plastocyanin (500 mVs^{-1}, pH 4) as the cathodic switching potential was varied between -150 and +50 mV vs. SCE (+108 and +308 mV vs. NHE). Consequently, the published working curve was adopted for kinetic calculations.

A typical initial-scan cyclic voltammogram measured at a scan rate of 500 mVs^{-1} is shown in Figure 8.9. By inspection, observed i_{pa}/i_{pc} ratios lie close to 1. A scan rate dependence in the range 10 - 500 mVs^{-1} showed that values of $E_{1/2}$ were independent of scan rate. Measurements of the ratio i_{pa}/i_{pc}, at 500 mVs^{-1}, were made after subtraction of the capacitative contribution, using a published semi-empirical procedure (see Appendix 8.1, (46)). Allowing for the uncertainty in the absolute switching potential, due to the limited response of the chart recorder at high scan rates, several estimates of i_{pa}/i_{pc} were taken. These all gave values of $i_{pa}/i_{pc} > 0.9$. To confirm this result, cyclic staircase voltammograms were run on a computer-controlled electrochemical rack system (potential step size = 1mV) with data acquisition and storage in a <u>digital</u> form. At scan rates in the range 500 mVs^{-1} to 4 Vs^{-1}, values of i_{pa}/i_{pc} were typically > 0.85. Adopting a cautious limit, $i_{pa}/i_{pc} > 0.75$, use of the working curve gives $\Psi < 1.0$. Consequently, at a scan rate (v) of 500 mVs^{-1} and using $pK' = 5.5$ (see Appendix 8.2), k_b must exceed 640 s^{-1}, that is, $t_{1/2}$ for deprotonation is < 1 ms. This result was confirmed in a control experiment using reduced plastocyanin and treating as for a C_rE_r system (44).

The limiting value for k_b may be compared with recent evidence (47), based upon NMR line-broadening measurements with <u>Anabaena variabilis</u> plastocyanin, which indicates that the

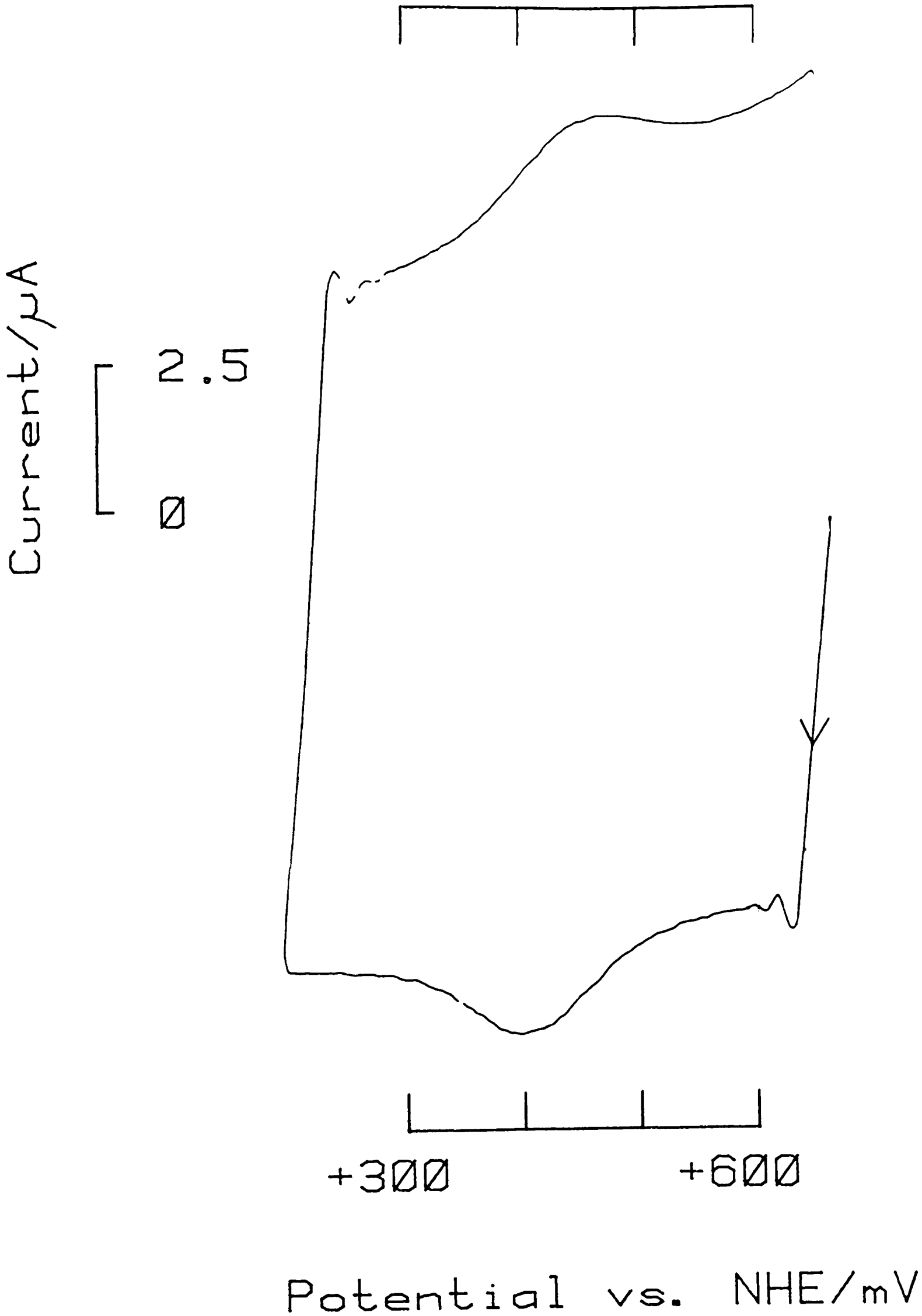

Figure 8.9: Initial scan cyclic voltammogram at 500 mVs^{-1} obtained for oxidised plastocyanin (28 μM) at pH 4.0 (5 mM acetate- 1 mM KCl, with the addition of 10 mM $MgCl_2$). Temperature = $3^{o}C$.

lifetime of a proton on the δ-nitrogen of His-87 is about 0.4 ms. Thus, the observation of well-behaved electrochemistry at low pH is due to the comparatively rapid proton transfer which maintains effective equilibrium between protonated (inactive) and unprotonated (active) forms of the reduced protein. The relevance of this equilbrium to the biological activity of plastocyanin, depends upon the time scale of electron transfer between photosystems I and II. Measurement (4) of the rates of oxidation and reduction of plastocyanin in intact chloroplasts, following a light flash, suggests half-lives of 20 - 200 μs and 100 - 500 μs, respectively. A redox inactive form of plastocyanin may be of significance on these time scales.

The results derived in this section serve to illustrate the mechanistic information and insight which may be drawn from direct electrochemical studies of redox proteins.

APPENDIX 8.1

Semi-Empirical Method for the Estimation of the Peak Current Ratio, i_{pa}/i_{pc}, from a Cyclic Voltammogram.

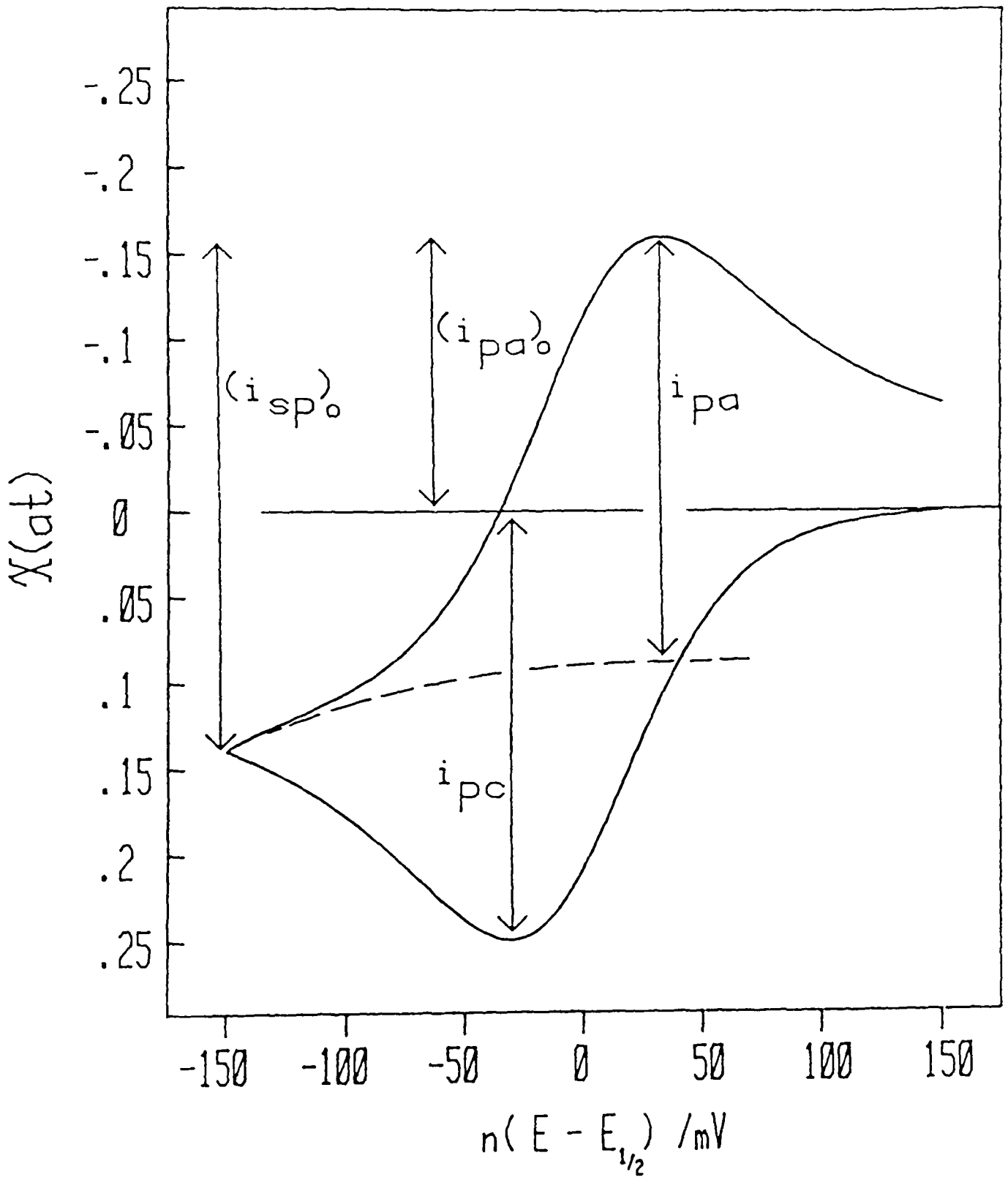

$$\frac{i_{pa}}{i_{pc}} = \frac{(i_{pa})_0}{i_{pc}} + \frac{0.485(i_{sp})_0}{i_{pc}} + 0.086$$

APPENDIX 8.2

Calculation of the De-protonation Rate Constant of the δ-Nitrogen of His-87 in Plastocyanin Cu(I).

According to the nomenclature of Nicholson and Shain (45) the equations for an E_rC_r reaction are written as:

$$O + ne^- \rightleftharpoons R$$

$$R \underset{k_b}{\overset{k_f}{\rightleftharpoons}} Z \qquad \text{where} \quad K = k_f/k_b$$

The corresponding expression for the protonation of reduced Pc is:

$$R + [H^+] \underset{k_b}{\overset{k_f'}{\rightleftharpoons}} Z \qquad \text{where } K' = k_f'/k_b$$

$$k_f = k_f'[H^+]$$

$$K = K'[H^+]$$

For plastocyanin, electrochemically-derived redox potentials give $pK' = 5.5$. Hence, at pH 4.0:

$$K' = 10^{5.5} = \frac{[Z]}{[R] \times 10^{-4}}$$

$$\text{therefore,} \quad K = k_f/k_b = 10^{1.5} = 31.6 \qquad (8.1)$$

From the working curve:

$$\Psi = \frac{K\sqrt{a}}{\sqrt{q}} < 1.0 \qquad \text{where } a = nF\upsilon/RT$$

$$q = k_f + k_b$$

Substituting $\upsilon = 0.5\ Vs^{-1}$ and $K = 31.6$ then $k_f + k_b > 20994$.

However, from equation (8.1), $k_f/k_b = 32$ and so $k_b > 644\ s^{-1}$.

APPENDIX 8.3

Initial Scan Cathodic Peak Currents[a] Obtained for Plastocyanin at an Edge Graphite Electrode under Various Conditions of pH and Mg^{2+} Concentration. Temperature = 3°C. Background Medium is 5 mM buffer - 1 mM KCl.

pH	Mg^{2+}/mM	i_{pc}/μA	pH	Mg^{2+}/mM	i_{pc}/μA	pH	Mg^{2+}/mM	i_{pc}/μA
4.0	0	0.2	5.0	5	0.22	7.0	0	b
	0.5	0.21		7	0.19		0.5	0.10
	1	0.19					1	0.14
	2	0.22	5.5	0	0.09		2	0.16
	4	0.20		0.5	0.15		3	0.16
	10	0.21		1	0.16		4	0.17
				2	0.17		5	0.17
4.5	0	0.21		5	0.18		6	0.17
	0.5	0.24		10	0.19		10	0.17
	1	0.21						
	2	0.22	6.0	0	b	8.0	0	b
	5	0.21		0.5	0.12		1	0.10
	10	0.21		1	0.15		3	0.14
				2	0.19		5	0.14
5.0	0	0.12		4	0.18		6	0.14
	0.5	0.16		5	0.22		8	0.15
	1	0.20		6	0.21		10	0.15
	2	0.18		10	0.18			
	4	0.19						

a. electrode surface area 0.20 cm^2, scan rate 20 mVs^{-1}. The concentration of plastocyanin is 25 μM.

b. faradaic peak current too low to measure.

References - Chapter 8

1) Haehnel, W., Berzborn, R. J. and Andersson, B., Biochim. Biophys. Acta 637, 389, (1981).

2) Katoh, S. in: Encyclopedia of Plant Physiology. Pirson, A. and Zimmerman, M., eds. Wiley: New York. 5, (1977).

3) Hauska, G., Hurt, E., Gabellini, N. and Lockau, W., Biochim. Biophys. Acta 726, 97, (1983).

4) Haehnel, W., Propper, A. and Krause, H., Biochim. Biophys. Acta 593, 384, (1980).

5) Nakatani, H. Y., Barber, J. and Forrester, J. A., Biochim. Biophys. Acta 504, 215, (1978).

6) Gray, J. C., Eur. J. Biochem. 82, 133, (1978).

7) Burkey, K. O. and Gross, E. L., Biochemistry 20, 2961, (1981).

8) Tamura, N., Yamamoto, Y. and Wishimura, M., Biochim. Biophys. Acta 592, 536, (1980).

9) Takabe, T., Ishikawa, H., Niwa, S. and Itoh, S., J. Biochem. 94, 1901, (1983).

10) Burkey, K. O. and Gross, E. L., Biochemistry 21, 5886, (1982).

11) Takabe, T., Ishikawa, H., Niwa, S. and Tanaka, Y., J. Biochem. 96, 385, (1984).

12) Farver, O., Shahak, Y. and Pecht, I., Biochemistry 21, 1885, (1982).

13) Willey, D. L., Auffret, A. D. and Gray, J. C., Cell 36, 555, (1984).

14) Hurt, E. and Hauska, G., Eur. J. Biochem. 117, 591, (1981).

15) Krinner, M., Hauska, G., Hurt, E. and Lockau, W., Biochim. Biophys. Acta 681, 110, (1982).

16) Sandmann, G. and Boger, P., Plant Sci. Lett. 17, 417, (1980).

17) Beoku-Betts, D., Chapman, S. K., Knox, C. V. and Sykes, A. G., Inorg. Chem. 24, 1677, (1985).

18) Takenaka, K. and Takabe, T., J. Biochem. 96, 1813, (1984).

19) Portis, A. R. and McCarty, R. E., J. Biol. Chem. 251, 1610, (1976).

20) Hind, G., Nakatani, H. Y. and Izawa, S., Proc. Natl. Acad. Sci. U.S.A. 71, 1484, (1974).

21) Katoh, S., Shiratori, I. and Takamiya, A., J. Biochem. 51, 32, (1962).

22) Segal, M. G. and Sykes, A. G., J. Am. Chem. Soc. 100, 4585, (1978).

23) Brill, A. S., Martin, R. B. and Williams, R. J. P. in: Electronic Aspects of Biochemistry. Pullman, B. ed. Academic Press: New York (1964).

24) Freeman, H. C., in: Coordination Chemistry-21. Laurent, J. P. ed. Oxford: Pergamon (1981).

25) Chapman, S. K., Sanemasa, I., Watson, A. D. and Sykes, A. G., J. Chem. Soc., Dalton Trans. 1949, (1983). Chapman, S. K., Watson, A. D. and Sykes, A. G., Ibid 2543, (1983). Chapman, S. K., Sanemasa, I. and Sykes, A. G., Ibid 2549, (1983).

26) Essen, L. N. in: Inorganic Syntheses. Parshall, G. W. ed. New York: McGraw-Hill 15, 93, (1974).

27) Ives, D. J. G. and Janz, G. J. Reference Electrodes. Academic Press: New York (1961).

28) Hill, H. A. O., Page, D. J., Walton, N. J. and Whitford, D., J. Electroanal. Chem. 187, 315, (1985).

29) Tanford, C. Physical Chemistry of Macromolecules. Wiley: New York (1960).

30) Matthews, B. W., J. Mol. Biol. 33, 491, (1968).

31) Johnson, R. C., Basolo, F. and Pearson R. G., J. Inorg. Nucl. Chem. 24, 59, (1962).

32) Eddowes, M. J. and Hill, H. A. O., Biosci. Reports 1, 521, (1981).

33) Sawyer, L. and James, M. N. G., Nature 295, 79, (1982).

34) Cookson, D. J., Hayes, M. T. and Wright, P. E., Nature 283, 682, (1980). Biochim. Biophys. Acta 591, 162, (1980).

35) Handford, P. M., Hill, H. A. O., Lee, R. W. K., Henderson, R. A. and Sykes, A. G., J. Inorg. Biochem. 13, 83, (1980).

36) Beattie, J. K., Fensom, D. J., Freeman, H. C., Woodcock, E., Hill, H. A. O. and Stokes, A. M., Biochim. Biophys. Acta 405, 109, (1975).

37) Driscoll, P. C., Part II Thesis. Oxford (1985).

38) Lappin, A. G., Segal, M. G., Weatherburn, D. C. and Sykes, A. G., J. Am. Chem. Soc. 101, 2297, (1979).

39) Lyklema, J., Colloids and Surfaces 10, 33, (1984).

40) Norde, W. and Lyklema, J., J. Coll. Interf. Sci. 71, 350, (1979).

41) Norde, W. and Lyklema, J., J. Coll. Interf. Sci. 66, 257, (1978).

42) Klotz, I. M., Science 128, 815, (1958).

43) Franks, F. and Eagland, D., Critical Rev. Biochem. 3, 165, (1975).

44) Armstrong, F. A., Hill, H. A. O., Oliver, B. N. and Whitford, D., J. Am. Chem. Soc. 107, 1473, (1985).

45) Nicholson, R. S. and Shain, I., Anal. Chem. 36, 706, (1964).

46) Nicholson, R. S., Anal. Chem. 38, 1406, (1966).

47) Kojiro, C. L. and Markley, J. L., FEBS Lett. 162, 52, (1983).

CHAPTER 9.

CATION-REGULATED ELECTROCHEMISTRY OF c-TYPE CYTOCHROMES

9.1 Introduction.

The crystal structures of most redox proteins display pronounced structural asymmetry, particularly in terms of the relative location of the redox centre within the tertiary configuration of the polypeptide chain. In many cases, this is often towards the periphery of the molecule as exemplified by the structures (see Chapter 1) of rubredoxin, flavodoxin, plastocyanin, azurin and cytochrome c. Furthermore, in the cases of flavodoxin and cytochrome c the redox centres may be regarded as having one edge exposed to solvent, which, therefore, represents a likely site through which electron-transfer occurs. It is perhaps significant that in both these proteins there is a region of uncompensated surface charge in the immediate environment of the exposed redox centre and that reactivity with physiological and non-physiological reagents is centred close to these points on the surface.

Clearly, the manner in which the electron-transfer site on the surface of a redox protein is brought into close proximity with an electrode surface, an electron-transfer reagent or a biological partner, is a fundamental problem and requires definition of the functional importance of protein charge and its non-uniform distribution in the crystal structures of redox proteins.

Considerable attention has been focussed on defining the binding domains of cytochromes. These are one of the best characterised groups of redox proteins, as a result of extensive

crystallographic and ^{1}H-NMR studies. Consequently, there is a firm structural foundation for comparing a range of c-type cytochromes with different charge characteristics but which retain the same basic cytochrome fold.

Chapman et. al. (1) and Moore et. al. (2) concluded, on the basis of ^{1}H-NMR and homogeneous kinetic studies, that local electrostatic effects and not net protein charges or dipolar effects were important in the binding of small molecules to a range of redox proteins, including cytochrome c. However, extensive chemical modification studies (3) have shown that the interaction domains for the binding of cytochrome c (cyt. c) to its physiological partners (cyt. c oxidase, cyt. c reductase, cyt. c_1, cyt c peroxidase, sulphite reductase) are found nearly to coincide with the point where the positive end of the molecular dipole moment emerges from the protein surface (see Chapter 1). This led Koppenol (4) to suggest that alignment and binding occur through dipolar effects.

Native cytochrome c carries a significant overall and conservatively-localised positive charge (pI = 9). The electrochemical effects of suppressing this basicity may be examined through chemical modification of one or more of the exposed lysine residues (e.g. with chloro 3,5-dinitro benzoic acid (CDNB) to give carboxydinitrophenyl (CDNP) derivatives of cytochrome c), or by comparison with cytochrome c_{551}.

Pseudomonas cytochrome c_{551} has a crystal structure (5) similar to that of mitochondrial cytochrome c, Figure 9.1. The major difference between the two structures is a fifteen residue deletion in the amino acid sequence of cytochrome c_{551}. This causes the loss of a polypeptide loop at the bottom of the

TABLE 9.1

Properties of c-Type Cytochromes

	Cytochrome c NATIVE	MULTI-CDNP	Cytochrome c_{551}
Radius / Å	16.5	\	15.2
5th/6th haem ligands	HIS/MET	\	HIS/MET
Amino acid residues	104	\	82
Lysine residues Total [haem face]	19 [8]	\	8 [4]
pI	10	n.a.[a]	4.7
Net charge (pH 7)	+7/+8	-ve	-4/-3
Dipole moment/ Debye	325/308	n.a.	n.a.

a. not available

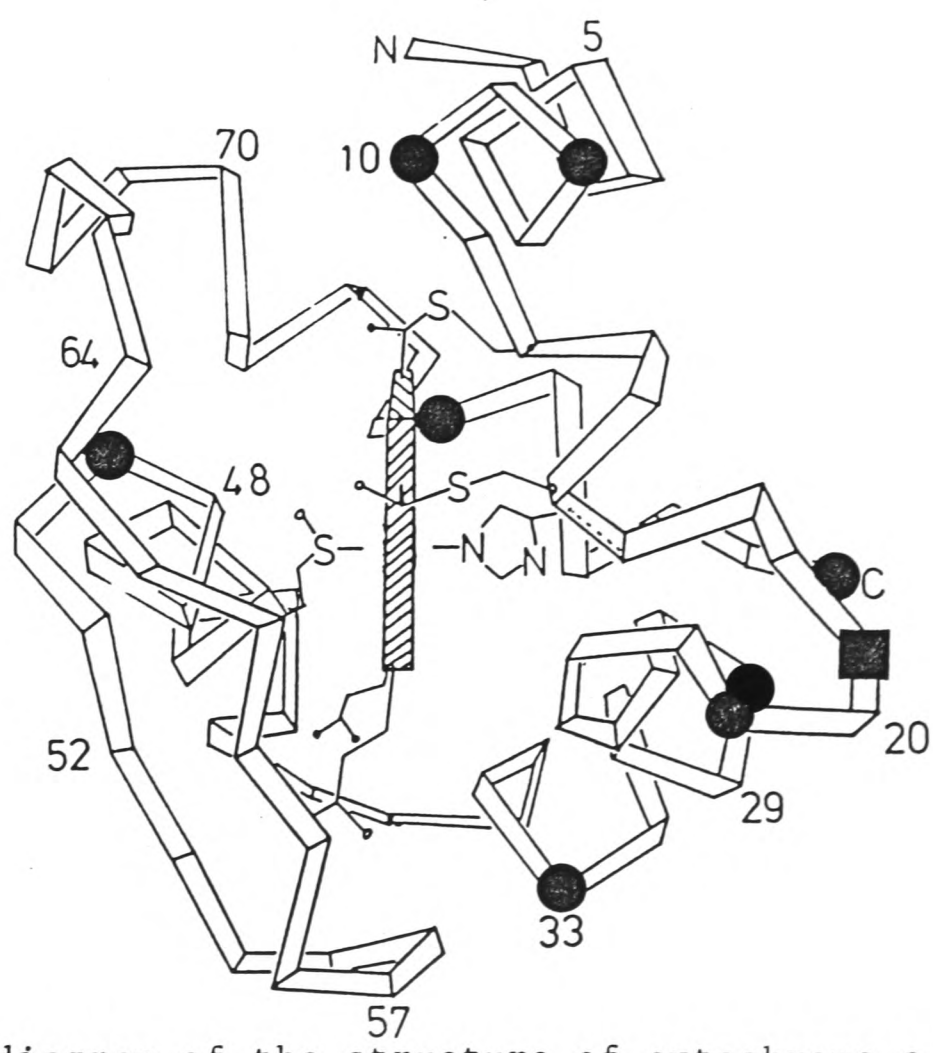

Figure 9.1: Ribbon diagram of the structure of cytochrome c_{551} showing the position of the α-carbon atoms. The molecule is viewed from the side bearing the exposed haem edge. All the lysine residues are marked (●) together with the only acidic residue (aspartate-19) on the haem face (■).

protein close to the haem propionates. However, the orientation and environment of the haem group is the same in both proteins and the distribution of lysine residues around the exposed haem edges is similar. The properties of 'native' cytochrome _c_ and cytochrome $\underline{c}_{551}$ are summarised in Table 9.1. A notable feature of cytochrome $\underline{c}_{551}$ is that this protein carries an overall negative charge at near neutral pH (6).

In the first section of this chapter the electrochemical characteristics of native cytochrome _c_ will be examined, with particular reference to the inhibition of electrochemical responses by multivalent cations. This is followed by a study of the direct electrochemistry of cytochrome $\underline{c}_{551}$ and a modified cytochrome _c_ (multi-substituted CDNP-cytochrome _c_) carrying a net negative charge.

9.2 Experimental Details.

The methodology of cation titrations follows that described in detail in Chapter 7. Ruthenium red (Sigma) was used as supplied. For those experiments performed with 1 mM cytochrome _c_, the support medium contained 100 mM NaCl to eliminate iR problems, and the reference arm of the electrochemical cell contained an identical solution (1 mM cytochrome _c_) to that in the working compartment, to minimise diffusive losses through the Luggin capillary.

9.3 Results: Native Cytochrome c.

9.3.1 Mg^{2+}

The addition of aliquots of a $MgCl_2$ solution to cytochrome c (5 mM Tricine, 100 mM NaCl, pH 8.0) inhibits the observed faradaic response at an edge graphite electrode (Table 9.2). The nature of this inhibition varies according to the concentration of cytochrome c. At low concentrations of cytochrome c e.g. 35 μM (Table 9.2 and Figure 9.2(a)) the addition of $MgCl_2$ effects a decrease in faradaic peak currents and an increase in the peak separation, but no loss of stability. At higher concentrations of cytochrome c (> 200 μM) (Table 9.2 and Figure 9.2(b)), the faradaic response in the absence of $MgCl_2$ is less reversible and impersistent. The addition of $MgCl_2$ inhibits the initial (scan 1) faradaic peak current and markedly amplifies the degree of impersistence observed on successive cycles. By contrast the response at a Au electrode surface-modified with bis(4-pyridyl)bisulphide is unaffected by changes in the concentration of cytochrome c or the addition of $MgCl_2$ (Figure 9.2(c); ΔE_p, scan 4 (1 mM cyt. c) = 62.5 mV [20 mVs^{-1}] in the range 1 - 100 mM Mg^{2+}), although the faradaic response is superimposed on a shifting background at high levels of Mg^{2+}. Complementary studies using the complex $Ru(NH_3)_6^{3+}$ as a test probe at edge graphite showed the faradaic response (ΔE_p = 60mV, 20 mVs^{-1}) to be independent of $Ru(NH_3)_6^{3+}$ concentration or added Mg^{2+} (0 - 100 mM) in 5 mM Tricine, 100 mM NaCl pH 8.0.

9.3.2 $Cr(NH_3)_6^{3+}$

The addition of $Cr(NH_3)_6^{3+}$ to 1 mM cytochrome c (5 mM Tricine, 100 mM NaCl, pH 8.0) effects a similar inhibition and

TABLE 9.2

Mg^{2+} Inhibition of the Direct Electrochemistry[a] of Cytochrome c

	35 μM Cyt. c			1 mM Cyt. c		
Mg^{2+}/mM	Scan	i_{pc}/μA	ΔE_p/mV	Scan	i_{pc}/μA	ΔE_p/mV
0	1,4[b]	0.21	<60	1	5.2	90
				4	4.5	118
22	1,4[b]	0.18	65	1	4.6	125
				4	3.2	160
54	1,4[b]	0.14	70-75	1	4	155
				4	2.5	220
108	1,4[b]	0.14	78-82	1	<3.2	>285
				4	c	c

a. data taken from cyclic voltammograms recorded at 20 mVs^{-1}.

b. measurements taken at scans 1 and 4 were identical.

c. faradaic current too small for accurate measurement.

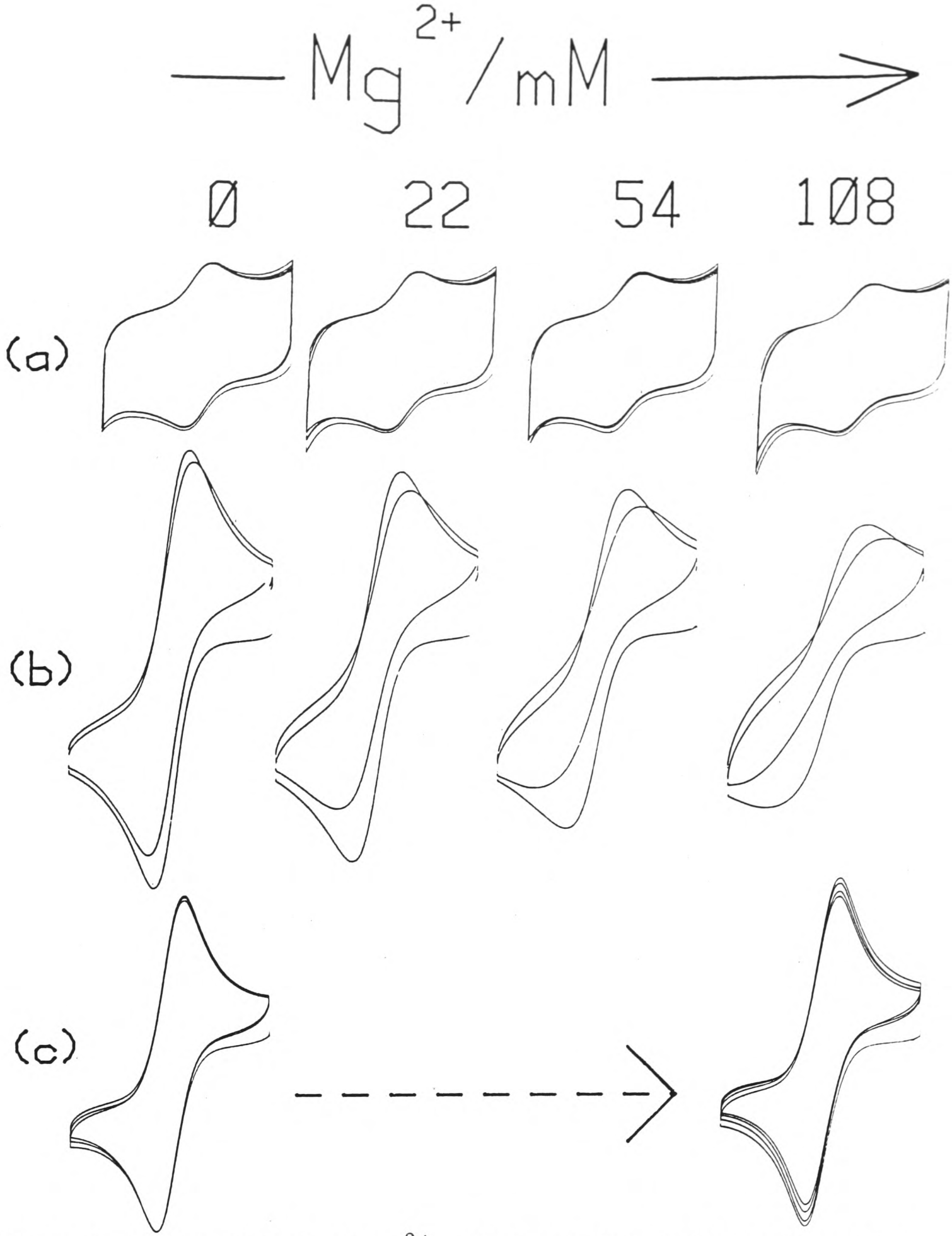

Figure 9.2: The effect of Mg^{2+} additions (as indicated) on the cyclic voltammetric responses of cytochrome c at edge graphite and surface-modified gold electrodes. All experiments carried out in 5 mM Tricine, 100 mM NaCl, pH 8.0. Scan rate 20 mVs^{-1}.
(a) 35 μM cytochrome c at edge graphite. Scans 1 - 4 shown for each Mg^{2+} concentration. Potential limits +530 to +20 mV vs. NHE.
(b) 1 mM cytochrome c at edge graphite. Scans 1 and 4 only are shown for clarity. Potential limits +550 to 0 mV.
(c) 1 mM cytochrome c at a gold electrode surface-modified with bis(4-pyridine)bisulphide. Scans 1 - 4 shown. Potentials as (b).
Data corresponding to (a) and (b) are presented in Table 9.2.
Voltammograms in (c) are on the same scale as those in (b).

destabilization of faradaic response to that seen following the addition of up to 0.1 M Mg^{2+} (Table 9.3). However, the trivalent cation is effective at concentrations below 10 mM, consistent with the importance of electrostatically-dominated inhibitory effects. At low cytochrome c concentrations, e.g. 50 μM the observed faradaic response is virtually insensitive to the addition of $Cr(NH_3)_6^{3+}$ (up to 10 mM).

9.3.3 $Pt(NH_3)_6^{4+}$

The tetravalent cation $Pt(NH_3)_6^{4+}$ is a most efficient inhibitor of cytochrome c electrochemistry when used at high cytochrome c concentrations (1 mM), and pH 6.0 (5 mM MES, 100 mM NaCl) to prevent hydrolysis. Destabilisation and inhibition of the faradaic response of 1 mM cytochrome c is evident at sub-millimolar amounts of $Pt(NH_3)_6^{4+}$, Figure 9.3(a). No significant effects are observed upon adding $Pt(NH_3)_6^{4+}$ to 1 mM cytochrome c at a Au electrode surface-modified with bis(4-pyridyl)bisulphide, Figure 9.3(b), (up to 3 mM $Pt(NH_3)_6^{4+}$) or to dilute cytochrome c (50 μM) at edge graphite.

9.3.4 Ruthenium Red $[(NH_3)_5Ru\text{-}O\text{-}Ru(NH_3)_4\text{-}O\text{-}Ru(NH_3)_5]^{6+}$

The complex cation ruthenium red shows no redox activity above +50 mV vs NHE and is irreversibly adsorbed at edge graphite simply by dipping an electrode into a 1 mM solution of the cation, followed by rinsing or stirring in buffer (7). Trial experiments showed that the response of cytochrome c (0.2 mM) at an edge electrode modified in this way is destabilised relative to the response of the 'bare' electrode.

TABLE 9.3

$Cr(NH_3)_6^{3+}$ Inhibition of the Direct Electrochemistry[a] of Cytochrome c

	50 μM Cyt. c			1 mM Cyt. c		
$Cr(NH_3)_6^{3+}$/mM	Scan	i_{pc}/μA	ΔE_p/mV	Scan	i_{pc}/μA	ΔE_p/mV
0	1,4[b]	0.31	<60	1	5	95
				4	4.5	112.5
2.5	1,4[b]	0.29	60	1	4.8	115
				4	3.7	140
5	1,4[b]	0.28	60	1	4.5	122
				4	3.5	150
7.5	1,4[b]	-	-	1	4	145
				4	3	195
10	1,4[b]	0.28	67.5	1,4	c	c

a. data taken from cyclic voltammograms recorded at 20 mVs^{-1}.

b. measurements taken at scans 1 and 4 were identical.

c. faradaic current too small for accurate measurement.

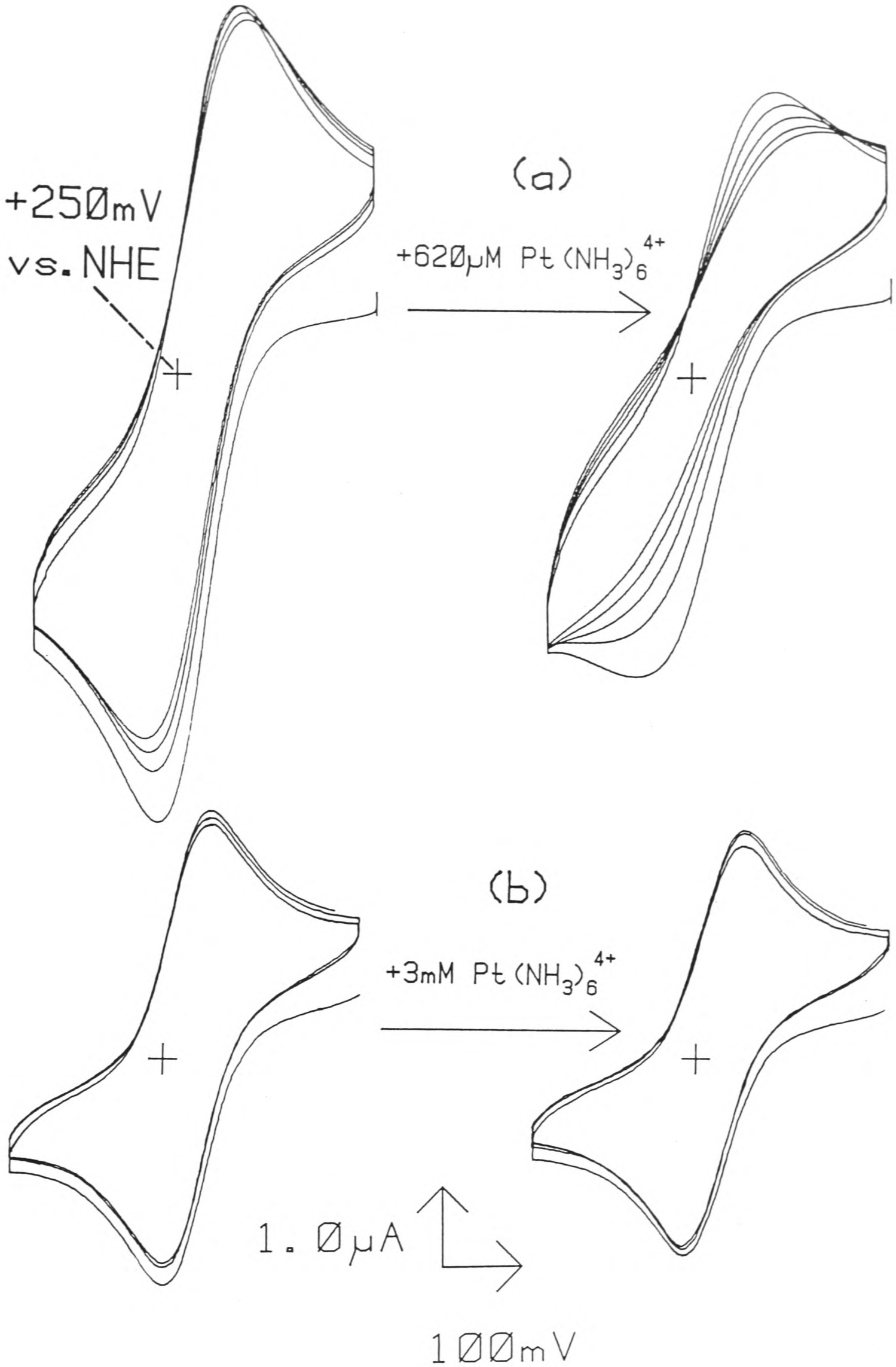

Figure 9.3: Cyclic voltammograms (20 mVs^{-1}) showing the effect of $Pt(NH_3)_6^{4+}$ additions (as indicated) on the direct electrochemistry of 1 mM cytochrome c (in 5 mM MES, 100 mM NaCl, pH6.0) at (a) edge graphite, and (b) a gold electrode surface-modified with bis(4-pyridine)bisulphide.

9.3.5 Competition Studies.

In the presence of multivalent cations (e.g. 10 mM $Cr(NH_3)_6^{3+}$) both cytochrome c (50 μM) and the 8Fe ferredoxin (150 μM) undergo quasi-reversible electron-transfer at an edge surface, despite the highly-contrasting net charge of these two proteins. Preliminary experiments were carried out at 'aged' electrodes and in solutions containing a mixture of the two proteins, in order to investigate site-selective interactions at edge graphite surfaces.

In a test solution containing cytochrome c (50 μM) and the 8Fe ferredoxin (67 μM), in the presence of 10 mM $Cr(NH_3)_6^{3+}$, each protein was observed to give the same stable, quasi-reversible electrochemical response as observed in the absence of the other protein. Similarly, at an electrode which has been previously 'aged' in a ferredoxin solution (67 μM) containing a sub-optimal level of $Cr(NH_3)_6^{3+}$ (50 μM), cytochrome c undergoes facile electron-transfer with no deterioration in response from that observed at the 'native' surface. The electrode showed no improvement in the ferredoxin response when returned to the ferredoxin solution.

9.4 Discussion of Cation Inhibition of Cytochrome c Electrochemistry.

Qualitative trends observed in the inhibition of cytochrome c electrochemistry by multivalent cations follow the order $M^{4+} > M^{3+} > M^{2+}$, in accord with the results previously described for the cation-promoted electrochemistry of negatively-charged redox proteins. This trend in cation effectiveness is consistent with the proposal that the basis for rationalising cation effects may rest on purely electrostatic grounds. In general terms, the quasi-reversible electrochemistry of cytochrome c in the absence of multivalent cations (100 mM NaCl) may be a consequence of favourable coulombic interactions between a negatively-charged electrode surface and an overall positively-charged redox protein. The addition of multivalent cations and their accumulation in the interfacial region, in response to a negative surface potential, will tend to weaken this electrostatic interaction.

In accord with previous discussions in this thesis, the inhibitory effect of cations may involve protein-cation association, electrode-cation association or simple diffuse layer effects. Despite the overall net positive charge of cytochrome c it is clear from equilibrium dialysis (8) (Ca^{2+}), electrophoresis (8) (Na^{+}, K^{+}, Mg^{2+}, Ca^{2+}), gel filtration (9) (Co^{2+}, Mg^{2+}) and NMR (2,10) ($Co(phen)_3^{3+}$, $Cr(NH_3)_6^{3+}$, $Cr(en)_3^{3+}$) studies that cations do bind to the surface of cytochrome c, although estimated binding constants (9) suggest only a weak association with divalent cations. This binding may involve association with acidic residues on the haem face of cytochrome c or at sites relatively far from the haem (2). However, it should be noted that $Pt(NH_3)_6^{4+}$ is an effective inhibitor of electrochemistry at

sub-stoichiometric amounts, which rules out protein-cation binding as the dominant effect in electrochemical studies with this cation. In addition, inhibition of electrochemistry in the presence of multivalent cations, such as $Pt(NH_3)_6^{4+}$, is observed at graphite but not at surface-modified gold electrodes. Clearly, the effect of multivalent cations is closely related to the nature of the electrode surface.

The involvement of diffuse, positive space charge density in cation de-promotion effects also seems unlikely at the high ionic stengths employed here (100 mM NaCl) where the diffuse layer is likely to be highly contracted. This observation suggests that the cations lie in a compact layer at the electrode surface and may serve to invert the potential at the OHP so presenting a positively-charged interface to freely-diffusing electroactive species. Preliminary experiments with the complex cation 'ruthenium red' provide direct evidence for the importance of irreversibly adsorbed cations in depromotion, although there is no evidence to suggest that $Pt(NH_3)_6^{4+}$ is similarly adsorbed at an edge surface through simple 'dip' experiments. However, it seems unlikely that a compact monolayer of cations is formed across the electrode surface in view of the differential inhibitory effects observed at low and high cytochrome c concentrations. Similarly, the apparent insensitivity of $Ru(NH_3)_6^{3+}$ to mobile, multivalent cations suggests that large regions of the surface may remain unpopulated by adsorbed cations. This is in accord with views as to the heterogeneous nature of edge graphite expressed earlier. Multivalent cations may be concentrated only at sites of high negative surface charge density.

The insensitivity of the faradaic response observed at surface-modified Au electrodes to additions of multivalent cations, may be a consequence of the nature of the binding domain at this surface. The bifunctional organic compounds used to modify this surface are typically dipolar in character rather than of discrete charge character. Thus, the binding interactions are postulated to involve discrete charge to dipole interactions (lysyl-NH_3^+ to pyridyl-N) which are less coulombic in nature than the discrete charge to discrete charge interactions which may occur at acidic (graphite) surfaces. This observation may be of relevance to the insensitivity of low cytochrome c concentrations to the addition of $Cr(NH_3)_6^{3+}$ and $Pt(NH_3)_6^{4+}$ at an edge graphite surface. Thus, the preferred protein-electrode interaction may be at sites affording charge-dipole or hydrogen-bonded interactions similar to those at surface-modified Au surfaces. As a consequence of the low cytochrome c concentration, less favourable binding sites carrying discrete negative charge density and a local surface excess of multivalent cations, may be successfully avoided. This is illustrated schematically in Figure 9.4. Plots of maximum peak current versus protein concentration for cytochrome c are linear only below 1 mM cytochrome c, suggesting that potentially productive sites for protein interaction do remain largely unoccupied at low cytochrome c concentrations.

The addition of Mg^{2+}, at low cytochrome c concentrations, to levels > 20 mM, does induce a decrease in electron-transfer rate (as evidenced by an increase in ΔE_p and a decrease in faradaic peak currents). However, no impersistence is observed under these circumstances. This may be indicative of a general repulsive effect at high levels of Mg^{2+}, exerted by regions of

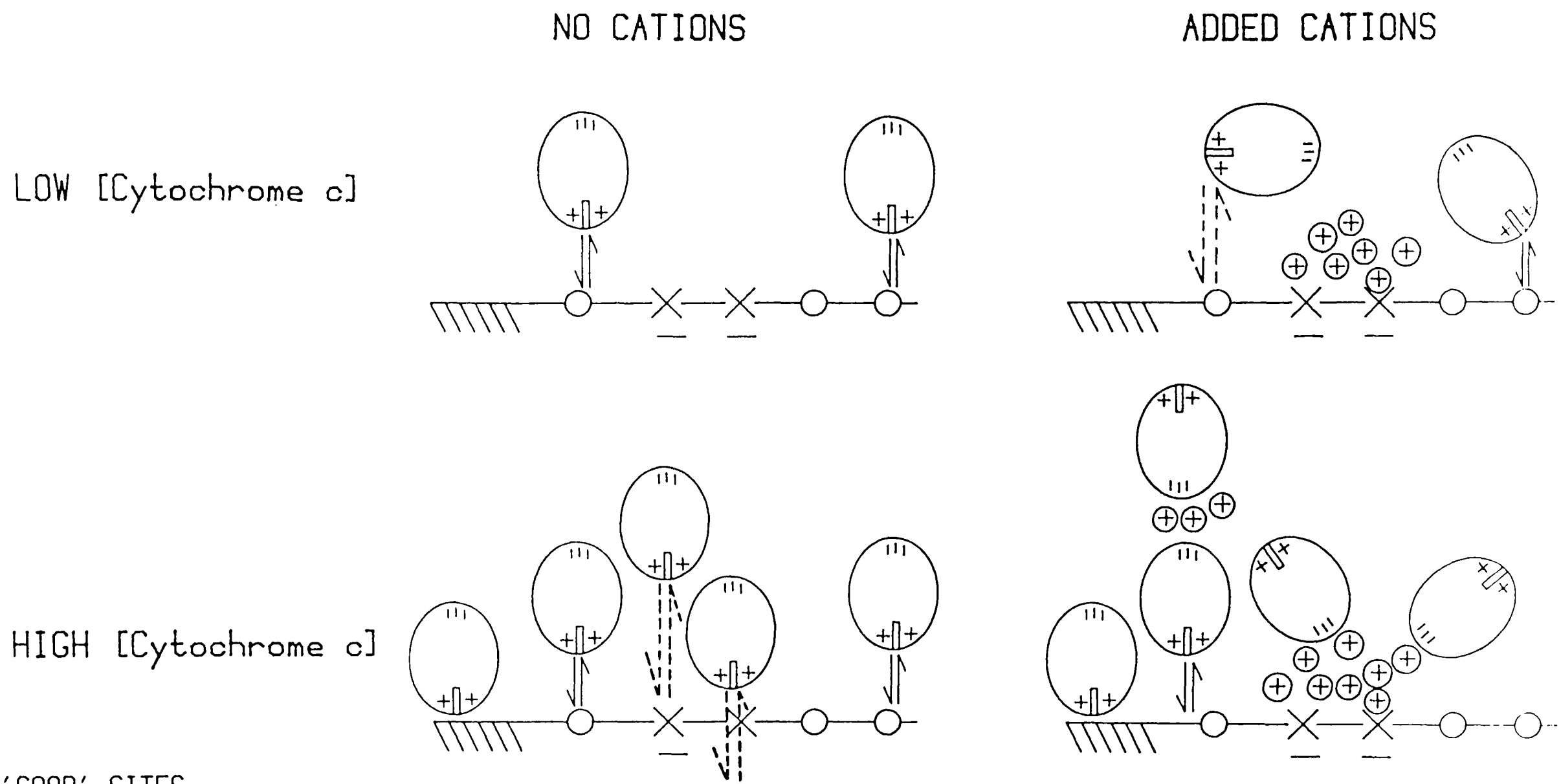

Figure 9.4: Schematic representation of the interaction between cytochrome c and edge graphite in the presence and absence of multivalent cations.

high, positive space charge density at the electrode surface. Although cytochrome c molecules will tend to avoid these sites, there may be an indirect effect as regions of high space charge density force re-orientation of the molecular dipole moment of cytochrome c molecules at adjacent sites in the interfacial region. As a consequence the exposed haem edge will become partially oriented away from the plane of the surface. This will increase the protein-electrode electron-transfer distance and may, additionally, weaken binding interactions, so decreasing, but not destabilising, the rate of heterogeneous electron-transfer.

Evidence to support a site heterogeneity model comes from (a) 'impersistence' studies and (b) the construction of a modified electrode bearing positive binding domains. At an edge surface modified with a high coverage of cationic Cr(III) complexes (ca. 50% monolayer with respect to C: see Chapter 11), the direct electrochemistry of cytochrome c is markedly de-promoted at **both** low (50 μM) and high (1 mM) protein concentrations. Clearly, at this modified surface, with a high coverage of Cr(III) complexes, cytochrome c molecules in the interfacial region are unable to 'avoid' positive-binding domains.

An edge electrode cycled in a solution of the 8Fe ferredoxin, at a sub-optimal level of $Cr(NH_3)_6^{3+}$, becomes inactive towards ferredoxin. However, the 'aged' electrode appears to retain full electron-transfer activity with 50 μM cytochrome c. Similarly, electrochemical responses are not perturbed in a mixture of the two proteins. This suggests that ferredoxin (67 μM) and cytochrome c (50 μM) utilise different functional sites at the electrode surface. Clearly, in this

instance, the edge surface behaves as if it were bifunctional. In a recent study of surface-modified Au electrode surfaces, an organic promoter has been reported which also facilitates bifunctional electrochemistry (11). This promoter 2-(pyridinylmethylene)hydrazinecarbothioamide allows quasi-reversible direct electrochemistry of plastocyanin, multi-modified cytochrome c and native cytochrome c.

At high protein concentrations (1 mM cytochrome c), the electrochemistry at an edge graphite electrode (1 mM cytochrome c in 100 mM NaCl alone) is an order of magnitude slower than in the low (35 μM) cytochrome c limit. This may reflect severe molecular crowding at the interface and repulsive protein-protein interactions, or the influence of surface heterogeneity i.e. there is a low density of productive binding sites at the surface. It is noteworthy that at high cytochrome c concentrations, the faradaic response at a surface-modified Au electrode is still essentially reversible. This reflects the more homogeneous nature of this surface associated with a surface 'carpet' of pyridyl functions.

The effect of crowding or heterogeneity at an edge graphite surface will be to force protein molecules on to disfavoured sites such as hydrophobic regions or regions of discrete negative charge density. The resulting impersistence indicates that these encounters are unproductive with a time-dependent blocking of the surface through permanent, or long-lived, protein-electrode interactions, which prevent exchange with the bulk of solution. This may occur through strong electrostatic interactions between lysyl residues and discrete surface charges. Alternatively, there may be strong hydrophobic

interactions between regions of basal plane character and the hydrophobic microenvironments located at the top and bottom of the haem crevice (12) on cytochrome c.

The addition of multivalent cations strongly destabilises the observed faradaic response of 1 mM cytochrome c. This supports the proposal that at high protein concentrations, cytochrome c is forced to bind at sites of discrete charge density. These sites will also bind multivalent cations. In accordance with this proposal, cation addition is ineffective at perturbing the electrochemical reponses of 1 mM cytochrome c at the dipolar, surface-modified Au electrode.

The nine acidic residues (4 aspartate and 5 glutamate) of cytochrome c are distributed inhomogeneously on the surface of the protein. The centre of negative charge calculated from the atomic co-ordinates of cytochrome c (4) is located at the back and right of the molecule i.e. the acidic face is essentially diametrically opposed to the haem face. It is the former which is the main contributor to the dipole moment of cytochrome c. In response to the generation of regions of positive space charge density in the Stern layer, by bound multivalent cations, there will be a reorientation of cytochrome c and approach to the surface in a 'backside' orientation. The acidic residues presented at or close to the surface in this orientation may be expected to bind strongly to the multivalent cations in the compact layer at the electrode surface, so forming unproductive protein-cation-electrode bridges, Figure 9.4. Another possibility is that multivalent cations cause protein-protein binding, through cation-bridged interactions between the acidic face of a cytochrome c molecule in the first layer at the electrode surface

and the acidic face of another molecule in the second layer at the surface. Unproductive binding interactions will block the electrode surface and cause a deterioration in the observed faradaic response.

Competition studies with two or more proteins in solution and further studies at electrodes which have been previously 'aged' in a ferredoxin solution, may provide the basis for future studies at edge graphite electrodes, with a view to elucidating the importance of site-selective interactions.

RESULTS:

9.5 Multi-Substituted CDNP Cytochrome c and Cytochrome c_{551}.

At an edge graphite surface in the absence of multivalent cations (5 mM Tricine, 1 mM NaCl pH 8.0), multi-substituted CDNP-cytochrome c (0.15mM) and cytochrome c_{551} (0.15mM) show no faradaic responses, Figure 9.5(a,b). However, the addition of 10 - 20 mM $MgCl_2$ is sufficient to stimulate persistent faradaic responses consistent with quasi-reversible electrochemistry: multi cytochrome c, ΔE_p = 65 mV (20 mVs^{-1}, scan 4, 10 mM $MgCl_2$); cytochrome c_{551}, ΔE_p = 80 mV (20 mVs^{-1}, scan 4, 20 mM $MgCl_2$). At a lower protein concentration (50 μM), the faradaic response of cytochrome c_{551} shows an improvement in the electron-transfer rate and a decrease in the overall Mg^{2+} requirement: ΔE_p = 67.5 mV (20 mVs^{-1}, scan 4, 6 mM $MgCl_2$).

The $E_{1/2}$ of cytochrome c_{551} (+267 mV vs NHE, pH 8.0) is in good agreement with one calculated (+257 mV vs. NHE, pH 8.0) from an $E_{1/2}$ vs pH curve (13). A potentiometric redox potential for multi-substituted CDNP-cytochrome c has not previously been reported. The electrochemically-derived $E_{1/2}$ of +422 mV vs. NHE shows a substantial positive shift in redox potential relative to native cytochrome c (+257 mV vs. NHE).

Electrochemical studies of cytochrome c_{551} and multi-cytochrome c at a cleaved basal plane surface revealed only weak faradaic responses in the expected potential domains (multi-cytochrome c: Figure 9.5(a)), although in each case the response was complicated by intrinsic 'surface' peaks.

9.6 Discussion

The electrochemical responses of multi-substituted CDNP-cytochrome c and cytochrome c_{551} show an edge-basal surface

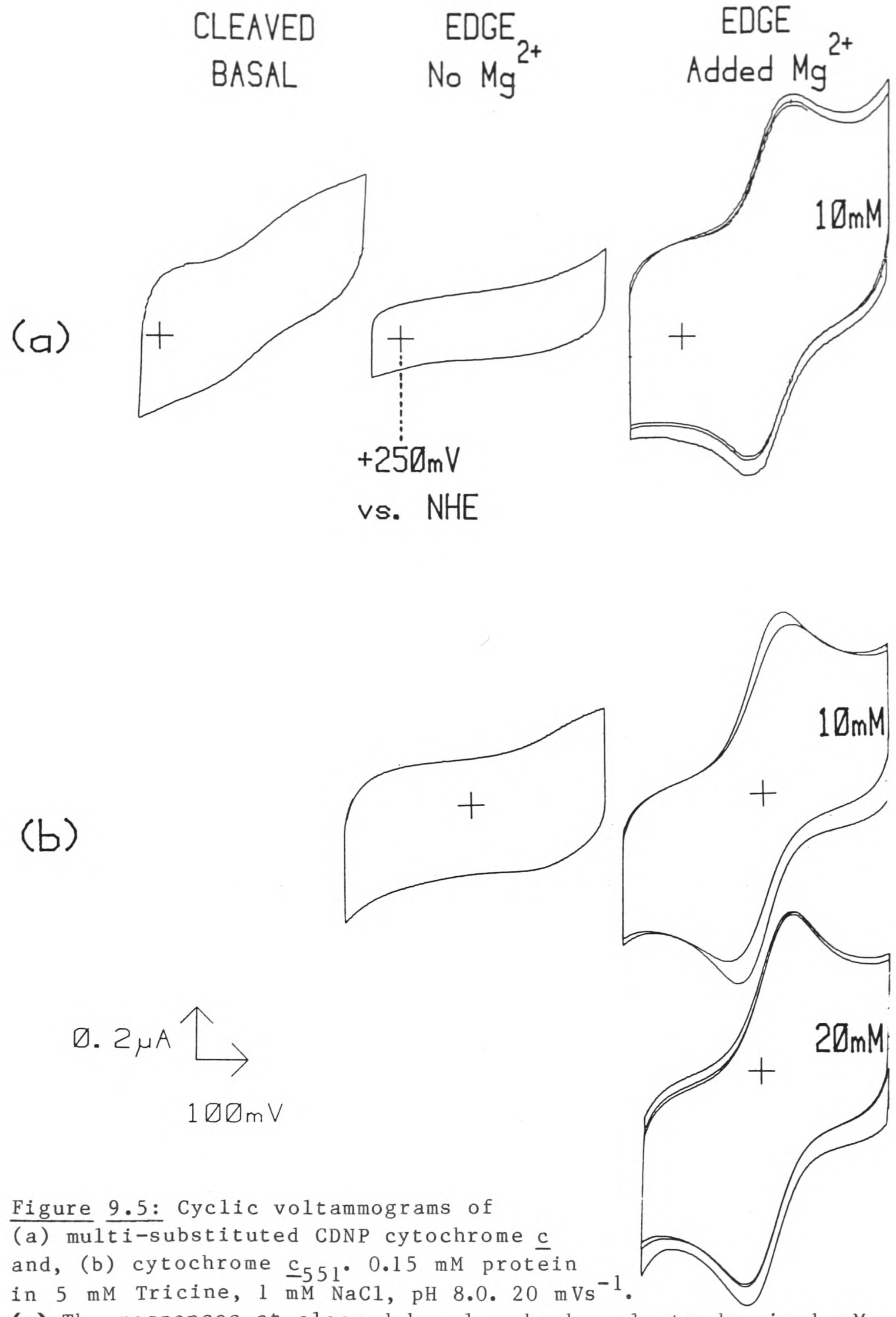

Figure 9.5: Cyclic voltammograms of (a) multi-substituted CDNP cytochrome c and, (b) cytochrome c_{551}. 0.15 mM protein in 5 mM Tricine, 1 mM NaCl, pH 8.0. 20 mVs^{-1}. **(a)** The responses at cleaved basal and edge electrodes in 1 mM NaCl only, are shown (scan 4). Also shown is the response at the edge following the addition of Mg^{2+} to 10 mM (scans 1 - 3). **(b)** The response at the edge in 1 mM NaCl only (scan 4), and after the addition of Mg^{2+} (10mM and 20mM) is shown (scans 1,4).

selectivity, a feature in common with the electrochemical responses of all other redox proteins at pyrolytic graphite. More importantly, perhaps, both proteins show a requirement for multivalent cation promoters, a characteristic feature of those proteins bearing negatively-charged binding domains or an overall net negative charge. This observation may be of significance in discussions of the fundamental importance of **net** protein charge, which will be important in determining diffuse layer effects at low ionic strengths, vs. **local charge**, which will influence specific binding interactions, in interfacial interactions.

Quasi-reversible electrochemistry of multi-substituted CDNP cytochrome c has also been reported (11) at surface-modified Au electrodes. Only those modifiers capable of providing a positively-charged interface were found to be effective (e.g. $HS-CH_2CH_2-NH_3^+$), in accord with the requirement for multivalent cation promoters at edge graphite. The $E_{1/2}$ of multi c at surface-modified Au (+412 mV vs NHE) shows the same positive shift as that observed at edge graphite.

It has been proposed that the redox potentials of c-type cytochromes are largely determined by the fifth and sixth iron ligands, the nature of the polypeptide environment surrounding the haem (14) and the degree of exposure of the haem to solvent (15). On this basis, the large positive shift in redox potential between native cytochrome c and multi-substituted cytochrome c implies a structural perturbation of the polypeptide chain in the region of the haem. It has been shown that 'open-closed' perturbations of the haem crevice, controlled by modification of surface lysine groups, may be linked with the pKa of the methionine[80]-haem link (12). This pKa may be conveniently

assessed by faradaic response pH titrations (see Chapter 6) and may warrant a future study to confirm the cause of the large shift in redox potential.

Clearly, direct electrochemical studies of multi cytochrome c can only be of limited mechanistic importance. Firstly, this protein is an inhomogeneous preparation lacking a well-defined specific number and spatial disposition of individual modified lysines. Secondly, although this protein has an overall net negative charge there may also be localised negative charges on the haem face. Similarly, native cytochrome c has both an overall positive charge and also localised positive charges on the haem face. Consequently, the switch from cation-inhibited (native) to cation-promoted (multi) electrode reponses may represent a complex interplay of local and net charge in interfacial interactions. Nevertheless, these studies have demonstrated the feasibility of specific residue modification in direct electrochemistry. A comparison of the electrochemical activity of closely related CDNP-cytochrome c derivatives, incorporating a single, well-defined, amino acid change, to eliminate specific lysine residues, may permit the specific importance and definition of local binding domains to be elucidated. Such a study is currently in progress in this laboratory (16).

A more informative protein, from the viewpoint of local vs. net charge is cytochrome c_{551}. However, there have been comparatively few direct electrochemical studies of this redox protein (17,18). It is clear that the individual lysine groups on the haem face are not solely important in determining the electrostatic interactions at edge graphite, since the

requirement for multivalent cationic promoters implicates a functional role for the acidic residues on this protein.

The specific role of acidic residues may be expressed in one of several ways. Firstly, this cytochrome carries an overall negative charge at neutral pH, as indicated by the pI of 4.7. Estimates of the total charge at this pH, based upon a charge count among the amino acid residues, suggest the net charge to be 1-. Under the conditions of low ionic strength (1 mM NaCl) employed in this study, the role of Mg^{2+} may simply be to relieve long range repulsive electrostatic interactions between electrode and protein surfaces, both of which carry net negative surface charge densities. Secondly, at distances of close approach between the two surfaces, cations may be involved in specific short range interactions by 'bridging' acidic residues on protein and electrode surfaces. This may involve only those acidic residues on the front half of the molecule (as drawn in Figure 9.1) to satisfy a likely constraint that the haem face be proximal to the electrode surface. The only suitable residue in this case seems to be Asp-19. However, unlike cytochrome c, that part of the haem edge exposed to solvent in cytochrome c_{551} bears the haem propionates. These propionic acids are more exposed and less hydrogen-bonded than in cytochrome c. The ionisation of one of the haem-linked propionic acids (pK_{ox} = 6.2) has been linked with the pH-dependent redox potential of cytochrome c_{551} (13). It may be that the requirement for multivalent cationic promoters arises from the discrete charge associated with a solvent-exposed, ionised haem propionic acid at pH 8.0.

Alternatively, in the absence of long range electrostatic repulsion, short range interactions may arise which are

independent of acidic residues. These may involve hydrophobic interactions between the hydrophobic haem face and areas of basal plane character on the electrode surface or specific hydrogen-bonding interactions to the haem face lysine residues. Interestingly, studies of cytochrome $\underline{c}_{551}$ at surface-modified gold surfaces (17) show that, at high ionic strength (100 mM $NaClO_4$), quasi-reversible electrochemistry is observed, not with positively-charged promoters, but at promoters bearing pyridyl-N functions, in accord with short range hydrogen-bonded interactions to haem-face lysine residues.

Clearly, these initial studies of cytochrome $\underline{c}_{551}$ do not unequivocally implicate the functional importance of either local or net charge, but suggest that at low ionic strengths (1 mM NaCl) the protein behaves as a net negatively-charged 'sphere' giving rise to long range electrostatic interactions. At high ionic strengths (100 mM NaCl) where long-range electrostatic interactions are effectively 'screened', there may be short-range interactions involving haem-face lysine residues.

References - Chapter 9

1) Chapman, S. K., Sinclair-Day, J. D., Sykes, A. G., Tam, S. C. and Williams, R. J. P., J. Chem. Soc. Chem. Commun. 1152, (1983).

2) Moore, G. R., Ragg, E., Eley, C. G. S. and Williams, G. in: Advances in Inorganic and Bioinorganic Chemistry. Sykes, A. G. ed. (1984).

3) Koppenol, W. H. and Margoliash, E., J. Biol. Chem. 257, 4426, (1982).

4) Koppenol, W. H., Vroonland, C. A. J. and Braams, R., Biochim. Biophys. Acta 503, 499, (1978).

5) Matsuura, Y., Takano, T. and Dickerson, R. E., J. Mol. Biol. 156, 389, (1982).

6) Horio, T., Higashi, T., Sasagawa, M., Kusai, K., Nakai, M. and Okuniki, K., Biochem. J. 77, 193, (1960).

7) Armstrong, F. A., unpublished result.

8) Magoliash, E., Nature 228, 723, (1970).

9) Margalit, R. and Schejjer, A., Eur. J. Biochem. 46, 387, (1974).

10) Williams, G., D. Phil Thesis. Oxford (1983).

11) Hill, H. A. O., Page, D. J., Walton, N. J. and Whitford. D., J. Electroanal. Chem. 187, 315, (1985).

12) Osheroff, N., Borden, D., Koppenol, W. H. and Margoliash E., J. Biol. Chem. 255, 1689, (1980).

13) Moore, G. R., Pettigrew, G. W., Pitt, R. C. and Williams, R. J. P., Biochim. Biophys. Acta 590, 261, (1980).

14) Kassner, R. J., J. Am. Chem. Soc., 95, 2674, (1973).

15) Stellwagen, E., Nature 275, 73, (1978).

16) Whitford, D., unpublished results.

17) Walton, N. J., D. Phil Thesis. Oxford (1984).

18) Bianco, P., Haladjian, J., Loutfi, M. and Bruschi, M., Biochem. Biophys. Res. Commun. 113, 526, (1983).

CHAPTER 10

THE ROLE OF MULTIVALENT CATIONS IN DIRECT ELECTROCHEMICAL STUDIES OF REDOX PROTEINS - SUMMARY AND DISCUSSION

The initial observations of the direct electrochemistry of redox proteins (Chapter 4) led to the proposal that due consideration of the net charge of a redox protein provides the basis for controlling direct electrochemical responses at polished graphite electrodes, based upon the presence or absence of multivalent cations [Mg^{2+} or $Cr(NH_3)_6^{3+}$]. The precise role of multivalent cations has been investigated in subsequent chapters through extensive studies of the direct electrochemistry of Fe-S proteins (Chapter 7), plastocyanin (Chapter 8) and c-type cytochromes (Chapter 9).

The general conclusion of these chapters, applicable to all the redox proteins studied, is that the order of effectiveness of multivalent cations is $M^{4+} > M^{3+} > M^{2+} > M^{+}$. This strongly suggests that the determining constraint, in direct electrochemical studies at graphite, is of an electrostatic nature. Studies of a range of cations, of the same charge type, were restricted to the 8Fe ferredoxin. However, it is clear, at least for this protein, that the important feature of a cation is simply the valence type of that cation, in accord with simple electrostatic effects. With few exceptions (e.g. the divalent cations: Mg^{2+} and $Fe(phen)_3^{2+}$) the specific chemical nature of a cation is only of secondary importance. No significant differences are observed between the effectiveness of various monovalent or trivalent cations.

At low concentrations (28 μM) of the 8Fe ferredoxin, the optimal faradaic response is independent of the cation charge, and the faradaic response promotion profiles differ only in the levels of cation required. However, the disparity between cations of differing charge type becomes especially marked at higher protein concentrations. In addition, the absolute level of any particular cation required to promote the optimal faradaic response of a negatively-charged redox protein is critically dependent upon protein concentration. At increased protein concentrations cation requirements are higher and faradaic responses less stable. It appears that the electrode processes, at high protein concentrations, are governed by electrode surface heterogeneity and lateral interactions between protein molecules.

Studies on the larger, more highly-charged proteins reveal a number of interesting features. Thus, $Cr(NH_3)_6^{3+}$, but not Mg^{2+}, stabilises quasi-reversible direct electrochemistry of plastocyanin (at room temperature) or the 2Fe ferredoxin. Furthermore, the problem of 'impersistence' (a gradual deterioration of faradaic response) is particularly marked for plastocyanin. Faradaic responses can be stabilised by the use of higher valent cations, low temperatures ($3^{o}C$), or low pH. The problem of impersistence may be traced to the properties of the protein in solution, in particular the structural rigidity of the protein. Thus, for flexible proteins, electrostatic interactions may not be the only factor governing binding interactions at electrode surfaces. The studies on plastocyanin indicate that the the most efficient cation at regulating electrochemical responses may always be a tetravalent cation, e.g. $Pt(NH_3)_6^{4+}$.

There is no clear correlation between cation requirements and the redox potential of a particular protein. Similarly, cation effects are evident in the potential range ca. -600 mV vs. SCE to ca. +200 mV vs SCE. This suggests that the important feature of the **electrode** surface appears to be oxidised C-O functional groups which provide sites of discrete charge character, as indicated by the control of electrochemical responses by edge-surface protonation equilibria, in the absence of multivalent cations.

Multivalent cations are effective at both low (1 mM NaCl) and high (100 mM NaCl) ionic strengths. It is also important to note that the $Cr(NH_3)_6^{3+}$ levels required to promote optimal faradaic responses of plastocyanin and ferredoxins (8Fe and 2Fe), increase with increasing ionic strength. At high ionic strengths diffuse-layer effects will be unimportant. Thus, highly-charged proteins will be able to approach the electrode surface unhindered by long-range electrostatic effects. Short-range interactions will then be the determining feature in orienting and binding redox proteins at the surface. However, at high ionic strengths, electrostatic binding interactions, such as those clearly implicated by the increase in $Cr(NH_3)_6^{3+}$ requirement with increasing ionic strength, will be weakened. At low ionic strengths, electrostatic binding interactions will be strong, although, under these conditions, diffuse-layer effects will provide an additional constraint upon interfacial interactions. These statements suggest that there will be a unique ionic strength, for any particular protein, at which diffuse layer effects and electrostatic binding interactions are finely balanced to give an optimal interaction at the surface.

Electrostatic association may occur through protein-cation binding or electrode-cation binding. There is firm experimental evidence that both of these association terms are important factors to be considered. ^{1}H-NMR studies of C. pasteurianum ferredoxin have shown that for $Cr(NH_3)_6^{3+}$ (but not Mn^{2+}) there is a protein-cation binding interaction which is electrostatic in nature. The binding of $Cr(NH_3)_6^{3+}$ to regions of uncompensated surface charge will facilitate protein-electrode and protein-protein interactions. The results of NMR studies reported by other workers (see Chapters 7 and 8) show that a similar conclusion may also apply to the 2Fe ferredoxin and plastocyanin.

The importance of electrode-cation binding is demonstrated by the irreversible adsorption of $Fe(phen)_3^{2+}$ and ruthenium red at edge graphite surfaces. The direct electrochemistry of the 8Fe ferredoxin is promoted at an $Fe(phen)_3^{2+}$-modified electrode in the absence of mobile, multivalent cations. The direct electrochemistry of cytochrome c is partially inhibited at a ruthenium red-modified surface. Moreover, the trivalent and tetravalent cations are often effective at sub-stoichiometric amounts, suggesting that there is prior association of these cations with the electrode surface and that the cationic sites so formed provide the basis for protein-cation interactions.

This proposal raises the intriguing possibility that direct electrochemical responses are regulated by the chance formation of protein-cation-electrode 'bridges'. It is notable that the most efficient divalent cationic promoters are the organic di-cations ($^{+}Me_3N(CH_2)_xNMe_3^{+}$; where x=6 or 10) and $Fe(phen)_3^{2+}$, which provide the opportunity for protein-electrode bridging interactions. In addition, the $Cr(NH_3)_6^{3+}$ binding site on the 2Fe

ferredoxin is in the same region as the binding site for the physiological redox partner (FNR). Thus, a protein-cation-electrode 'bridge' may orient this protein in such a way that the electron-transfer site is in close proximity to the electrode surface. Any further discussion of the 8Fe and 2Fe ferredoxins must await the assignment of specific resonances in the ^{1}H-NMR spectra of these proteins. However, it is relevant to note, in the context of this discussion, that a more precise definition of the nature of cation binding sites has been made in the case of flavodoxin, which is known to undergo $Cr(NH_3)_6^{3+}$-promoted direct electrochemistry at edge (1) and polished basal (Chapter 4) plane electrodes.

Preliminary experiments by ^{1}H-NMR (2) on the association of $Cr(NH_3)_6^{3+}$ to <u>D. vulgaris</u> flavodoxin have clearly demonstrated that binding sites both close to, and distant from the prosthetic group exist. Resonances broadened by the binding of $Cr(NH_3)_6^{3+}$ to the oxidised protein are also selectively broadened by one electron reduction of the protein to the semiquinone form (in the absence of $Cr(NH_3)_6^{3+}$). This shows that there is a cation binding site close to the flavin moiety. The peak most affected by $Cr(NH_3)_6^{3+}$, which is also affected by reduction of the flavin, arises from the H9 proton of the isoalloxazine ring system or from the H2 proton of Trp-60, both of which would suggest that the $Cr(NH_3)_6^{3+}$ might bind somewhere between strands 59-62 and 65-67, as shown in Figure 10.1, coordinated possibly to Asp-63 and/or Glu-66. It is interesting to note that kinetic studies with flavodoxins have suggested (3) that the "point of entry and exit of the electron" is the exposed dimethylbenzene ring of the flavin. This point is in close proximity to the $Cr(NH_3)_6^{3+}$

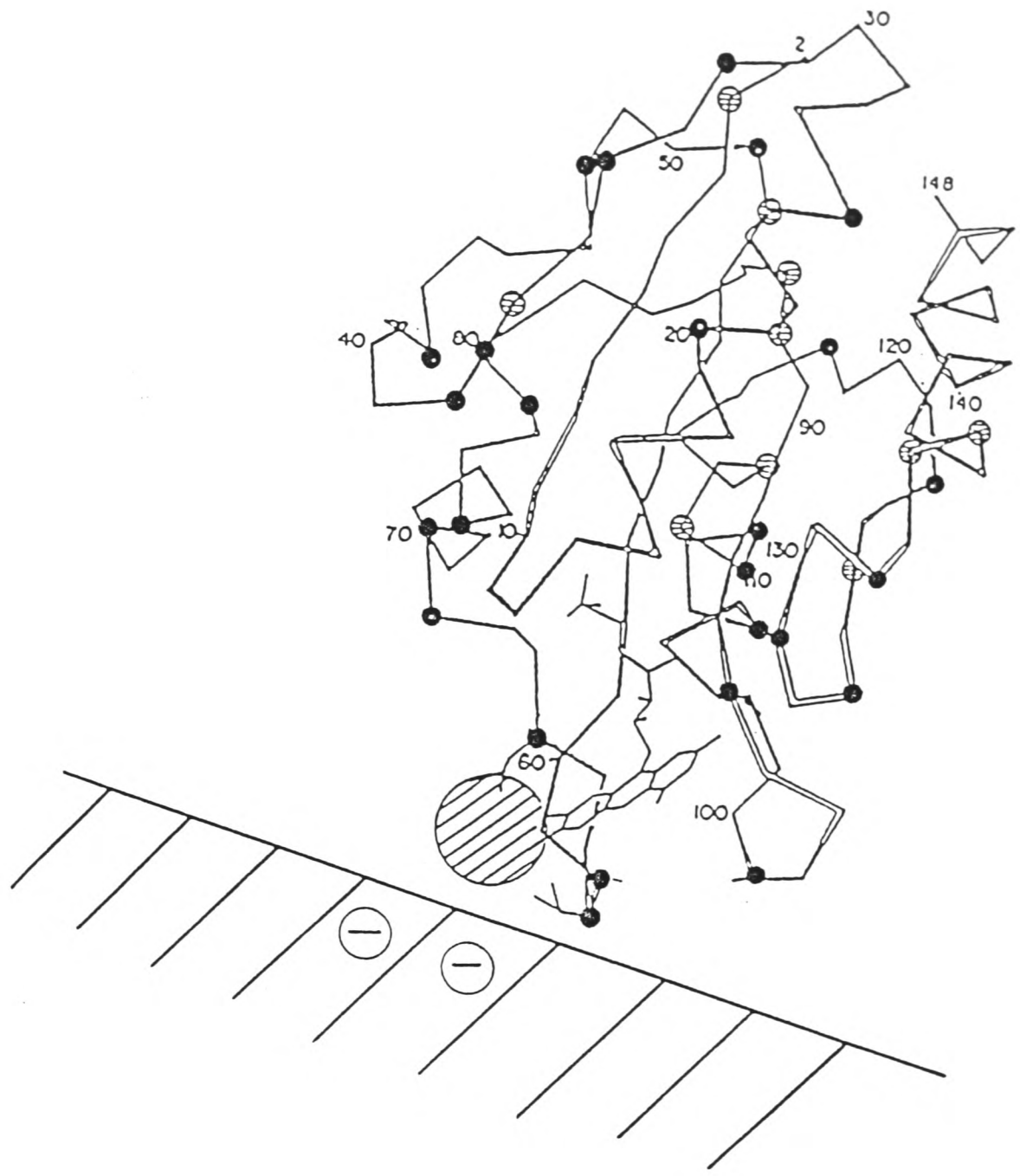

Figure 10.1: The backbone structure of D. vulgaris flavodoxin showing the positions of acidic (●), and basic (◍) residues. The position of a binding site of $Cr(NH_3)_6^{3+}$ close to the FMN group (◍), which may serve to 'bridge' a protein-electrode interaction, is indicated.

binding site. Therefore, it appears that a specific cation-protein-electrode 'ternary' bridge would facilitate the attainment of an (ideally) optimal orientation of the protein at the electrode with the shortest possible electron-transfer distance, as illustrated in Figure 10.1. A similar 'model' of the interfacial binding interactions has been proposed for plastocyanin (Chapter 8).

The only suitable 'general' model of the interface which may be proposed at present is one in which electrostatic stabilisation of the interfacial region occurs by condensation of counter-ions around protein molecules to form an irregular lattice framework of proteins and cations localised over specific regions on the electrode surface. Within this lattice there may be specific and local effects involving cation-protein ion-pairing, ion adsorption at the surface and, possibly, protein-cation-electrode 'bridge' interactions. Further, since the edge is hydrophilic, since water molecules solvate the counter-ions and since protein molecules may be heavily hydrated then there may be collective protein + water + counter-ion effects. The concept of molecular assemblies and the role of boundary water has been discussed recently by Parsegian and Rau (4).

References - Chapter 10

1) Armstrong, F. A., unpublished results.

2) Kitchen, N. A., D. Phil. Thesis. Oxford (1984).

3) Jung, J. and Tollin, G., Biochemistry 20, 5124, (1981).

4) Parsegian, V. A. and Rau, D. C., J. Cell Biol. 99, 196, (1984).

CHAPTER 11

A CHARGE-MODIFIED GRAPHITE ELECTRODE

11.1 Introduction.

The direct (un-mediated) electrochemistry of redox proteins has been readily achieved at edge-plane oriented pyrolytic graphite electrodes (see, for example, Chapter 4), at whose surface, mammalian cytochrome c, positively-charged at pH 7, undergoes stable and quasi-reversible electron transfer. However, most redox proteins carry a significant overall negative charge at pH 7. For these proteins, the observation of direct electrochemistry necessitates the inclusion of mobile multivalent cations such as Mg^{2+}, $Cr(NH_3)_6^{3+}$ or $Pt(NH_3)_6^{4+}$.

Direct electrochemical studies of negatively-charged redox proteins at polished graphite surfaces are often subject to a gradual deterioration of faradaic response, termed 'impersistence', which is particularly marked under sub-optimal conditions. It has been shown that a suitable combination of low protein concentration, low temperature (ca. 3°C), and higher-valent cations can effectively stabilise electrochemical responses.

The observation of 'impersistence' suggests that the electrode surface is highly heterogeneous and may have a wide range of binding environments, some offering more productive binding domains than others. Redox proteins may interact with the surface through hydrophobic or ionic interactions. The effects of 'impersistence' are noticeably less marked at surface-modified Au surfaces, which may present a more controlled, 'homogeneous' binding domain at the electrode-solution interface.

A functional graphite electrode, permitting reversible binding of negatively-charged redox proteins, needs to incorporate well-defined positively-charged binding domains. However, few 'native' electrode surfaces are positively-charged at neutral pH. Thus, the generation of positively-charged binding domains necessitates specific electrode modifications. This chapter describes the construction of surface-bound cationic sites at an edge-oriented graphite electrode. The modification strategy follows one of specific chemical modification of surface C-O groups, so utilising the readily-generated, rich functional chemistry of the edge surface.

The basis of the modification technique arises from homogeneous kinetic and ^{1}H-NMR studies of protein-cation binding (see Chapter 7). These studies have shown that there is preferential association of Pt(IV), Cr(III) and Co(III) hexa-ammine complexes with a single (dominant) region of negatively-charged redox proteins, such as plastocyanin, flavodoxin, 8Fe ferredoxin and 2Fe ferredoxin. There is every likelihood that the cationic binding domains are also sites relevant to physiological electron-transfer reactions. The generation of electrode surface-bound cationic ammine complexes may then provide a binding site for freely-diffusing protein molecules, in which the site on the protein surface used for electron-transfer is in a favourable position for rapid protein-electrode electron transfer to occur.

A projected reaction scheme, outlined as shown in Scheme 11.1, involves the electrochemical generation of reactive, substitution-labile Cr(II) species, a proportion of which may coordinate to surface C-O functional groups, yielding substitution-inert Cr(III) complexes incorporating electrode

SCHEME 11.1

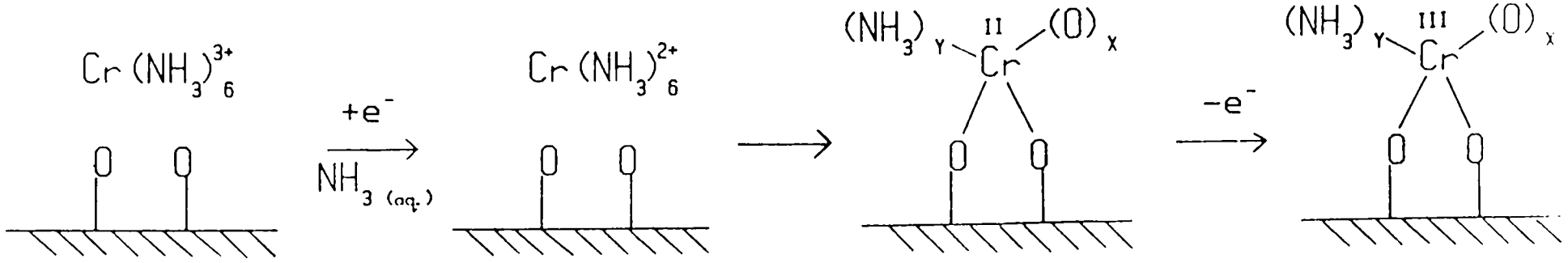

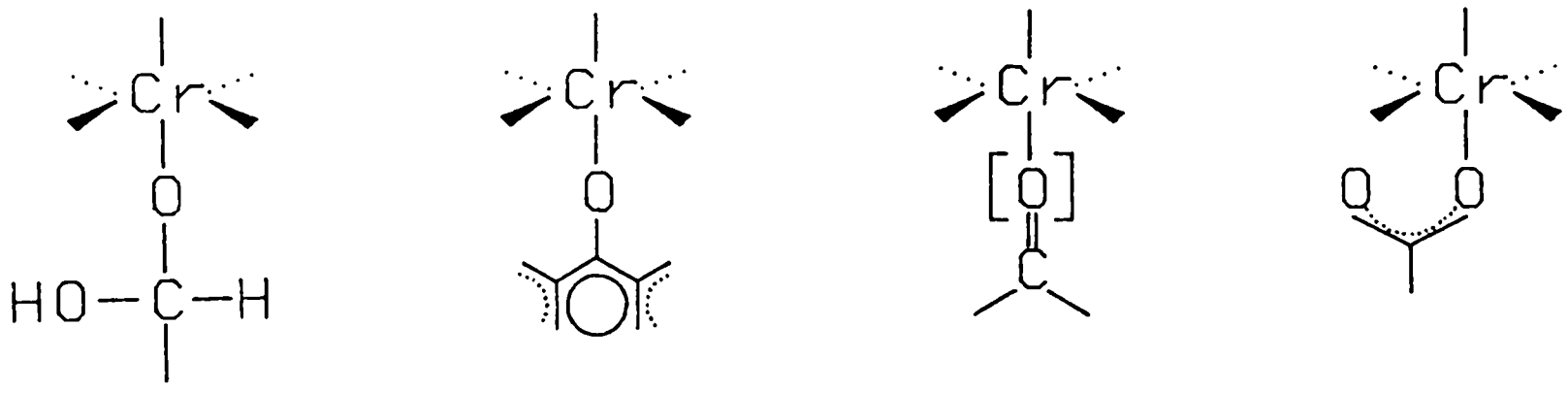

Figure 11.1: Examples of the electrode surface C-O groups which may be incorporated into Cr(III) surface complexes.

surface C-O groups. The various possible linking groups which may be provided by an edge surface are illustrated in Figure 11.1. Comparable Cr(III)-oxygen bonds have been reported in the cathodic pinacolisation of benzaldehyde and benzophenone by $CrCl_3$ (Cl_3Cr-O=CR_1R_2) (1), and in the Cr(II) reduction of maleatopentaamminecobalt(III) (Cr(III)-carboxylate chelate complex) (2).

The complex $Cr(NH_3)_6^{3+}$ was used to permit surface modification to be carried out in concentrated aqueous ammonia solution without complications due to insoluble Cr(III) hydroxy species. The use of aqueous ammonia ensures de-protonation of acidic surface groups, and the competition of NH_3 with H_2O (OH^-) for the remaining co-ordination sites is expected to minimise formation of lower-charged polymers through olation and oxolation (3).

11.2 Experimental Details

The all-glass electrochemical cell used in modification cycles was a large volume (ca. 10 mL total), three compartment cell. The reference electrode (saturated calomel [SCE]) compartment was connected to the working compartment through a Luggin capillary. The counter electrode was a platinum gauze, separated from the working compartment by a glass frit. Both of the side arms were filled with an aqueous solution of NH_4Cl [30 mM] (BDH, Analar). The working compartment was carefully dried with a cotton wool bud before adding 3 mL of concentrated aqueous ammonia solution (BDH, Analar). Reproducible modifications were only obtained when a new winchester of 880 ammonia was opened immediately prior to use. The use of 'old' ammonia solutions gave

irreproducible results and poor electrode modification. For modification cycles, the cell contained an ammonia solution of $Cr(NH_3)_6Cl_3$ (typically 10 mM). In between modification cycling, a close-fitting Teflon cap was placed over the working compartment. Modification solutions were frequently renewed during several hours of modification. Control experiments were performed in a concentrated aqueous ammonia solution of NH_4Cl (typically 100 mM).

Electrode discs were cut from standard pyrolytic graphite (Le Carbone, Portslade, Sussex) with the a-b (basal) plane perpendicular to the disc face. For examination of protein electrochemistry, a 5 mm disc was sealed in a Teflon electrode sheath. For parallel studies in which modification was examined by X-ray photoelectron spectroscopy, a 9 mm disc was mounted in a PVC girdle and electrical contact was achieved by insertion of a stainless steel needle into the intersection. Spectra were obtained with an ESCALAB 5 spectrometer (VG Scientific, U.K.) with a Mg $K\alpha_{1,2}$ excitation source (1253.6 eV) (see Chapter 5). Spectroscopic analysis of modified edge graphite discs was carried out in subdued lighting conditions to prevent photolysis of Cr(III) ammine surface complexes. The apparatus and conditions used in direct electrochemical studies were as described in Chapters 4 and 7.

Results and Discussion

11.3 Surface Modification of Edge-oriented Graphite by Reductive Cycling.

An edge-oriented pyrolytic graphite electrode cycled (20 mVs^{-1}) over the range 0 to -1500 mV vs. SCE in a concentrated aqueous ammonia solution of $Cr(NH_3)_6^{3+}$ (10 mM, plus 0.1 M NH_4Cl) gives the voltammetric response shown in Figure 11.2(a). Two features are seen in the initial (scan 1) reduction cycle. A strong peak at ca. -1350 mV and a small shoulder at -1050 to -1150 mV vs. SCE. These reductions appear irreversible i.e. no re-oxidation waves are visible in the reverse (anodic) sweep. In the absence of $Cr(NH_3)_6^{3+}$, no faradaic processes were observed at potentials positive of -1500 mV. It appears that the observed electrode processes are associated with the reduction of $Cr(NH_3)_6^{3+}$. Indeed, the observed electrochemical activity lies close to reported values of the polarographic reduction potential for $Cr(NH_3)_6^{3+}$ [-0.93 V vs. SCE in Divers' liquid (NH_3/NH_4NO_2) (4); -0.97 V vs. SCE in acetate buffer (5)].

Successive cycles in the $Cr(NH_3)_6^{3+}$- aqueous NH_3 solution show a cathodic shift in the voltammetric response, in parallel with a decrease in the cathodic peak currents. This effect is not simply due to depletion of the electroactive species in the diffusion layer. Agitation of the electrode between consecutive scans does not restore the initial (scan 1) faradaic response.

Following reductive cycling (11 scans) in the $Cr(NH_3)_6^{3+}/NH_3$ solution, the electrode was rinsed and then vigorously stirred, or sonicated, in buffer solution for up to 10 mins. Subsequent voltammetric cycling (Figure 11.2(b): -400 to -1500 mV; 20 mVs^{-1}) in deoxygenated buffer solution (20 mM Tricine, 100 mM KCl, pH8.0),

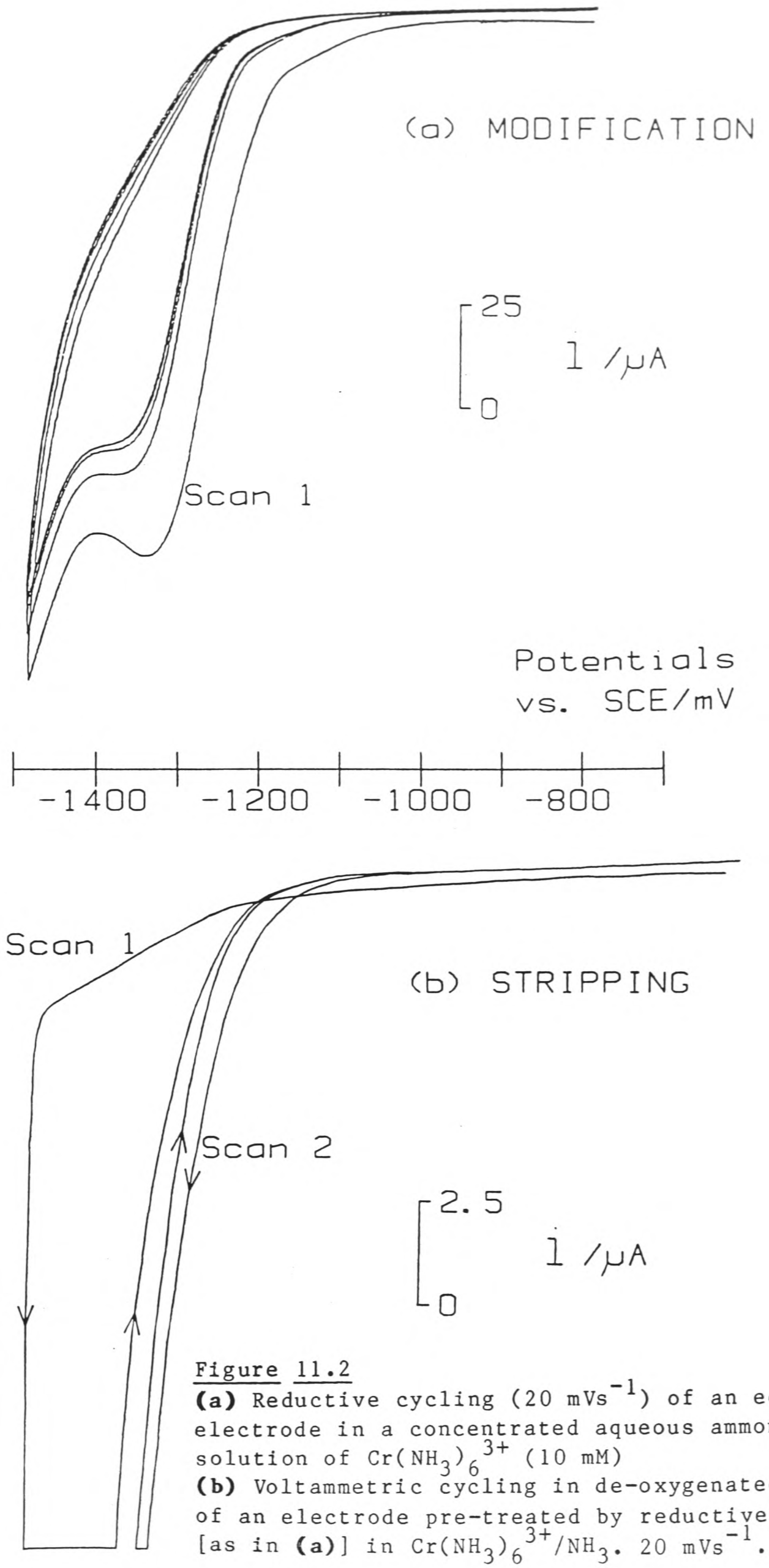

Figure 11.2
(a) Reductive cycling (20 mVs^{-1}) of an edge electrode in a concentrated aqueous ammonia solution of $Cr(NH_3)_6^{3+}$ (10 mM)
(b) Voltammetric cycling in de-oxygenated buffer, of an electrode pre-treated by reductive cycling [as in **(a)**] in $Cr(NH_3)_6^{3+}/NH_3$. 20 mVs^{-1}.

reveals large shifts in the overpotential for H_2 evolution. In the initial cathodic scan, H_2 evolution is suppressed and a broad shoulder is seen which extends over a region corresponding to the maximal faradaic activity in the ´modification´ cycles. Following this shoulder, there is a precipitous increase in cathodic current and a large hysteresis in the reverse (anodic) cycle. Subsequent cycles reveal a large (ca. 250 mV) positive shift in the cathodic discharge wave, Figure 11.2(b) (scan 2), with no further hysteresis in the anodic cycle. Similar electrochemical characteristics were observed after a single reductive cycle.

Preliminary tests of the biological electron-transfer activity of a reductively-cycled ($Cr(NH_3)_6^{3+}/NH_3$) edge surface were carried out with the 8Fe ferredoxin (0.2 mM in 20 mM Tricine, 100 mM NaCl pH 8.0). A square-wave voltammetric response with well-defined forward and reverse current contributions to the net current, Figure 11.3, was observed following reductive cycling in $Cr(NH_3)_6^{3+}/NH_3/NH_4Cl$ (4 scans). No faradaic response was detectable after cycling in NH_3/NH_4Cl alone.

The electrochemical characteristics observed in reductive-cycling experiments ($Cr(NH_3)_6^{3+}/NH_3$) are consistent with the projected reaction scheme, as outlined in Scheme 11.1. In particular, reductive cycling in $Cr(NH_3)_6^{3+}/NH_3$ shows faradaic activity close to the expected reduction potential for $Cr(NH_3)_6^{3+}$. Moreover, this faradaic activity is retained at the electrode surface, even after sonication, as judged by the initial cycle in buffer alone. The observation of the direct electrochemistry of ferredoxin, in the absence of multivalent cations, implies a modification of the edge graphite surface, such that there is a reduction in the negative surface charge density of this

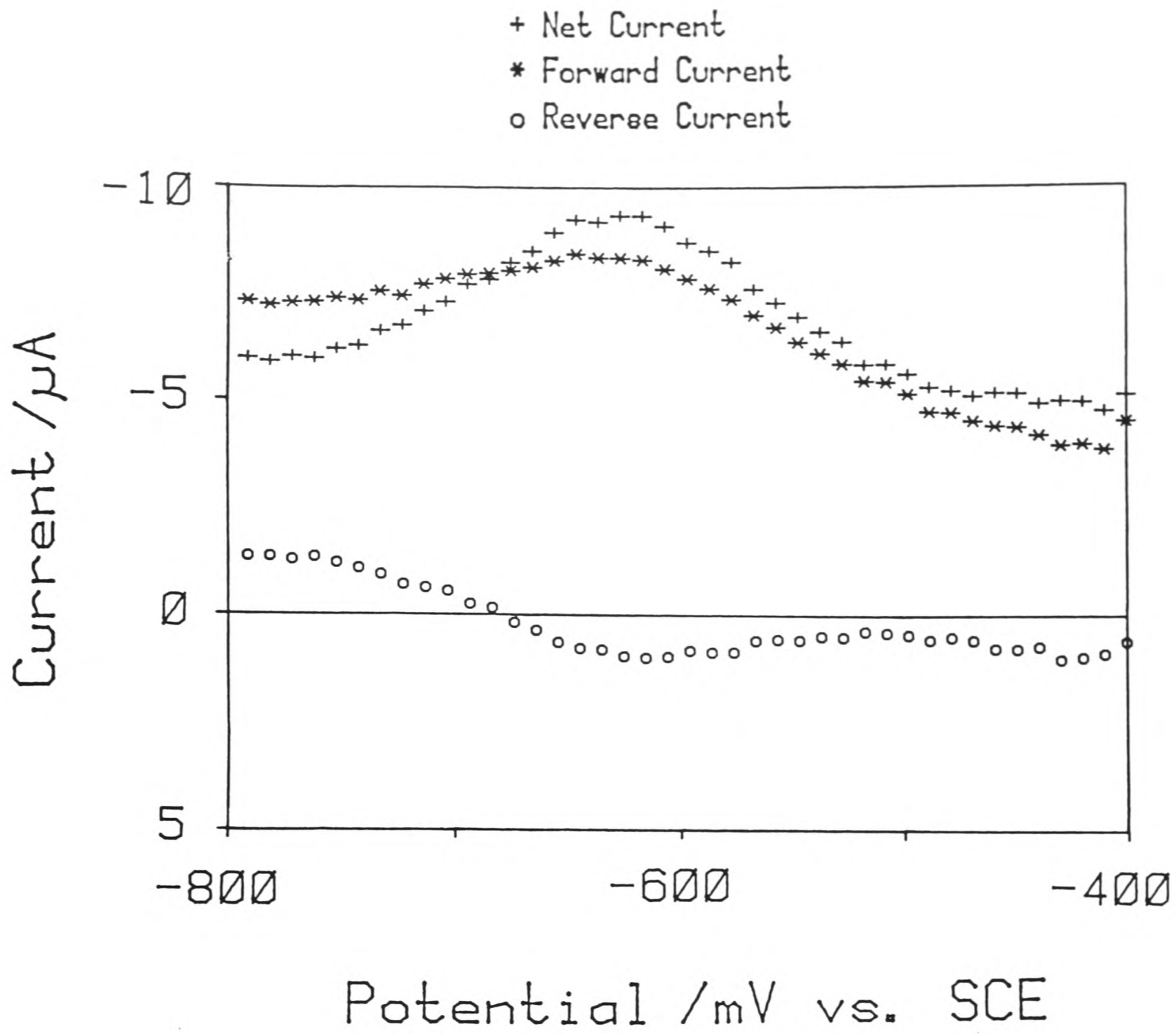

Figure 11.3: Square-wave voltammogram of 0.18 mM C. pasteurianum 2[4Fe-4S] ferredoxin (in 20 mM Tricine, 100 mM NaCl, pH 8.0) at an edge graphite electrode modified by reductive cycling as in Figure 11.2(a). Square-wave parameters of frequency 31 Hz, amplitude (half-peak-to-peak) 50 mV.

electrode. Similarly, the profound suppression of H_2 evolution in buffer (pH 8.0), at a reductively-cycled electrode, suggests a modification of the electrode such that the active sites for H_2 evolution are effectively 'masked'. Even in the reductive pre-treatment itself, there is a decrease in the faradaic peak current and an increase in overpotential upon cycling, suggesting a change in the surface characteristics.

When considered together, the electrochemical observations described in the previous paragraph are all consistent with a change in surface potential upon reductive-cycling, through the generation of positively-charged surface domains. A more positive surface potential will increase the cathodic overpotential for both H^+ and $Cr(NH_3)_6^{3+}$ reduction, while facilitating reduction of the highly-negatively charged 8Fe ferredoxin. A single cathodic cycle of a 'modified' electrode in buffer, causes a large (ca. 200 mV) anodic shift in the overpotential for H_2 evolution. This is consistent with the reductive 'stripping' of a positively-charged surface species, so restoring a negative surface potential. Moreover, a 'stripping' feature is seen in the initial cathodic scan, close to the half-wave potential of $Cr(NH_3)_6^{3+}$. This may correspond to the formation of labile Cr(II) species with subsequent dissociation of surface-bound Cr(III) ammine complexes.

11.4 Direct Electrochemical Studies of Plastocyanin and Cytochrome c.

In order to characterise further the nature of the 'charge-modified' edge graphite surface, direct electrochemical studies of redox proteins with well-defined positive (cytochrome c) and negative (plastocyanin) binding domains were undertaken.

PLASTOCYANIN.

An edge graphite electrode was subjected to (a) single-scan reductive cycling or (b) multiple-scan reductive cycling (typically 4 scans), at 20 mVs^{-1} in $Cr(NH_3)_6^{3+}/NH_3$, in the potential range -400 to -1500 mV vs. SCE. Following the pre-treatment procedure the electrode was rinsed and then sonicated in buffer for ca. 4 minutes. After a single reductive cycle, a stable, but highly asymmetric ($i_{pa}>>i_{pc}$), voltammetric response was observed at 20°c in the expected potential domain for plastocyanin (30 μM in 5 mM HEPES, 1 mM KCl pH 7.0). Upon multiple cycling, the faradaic response was barely detectable above the background response.

Following the addition of KCl to a final concentration of 100 mM, stable and symmetric plastocyanin electrochemistry was observed at 20°C ,after a single-scan reductive cycle in the range -400 to -1500 mV vs. SCE (followed by 4 minutes sonication). Subsequent experiments showed that this result is reproducibly obtained upon $Cr(NH_3)_6^{3+}/NH_3$ modification, either by a single voltammetric cycle (20 mVs^{-1}) between the restricted limits -400 to -1200 mV vs. SCE, or by poising at a potential of -1000 to -1130 mV vs. SCE for ca. 1 minute. These limits encompass only the small cathodic peak in the reductive cycle. A typical result for plastocyanin is shown in Figure 11.4(a). The half-wave potential ($E_{1/2}$) is +385 mV vs. NHE, close to the potentiometrically-determined value (Chapter 7). Faradaic peak separations were reproducibly 60 mV (20 mVs^{-1}, scan 5) and a plot of i_{pc} versus (scan rate)$^{1/2}$ was linear up to 100 mVs^{-1}. No deterioration of this electrochemical response was evident after prolonged cycling in the plastocyanin solution (>10 mins.) or after

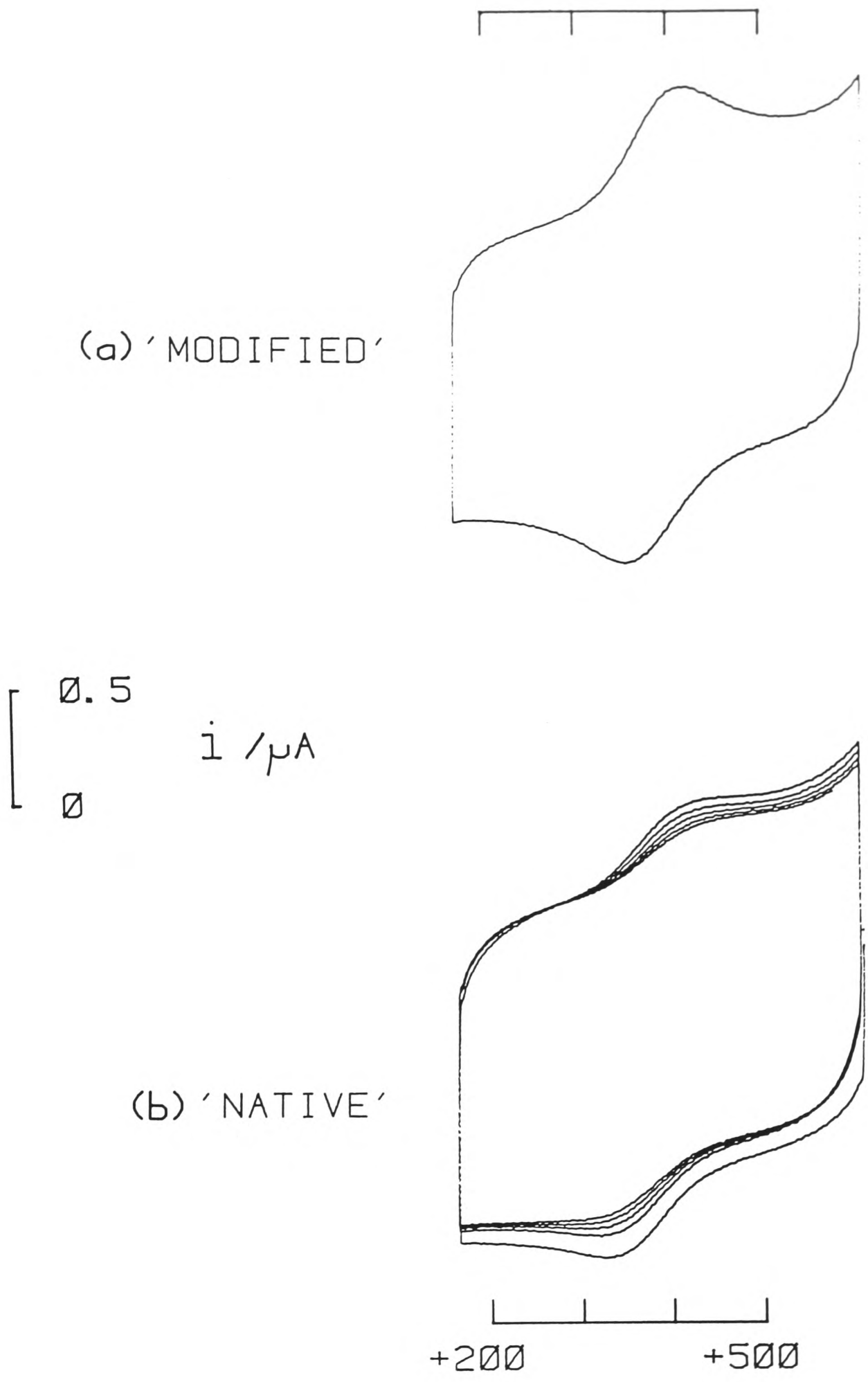

Figure 11.4: Cyclic voltammograms (20 mVs^{-1}) of plastocyanin at an edge-oriented electrode pre-treated by a single voltammetric cycle in $Cr(NH_3)_6^{3+}$/aqueous NH_3. 30 μM plastocyanin in 0.1 M KCl, 5 mM HEPES, pH 7.0. Temperature = 20°C.
(a) Pre-treatment range -400, -1200mV vs. SCE. 4 min. sonication. For clarity only the 5th cycle is shown.
(b) Cycling restricted to -400, -800mV. Scans 1 - 5.

sonicating the 'modified' electrode for 90 minutes.

Control experiments show that restricting potential cycling in $Cr(NH_3)_6^{3+}/NH_3$ to the region positive of -1000 mV vs. SCE, cycling in aqueous ammonia alone, cycling in buffer solution, or simply 'dipping' (1 minute) an electrode into the $Cr(NH_3)_6^{3+}/NH_3$ solution, gives only an impersistent and rather irreversible response, similar to that obtained for a routinely-polished electrode, Figure 11.4(b). Typical peak separations [ΔE_p/mV: scans 1 [5], 20 mVs^{-1}] are 100 [>130]: polished electrode; 85 [>120]: electrode cycled (1 scan) -400 to -800 mV vs. SCE in $Cr(NH_3)_6^{3+}/NH_3$.

A single reductive cycle (-400, -1200 mV vs. SCE) of an edge electrode in a concentrated aqueous ammonia solution of $Ru(NH_3)_6^{3+}$ ($E_{1/2}$ ca.-625 mV vs. SCE in aqueous ammonia) did not generate a detectable faradaic response attributable to plastocyanin (50 μM plastocyanin in 5 mM HEPES, 1 mM KCl pH 7.0).

Cathodic 'stripping' experiments were carried out by cycling (-400 , -1500 mV vs. SCE) or poising (-1400 mV, ca. 1 minute) a 'modified' electrode in concentrated aqueous ammonia, or de-oxygenated buffer solution, followed by sonication in buffer (4 minutes). 'Stripping' in aqueous ammonia solution produced no detectable change in the faradaic response of plastocyanin (ΔE_p = 60 mV, scan 4), although a slight deterioration of response was evident after stripping in buffer alone.

CYTOCHROME c.

An edge graphite electrode was 'modified' by single-scan reductive cycling (-400 , -1200 mV vs. SCE) or poising (ca. -1100 mV, 1 minute) in 10 mM $Cr(NH_3)_6^{3+}/NH_3$, followed by

sonication for 4 minutes. Examination of cytochrome c electrochemistry (in 5 mM Tricine, 100 mM NaCl pH 8.0) at the ´modified´ surface shows a marked inhibition of the faradaic response due to cytochrome c, at both low (50 μM) and high (1 mM) protein concentrations, when compared with the response at a polished surface, Figure 11.5(a-d). Control experiments showed that no inhibition of the faradaic response was observed when reductive-cycling in $Cr(NH_3)_6^{3+}/NH_3$ was restricted to potentials positive of -1000 mV vs. SCE.

The response at the ´modified´ electrode is consistent with a surface bearing positively-charged domains which function to promote reversible binding of the negatively-charged protein plastocyanin at high ionic strength (100 mM KCl). At low ionic strength (1 mM KCl), the ´modified´ surface is also active towards plastocyanin, but the voltammetric responses are asymmetric and characteristic of less reversible adsorption processes at the surface. This suggests that the electrostatic interactions between the protein (negatively-charged) and electrode (positively-charged) are too strong and are not adequately ´screened´ in 1 mM KCl. As expected, cytochrome c (positively-charged) shows only highly irreversible faradaic reponses at the ´modified´ surface, consistent with the absence of suitable electrostatic interactions between an electrode surface bearing positively-charged domains and positively-charged lysine residues on the haem face. The preferred electrostatic interaction may be with the acidic ´backside´ of cytochrome c, leading to binding in an unproductive orientation.

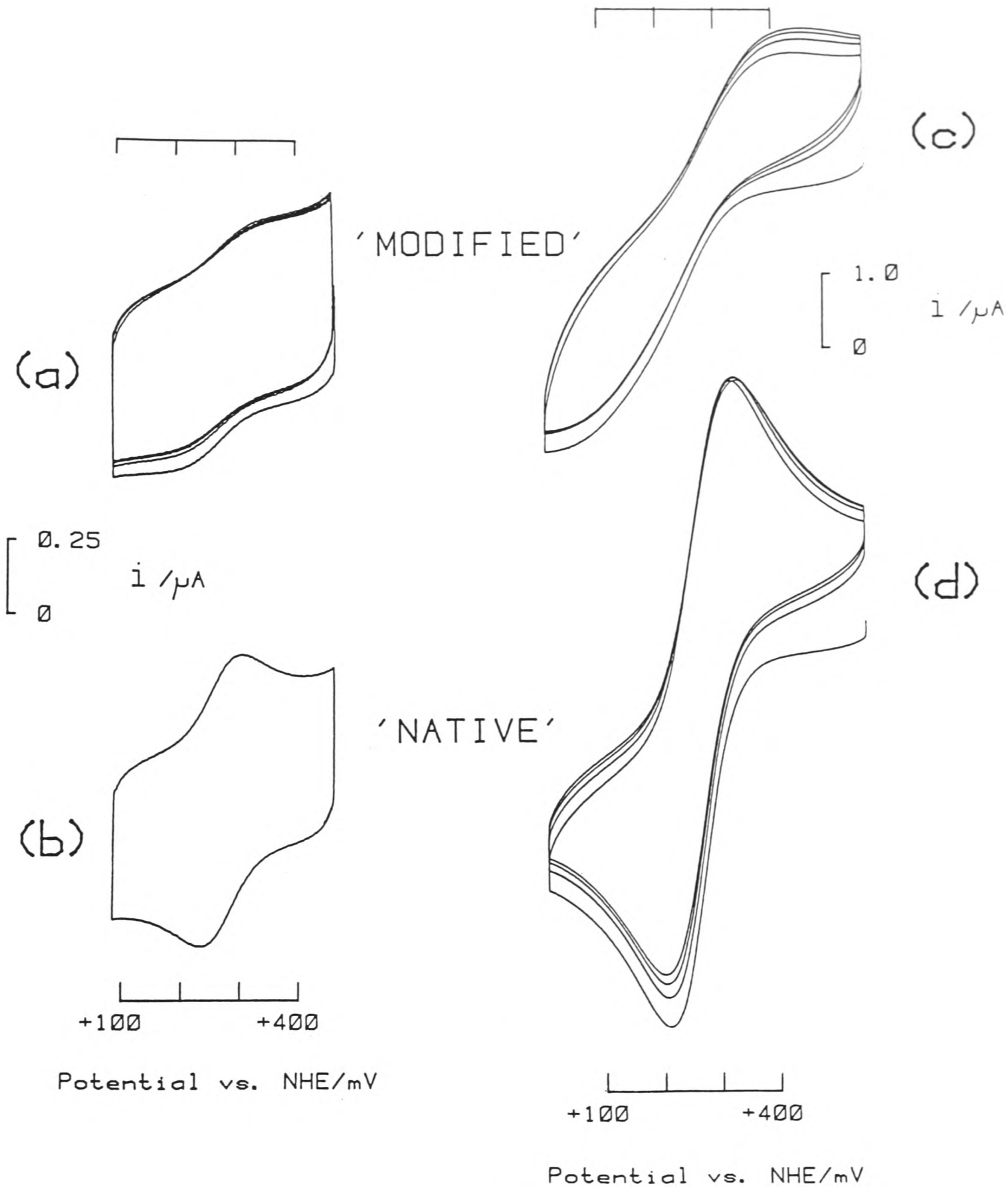

Figure 11.5: Cyclic voltammograms (20 mVs^{-1}) of cytochrome c in 5 mM Tricine, 100 mM NaCl, pH 8.0.
(a,b) 50 μM protein, at (a) a surface pre-treated by a single voltammetric cycle in $Cr(NH_3)_6^{3+}/NH_3$. Treatment range -400, -1200mV vs. SCE, followed by 4 minutes sonication; (b) a routinely-polished ('native') edge graphite electrode.
(c,d) 1 mM protein at (c) pre-treated, and (d) 'native' edge graphite. Conditions as in (a,b).

11.5 Spectroscopic Studies of 'Charge-Modified' Surfaces.

Parallel investigations with ESCA were used to confirm the incorporation of Cr (and N) at a reductively-cycled, edge-oriented graphite disc. The ESCA spectra shown in Figure 11.6, were obtained following electrode pre-treatment by single-scan reductive cycling in a concentrated aqueous ammonia solution of $Cr(NH_3)_6^{3+}$ (10mM) and, subsequently, 4 minutes sonication in buffer. The spectrum of an electrode subjected to a single cycle between the limits ca. -400 to -1200 mV vs. SCE, shows large C_{1s} and O_{1s} signals, as expected for a polished edge graphite surface (see Chapter 5). However, the spectrum also reveals the incorporation of Cr and N, as confirmed by the comparison of experimentally-observed binding energies with those expected for Cr_{2p} and N_{1s} levels, Table 11.1. The corresponding spectrum of an electrode at which the reductive cycle was restricted to -400 to -900 mV vs. SCE, shows that any Cr_{2p} signal lies within the noise level, although there is a small amount of N, most likely representing adsorbed NH_3.

A compilation of intensity data for C_{1s}, N_{1s}, O_{1s}, and Cr_{2p} peaks at 'modified', control and native edge surfaces, is given in Table 11.1. The O coverages at 'modified' electrodes (as estimated from C_{1s}/O_{1s} ratios: 3.1, 3.7, 2.6) are in good agreement with values derived from ESCA studies of 'native' edge electrodes (3.33 $\pm$ 0.73), Table 11.1 and Table 5.2.

The surface coverage of Cr, with respect to C, was estimated from C_{1s}/Cr_{2p} intensity ratios, for 'modified' electrodes subjected to various lengths of sonication pre-treatment (20 seconds; 4 minutes) or stirring in buffer solution (4 minutes). This calculation was based on the attenuation of

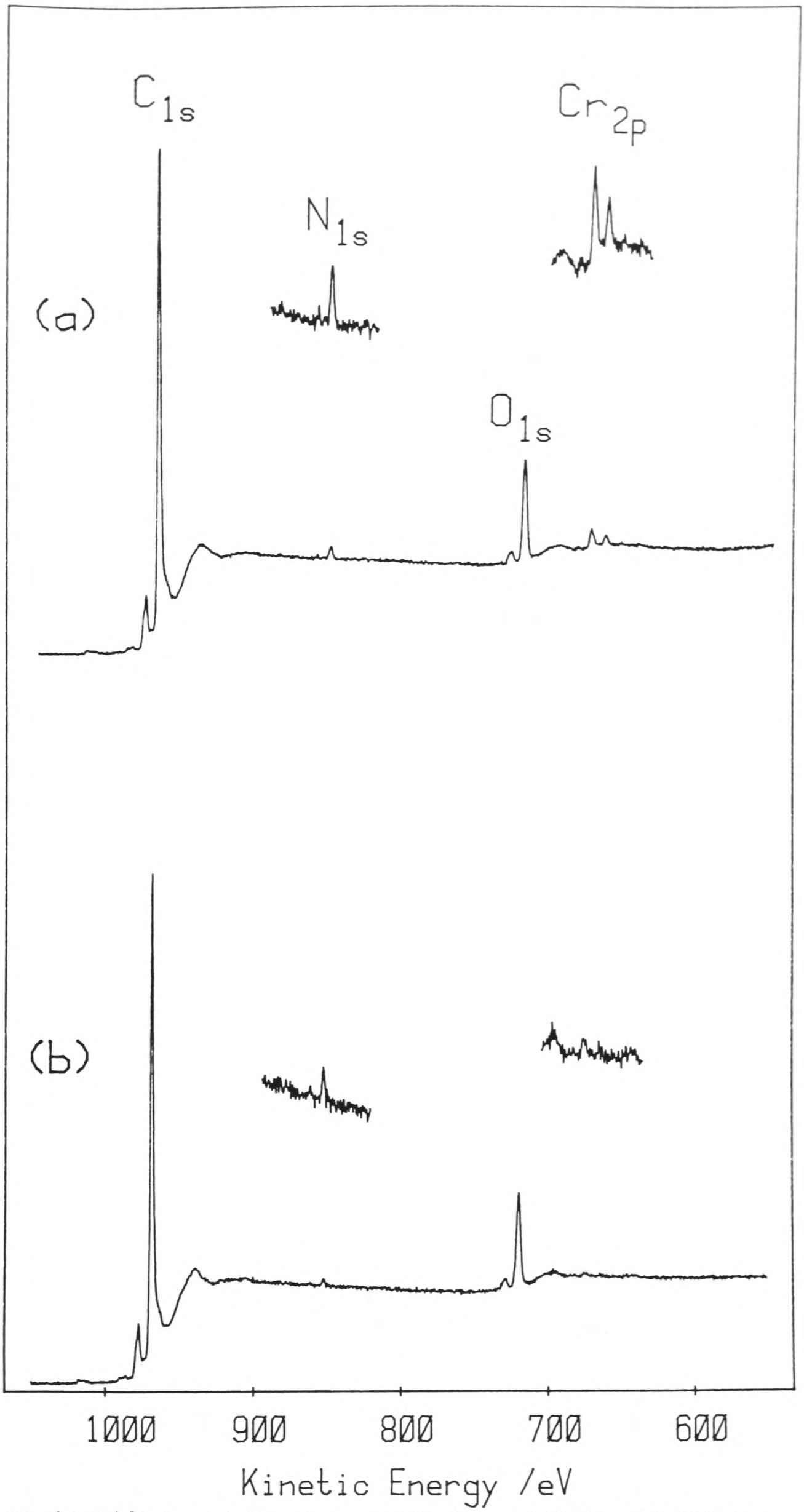

Figure 11.6: Wide scan ESCA spectra of edge graphite electrodes. Scale expansions (x 5) of Cr_{2p} and N_{1s} spectral regions. (a) Modified surface. (b) Control surface. (Conditions given in Table 11.1). Electrodes sonicated for 4 minutes prior to analysis.

Table 11.1

ESCA Analysis of Modified 'Edge' Graphite

Sample	Treatment Range		Standardised Intensity[1] (Band energy[2]/eV)			
			Cr_{1s}	O_{1s}	N_{1s}	Cr_{2p}
Modified	Cycle or poise	**a**	7658(969)	2439(120)	160(825)	698(674,664)
	below -1000 mV	**b**	8006	2190	137	763
	vs. SCE	**c**	5641	2169	285	1332
Control	Cycle or poise	a	7431(969)	2084(719)	74(853)	n.d.
	in range -400	**c**	6484	1741	76	n.d
	to -900 mV					
Polish	----------	a	7742(969)	2574(720)	n.d.	n.d.
		a	8178	2013	n.d.	n.d.

1. Band intensities were derived by integration of experimental data and are standardised for the number of scans and the width of scan. Prior to integration, background and satellite structure were subtracted. All values are corrected for the observed transmission characteristic of the electron energy analyser. (See Appendix 5.1 for further discussion).
2. Typical literature values: $Cr_{2p(1/2,3/2)}$ 670,669eV; N_{1s} 855eV

a. 4 minutes sonication in buffer prior to examination.

b. 20 seconds sonication in buffer prior to examination.

c. 4 minutes stirring in buffer prior to examination.

n.d. not detected

photoelectron flux with depth expected for a model of the 'modified' surface, in which an overlayer of Cr is formed on an array of C-O groups at a periodic edge lattice structure (see Appendix). This analysis, using estimated ESCA cross-sections and mean free paths, yields Cr coverages (with respect to C) of ca. 9% (after 20 seconds sonication), ca. 9% (after 4 minutes sonication) and ca. 23% (after 4 minutes stirring). These estimates show that, after a short sonication pre-treatment, a stable Cr-modified electrode is achieved with no decrease in coverage at longer sonication times. This is consistent with the stability of the electrochemical response of plastocyanin as observed after 4 minutes and then 90 minutes sonication. These observations strongly support the proposal that reductive-cycling produces an inner-sphere reaction at the electrode surface leading to covalent-modification. Stirring a 'modified' electrode in buffer yields a higher surface coverage of Cr. This treatment is apparently not sufficiently vigorous to remove strongly physisorbed Cr complexes.

The ESCA peak intensities suggest that at the 'modified' surface there is an increase in the N_{1s} signal over the residual N_{1s} signal detected at the control surface. This increase is most likely due to ammine co-ordination of the surface bound Cr species. The N_{1s} intensities at the modified (sonicated) surfaces may be corrected ($N_{1s,corr.}$) by subtraction of the N_{1s} intensity at the control surface. This gives $Cr_{2p}/N_{1s,corr.}$ intensity ratios at the modified (sonicated) surfaces of 8 and 12. The ratio (Cr_{2p}/N_{1s}) of estimated ESCA cross-sections is 6. This suggests that the stoichiometry, N/Cr, of the surface bound Cr(III) species is <1. However, this ratio should be treated with

caution, in view of the use of estimated ESCA cross-sections, the retention of NH_3 at 'native' surfaces and the disregard for the attenuation of photoelectron flux with depth. EELS studies were used to probe further into the nature of the ligand donors to the surface Cr(III) complexes, through d-d transitions. However, these features were too weak to detect above intense transitions attributable to the native surface (Chapter 5).

11.6 Summary and Concluding Discussion.

An edge graphite electrode surface was reductively-cycled in a concentrated aqueous ammonia solution of $Cr(NH_3)_6^{3+}$ (typically 10 mM). Direct electrochemical studies at native and pre-treated surfaces, using redox proteins with significant overall (and conservatively-localised) negative (plastocyanin) and positive (cytochrome c) charges, are consistent with the formation of positively-charged binding-domains at the pre-treated surface. This is illustrated schematically in Figure 11.7.

ESCA studies confirm that a reductively-cycled electrode is modified by the incorporation of Cr (and N). The potential threshold for modification, as judged by ESCA and plastocyanin electrochemical activity, lies in the region of -1000 mV vs. SCE. This is close to reported values of the polarographic reduction potential for $Cr(NH_3)_6^{3+}$ and corresponds to the appearance of a small cathodic peak at ca -1100mV in the reduction cycle. Analogous experiments performed with a concentrated aqueous ammonia solution of $Ru(NH_3)_6^{3+}$ (10 mM) do not generate plastocyanin electrochemical activity.

The key feature distinguishing the Cr^{3+}/Cr^{2+} couple from the Ru^{3+}/Ru^{2+} couple, is that Cr^{2+} is extremely substitution

'CHARGE-MODIFIED' SURFACE

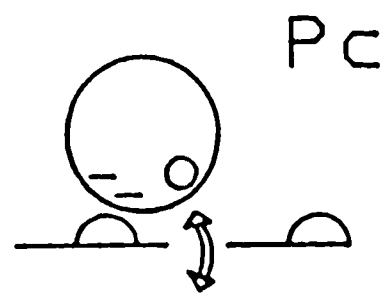

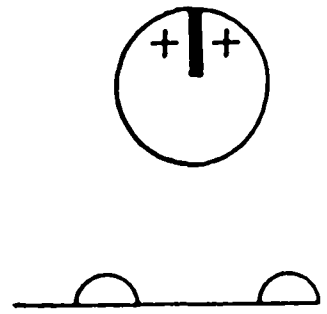

'NATIVE' SURFACE

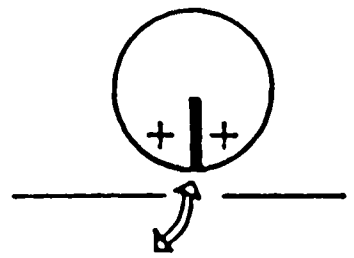

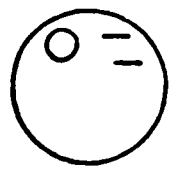

CURRENT OBSERVED

NO CURRENT OBSERVED

Figure 11.7: Schematic representation of the interaction between redox proteins and 'native' or modified edge graphite electrodes.

labile (rate constant for ligand exchange, $k_{ex} > 10^9\ s^{-1}$), whereas Cr^{3+} is extremely substitution inert ($k_{ex} \sim 10^{-6}\ s^{-1}$) (6). Consequently, the electroreduction of $Cr(NH_3)_6^{3+}$ produces a labile Cr(II) species, a proportion of which may co-ordinate to surface C-O functional groups, followed by re-oxidation to give a modified electrode. However, the observed electrochemical reductions appear irreversible i.e. there are no reverse (anodic) waves consistent with the re-oxidation of Cr(II) species. This observation can be reconciled with the projected reaction scheme, if a thermodynamically stable Cr-surface species is produced in the ligand exchange reactions of $Cr(NH_3)_6^{2+}$ e.g. two or more Cr-O surface bonds may be involved. Support for this proposal comes from 'stripping' experiments. The electrochemical activity of plastocyanin, at a Cr-modified electrode, is not significantly perturbed by cathodic 'stripping' cycles utilising a potential range identical to that used in the modification cycle. This indicates that stable Cr(III)-surface complexes are important in promoting the electrochemical activity of plastocyanin. Thus, the precursor Cr(II)-surface complexes will be rapidly oxidised at the same potential as which electroreduction of $Cr(NH_3)_6^{3+}$ occurs. This re-oxidation may occur through an intermediate reaction, as illustrated below. In this reaction scheme, the re-oxidation step, (C), occurs with no charge flow to the electrode. In the overall scheme, electrons need only be consumed in the formation of a catalytic amount of $Cr(NH_3)_6^{2+}$. A similar catalytic electrode process has been proposed to account for the de-activation of a Hg-pool electrode following $Cr(NH_3)_6^{3+}$ reduction (7). The catalytic activity of Cr^{2+} is well-known through its ability to catalyse dissolution of insoluble $CrCl_3$.

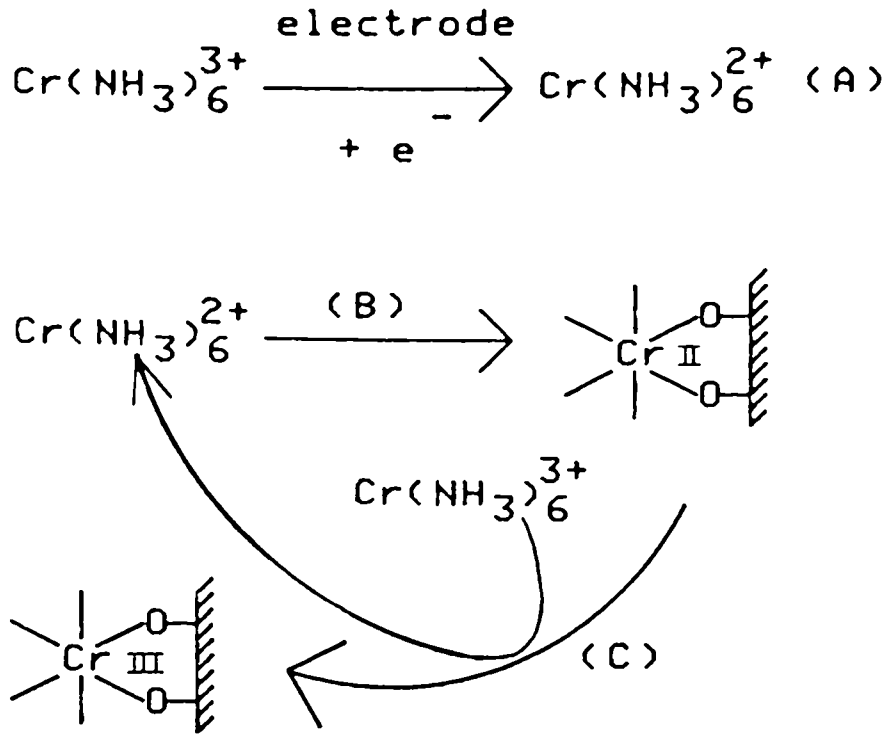

ESCA studies of the Cr-modified surface are consistent with a surface coverage of Cr (with respect to C) of ca. 9%. It is interesting to note that ESCA studies of silylated edge graphite surfaces (8) have led to a similar estimated coverage (ca. 10%) for Si (with respect to C). However, in the absence of specific chemical and structural information concerning the heterogeneity of the edge surface, these results must be treated with caution.

An estimate of the maximal coverage of $Cr(NH_3)_6^{3+}$, which may be achieved at an edge surface, can be made based upon the close packing of spheres of radius ca. 3 Å (Stokes radius of $Cr(NH_3)_6^{3+}$= 2.75 Å(9)) across a periodic edge lattice structure. This indicates that maximum coverage will be achieved at only ca. 20% Cr, with respect to C. Thus, reductive cycling in $Cr(NH_3)_6^{3+}/NH_3$ may lead to a high surface coverage (ca. 50% monolayer) of surface-bound Cr(III) complexes.

Electrochemical responses recorded for cytochrome c (35 μM) at a routinely-polished edge electrode, are relatively unaffected by the addition of mobile multivalent cations e.g. 10 mM $Cr(NH_3)_6^{3+}$. By contrast, the response at high (1 mM) cytochrome c

is markedly de-stabilised by the addition of $Cr(NH_3)_6^{3+}$. It has been suggested (see Chapter 9) that 'mobile', multivalent cations are only localised at specific regions of the electrode surface. Thus, only at high protein concentrations is cytochrome c forced to populate sites carrying local surface excesses of $Cr(NH_3)_6^{3+}$, with subsequent de-stabilisation and 'impersistence' of faradaic responses. However, the electrochemical responses of both low (50 μM) and high (1 mM) cytochrome c concentrations are markedly de-promoted following reductive modification of an edge surface. This observation is consistent with the proposal that the Cr-modified electrode carries a high surface coverage of positively-charged binding domains.

The precise nature of the chromium surface species generated by reductive cycling remains to be determined. It is likely that the complexes will comprise variable ammine, aquo and surface groups and be appreciably heterogeneous. The complexes may, thus, be comparable to those implicated in chrome tanning and dyestuffs technology (10), and in recent chromium polymer derivatisations of semi-conductor surfaces (11). The poorly-defined electrochemical activity of plastocyanin at an edge surface, following multiple reductive cycling, contrasts with the quasi-reversible faradaic responses observed after single-scan reductive cycles. It may be that multiple reductive cycles lead to extensive polymerisation of Cr(III) complexes formed at the surface.

It will be of interest to pursue the electrochemical generation of surface complexes, as described in this chapter, with the aim of achieving, via chromium coordination, rapid electrochemical incorporation of a wide range of biologically

important ligands at the electrode surface. Specific interest may be directed towards the incorporation of amino acids, of which there already exists well characterised $Cr(NH_3)_x$(amino acid)$_y$ complexes (12), or perhaps proteins themselves.

Appendix

Calculation of the Cr(III) Coverage from the ESCA Peak Intensity Ratio, C_{1s}/Cr_{2p}.

Assume a simple layer-structure model of the modified edge surface in which an overlayer of Cr(III) species is formed on an array of C-O groups, at a periodic 'edge' lattice structure:

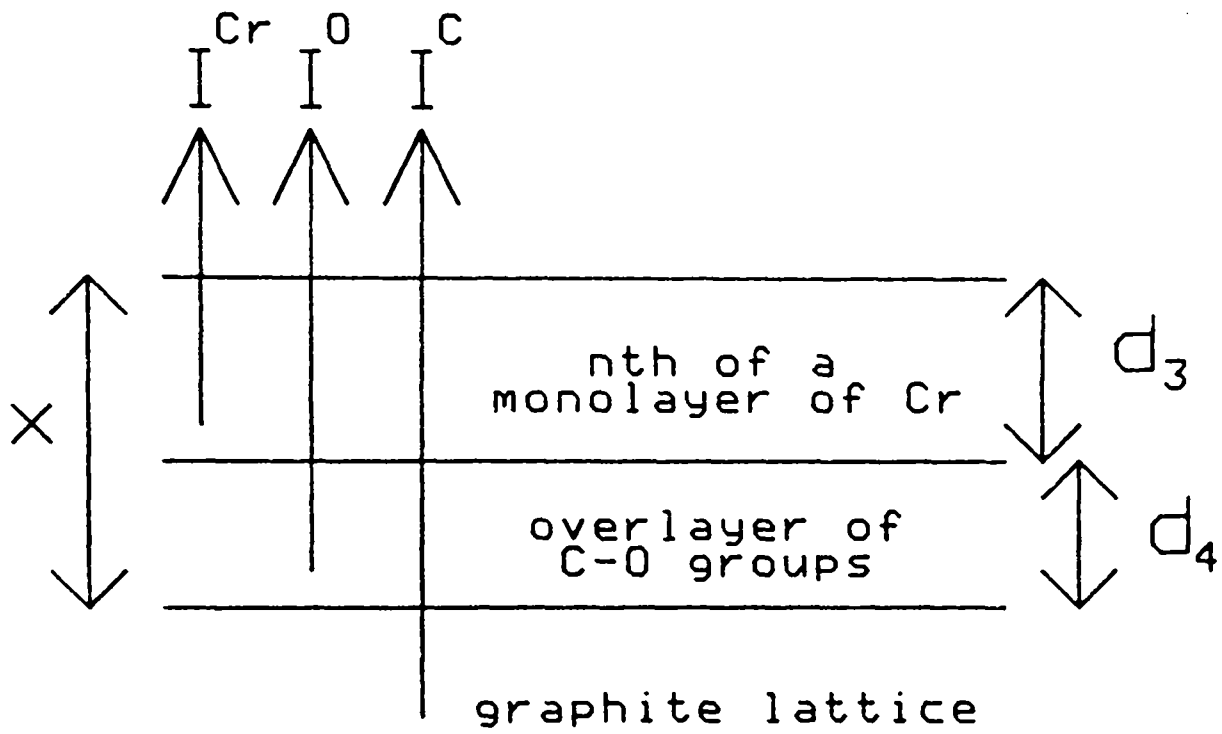

From Chapter 5 (Appendix 5.2) the total emergent C_{1s} intensity from graphitic layers with an overlayer of thickness x is given by:

$$I^C = I_o{}^C . \frac{\exp(-x/\lambda_c) + \exp(-[x+d_2]/\lambda_c)}{1 - \exp(-d_1/\lambda_c)}$$

$$= I_o{}^C . f(x, d_1, d_2, \lambda_c) \qquad (11.1)$$

where d_1, d_2 are lattice dimensions

λ_c = mean free path for the C_{1s} region

For nth of a monolayer of Cr(III) surface complexes:

$$I^{Cr} = nI_o{}^{Cr} \qquad (11.2)$$

where $I_o{}^{Cr}$ is the tabulated ionisation cross-section for Cr_{2p}

Therefore from equations (11.1) and (11.2):

$$\frac{I^C}{I^{Cr}} = I_o{}^C . \frac{f(x,d_1,d_2,\lambda_c)}{n.I_o{}^{Cr}} \qquad (11.3)$$

For a monolayer of sp^2 C-OH functionalities, d_4 = 1.34 Å.

Assuming the width (d_3) of the surface-bound Cr complex is 4 Å, then using equation (11.3):

$$\frac{I^C}{I^{Cr}} = \frac{0.225}{2.34n} \cdot \frac{\frac{\exp(-1.34+4n)}{12} + \frac{\exp(-1.34+4n+0.7075)}{12}}{1 - \exp(-2.1225)}$$

Inserting typical ESCA intensities gives:

$$\frac{8006n}{763} = e^{-n/3} \qquad (11.4)$$

Equation (11.4) is solved for n, the surface coverage of Cr with respect to C.

References - Chapter 11

1) Sopher, D. W. and Utley, J. H. P., J. Chem. Soc., Perkin Trans. II, 8, 1361, (1984).

2) Olson, M. V. and Taube, H., Inorg. Chem. 9, 2072, (1970).

3) Rollison, C. L. The Chemistry of Cr, Mo and W. Pergamon Topics In Inorganic Chemistry. Oxford: Pergamon. 21 (1973).

4) Tanaka, N., Nature 197, 176 (1963).

5) Ichniowski, T. C. and Clifford, A. F., J. Inorg. Nucl. Chem. 22, 133, (1961).

6) Taube, H. Electron Transfer Reactions of Complex Ions in Solution. New York: Academic Press (1970).

7) Fischer, O. and Dracka, O., Collect. Czech. Chem. Commun. 38, 645, (1973).

8) Brown, K. J. Part II Thesis. Oxford (1985).

9) Weaver, M. J. and Satterberg, T. L., J. Phys. Chem. 81, 1772, (1977).

10) Bird, C. L. The Theory and Practice of Wool Dyeing. Bradford: Society of Dyeists and Colourists (1972).

11) Malpass, R. E., Mayers, F. R. and Osborne, A. G., J. Electroanal. Chem. 153, 97, (1983).

12) Cooper, J. A., Blackwell, L. F. and Buckley, P. D., Inorg. Chim. Acta 92, 23, (1984).

CHAPTER 12

THE DEVELOPMENT OF AN ENZYME-BASED ELECTROSYNTHETIC DEVICE

12.1 Introduction.

In recent years there have been a number of developments in electrocatalysis, mainly resulting from advances in material science (1). New materials are now available for electrodes, cell parts and membranes, which can withstand chemical attack (e.g. "dimensionally stable" anodes), reduce overpotentials (e.g. of $2H_2O \xrightarrow{2e^-} H_2$), or increase current densities (e.g. two-dimensional or fluidised-bed electrodes). However, the development of specific and selective catalysts for individual electro-organic reactions has received less attention, although selectivity is of paramount importance to process economics. A current approach to highly-selective electrochemistry is through the construction of electrode surfaces with a well-defined molecular architecture (2). This is exemplified by the preparation of electrode surfaces that can be used for partially stereoselective electro-organic syntheses (3,4). Enzymes catalyse specific transformations in a given range of substrates. In addition, these transformations are stereoselective. Thus, it is of interest to combine electrochemistry with the speed, selectivity and mild reaction conditions of enzymic transformations.

In principal, electroenzymology may be exploited for analytical purposes, for the development of bio-fuel cells and for efficient synthesis. A fuel cell based on methanol dehydrogenase (5), and an amperometric glucose sensor using immobilised glucose oxidase (6), have been previously described. The use of purified enzymes to functionalise carbon skeletons,

through the selective introduction of hydroxyl or carbonyl groups, presents a valuable synthetic opportunity. These conversions are not easily achieved with selectivity, control, and high yields, by conventional methods, and often require multi-stage syntheses.

The mono-oxygenases (e.g. methane mono-oxygenase or cytochrome P-450) are an attractive group of redox enzymes for incorporation into electro-organic devices. These enzymes catalyse dioxygen-dependent hydroxylation reactions with a broad substrate specificity ranging from methane or chloroform to complex organics. Hydroxylation requires a source of reducing equivalents furnished by NAD(P)H, via a low potential redox protein. However, the practical use of these enzyme systems, in enzyme reactors or electroenzymological devices, has been limited by the relative instability of the enzymes, the oxygen-sensitivity of the low potential redox proteins and the requirement for a source of reduced NAD(P)H. The cost of these co-factors is sufficiently high to exclude their use in stoichiometric amounts. This problem may be overcome by using enzymatic or electrochemical regeneration of the reduced co-factor. Although there is no satisfactory method for the direct electrochemical reduction of $NAD(P)^+$, mediated electrochemical regeneration of NADH (or NADPH), using, for example, methyl viologen and lipoamide dehydrogenase (or ferredoxin-NADP-reductase), has been described (7,8), and this could be used to drive enzymatic hydroxylations in an electrochemical closed loop. However, the ultimate aim of electroenzymology is to simplify catalytic systems and eliminate any dependence on co-factors or low potential mediators.

An attractive alternative in the design of electroenzymological devices is to establish direct (unmediated) electron-transfer between the enzyme system and an electrode. This may be effectively achieved by coupling through the redox proteins which provide an electron pathway, *in vivo*, to the active enzyme centre. Thus, the synthetic activity of an enzyme may be coupled, through the direct electrochemistry of a redox protein, to an electrochemical device. A similar coupling has been described between cytochrome oxidase, in intact mitochondria, and exogenous cytochrome *c* (9).

A number of hydroxylases have been isolated from bacteria of the *Pseudomonas* family, which are effective catalysts for the oxidation of *p*-cresol and related alkyl-substituted phenols. These enzymes are not mono-oxygenases, since molecular oxygen is not incorporated into the products, but act by dehydrogenating the substrate to a quinone methide, followed by *hydration* to the corresponding alcohol (10), as shown below. The di-alcohol acts as the substrate for a further enzyme-catalysed dehydrogenation to give the carbonyl compound.

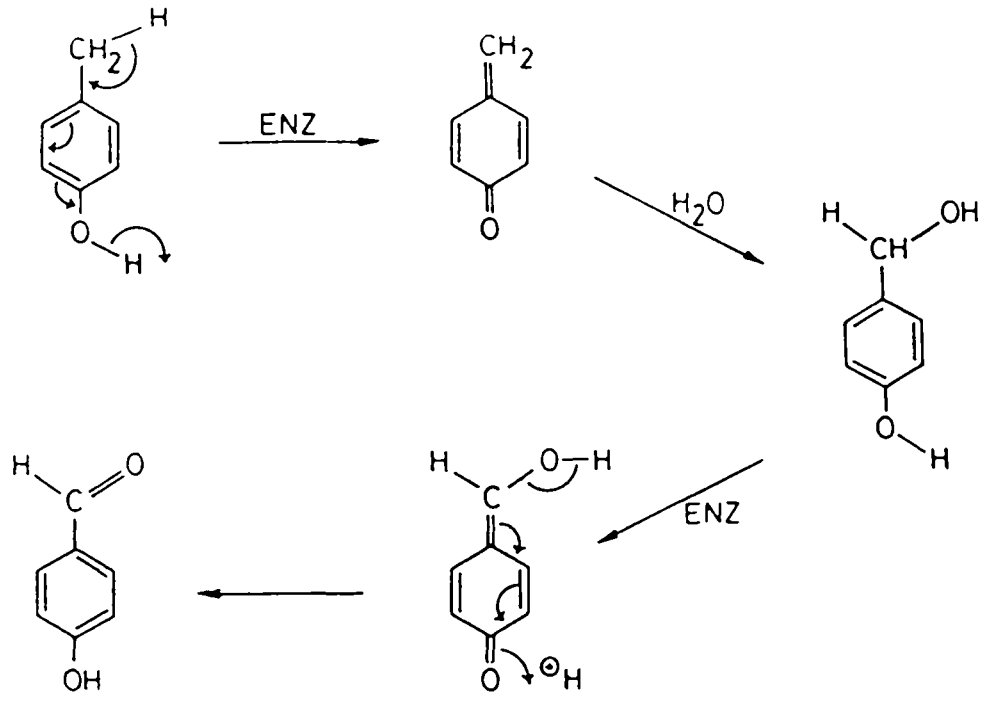

In contrast to the mono-oxygenases, the enzyme requires an electron-acceptor and azurin is thought to be the physiological electron-transfer protein involved in this process (11). The direct electrochemistry of azurin is readily observed at surface-modified gold and carbon electrodes (see Chapter 4) and may provide the key to the electrosynthetic coupling of the p-cresol hydroxylases.

12.2 Experimental Details.

Cu(I) azurin was prepared by reduction of the oxidised protein with a stoichiometric quantity of dithionite, followed by extensive diafiltration (Amicon 8-MC) against buffer (Tris-HCl, pH 7.6). p-Cresol (Aldrich, 'Gold Star') and p-hydroxybenzaldehyde (Aldrich) were recrystallised from H_2O. p-Hydroxybenzylalcohol (Aldrich) and ferrocene boronic acid (Koch-Light) were used as supplied.

Cyclic voltammetric experiments.

Cyclic voltammetry was carried out as described in previous chapters. The electrochemical cell was thermostatted at 25°C. The working electrode, a 4 mm. diameter gold disc, housed in an epoxy sheath, was precycled (-800 to +1200 mV vs SCE, 50 mVs^{-1}) in 0.1 M $NaClO_4$ + 20 mM phosphate (pH 7.0) at the start of each experimental session. Solutions (ca. 1 mM) of bis(4-pyridyl) bisulphide [Aldrich] and 2-(pyridinylmethylene)hydrazine-carbothioamide were prepared in the working buffer, which was 50 mM Tris [tris(hydroxymethyl)aminomethane]-HCL, 10 mM KCl, pH 7.6 (optimal pH for enzyme activity (12)). Surface modification was carried out by dipping an alumina (0.3μ)-polished gold electrode

into a solution of the surface modifier for 2 minutes, followed by copious washing with doubly-deionised water.

Bulk electrosynthetic experiments.

The electrocatalytic system was scaled up for preparative experiments by using a two-compartment stirred cell, divided by a salt (1 M KCl) bridge. The cell was thermostatted at 30°C. The anode (gold foil) and cathode (gold or platinum foil) compartments contained electrodes giving high surface area (ca. 50 cm^2) to volume (50 cm^3) ratios. In between runs the electrodes were removed and polished with a detergent ('Micro', International Products Corp.) followed by extensive sonication in doubly-deionised water. The reference electrode (saturated calomel[SCE]) was housed in a glass tube with connection to the working compartment through a sintered glass frit. The potentiostat (PAR model 173 polarographic analyser) used for potential control and current measurement was equipped with a digital coulometer (PAR model 179). The buffer used in the working compartment, for all experiments, was 100 mM Tris-HCl/50 mM KCl, 30% MeOH, pH 7.6. MeOH was used to increase the solubility of ferrocene boronic acid, and p-cresol and its oxidation products. The use of MeOH did not affect the activity of p-cresol hydroxylase. Various buffers were used in the cathodic compartment (0.5 M H_2SO_4; 100 mM Tris-HCl/50 mM KCl (pH 7.6) or 100mM Glycine-NaOH/50 mM KCl (pH 9.6)).

Product analysis.

2,4-dinitrophenylhydrazone derivatives were prepared by incubating reaction mixtures at 30°C for 30 mins. with a solution

of 2,4-dinitrophenylhydrazine (Aldrich) in 2 M HCl. The precipitated 2,4-dinitrophenylhydrazone was collected by centrifuging at 10000g for 10 mins. The pellet was washed several times with 2 M HCl and then dissolved in ethyl acetate. This solution was dried *in vacuo.*

HPLC analysis (LCD/Milton Roy computing integrator) was carried out on a Spherisorb S5C8 column (Phase Separations, U.K.) in a gradient (22 mins.) of water modified with acetonitrile, at 3.1 - 3.7 kpsi (1.4 mL/min.). Standard solutions of *p*-cresol, *p*-hydroxybenzaldehyde and *p*-hydroxybenzylalcohol were prepared in EtOH. Samples were loaded by using a 100 µL injection loop. The detector was set at 280 nm.

Experimental Results and Discussion.

12.3 Direct Electrochemistry of Azurin.

The direct electrochemistry of azurin (0.25 mM) from Pseudomonas putida was investigated at pH 7.6, at a range of electrode surfaces. The faradaic responses were identical to those for azurin from Pseudomonas aeruginosa. At gold electrodes surface-modified with organic promoters (e.g. bis(4-pyridyl) bisulphide or 2-(pyridinylmethylene)hydrazinecarbothioamide [2-PMHC], whose structure is shown in Figure 12.1), faradaic responses were symmetrical and consistent with diffusion-dominated, quasi-reversible electrochemistry. This is illustrated in Figure 12.1, for Au-PMHC (ΔE_p /mV: 72.5 (20 mVs^{-1}); 82.5 (100 mVs^{-1}). However, at these surfaces the faradaic peak current became smaller with time. This may be due to slow desorption of the organic modifier, or displacement of the modifier from the surface by protein molecules. The action of 2-PMHC, and similar compounds, as surface-modifiers of gold electrodes, has been described recently (13). The faradaic responses at edge graphite electrodes were less reversible than those at gold electrodes and were noticeably asymmetric with a rounded and depressed anodic peak. A gold electrode surface-modified with 2-PMHC was chosen for use in electrosynthetic studies. At the same electrode, p-cresol hydroxylase did not exhibit any observable electrochemistry. However, at potentials greater than +550 mV vs. NHE, a strong oxidation wave was seen in solutions containing only p-cresol.

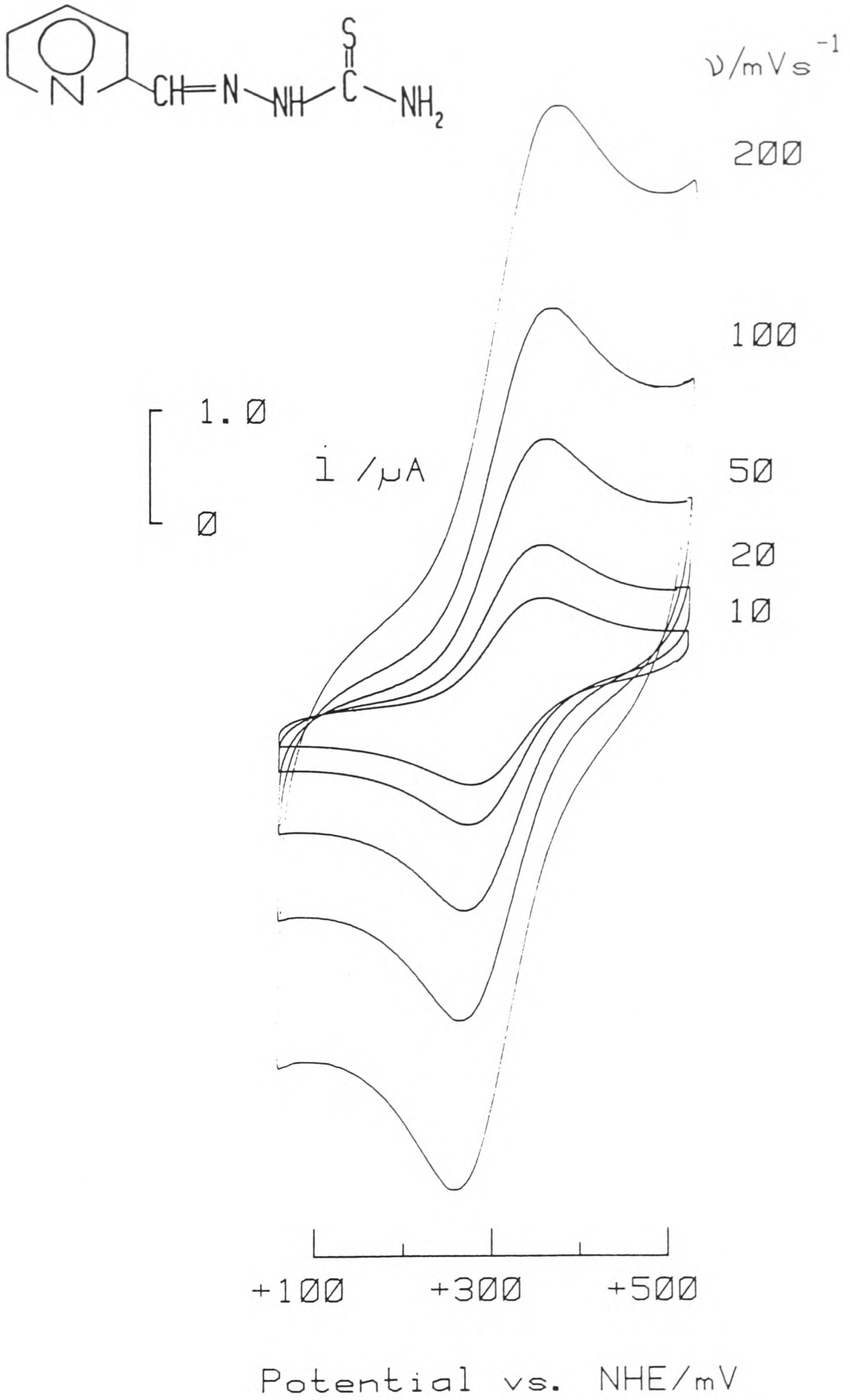

Figure 12.1: Cyclic voltammograms for azurin (0.25 mM in 50 mM Tris-HCl, 25 mM KCl, pH 7.6) at various scan rates, recorded at a gold electrode surface-modified with 2-(pyridinylmethylene)hydrazinecarbothioamide. The inset shows the structure of the surface modifier.

12.4 Azurin as an Oxidant for p-Cresol Hydroxylase.

The addition of either p-cresol hydroxylase (e.g. from P. putida; < 1 μM) or p-cresol (3 mM) to a solution of Cu(I) azurin (0.25 mM P. aeruginosa or P. alcaligenes azurin) has no significant effect upon the electrochemistry, as illustrated in Figure 12.2(a,b). However, the addition of both p-cresol and the enzyme to a solution of Cu(I) azurin causes a striking change in the voltammetric response, particularly at low scan rates (e.g. 5 mVs^{-1}), Figure 12.2(c). No peaks are observed and a large current flows at oxidising potentials. This is indicative of the catalytic regeneration of Cu(I) azurin from Cu(II) azurin by the reduced enzyme. A diagnostic plot (see Figure 12.2(d)) of $i_{pa}/v^{1/2}$ versus $\log_{10}v$, is similar to that of Figure 2.4 (case e), and indicates that the experimental result conforms to the theoretical model for a coupled catalytic reaction:

$$O + Z \xrightarrow{k_f} R \qquad (12.1)$$

$$R + e^- \rightleftharpoons O$$

Electrochemically-generated Cu(II) azurin is acting as an electron acceptor for the enzyme-catalysed oxidation of p-cresol (scheme 12.1) within the diffusion layer. The reduced azurin is continuously recycled electrochemically. Thus, direct electrochemistry of azurin has coupled electron-flow between a synthetically-useful enzyme and an electrode. However, a decrease in catalytic peak current was observed with successive voltammetric cycles, consistent with a decrease in the number of effective sites for protein-electrode electron transfer. This

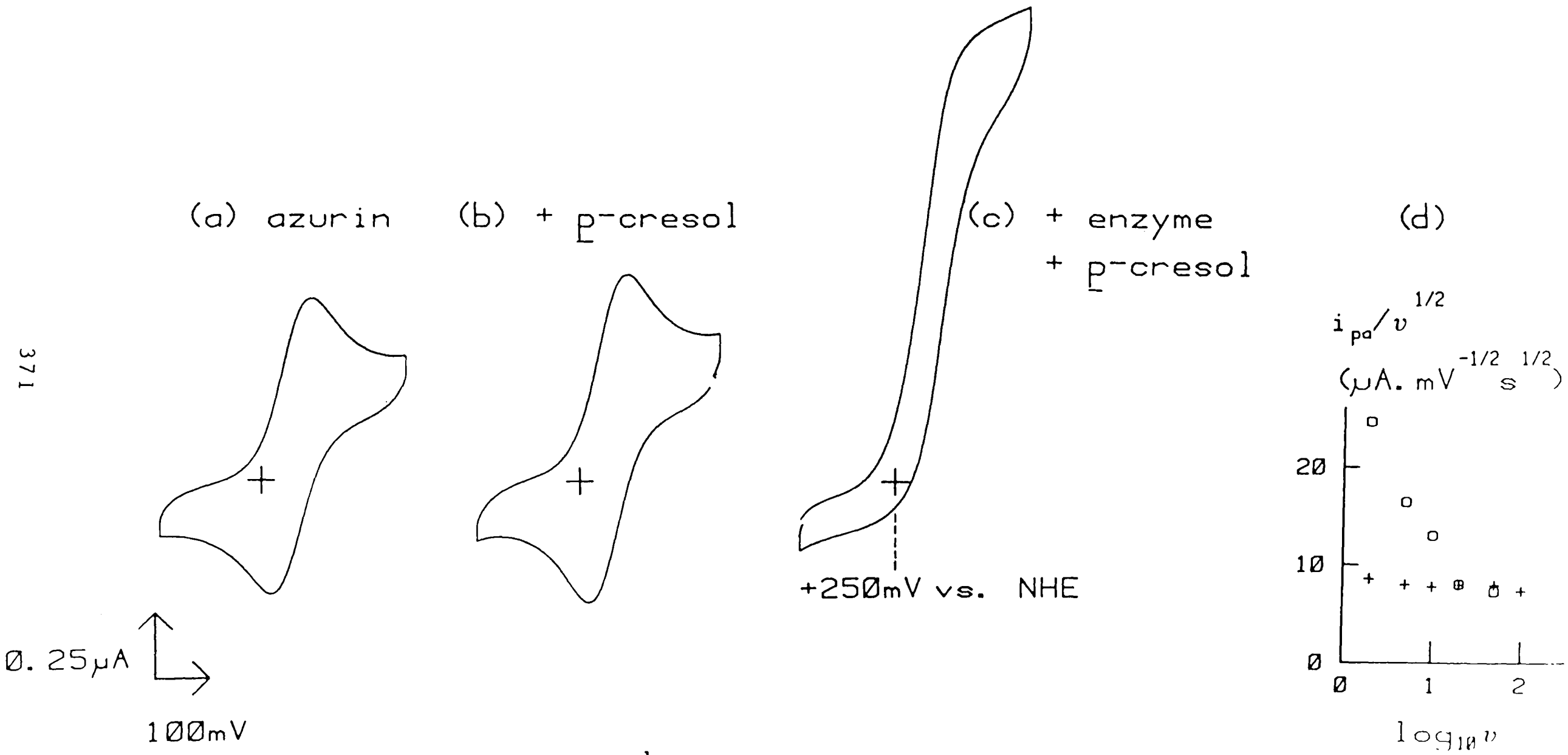

Figure 12.2: Cyclic voltammograms (5 mVs^{-1}) recorded at a gold electrode surface-modified with 2-(pyridinyl methylene)hydrazinecarbothioamide. **(a)** 0.25 mM azurin in 50 mM Tris-HCl, 10 mM KCl, pH 7.6; (b) as (a), with the addition of p-cresol to 3 mM; (c) as (b), with the addition of p-cresol methylhydroxylase (from P. putida) to 0.7 μM; (d) diagnostic plots of the peak current function at p-cresol methylhydroxylase concentrations of (o) 0.21 μM, (+) zero, in the presence of 7 mM p-cresol. Other conditions as given in (a).

Scheme 12.1
372

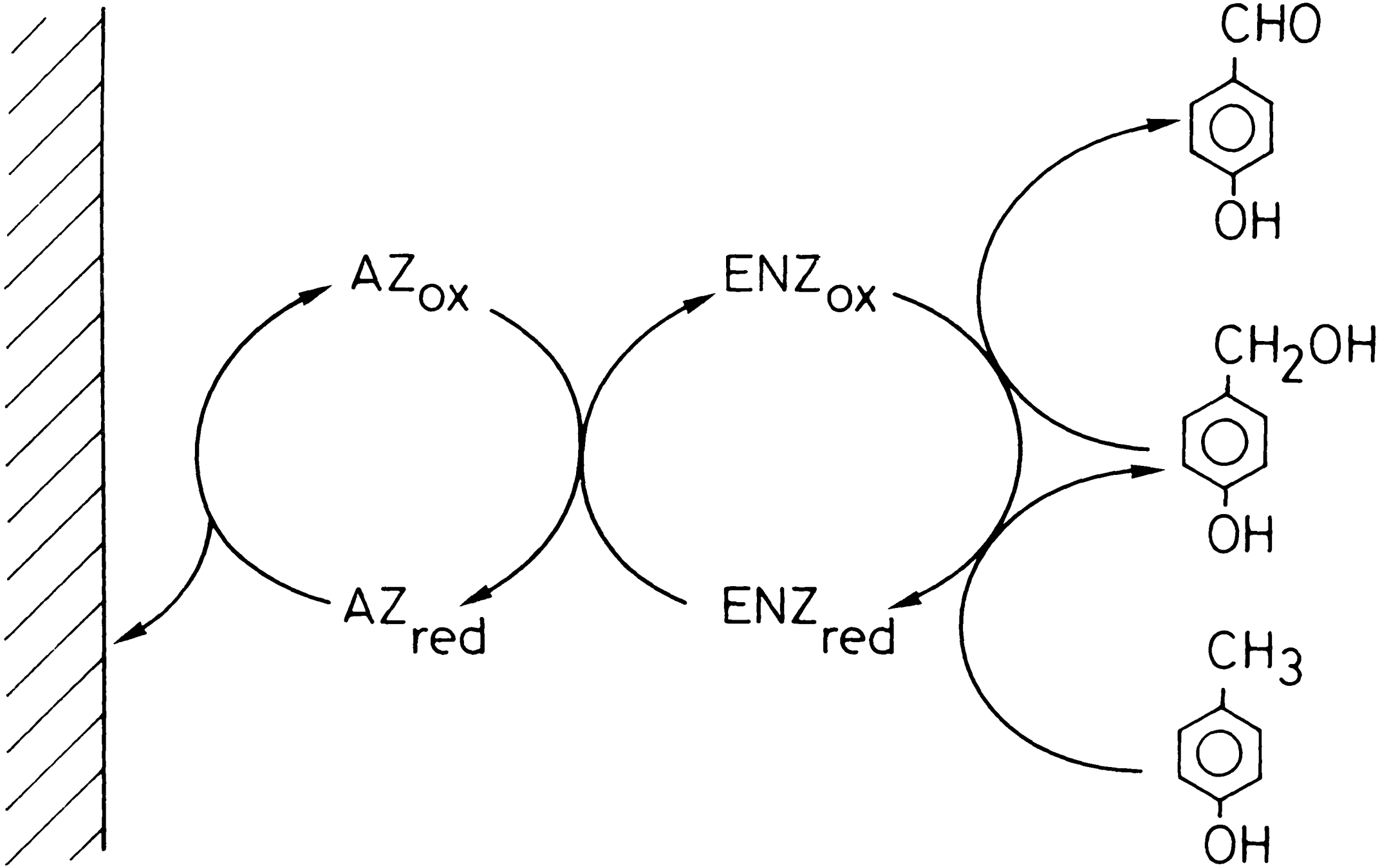

limited any further development of the azurin-coupled enzyme system into a larger-scale synthetic device.

12.5 Ferricinium Ion as an Oxidant for p-Cresol Hydroxylase.

A suitable low molecular weight mediator was sought in order to effect coupling between an electrode and p-cresol hydroxylase. In a homogeneous study (10), phenazine methosulphate was used to assess p-cresol hydroxylase activity. However, a disadvantage of using this mediator is its light sensitivity. It has been shown that ferrocenes can act as effective mediators to a variety of oxido-reductases (6,14). Ferrocene derivatives have many advantages as mediators, including rapid homogeneous and heterogeneous electron transfer and little tendency to auto-oxidise in the reduced form. A particularly attractive feature is that a wide range of redox potentials is available through derivatisation of the cyclopentadienyl rings, while still retaining well-behaved, one-electron transfer.

The half-wave potential of ferrocene boronic acid (FBA) ($E_{1/2}$= +323 mV vs. NHE, pH 7.6) is closely similar to that of azurin ($E_{1/2}$= +307 mV vs. NHE, pH 7.6). In addition, ferrocene boronic acid gives stable well-behaved electrochemistry at a 'bare' gold electrode (Figure 12.3(a)), ΔE_p = 78 mV (20 mVs^{-1}); $i_p/v^{1/2}$ = constant; D_o= 9.3 x 10^{-6} cm^2s^{-1}. Thus, azurin was replaced by FBA as a mediator of electron-transfer. The addition of p-cresol or p-cresol hydroxylase to a solution of ferrocene boronic acid (0.5 mM) did not significantly effect the faradaic response, Figure 12.3(b). However, when both the enzyme and substrate are present (Figure 12.3(c,d)) an enhancement of the anodic response is seen, which is more pronounced at low scan

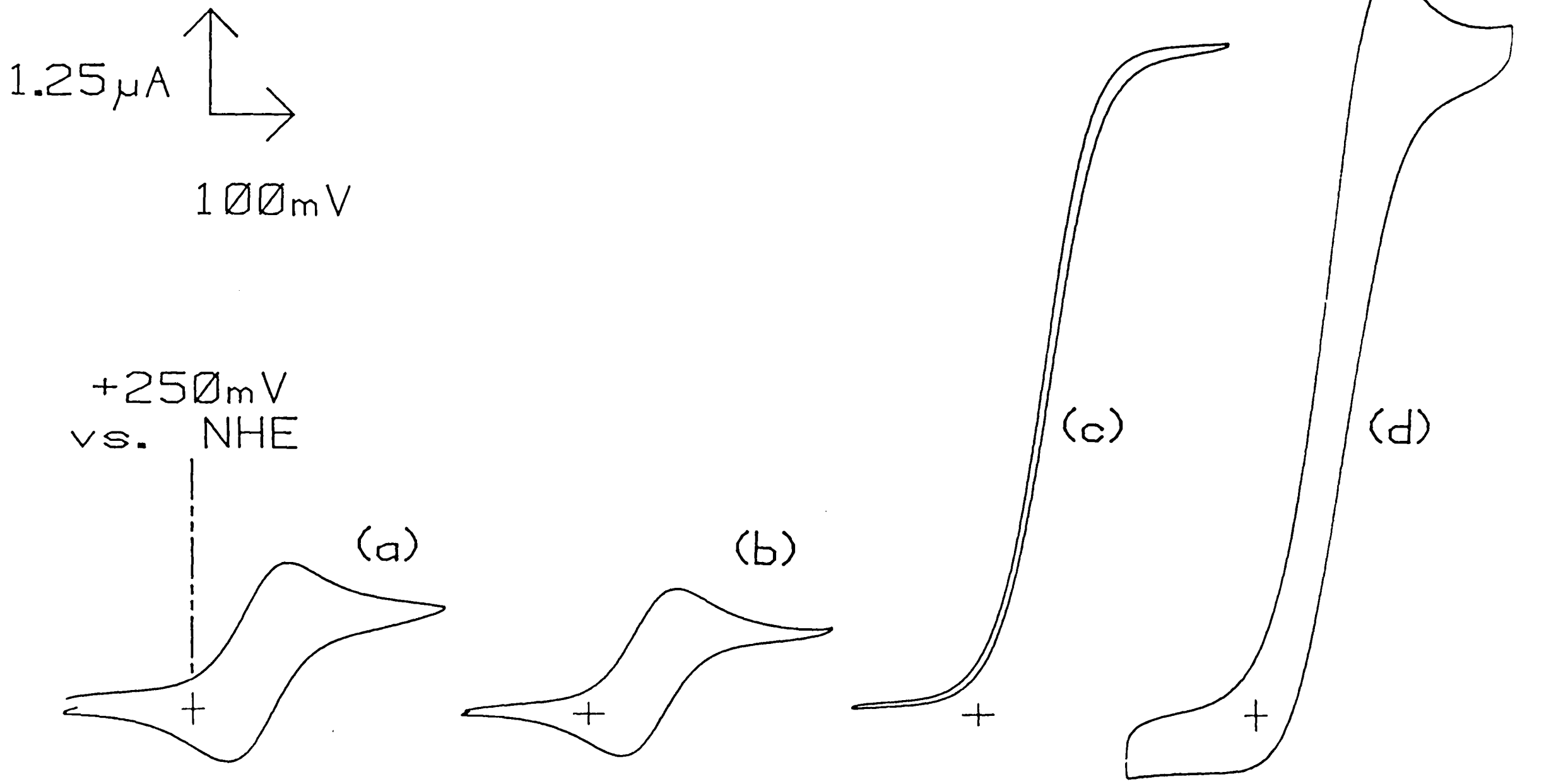

Figure 12.3: Cyclic voltammograms recorded at a 'bare' gold electrode. **(a)** 0.25 mM ferroceneboronic acid in 50 mM Tris-HCl, 10 mM KCl, pH 7.6; (b) as (a), with the addition of p-cresol to 7 mM; (c) as (b), with the addition of p-cresol methylhydroxylase (from *P. putida*) to 1.4 μM; (d) as (c).
(a,b,c): scan rate of 5 mVs^{-1}. (d): scan rate of 100 mVs^{-1}.

rates. A diagnostic plot, Figure 12.4, confirms that this reaction also conforms to the theoretical model for a coupled catalytic reaction (equation (12.1)).

The addition of o-cresol to a solution containing ferrocene boronic acid and p-cresol hydroxylase does not significantly affect the faradaic response, Figure 12.5(a,b). All that is observed is the unperturbed, diffusion-controlled response of ferrocene boronic acid. Similarly, the addition of m-cresol to the same solution does not affect the faradaic response, Figure 12.5(c). However, the addition of p-cresol to the same solution leads to a large catalytic enhancement of the anodic response, Figure 12.5(d). This clearly demonstrates a marked isomer selectivity in the activity of p-cresol hydroxylase and emphasises that selective chemistry is an important feature of enzyme-catalysed reactions.

$K_3Fe(CN)_6$ and N,N,N´,N´-tetramethyl-p-phenylenediamine were also evaluated as potential mediators. However, these couples gave no significant enhancement of the anodic response following the addition of p-cresol and p-cresol hydroxylase.

12.6 The Estimation of Kinetic Data for the Oxidation of p-Cresol Hydroxylase.

The rate of reaction between the reduced enzyme and the oxidised ferrocene, can be derived from an analysis of the cyclic voltammograms (Chapter 2) provided that the rate of heterogeneous electron transfer, for ferrocene boronic acid, is fast compared to the homogeneous rate between the ferricinium ion and p-cresol hydroxylase. Furthermore, there should be excess substrate to ensure that the enzyme is fully reduced. In the presence of a

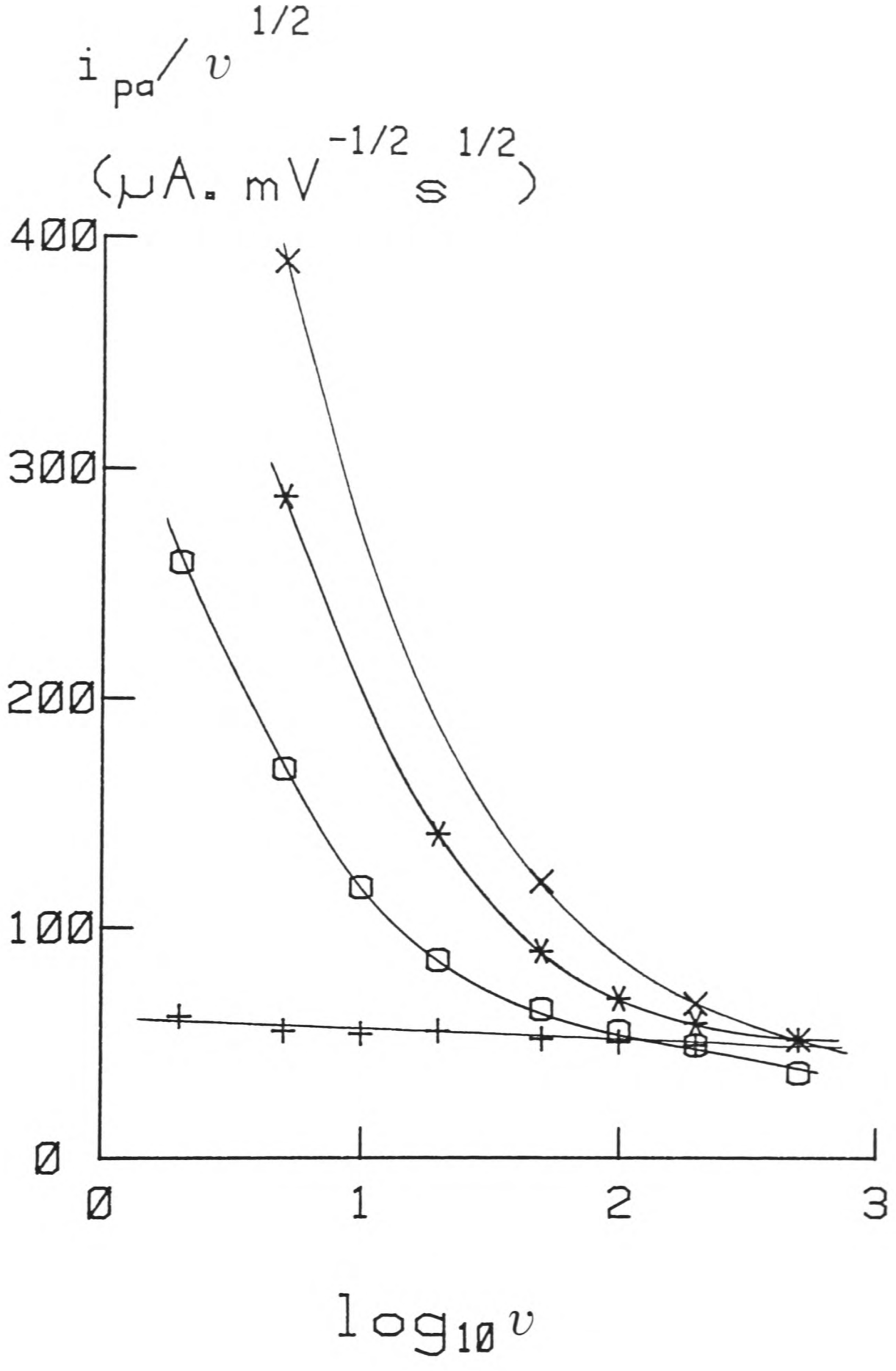

Figure 12.4: Diagnostic plots of the peak current function at p-cresol methylhydroxylase concentrations of: (+) zero, (o) 0.7 μM, (*) 2.1 μM, and (x) 4.2 μM. 0.5 mM ferroceneboronic acid in 50 mM Tris-HCl, 10 mM KCl, pH 7.6 with 10 mM p-cresol.

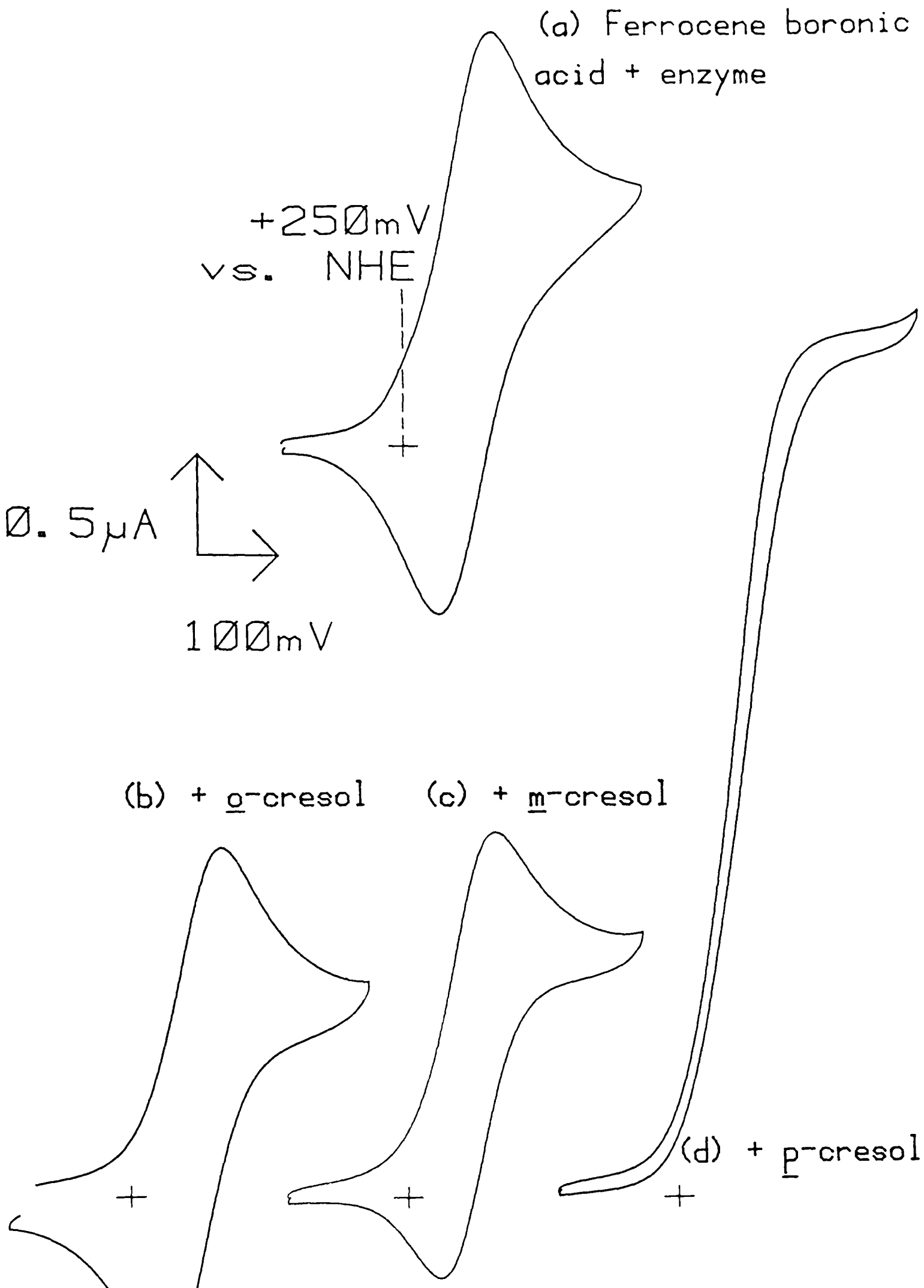

Figure 12.5

Cyclic voltammograms (5 mVs^{-1}) recorded at a 'bare' gold electrode. **(a)** 0.25 mM ferroceneboronic acid in 50 mM Tris-HCl, 10 mM KCl, pH 7.6 containing 0.53 μM p-cresol methylhydroxylase; (b) as (a), with the addition of o-cresol to 7 mM; (c) as (b), with the addition of m-cresol to 7 mM; (d) as (c), with the addition of p-cresol to 7 mM.

high ferrocene to enzyme ratio, the pseudo first order rate constant (k_f) is related to the average second order rate constant (k^s) by $k_f = k^s$ [enzyme].

To obtain quantitive kinetic information, an experimentally-determined ratio of catalytic to diffusion-controlled currents (i_k/i_D) is taken at each scan rate. The value of i_D is the mean value of $i_{pa}/\upsilon^{1/2}$ for ferrocene boronic acid alone. This ratio is related to a kinetic parameter $(k_f/a)^{1/2}$ by a working curve (Chapter 2), where $a = nF\upsilon/RT$. The data are re-plotted, for a series of enzyme concentrations, as k_f/a versus $1/\upsilon$ (Figure 12.6(a)) which is linear, corresponding to pseudo-first order conditions.

From the slope of each curve in Figure 12.6(a), which equals $k_f nF/RT$, a scan-rate independent pseudo-first order rate constant is obtained for each p-cresol hydroxylase concentration. A plot of k_f against enzyme concentration, Figure 12.6(b), is also linear, with a slope equal to the average second order rate constant k^s. The rate constant derived from the reaction of the oxidised form of ferrocene boronic acid with p-cresol hydroxylase (from *P. putida*) is *ca.* 5×10^5 $M^{-1}s^{-1}$. This compares with a rate constant estimated by the same method, for the reaction between azurin (from *P. aeruginosa*) and p-cresol hydroxylase (from *P. putida*), of *ca.* $6 - 9 \times 10^4$ $M^{-1}s^{-1}$. It appears that ferrocene boronic acid acts as a rapid oxidant of p-cresol hydroxylase. The kinetics of the glucose/glucose oxidase/ferrocene system have been derived by a similar method using various ferrocene derivatives (6). Most of the ferrocenes investigated acted as rapid oxidants for the enzyme (e.g. for methyl(trimethylamino) ferrocene, $k^s = 5.25 \times 10^5$ $M^{-1}s^{-1}$) although rates were lower than

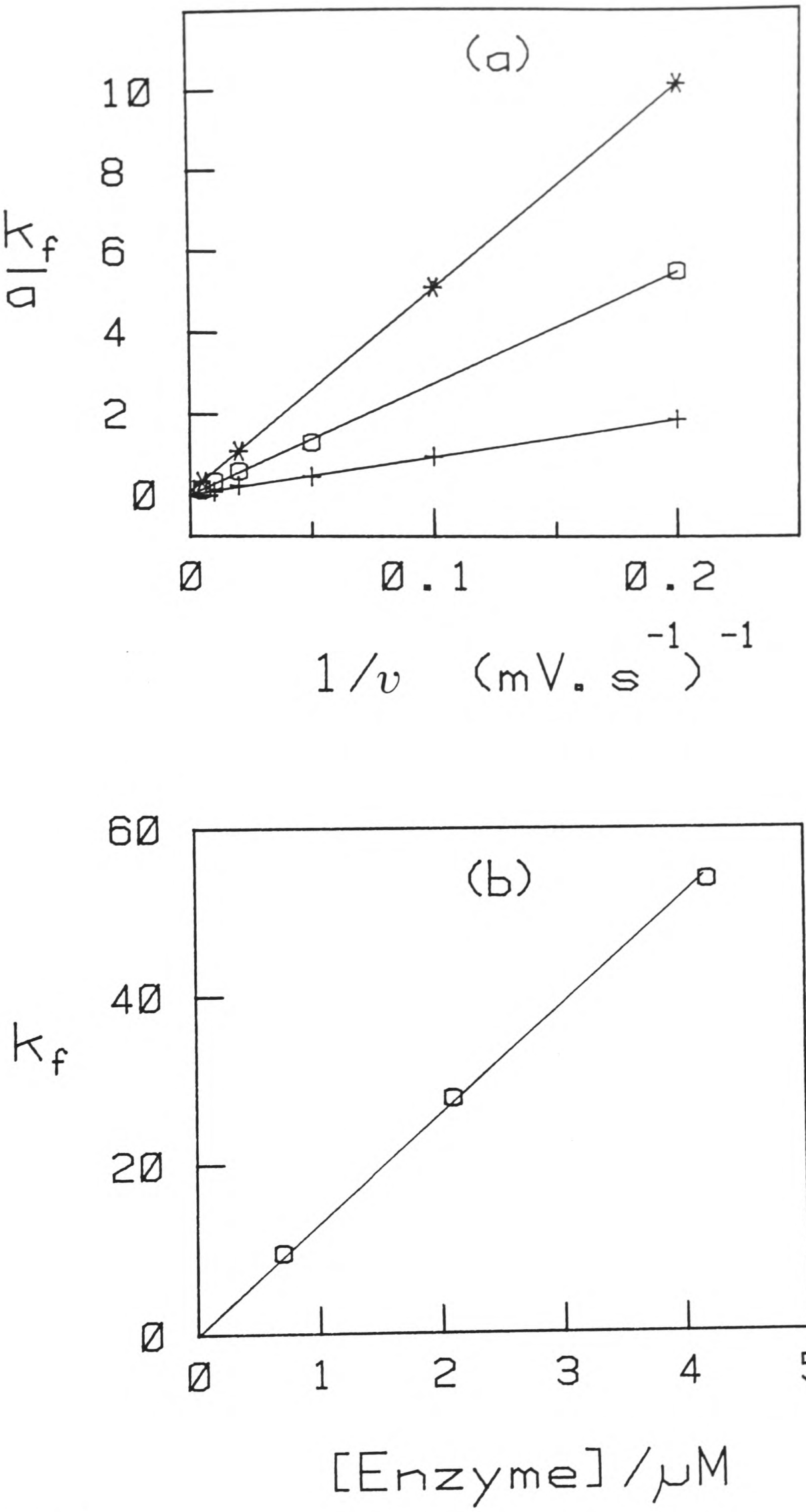

Figure 12.6: **(a)** Plot of kinetic parameter k_f/a as a function of 1/(scan rate) at p-cresol methylhydroxylase concentrations, (+) 0.7 μM, (o) 2.1 μM, and (*) 4.2 μM.
(b) Pseudo-first order rate constants [taken from the slopes of the lines in Figure 12.6(a)] plotted as a function of p-cresol methylhydroxylase concentration. Conditions as given in Figure 12.4.

that for the reaction between reduced glucose oxidase and its natural redox partner, dioxygen (k^s= 1.5 x 10^6 $M^{-1}s^{-1}$).

12.7 The Exploitation of the p-Cresol Hydroxylase for Bulk Electro-synthesis.

The ready availability of ferrocene boronic acid, its ease of use, and the stability of the coupled electrochemistry with this mediator, made the FBA/p-cresol hydroxylase system ideal for incorporation into a bench-scale synthetic device. A simple two-compartment stirred cell, with large surface area electrodes (anode: gold foil; cathode: gold or platinum foil) was used as a prototype reactor.

A current-time trace resulting from a typical bulk electrosynthetic run is shown in Figure 12.7. In the initial stage, monitored by a yellow [ferrocene] to blue [ferricinium] colour change, ferrocene boronic acid (50 cm^3 of 1 mM FBA, pH 7.6, 30°C.) was completely oxidised to the ferricinium (FBA^+) state. The addition of p-cresol (125 μmols) to the ferricinium solution caused no significant change in the anodic current. However, the addition of a catalytic quantity (90 nmols) of p-cresol hydroxylase stimulates a profound change in electrochemical activity, marked by the onset of a ´limiting´ anodic current (ca. 10 mA) and the rapid (<5 secs.) reduction of the ferricinium solution (blue to yellow colour change). These observations are consistent with the flow of reducing equivalents, from the oxidation of p-cresol, through the ferrocene boronic acid-mediated electrocatalytic system, as described above. In the prototype cell, the current derived from this oxidation was used to evolve H_2 from H_2O at the cathode. The rate of substrate

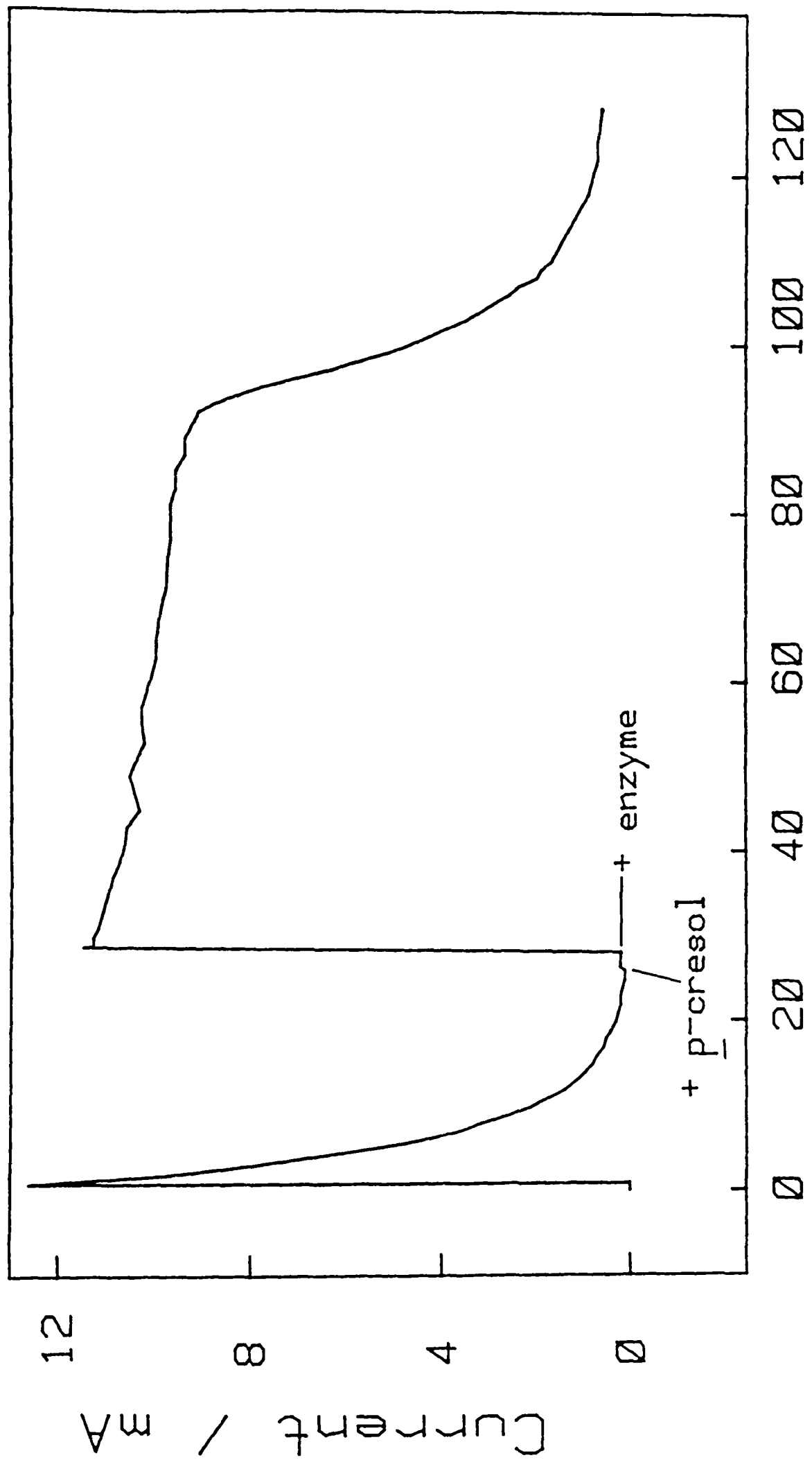

Figure 12.7: Current-time response obtained in a stirred, bulk electrolysis cell. Solution contained initially 1 mM FBA in 100 mM Tris-HCl, 50mM KCl, pH 7.6. Applied potential switched from E = +250 mV to +600 mV vs. NHE at time = 0. Additions of p-cresol (125 µmols) and p-cresol methylhydroxylase [from P. alcaligenes] (90 nmols) were made as indicated.

transformation was independent of the conditions used in the cathode compartment (pH 1, pH 7.6 or pH 9). This suggests that the limiting anodic current observed is a consequence of the limited solubility (ca. 1 - 2 mM) of ferrocene boronic acid, under the conditions used.

The completion of enzyme activity (Figure 12.7) was marked by an abrupt decay in the faradaic current, corresponding to the re-oxidation of FBA to FBA^+, as monitored by the change in colour (yellow to blue) of the solution. Further enzyme activity could be stimulated simply by the addition of a second batch of p-cresol (125 μmols) to the same cell. In fact, there was no apparent loss of enzyme activity (30°C) after at least 12 hours of batch-wise processing. Enzymic activity was also maintained at higher levels (ca. 1.25 mmol additions) of p-cresol.

Initial confirmation of p-hydroxybenzaldehyde as a product in reaction mixtures was provided by the preparation of a 2,4-dinitrophenylhydrazine derivative. The melting point of the 2,4-dinitrophenylhydrazone (275 - 277°C) was in good agreement with that for a derivative obtained from authentic material (280°C). HPLC analysis (Figure 12.8) of typical product mixtures resulting from an electrosynthetic experiment confirms that there is complete turn-over of p-cresol. The only significant product is p-hydroxybenzaldehyde. The yield of p-hydroxybenzaldehyde, as measured by the integration of current-time profiles, varies according to the source of the enzyme. Using p-cresol hydroxylase from P. alcaligenes, yields were typically ca. 85% of the expected coulometric maximum.

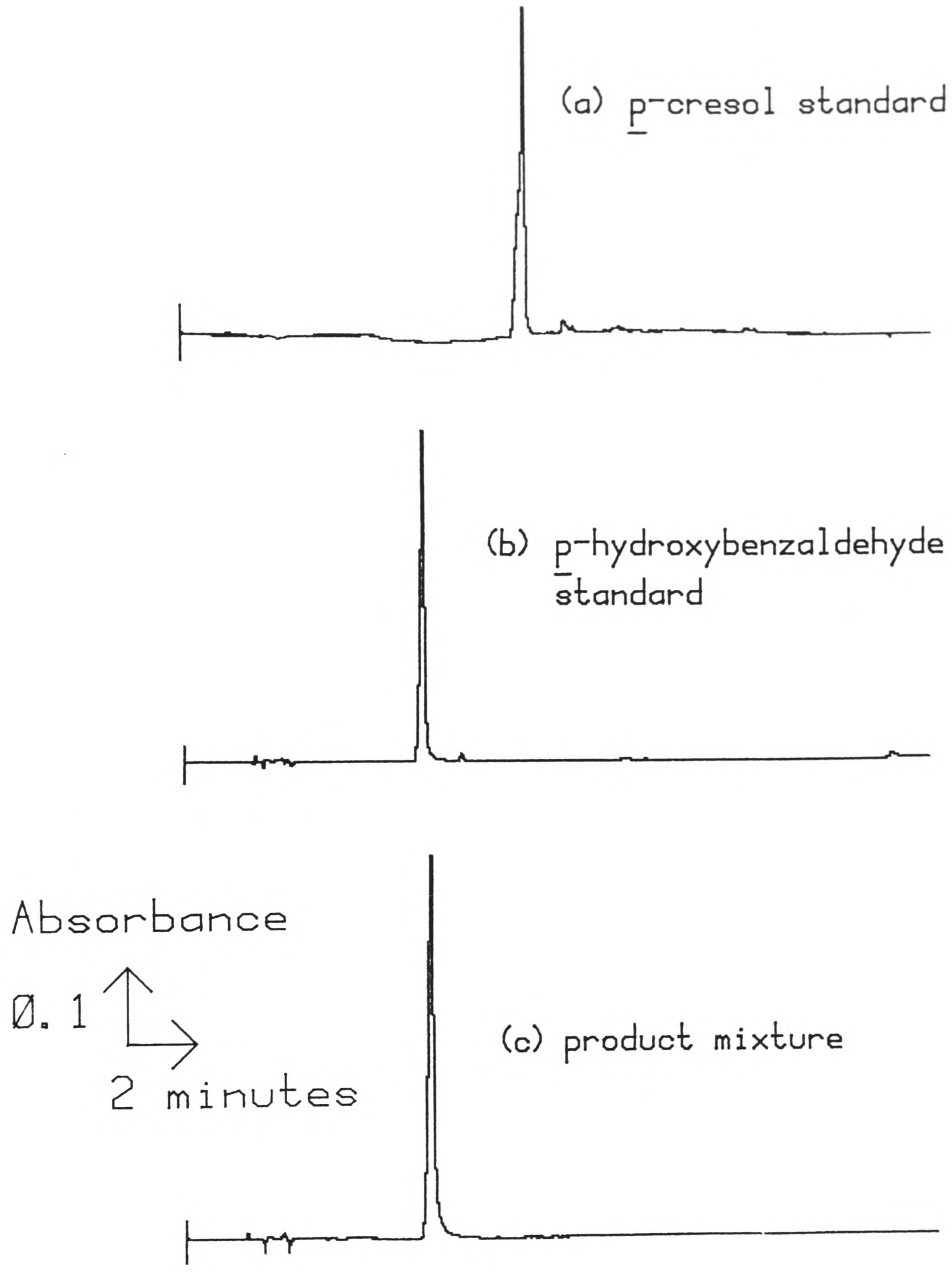

Figure 12.8: HPLC analysis of a product mixture resulting from an electrosynthetic run as in Figure 12.7. Standard solutions (1 mg in 100 mL) were made up in ethanol. Other conditions were as given in the experimental details section.

12.8 Summary and Final Discussion.

This chapter describes the coupling of an electrochemical device to a synthetically-useful enzyme and the development of a prototype bulk electrosynthesis cell. This is one of the first examples of enzyme-catalysed electro-organic synthesis. The electrochemical oxidation of p-cresol is effected enzymically using either a redox protein, azurin, or ferrocene boronic acid as a mediator of the anodic reaction. The reaction of enzyme, substrate and electrochemically-regenerated mediator (ferrocene boronic acid), in a bench-scale device, converts p-cresol to p-hydroxybenzaldehyde under mild conditions (pH 7.6, 30°C.). Although the yield of this prototype reactor is not as high as expected and remains to be optimised, the use of p-cresol hydroxylase demonstrates the advantages of bioelectrosynthetic routes, in particular, the stereoselectivity of substrate transformation, rapid turn-over of substrate and mild reaction conditions.

A critiscism of enzyme-catalysed organic synthesis is the high substrate specificity of some enzymes, which limits the scope for effecting commercially-valuable conversions. It is worth noting that, although p-cresol hydroxylase is highly stereoselective, the enzyme has a low substrate specificity and will oxidise a wide range of substituted phenols (15). It is anticipated that the rate of substrate transformation and, hence, the productivity of the prototype cell, could be increased by the use of a more soluble ferrocene derivative. In addition, the current derived from the oxidation of p-cresol could be used to drive a second enzyme-controlled electrosynthetic reaction in the cathode compartment.

References - Chapter 12

1) Jansson, R., Chem. and Eng. News 62, 43, (1984).

2) Faulkner, L. R., Chem. and Eng. News 62, 28, (1984).

3) Matsue, T., Fujihira, M. and Osa, T., J. Electrochem. Soc. 126, 500, (1979).

4) Firth, B. E., Miller, L. L., Mitani, M., Rogers, T., Lennox, J. and Murray, R. W., J. Am. Chem. Soc. 98, 8271, (1976).

5) Davis, G., Hill, H. A. O., Aston, W. J., Higgins, I. J. and Turner, A. P. F., Enzyme Microb. Technol. 5, 383, (1983).

6) Cass, A. E. G., Davis, G., Francis, G. D., Hill, H. A. O., Aston, W. J., Higgins, I. J., Plotkin, E. V., Scott, L. D. L. and Turner, A. P. F., Anal. Chem. 56, 667, (1984).

7) Allen, P. M. and Bowen, W. R., Trends in Biotech. 3, 145, (1985).

8) Walt, D. R., Findeis, M. A., Rios-Mercadillo, V. M., Auge, J. and Whitesides, G. M., J. Am. Chem. Soc. 106, 234, (1984).

9) Coleman, J. O. D., Hill, H. A. O., Walton, N. J. and Whatley, F. R., FEBS Lett. 154, 319, (1983).

10) Hopper, D. J. and Taylor, D. G., Biochem. J., 167, 155, (1977).

11) Causer, M. J., Hopper, D. J., McIntire, W. S. and Singer, T. P., Biochem. Soc. Trans. 12, 1131, (1984).

12) Hopper, D. J., personal communication.

13) Hill, H. A. O., Page, D. J., Walton, N. J. and Whitford, D., J. Electroanal. Chem. 187, 315, (1985).

14) Cass, A. E. G., Davis, G., Green, M. J. and Hill, H. A. O., J. Electroanal. Chem. 190, 117, (1985).

15) McIntire, W. S., Hopper, D. J. and Singer, T. P., Biochem. J. 228, 325, (1985).